Department of Imaging and Applied Physics
Centre for Marine Science and Technology

Oceanographic Processes in the Perth Canyon and Their Impact on Productivity

Susan Jane Rennie

This thesis is presented for the Degree of
Doctor of Philosophy
of
Curtin University of Technology

December 2005

Declaration

To the best of my knowledge and belief this thesis contains no material previously published by any other person except where due acknowledgment has been made.

This thesis contains no material which has been accepted for the award of any other degree or diploma in any university.

Signature: …….

Date: ……...

Abstract

Submarine canyons are important to continental shelf ecosystems. They have a strong influence on shelf circulation and the distribution of biota. The Perth Canyon is a long, deep canyon on the Western Australian coastline that has attracted attention as a feeding area for pygmy blue whales (*Balaenoptera musculus brevicauda*). Despite existing on a highly oligotrophic coast, the Perth Canyon has the ability to support sufficient krill to feed these massive mammals. The aim of this study was to examine the physical processes within the Perth Canyon, and consider how these could affect productivity. Research areas included the interaction of the Leeuwin Current and Leeuwin Undercurrent with the canyon, the circulation within the canyon, the effect of wind forcing and the occurrence of upwelling. The oceanography of the Western Australian coast including seasonal productivity changes was also examined.

This study utilised numerical modelling and collection of field data to develop a thorough understanding of the Perth Canyon. The numerical model ROMS (Regional Ocean Modelling System) was used to simulate a long stretch of coastline in which the Perth Canyon was centrally located. The model forced the Leeuwin Current and Undercurrent using density gradients, and the seasonal Capes Current was then generated by applying a surface wind stress. The simulations showed that primarily the Leeuwin Undercurrent interacted with the canyon. Eddies continually formed within the canyon, which enhanced vertical transport and could contribute to entrapment of passive drifters. The addition of wind had no discernible effect on canyon circulation although vertical velocities increased everywhere and shallow upwelling occurred along the shelf.

The field data comprised moored temperature loggers, field cruises, and sundry data from satellite imagery, weather stations and whale observations. The temperature loggers, located on the canyon rim, indicated the range of processes that affect the canyon region. These processes included seasonal changes in the wind, the seasonal changes and meanders of the Leeuwin Current, storms, the near-diurnal sea breeze and inertial period changes, and other internal waves. The temperature loggers also

indicated sporadic upwelling at the canyon rims, although this upwelling rarely extended into the Leeuwin Current. The field cruises gathered CTD, ADCP, nutrients and acoustic backscatter data. The water masses near the canyon were identified from their temperature, salinity and oxygen signatures. The deep chlorophyll maximum exhibited high spatial variability around the canyon. The circulation, in conjunction with the simulated circulation from ROMS, reiterated that eddies filled the canyon below its rims, and suggested that passive drifters would aggregate within the head. The acoustic backscatter reinforced this, showing that biota concentrated near the head of the canyon, which is where the whales were most often sighted feeding.

The conclusions of this study were that the canyon is a region of enhanced productivity where upwelling is enhanced and aggregation of passive drifters is likely. Upwelling occurs more strongly when the Leeuwin Current is weakened or has meandered out of a region. Seasonal changes in productivity in the canyon conform to seasonal productivity arguments for the entire coastline, which accounts for the seasonal aggregation of blue whales. The physical processes in the Perth Canyon are variable and all are important to this marine ecosystem.

Acknowledgements

The foremost acknowledgements are to my supervisors Dr. Rob McCauley and Professor Chari Pattiaratchi, for all their guidance, feedback and assistance. Thanks also to Emeritus Professor John Penrose for his suggestions.

Funding for this study was provided through the WAXA (Western Australian Exercise Area) Blue Whale Project, which Australian Defence Forces funded to study the blue whales and their habitat. I received an Australian Postgraduate Award with a top-up from the WAXA BW Project.

The survey of blue whales, and processing and analysis of survey data, was undertaken by the Centre for Whale Research (boat surveys), Western Whale Research (aerial surveys), and Dr R. McCauley, Curtin University of Technology (passive acoustic detection), as part of the WAXA Blue Whale Project. Dr McCauley, as Project Leader, assimilated the whale survey data that was provided for Chapter 6 to assist with analysis of the Perth Canyon. The summary report "McCauley, R., Bannister, J., Burton, C., Jenner, C., Rennie, S. & Salgado Kent, C. (2004) *Western Australian Exercise Area Blue Whale Project - Final Summary Report - Milestone 6*" is available at:
http://www.cmst.curtin.edu.au/publicat/index.html.

Dr Rob McCauley conducted the deployment and recovery of the temperature logger mooring equipment. Paul Pettorini and the crew of the fishing vessel *Reliance II* were crucial for mooring deployment and recovery. The Centre for Whale Research assisted with mooring deployments.

NOAA satellite images of the Leeuwin Current (Chapter 3) were provided by Alan Pearce, courtesy of WASTAC (Western Australian Satellite Technology and Applications Consortium). Additional unpublished satellite SST images were obtained from the Western Australian Department of Land Information through the Land Online website at www.landonline.com.au and POET at poet.jpl.nasa.gov.

The Australian Bureau of Meteorology supplied the meteorological data from the Rottnest Island station.

The bathymetric data is © Commonwealth of Australia (Geoscience Australia) 2003. The Data (Australian Bathymetry and Topography Grid) has been used in this model with the permission of Geoscience Australia. Geoscience Australia has not evaluated the Data as altered and incorporated within this model, and therefore gives no warranty regarding its accuracy, completeness, currency or suitability for any particular purpose.

The numerical model was run on the supercomputer Carlin at the Interactive Virtual Environment Centre (IVEC), Perth, Western Australia.

The CTD and hydrology data collected on the RV Southern Surveyor was processed by CSIRO. Christine Hanson kindly provided the chlorophyll *a* extractions used to convert the fluorescence data. The acoustic backscatter data was processed and analysed, and the species netted and identified from backscatter targets, by Dr Rob McCauley.

Chapter 4 "Dynamics of the surface and sub-surface currents off south-western Australia: a numerical study" was submitted in a slightly modified form for a special issue of Deep-Sea Research II regarding the Leeuwin Current and its Eddies.

Special thanks to Miguel Lievano for his friendship and support, my parents for all their good advice, and my office co-workers over the years (Chris van Etten, Marco Marinelli, Luigi Renzuello, Tseng Yao-Ting, Iain Parnum, Miles Parsons, Matthew Legg, and of course Matthew Rowles, who said it was easy).

Table of Contents

List of Figures

List of Tables

CHAPTER 1

Introduction

Submarine canyons are an important part of a continental shelf ecosystem, where the interaction between physical and biological systems create highly productive regions with high biodiversity. Canyons are popular locations for fishing, but are also preferred areas for marine conservation. To ensure these regions (and their inhabitants) are not abused, a thorough understanding of the dynamics of a submarine canyon is imperative. Furthermore, submarine canyons act as conduits between the shelf and deeper ocean, transporting water, sediment and pollution on or off the shelf, so an understanding of the circulation within canyons is important.

The Perth Canyon is located about 50 km offshore, west of Perth, the capital city of Western Australia. The region it occupies experiences heavy human usage comprising shipping, commercial fishing and naval training exercises. The Perth Canyon also hosts feeding pygmy blue whales during summer. Pygmy blue whales (*Balaenoptera musculus brevicauda*) are an endangered species that migrate along the Western Australian coast during summer and autumn. They have regularly been sighted feeding around the Perth Canyon's head and, in recent years, a concerted effort has been made to estimate population numbers, track their migration and characterise behaviour. To this end the Western Australian Exercise Area (WAXA) Blue Whale Project was initiated (see Acknowledgements), which provided the setting for the oceanographic study of the Perth Canyon presented here.

The role of this study was to investigate the physical oceanographic processes associated with the Perth Canyon. The physical oceanography was elucidated with diverse field data and numerical simulations of the circulation, which were ultimately combined in a multidisciplinary analysis. One focus was to determine conditions that could increase the density of krill swarms, the whales' prey. This information might be used to predict the whales' arrival and so assist in the conservation of the blue whales by limiting contact with humans.

1.1 Setting for the Project

The Western Australian (WA) coastline has been the subject of many oceanographic studies regarding its unusual current—a year-round poleward eastern boundary current named the Leeuwin Current. The Leeuwin Current dominates the coastline from the North-West Shelf around to the Great Australian Bight (Ridgway & Condie 2004). The warm, narrow current suppresses the upwelling of cool nutrient-rich water that would be expected on an eastern oceanic boundary, despite strong upwelling-favourable winds during summer. Few studies have been conducted on the Leeuwin Undercurrent, which is a weak net northward flow along the shelf slope at ~450 m depth (Woo 2005), or the Capes Current, a seasonal northward shelf current (Gersbach et al. 1999; Pearce & Pattiaratchi 1999). There is also a paucity of work on submarine canyons of the Western Australian coastline. The Perth Canyon is one of the most individual, being long, deep and narrow, and isolated from any other canyon that incises into the shelf break above the 1000 m contour. The interaction of this canyon with an unusual current system is of great interest to the field of submarine canyon research and to WA continental shelf research.

This Perth Canyon study is important for environmental impact concerns. The confluence of different users, both human and sea-creature, makes understanding the region important in a world that is now more environmentally aware. The Western Australian (Naval) Exercise Area (WAXA) extends along a large portion of the west coast and has a focus within 50 nm of the Perth Canyon, which as the nearest deep water, is commonly used for deep water exercises and submarine diving. With HMAS Stirling Naval Base situated nearby, and Fremantle as Perth's major port, the area has heavy transport both with shipping and military vessels.

The oldest records of blue whales along the WA coast include sporadic sightings and whale catch information from Soviet pelagic catches during the twentieth century, which became available to the Western Australian Museum during the 1990's. In the late 1960's, blue whale numbers had diminished to the point that they became an endangered species. The pygmy blue whales commonly seen in the Perth Canyon are a subspecies which is slightly smaller (~22 m) than the 'true' blue whales which

are found near the Antarctic ice shelf in summer. Pygmy blue whales have been sighted throughout much of the year around Exmouth (22°S), near Geraldton and Jurien Bay (29-30°S), and in Geographe Bay (33°S) around November. Sightings in the Perth Canyon are most common in summer and early autumn (February–March). Little is known of the migration patterns of the pygmy blue whales or where they are during other parts of the year, although sightings have occurred along the western and southern coasts of Australia. More information is available from the Australian Government's Department of the Environment and Heritage website at http://www.deh.gov.au/coasts/publications/cetaceans-action-plan/whaleap5a16.html.

A blue whale cruise instigated by the joint Japan/International Whaling Commission in December-January 1995-1996 off WA immediately sighted a number of blue whales around the Perth Canyon. A group of WA researchers including the Western Australian Museum, Curtin University of Technology, Western Whale Research and the Centre for Whale Research, received funding from Environment Australia (now the Department of the Environment and Heritage) to study the whales around the canyon by aerial, boat and acoustic surveys. These took place over 1999-2001 at the Perth Canyon, and identified that whales frequented the area and seemed to be often feeding.

In 2001 the research continued under the WAXA Blue Whale Project, with funding from Australian Defence Forces, as part of a collaborative effort between the various whale research groups, researchers at Curtin University of Technology, environmental groups, Royal Australian Navy (RAN), Defence Science and Technology Organisation (DSTO) and others. The object of the WAXA Blue Whale Project was to learn more about the blue whales that visit the Perth Canyon region and WA's coast, in order to observe their behaviour, estimate population numbers and determine their migration patterns. The Navy's interest stemmed from an obligation to understand the impact their use of the area will have on the whales, and to be able to implement practices that minimise this impact, specifically by knowing when and where the whales are likely to be present or absent.

The WAXA Blue Whale Project implemented several research techniques. Boat and aerial surveys estimated population numbers, and the boat surveys also documented

whale behaviour, took samples for genetic studies and satellite-tagged several whales. Individuals were photographed for identification in subsequent resightings. A passive acoustic array moored on the canyon rim detected whale calls, to count and track whales. The zooplankton in the canyon were sampled with nets and acoustic backscatter. The physical oceanographic study of the Perth Canyon was intended to learn more about the whales' habitat, which might indicate why, how or when it is a feeding ground for the whales.

1.2 Aims

The objective of this study, as part of the WAXA Blue Whale Project, was to investigate the physical oceanographic processes in the Perth Canyon and its physical impact on the local ocean. Processes, such as upwelling, that would favour the formation of the dense krill aggregations that the whales feed upon were given particular attention. Specific aims of this study were to:

- examine the Leeuwin Current and Leeuwin Undercurrent interaction with the canyon, and increase understanding of the Leeuwin Undercurrent,
- consider the effect of seasonal wind forcing on the circulation on the coast and in the canyon, and
- investigate the circulation within the canyon, particularly with regard to upwelling and eddy formation.

An addition to these aims was to discover the physical factors that could affect distribution of biota in the canyon, and recognize how other (non-canyon) physical factors affect productivity in the canyon region.

1.3 Outline

This study used several different techniques, for which the results were analysed separately, and then the outcomes were combined to produce a broad picture of the Perth Canyon's oceanography. These techniques included numerical simulation and analysis of field data.

The canyon's circulation was simulated using ROMS (Regional Ocean Modelling System), to investigate the effect of the topography on the ocean currents. The objective of the numerical simulation was to understand how the ocean currents interact with the canyon, if upwelling or downwelling is induced by the canyon, and what effect wind forcing has on the circulation. The model used realistic bathymetry, ocean properties and wind forcing. As ROMS uses *s*-coordinates, the error associated with vertical interpolation of the horizontal pressure gradient was also assessed. The initial simulation used only salinity and temperature gradients to produce the Leeuwin Current and Undercurrent. Wind forcing was then applied to generate the Capes Current and examine changes to the circulation and vertical transport. Although the canyon was of primary interest, an examination of the currents and eddy formation was included, which arose from ground-truthing the model.

The field data analysis utilised many types of data relevant to the region of interest. However, two primary sources were employed specifically for this study. The first source involved strings of temperature loggers moored on the canyon rims discontinuously over four years. Two field cruises on the RV *Southern Surveyor* constituted the second source of field data. The field cruises collected CTD, ADCP, hydrology, and acoustic backscatter data. Sundry other data included wind from Rottnest Island (from the Australian Bureau of Meteorology), chlorophyll *a* estimates from ocean colour (SeaWIFS satellite data from NASA), sea surface temperature from NOAA satellites, and other historical oceanographic data. The whale sighting data collected by the WAXA Blue Whale Project were also utilised.

This thesis has been written in the format of a series of papers. The literature review in Chapter 2 reviews a broad field of relevant literature. Chapters 3 through 6 constitute the research effort and results. Each of these chapters has been written in the format of a paper, with individual literature review, description of methods and results, with some repetition so that each chapter can stand alone. Chapter 3 deals with the set of field data gathered from moored temperature loggers, which displayed the response of the water over the canyon to weather forcing, and other non-windforced effects. Chapter 4 introduces the numerical modelling effort, dealing with the model development and ground-truthing, the behaviour of the major

currents and formation of eddies. Chapter 5 presents the analysis of the canyon's circulation in the numerical simulations, describing how eddies tend to form within the canyon and impact on the vertical transport. Chapter 6 deals with the results from field cruises and combines this with the results from the previous chapter and the results from the research of the WAXA Blue Whale Project. The properties of the canyon waters are revealed, and the field measurements are integrated with the circulation from the model. Finally, the results are considered with regard to the annual appearance of blue whales. Chapter 7 summarises the findings of this study and suggests future oceanographic work for the Perth Canyon and the blue whales.

CHAPTER 2

Literature Review

2.1 Introduction

Ubiquitous around the world's coastlines, submarine canyons are intrinsic to the oceanography of continental shelves. Submarine canyons' realm of influence extends from the flow of ocean currents to the distribution of marine fauna. Consequently they have been the subjects of various studies in different disciplines.

There are several focus areas in this project and correspondingly in this literature review. The primary focus of the study is the Perth Canyon and the role it plays in the physical oceanography of the southwestern Australian coast. The location of the Perth Canyon is indicated in Figure 2.1. The secondary focus is the relationship of the pygmy blue whales (*Balaenoptera musculus brevicauda*) to the Perth Canyon. There is not a great deal known about blue whales in general, or those seen in Western Australia (WA). Recent surveys by whale research groups[1] have provided more information on their activities, and other fauna, during the year. By understanding the influence of the Perth Canyon, the visitation of blue whales in that region may be understood also.

The effect of a submarine canyon is dependent upon the currents that impinge on it, so an ancillary focus of this study is the unusual current system of the WA coastline. In the case of the Perth Submarine Canyon, the Leeuwin Current (a year-round poleward eastern boundary current) and the equatorward Leeuwin Undercurrent are most relevant. There is also the seasonal Capes Current, which appears on the shelf during summer. The Leeuwin Current has been the subject of many studies for its uniqueness as a year-round poleward eastern boundary current. The Leeuwin

[1] Western Australian Museum, Centre for Whale Research, Western Whale Research and Curtin University, funded through the Commonwealth Department of Environment and Heritage (1999-2000), and Australian Defence for the Western Australian Exercise Area (WAXA) Blue Whale Project (2001-2004).

Current also causes the WA coast to be oligotrophic, which thwarts the typical productivity arguments for canyons.

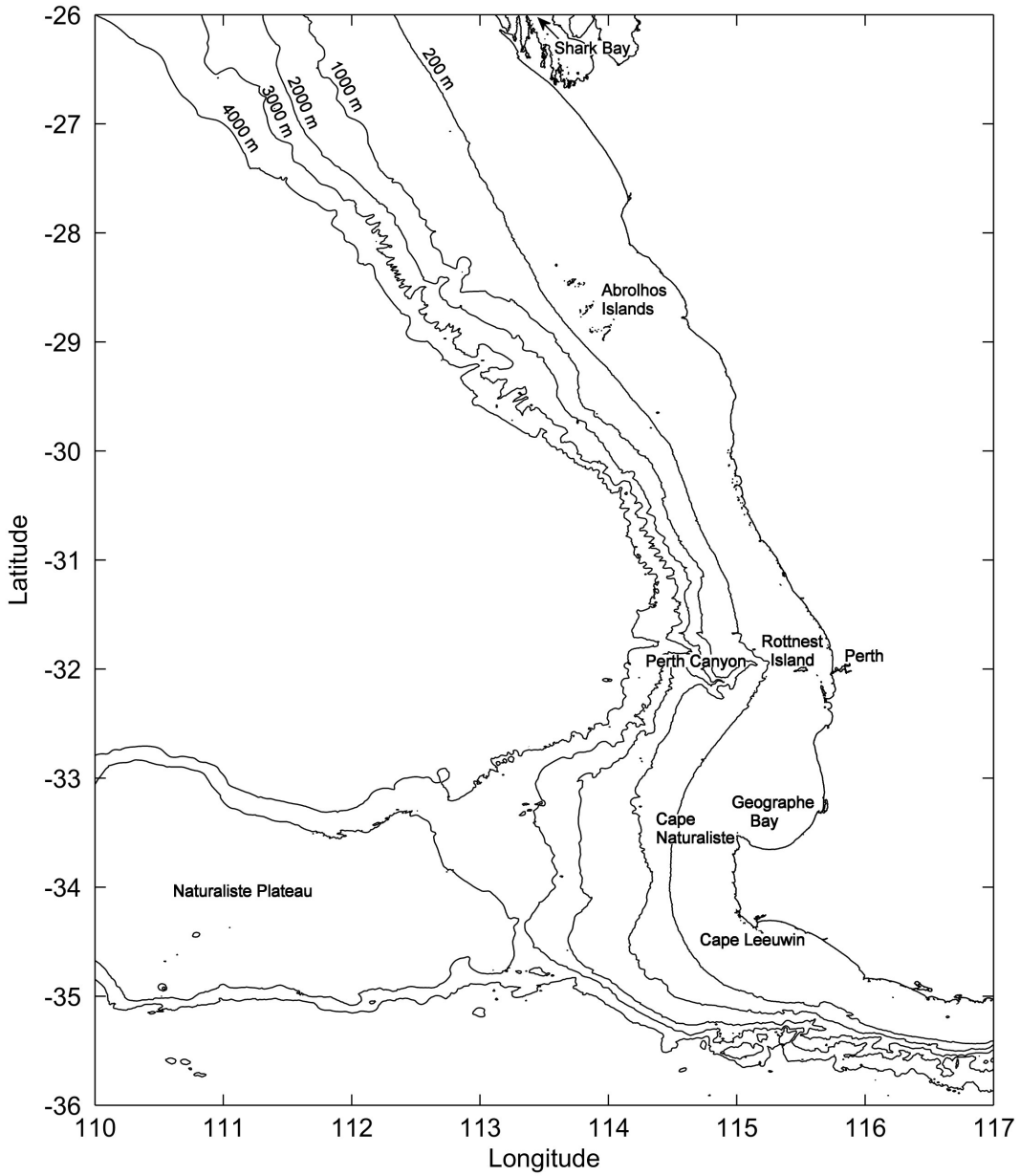

Figure 2.1. Map of part of the Western Australian coastline, showing key landmarks.

Studies of canyons, whether general or specific, are diverse. The focus may be, for example, on measuring currents or plankton around a canyon, or the visitation of megafauna. Some studies show a relationship between canyons and whales exists in other canyon systems (e.g. Hooker, Whitehead & Gowans 2002; Schoenherr 1991), which supports the theory that the Perth Canyon plays a role in attracting the whales. Other studies examine the effect of canyons on fluid flow by numerical and

analytical modelling, and occasionally by laboratory experiment. Water flowing across a canyon will be diverted by the canyon. Movement of water down into the canyon or up on to the shelf is also produced. The unusual oceanography of the Leeuwin Current makes this system studied here different to many previous studies' scenarios.

This literature review starts by examining the principles of oceanography and theory relevant to this study. Next it examines the oceanography of WA and relevant climatological factors. Studies of submarine canyons are reviewed by study type, and finally literature relevant to canyon modelling with ROMS is reviewed.

2.2 Physical Oceanography Principles

The two most important ocean water properties are temperature and salinity, which control density. Depth (pressure) also affects density, as water is slightly compressible. The density can be calculated using the International Equation of State of Seawater (1980), which is an empirical function of salinity and temperature at one standard atmospheric pressure, i.e. $\rho(s,t,0)$. The ocean salinity, which is a measure of total salts content, often indicated by Cl^- concentration, falls into a narrow range of (34–36 psu), excluding near freshwater sources. Salinity is calculated empirically from conductivity measurements, combined with temperature and pressure. These complex empirical equations may be found in the literature (JPOTS, 1991). The temperature at the surface varies due to insolation, but decreases rapidly with depth, and is laterally quite uniform below ~2000 m. Bottom (>3000 m) temperatures of ~1 °C are common everywhere, as the bottom water is sourced from few places, circulates throughout the oceans and mixes very slowly (Tomczak & Godfrey 1994). Salinity and temperature are also altered by precipitation, evaporation and inflow from rivers. Juxtaposed waters of different properties will undergo physical mixing and diffusion, which result in water of averaged properties. Regions of the earth's oceans, distinguished by depth as well as latitude and longitude, have distinct properties so that the salinity and temperature may identify the water mass.

The driving forces of the ocean include gravity, pressure gradients, friction, and the Coriolis force. The Coriolis force arises because the Earth is rotating. If an observer views the Earth as stationary, they will perceive a force acting on moving water, causing it to be deflected to one side as a centripetal acceleration. The equations of motion for oceanic flow are:

$$\left.\begin{aligned} \frac{du}{dt} &== \alpha\frac{\partial p}{\partial x} + 2\Omega\sin\phi v - 2\Omega\cos\phi w + F_x \\ \frac{dv}{dt} &== \alpha\frac{\partial p}{\partial y} - 2\Omega\sin\phi u + F_y \\ \frac{dw}{dt} &== \alpha\frac{\partial p}{\partial z} + 2\Omega\cos\phi u - g + F_z \end{aligned}\right\} \text{ Equations of motion} \qquad (1)$$

$$\frac{\partial u}{\partial x} + \frac{\partial v}{\partial y} + \frac{\partial w}{\partial z} = 0 \qquad \text{Equation of continuity} \qquad (2)$$

u, v and w are the vectors of three-dimensional motion, u representing zonal, v meridional and w vertical motion. x, y and z are the corresponding three vector components of direction. t is time and the total derivative is given by $\frac{dq}{dt} = \frac{\partial q}{\partial t} + \left(u\frac{\partial q}{\partial x} + v\frac{\partial q}{\partial y} + w\frac{\partial q}{\partial z} \right)$. p is pressure, α the specific volume, Ω the frequency of the earths rotation and ϕ the angle of latitude. g represents acceleration due to gravity and F terms represent body forces on the fluid and may include friction and tidal forces. The Coriolis term $2\Omega\sin\phi$ is usually represented as f. These equations are usually solved numerically or by making approximations.

2.2.1 Upwelling

The importance of upwelling relates to its impact on productivity. Upwelling is a mechanism for providing nutrients to the photic zone; below the depth at which nutrients are utilised the nutrient concentration increases rapidly in most ocean regions. Major upwelling zones constitute the areas of the world's major fisheries.

Upwelling is generally defined as a vertical displacement of water, usually with a small velocity which is unable to be measured directly but which may be calculated from horizontal velocities using the equation of continuity (2). Cases of upwelling

(or downwelling) may also be detected by the deflection of isotherms, isopycnals, etc. up a shelf slope, or within the water column.

Upwelling is produced by the divergence of surface water, resulting in vertical flow to replace the water. Downwelling occurs in the convergence of surface water. Convergence and divergence can occur with respect to the coast, i.e. onshore and offshore flow, and mid-ocean. Both of these cases are illustrated in Figure 2.2.

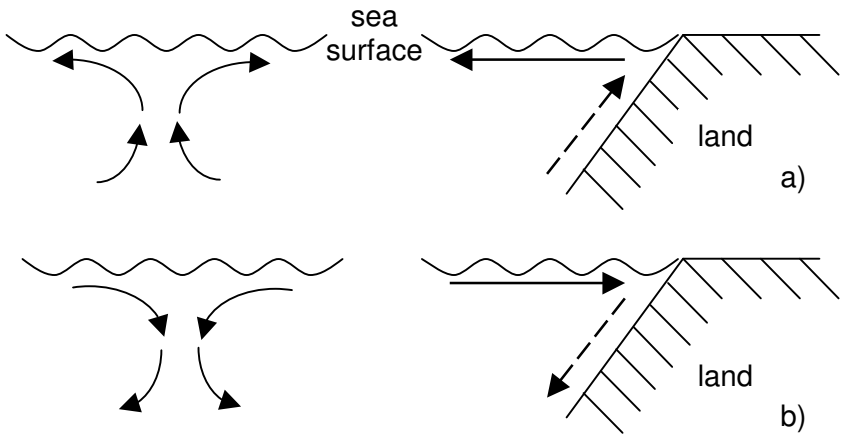

Figure 2.2. Schematic of vertical cross section showing a) upwelling, and b) downwelling, away from and against a shelf slope.

Upwelling and downwelling occur through various mechanisms. Wind is one common forcing mechanism that is easy to understand. Currents driven by the wind, or wind combined with the Coriolis force, can transport water onshore or offshore (Ekman transport), which can result in downwelling or upwelling respectively. Away from the coast, wind gradients of direction or strength can produce convergence or divergence (Pond & Pickard 1983).

Bathymetry changes also affect upwelling and downwelling. It is discussed in Section 2.4 that abrupt changes in bathymetry cause deflection of currents, and may cause the water to cross isobaths, forcing the water up or down the slope. Conservation of potential vorticity

$$\left(\frac{\xi + f}{D} \right) \qquad (3)$$

is important when depth changes occur (Pond & Pickard 1983). Changes of water layer depth D must be accompanied by changes in f (planetary vorticity) or ξ. (relative vorticity). Changes in f are produced by changes in latitude, so if f is constant then ξ must change to compensate. How it changes depends on the change in D and the hemisphere (north or south). Generally ξ is very small away from the coast. By convention anticlockwise constitutes positive vorticity and clockwise negative vorticity. Thus a water column flowing over a canyon can stretch and its vorticity will change (Pond & Pickard 1983). Stretching or compression must be compensated by convergence or divergence.

2.3 WA Oceanography and Climatology

It is difficult to discuss WA's oceanography without considering the Leeuwin Current, which has a profound effect on the marine flora and fauna. Within its domain the water properties, such as salinity, temperature and nutrient content, are significantly different to adjacent waters. It can be identified from its start on the North-West Shelf right down the west coast continental shelf, around Cape Leeuwin (Figure 2.1) and into the Great Australian Bight (Figure 2.3). The Leeuwin Current is not comparable to the conventional southern hemisphere eastern boundary currents; it flows contrary to the normal equatorward current and is far more intense (faster and narrower). As such, the marine ecosystem is of a very different nature to that of the west coasts of Africa and South America (Gentilli 1991).

2.3.1 Eastern boundary current systems

Eastern boundary currents (EBC) occur along most eastern ocean boundaries as slow and broad equatorward currents (in contrast to the intensified poleward western boundary currents) making one part of the anticyclonic subtropical gyre in each hemisphere's oceans. These gyres result from a combination of wind stress, pressure gradients and Coriolis acceleration. The EBC regions are characterised by cool

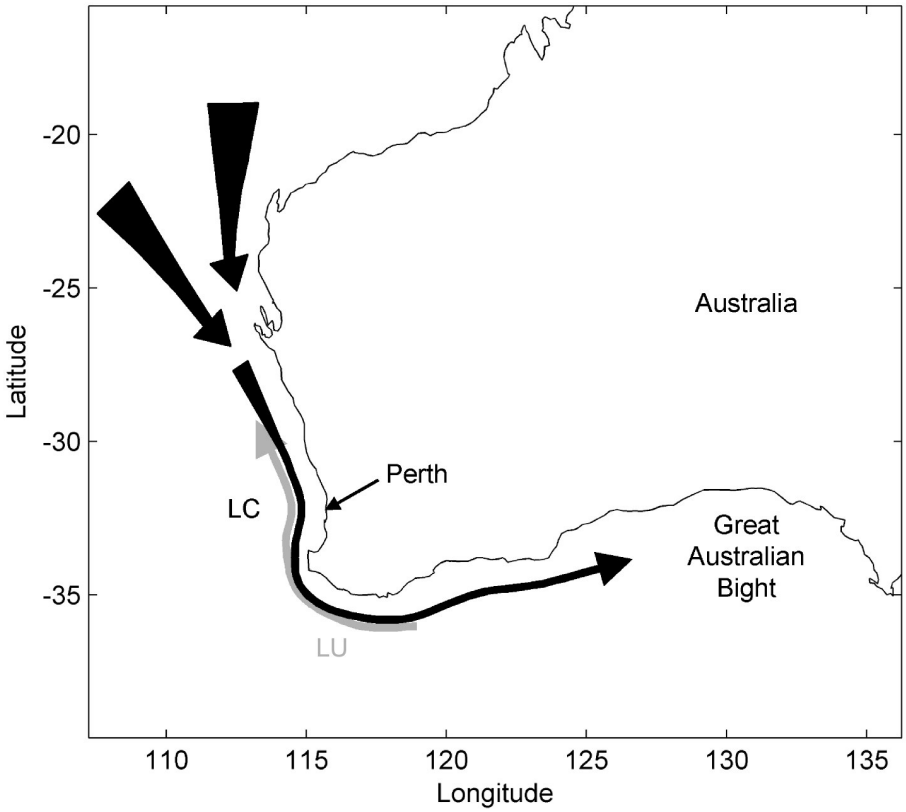

Figure 2.3. Path of the Leeuwin Current (LC) and Leeuwin Undercurrent (LU).

subsurface upwelled water and high biological productivity, so they support major fishing industries. Western Australia does not have the level of biological productivity induced by the Humboldt Current off Africa or the Benguela Current off Peru because the Leeuwin Current suppresses the upwelling of cooler nutrient-rich water along the continental shelf. The continuity of mass required in the oceanic circulation is achieved through the Western Australian current, which is slow and runs deeper than the Leeuwin Current, and is located further offshore.

2.3.2 Source of the Leeuwin Current

The Leeuwin Current is driven by a large longshore sea height gradient North-South along the WA coast (Smith et al. 1991; Thompson 1984). This is facilitated by the connection between the Pacific and Indian Oceans through the Indonesian archipelago. The Indonesian flow-through and the Indian Ocean equatorial countercurrent both contribute water to the Leeuwin Current (Figure 2.3) (Tomczak & Godfrey 1994). Coming from a tropical region, the Leeuwin Current in the north is warmer and less saline that the South Indian Central Water with which it mixes

(Cresswell 1991; Woo 2005). The Coriolis force deflects the current onshore so it follows the coastline closely. In the north it is shallow and wide (around 400 km wide and 50 m deep) with speed exceeding 0.5 m s^{-1} (Smith et al. 1991). Further south it becomes deeper and narrower (around 100 km wide and 150 m deep). Around Cape Leeuwin and into the Great Australian Bight it accelerates and can be >1.5 m s^{-1} (Ridgway & Condie 2004). As it progresses it mixes with local water, decreasing in temperature while increasing in salinity. Near Rottnest Island (Figure 2.1), the Leeuwin Current in June 1987 was measured as 21 °C, 2 °C higher than offshore, with salinity near 35.4 psu, 0.4 psu lower than offshore. Chlorophyll *a* concentrations increased in the onshore and offshore boundaries of the current and nitrate concentration increased in the current, due to mixing (Cresswell 1996).

The Leeuwin Current has been associated with mesoscale eddies and meanders (Fang & Morrow 2003; Feng et al. 2005; Fieux, Molcard & Morrow 2005; Morrow et al. 2003; Pearce & Griffiths 1991) which the offshore boundary comprises, with eddies eventually separating from the current and drifting seaward. These are apparent in sea surface temperature satellite imagery (Griffin, Wilkin, Pearce et al. 2001).

Analysis of temperature data from the south west of Western Australia, from, for example, bathythermographs or CTDs, reveals the general structure of the water. Usually a well-mixed layer (WML) exists at the surface, which is produced by turbulent mixing, e.g. by surface wind stress, and also the presence of the Leeuwin Current. The WML is deeper in the Leeuwin Current than onshore or offshore. The variation in the WML can be greater than 100 m. The mixed-layer depth varies with season and with El Niño (Feng et al. 2003). Below the WML the thermocline usually descends to around 400 m, although sub-layers may exist in this depth range. The seasonal changes include a cooler sea surface temperature (SST) corresponding to the austral winter, and warmer SST in the austral summer, with the deepest mixed-layer depths occur during winter (Feng et al. 2003; Hamilton 1986).

2.3.3 The Leeuwin Undercurrent

The Leeuwin Undercurrent has had little study devoted to it. Measurements of the deeper current indicated an equatorward flow of 0.1–0.4 m s^{-1} below the Leeuwin

Current (below 250 m depth) that is stronger during November to January, and showed a maximum around 450 m, which is driven by a density gradient (Smith et al. 1991; Thompson 1984; Woo 2005). The Undercurrent is associated with Sub-Antarctic Mode Water and generates upwelling beneath the Leeuwin Current (Woo 2005).

2.3.4 El Niño – Southern Oscillation

The main influence on the Leeuwin Current's strength is the geopotential gradient variations. This is fairly constant over a year, but will vary with the El Niño – Southern Oscillation (Feng et al. 2003). The higher sea level near Indonesia is due to the southeast trade winds pushing water across from the Pacific Ocean, so in La Niña years there is low pressure over Indonesia, bringing rainfall. During El Niño years the Walker cell (atmospheric cell containing trade winds stretching from Peru to Indonesia) contracts and the trade winds weaken, allowing water levels to even out. Thus the water level in Indonesia decreases. An indicator for this is the Southern Oscillation Index (SOI), which may be measured by e.g. the Mean Sea Level Pressure difference between Tahiti and Darwin (Troup SOI)[2]. A strong negative SOI indicates El Niño conditions. During El Niño years the geopotential gradient is less, the Leeuwin Current is weaker and consequently sea levels along the WA coast decrease (Feng et al. 2003; Pearce 1991).

2.3.5 Wind and the Capes Current

The Leeuwin Current exhibits considerable seasonal variations as a result of the seasonal winds of WA. During October to March, wind measurements up and down the WA coast (Smith et al. 1991), with the exception of the southern coast, show strong equatorward winds. From March to mid May the winds become more variable in strength and direction though are still equatorward on average. From late autumn to early spring the winds are rotary in direction, due to the passage of low pressure systems below 30°S, and of variable direction and strength northwards to 22°S. Recent wind data from Rottnest Island[3] agree with this, finding strong south-

[2] From Australian Bureau of Meteorology web glossary at http://www.bom.gov.au/climate/glossary/soi.shtml.
[3] From the Meteorological station at Rottnest Island, courtesy of the Australian Bureau of Meteorology.

southwest winds with occasional easterly winds during summer (October-March) and weaker, variable direction winds during winter. In effect, this means that during summer winds are stronger and oppose the Leeuwin Current in direction, forcing it to weaken and broaden (Smith et al. 1991). The LC also shifts further offshore, allowing the Capes Current to develop and flow northward from the south west, between the Leeuwin Current and the shore (Figure 2.4). In winter, the LC is stronger and deeper, and the Capes Current is not present.

The Capes Current is sourced from shallow upwelling of water from the bottom of the Leeuwin Current (~100 m) (Gersbach et al. 1999; Pearce & Pattiaratchi 1999). This water mostly comes from the region between Capes Naturaliste and Leeuwin, hence the name. The Capes Current signal eventually disappears near Shark Bay, due to mixing (Woo 2005).

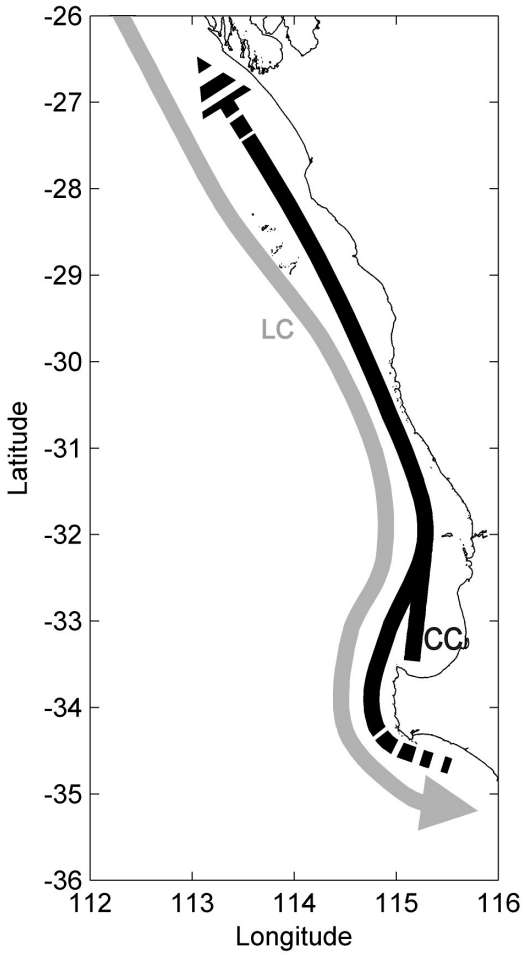

Figure 2.4. The Leeuwin Current (LC, grey) and Capes Current (CC, black).

2.4 Submarine Canyons

Submarine canyons were first recognised over 100 years ago and their origins were the subject of much speculation (Heezen 1956; Johnson 1967). Some are considered to be drowned river valleys, some developed from relicts of old drainage systems, and some are eroded down through turbidity currents. There are many different types of canyons if formation is considered. However, the effect of the canyon depends upon the configuration of the deep incision into a coastal shelf, regardless of how it formed. Important parameters include shelf depth, canyon depth below the shelf, canyon width, length, distance from coast, intrusion into bay areas and depth of the mouth. Commonly, canyons in continental shelves are within a few hundred metres of the surface, 10-30 km wide, and around 2 km deep, though the length may vary greatly (Hickey 1995).

Earliest studies of shelf dynamics were conducted by avoiding the areas with canyons and focussing on sections of straight shelf. Results demonstrated that inaccuracies arose from avoiding the effects of the canyons (Hickey 1995). Canyons have an impact on the shelf beyond their immediate vicinity and are common enough that no coast may be unaffected. (Interestingly, the Perth Canyon has no such neighbouring canyons.) Thus the effects of canyons are important to the coastal and shelf systems.

There exists plenty of anecdotal evidence that canyons' influence extends to biota right through the food chain. Compared to their surroundings, canyons exhibit higher biodiversity and biological productivity (Hickey 1995). This is often attributed to upwelling at the canyon site, enriching the photic zone with nutrients. Canyons are the focus of many studies encompassing physical and biological oceanography, sediment transport, biodiversity and marine conservation. The higher productivity means that marine megafauna often inhabit or feed in canyons (D'Amico et al. 2003; Hooker, Whitehead & Gowans 2002; Schoenherr 1991; Vetter & Dayton 1998) which make them important marine conservation areas.

2.4.1 Physical oceanography of submarine canyons

The abrupt changes in isobath direction and depth when encountering submarine canyons can affect a current strongly. Generally currents will follow isobaths rather than cross them. However, when the change of direction becomes too great, the flow will break away and cross the isobaths. The change in depth produced by this will affect the vorticity as described in Section 2.1. Water flowing over deeper topography will 'drop' or stretch over a greater depth, and find the increase in h from (3) must be balanced by a change in ξ such that $|\xi + f|$ increases. Similarly, water crossing to shallower areas will be pushed up and compressed, changing the vorticity. The result is rotation of the fluid, which can form eddies or meanders. Eddies are often trapped around canyons and seamounts for the same reason. As described in Section 2.1, cyclonic circulation is associated with upwelling and anticyclonic circulation is associated with downwelling, so the direction of flow over the canyon will determine whether downwelling or upwelling is the predominant result. The direction of flow along a continental shelf will normally incite upwelling or downwelling, due to the Coriolis force acting on the boundary current. Where the current is pushed onshore, downwelling ensues, and where the current is pushed offshore, water is upwelled against the shelf to replace it. For $-f$, i.e. southern hemisphere, left-bounded flow (looking downstream) will produce downwelling and right-bounded flow will produce upwelling. In the case of the flow crossing a submarine canyon, the amount of upwelling or downwelling is enhanced.

There have been many studies that examine the role of submarine canyons on continental shelves (e.g. Allen 1996; Boyer, Zhang & Pérenne 2000; Hughes, Ofosu & Hickey 1990; Klinck 1996; She & Klinck 2000; Skliris et al. 2001). Some general descriptions arise. The flow is usually alongshore and in most studies the flow is perpendicular to the canyon axis, particularly with idealised models but often also in real canyon studies. Upwelling or downwelling occurs according to the effects mentioned above. The wind can be an important factor as it can affect the direction of the flow over the canyon. As cross-shelf transport is enhanced within a canyon, canyons also facilitate the transport of sediment off the shelf and nutrients onto the shelf. Eddies can form over a canyon and can also be trapped in a canyon.

2.4.2 Model circulation studies

Analytical model studies of canyons began some decades ago, although studies examining the flow at all levels of a canyon increased greatly from the late eighties. Due to the complexity of the equations, simplifications were needed for an analytical solution. Canyon bathymetry was also simplified, for example using an infinitely long canyon (a channel), vertical sides or infinitesimal width. The earliest numerical modelling studies used similarly simplified bathymetry (e.g. Klinck 1988; Klinck 1989).

Allen (1996) investigated a finite length, very thin canyon using both analytical and numerical model solutions. The analytical model contained an infinitesimally thin canyon but the canyon in the numerical model had a finite width. The analytical solution indicated that for a canyon in a homogenous fluid there was additional flux through the canyon, in part at the expense of flux across the shelf break. The result was an increased surface elevation over the canyon. With a three-layer stratified fluid, the upper layers were deflected around the head of the canyon, which required the interface between layers to rise within the canyon, causing an influx of deeper water into the canyon. The analytical model compared well with the numerical model for the linear solutions. A non-linear solution caused the flow pattern to be advected downstream, which increased upcanyon (towards the head) flow. For the nonlinear, stratified flow, anticyclonic circulation was generated at the head of the canyon in the upper layer, while the layer in contact with the topography generated anticyclonic flow on the downstream rim but cyclonic vorticity on the upstream rim. The deeper flow within the canyon was cyclonic.

Klinck (1996) simulated a smooth-bathymetry canyon with a semi-spectral primitive equation model (SPEM v3) using periodic along-shore boundaries. The variables investigated included strong and weak stratification, and upwelling and downwelling-favourable flow directions. The weakly stratified case for downwelling flow produced cyclonic circulation over the canyon, with enhanced velocity around the head but weakened velocity above the canyon. Downwelling occurred on the upstream rim and upwelling on the downstream rim, which produced a warm temperature anomaly over the canyon. The strongly stratified downwelling case produced a similar pattern to the weak stratification but with more small-scale

structure due to internal waves. For the upwelling cases, the weak stratification produced onshore flow over the canyon and a downstream coastal jet. A plume of colder water upwelled through the canyon was transported along the shelf. The flow off the shelf turned offshore after passing the canyon and some downwelling occurred. For strong stratification the flow was very similar. The main difference due to stratification in both cases (upwelling and downwelling) was to limit the vertical extent of the effect of the canyon on the flow. The strongest cross-shelf exchange arose in the upwelling scenario.

She and Klinck (2000) used ROMS to study wind-driven circulation over a submarine canyon. The model emulated Astoria Canyon in the west coast of North America but used idealised bathymetry. The simulated canyon was shallow and the mouth of the canyon was located above the bottom of the shelf slope. The variables examined included wind direction and stratification. For normal stratification and upwelling-favourable winds, after reaching a quasi-steady state, a closed cyclonic circulation formed within the canyon below the rims, but located towards the upstream rim. Deeper in the canyon, the flow followed isobaths but with stronger onshore flow producing upwelling. During the simulation, the flow within the canyon strengthened. Reducing the stratification by a factor of four increased the influence of the canyon near the surface, and the flow within the canyon was weaker. However, using four times the realistic stratification produced very little difference in flow to normal stratification. Downwelling winds produced a reverse situation with an anticyclone over the canyon. The net cross shelf exchange was less than for the upwelling case, though not as small as Klinck (1996) found. This presented the assumption that in the presence of a canyon, variable winds may still result in a net upwelling as downwelling does not occur equally.

Hughes, Ofosu and Hickey (1990) analysed the interaction of an undercurrent near a canyon using a simple model with parameters to mimic the California Undercurrent. This undercurrent flowed against the continental shelf break in a poleward direction. The model considered the flow to be uniform, and of even thickness parallel to the slope. Three regimes were identified depending on the relative importance of the Rossby number and Froude number. For the California Undercurrent scenario both terms were determined to be important. Another important factor was the width of

the canyon in comparison to the Rossby Radius. It was found that for narrow canyons the undercurrent would separate from the shelf slope within the canyon and be subject to vorticity changes as the depth changed. For wide canyons there would be an onshore excursion of the flow, with the flow steered by the topography. However, with deep canyons, the assumptions made did not hold true. In deep canyons the flow could not realistically undertake the excursion predicted, so also separated from the slope. The flow of underlying water between the undercurrent and slope was then of interest. It was concluded that upwelling would occur within the canyon, with cyclonic flow close to the canyon head trapped by anticyclonic flow further offshore. This pattern shifted offshore with depth and the slope of the shelf within the canyon, so that deep within the canyon the cyclonic flow dominated.

Boyer, Zhang and Pérenne (2000) conducted a laboratory experiment using an rotating tank to observe oscillating flow around a canyon bathymetry. One focus of the experiment was to provide a benchmark for numerical modelling. The laboratory experiment indicated that stratification limited the influence of the canyon towards the surface, which numerical studies had also found (Klinck 1996; She & Klinck 2000). The circulation was asymmetrical with respect to direction of flow, with a net flow upcanyon and alongshore despite the symmetric oscillation. Similar asymmetry was found in non-linear models (e.g. Allen 1996).

The use of idealised canyon models is due to their ease of operation and analysis as well as evaluation. Comparisons are easy to make because of the similarities between studies. However, simulations of real or realistic submarine canyons have further useful applications. The most recent model studies have been aimed at reproducing flow around actual canyons, which is easier than field measurements of circulation if the model is demonstrably accurate.

The Calvi Canyon of northwest Corsica in the Mediterranean Sea has been studied using a numerical model with realistic bathymetry (Skliris et al. 2001; Skliris, Hecq & Djenidi 2002; Skliris, Lacroix & Djenidi 2004). Calvi Canyon is small, but narrow and deep. The model was non-linear and used a double σ coordinate system. Other realistic parameters included the shoreline and the application of wind. Model simulations were run with negligible wind, and with wind in the two prevailing

directions. The volume transport was calculated by the flux through sides of a closed box around the canyon. With negligible wind the flow was consistent with field observations: deflected around the canyon, but not forming closed circulations, which may have been because of the weak stratification (Skliris et al. 2001). Vertical flow around the canyon was enhanced, with upwelling on the downstream side and downwelling on the upstream side, and maximum vertical velocities on the rim. The cross-shelf transport was an order of magnitude higher in the canyon, with cyclonic circulation over the canyon, but anticyclonic circulation in the bay on the western (upstream) side. Incorporating wind forcing increased the circulation in the bay and controlled its direction, and also enhanced the vertical flow within the canyon. Cross-shore transports were also larger with wind forcing. To represent a different season's stratification, Calvi Canyon was also simulated with strong stratification. This had the effect of limiting the influence of the canyon topography on surface flows. The direction of the wind determined whether upwelling or downwelling occurred and also affected the cyclonic circulation in the canyon, either enhancing or reducing it. These results agreed with the findings from idealised canyon models described above in this section. For Calvi Canyon, the results indicated that it could increase the flow of nutrients to the shelf, and also act to channel pollutants and particulate matter offshore (Skliris, Hecq & Djenidi 2002).

This model was subsequently applied to simulate a storm event over Calvi Canyon (Skliris, Lacroix & Djenidi 2004). Meteorological conditions recorded from the storm were applied to the Calvi Canyon model. During this storm event the wind was largely southwesterly. The strong winds increased the cross-shelf flow and engendered marked downwelling in the model, filling the canyon with shelf water. It was concluded that this storm caused considerable flushing of the shelf.

Ardhuin, Pinot and Tintore (1999) simulated the northwest Mediterranean where the Liguro-Provençal Current flows across Blanes Canyon, with the coastline on the right. The model was applied with no wind and with strong northerly (seaward) and easterly (right-bounded alongshore) wind bursts to simulate different seasons. Geostrophic flow formed an anticyclonic eddy and deep upwelling toward the head. The anticyclonic eddy flow diverged against the rim and accelerated onshore in a secondary circulation. Easterly wind promoted downwelling with onshore surface

flow causing deeper downcanyon flow. Northerly wind promoted upwelling, with a strong anticyclonic eddy and deeper upcanyon flow. Upwelling resulted from flow directed into the canyon rim. At the canyon bottom the flow was up or downcanyon. Subsequent to wind relaxation, the vertical transport reversed direction. Similar behaviour was reported for Astoria Canyon in field measurements by Hickey (1997).

2.4.3 Field circulation studies

Physical field studies of canyons are rare because of the difficulty involved in taking measurements, particularly over long periods of time. Equipment malfunctions and losses are a problem, as is the sparsity of economical spatial sampling.

Astoria Canyon is one of the best-studied canyons on the west coast of North America. Hickey (1997) reported on moored current meter arrays and CTD surveys from around Astoria Canyon, examining spatial patterns, phase relationships between currents and winds, and vertical velocity. Upwelling coincided with strong equatorward winds and downwelling occurred when these winds relaxed or reversed. The upwelling velocity reached 50 m d^{-1}; downward velocity during relaxation after upwelling reached 90 m d^{-1}. The vertical velocity within the canyon was strongly related to vorticity. Cyclonic circulation decreased during upwelling and was strongest during the relaxation phase after upwelling.

Above the canyon, relative vorticity was related to and in phase with incident alongshore flow. Above and below the rim vorticity was cyclonic. Below the shelf break, this may have been due to separation of the upstream slope flow on encountering the canyon. Above the shelf break, it was more likely due to the shape of the canyon topography. The flow was funnelled west-southwest across local isobaths, causing it to stretch and increase cyclonic vorticity. Due to limited upwelling events, it could not be verified whether the cyclonic mean flow below canyon rims was caused or enhanced by upwelling events. However, the cyclonic circulation that occurred during relaxation after upwelling appeared to be driven by upwelling. This also showed that after upwelling the canyon system did not just return to the same mean state.

Temperatures above and below the canyon rim were markedly different over time, and seemed to be out of phase. Below the rim, the time rate of change of temperature was in phase with wind (maximum cooling with maximum southward wind) and above the rim, temperature was in phase with wind (coolest water with southward wind). The time rate of change of temperature above the canyon was in phase with the vertical velocity below the canyon. This all suggested that during upwelling the temperature reached a minimum when the south wind was a maximum and after that upwelled water exited laterally on the downstream side of the canyon.

Bosley et al. (2004) conducted a physical, isotopic and biological survey of Astoria Canyon. The physical study utilised temperature and current meters at two moorings on the rim and in the canyon. The mooring data indicated a diurnal frequency within the canyon, the inertial period signal above the shelf and a strong semi-diurnal signal at all locations. The temperature and the surface sub-tidal currents were correlated, with the currents leading the temperature slightly. The strength of the sub-tidal alongshore current, which is a proxy for the alongshore pressure gradient, controlled the upcanyon flow which resulted in upwelling. Upwelled water would be advected downstream and enhance productivity on the south rim of the canyon. Upwelling and downwelling would not occur uniformly but a cyclonic eddy could arise which could prolong the residence time of nutrients. These results matched Hickey's (1997) work on currents.

Biobío Canyon on the coast of Chile was studied using moored temperature and current meters (Sobarzo, Figueroa & Djurfeldt 2001). The moorings were in position on the canyon rim at 10 m, 40 m and 80 m for two periods in March-April and August. The motivation behind this study was that the Chilean fishing industry relies heavily on the upwelling-favourable Chilean Eastern Boundary Current. Higher fishing areas are associated with bathymetric or coastal features and trapped eddies.

Biobío Canyon appeared to be associated with occasional upwelling in the order of 20 m per day. A strong upwelling occurred in response to a storm during the second measurement period, with strong northerly wind. The upwelling was subsequent to the storm winds, which were downwelling-favourable. The shallower temperature loggers indicated surface mixing while the deeper logger showed cooling a few days

after the storm began. At restratification after the wind relaxed, the 40 m logger also indicated cooling. During other, non-stormy times, it was apparent that the canyon caused the currents to intensify towards the head of the canyon (Sobarzo, Figueroa & Djurfeldt 2001).

The interaction of undercurrents with topographic features along the coast of Portugal was examined by Cherubin et al. (2000). These undercurrents formed from Mediterranean Sea outflow, which sinks and mixes with Atlantic Ocean water. The data collection included XCTD, XBT, CTD, and LADCP. Drogued buoys and floats were used to track flow between 700 and 1400 m. Crossing the Portimão Canyon, the lower core of Mediterranean water formed two branches, one of which passed across the canyon, sometimes forming small eddies, while the other follows the isobaths around the canyon. The potential vorticity gradients were reinforced within the canyon, which encouraged barotropic and baroclinic instabilities.

Granata et al. (1999) studied Blanes Canyon in the northwest Mediterranean by field measurements with good spatial coverage. The measurements were used to determine velocity, vorticity and sediment flux within the canyon. The study examined the role of the canyon in supporting detritivore populations. Regarding the interaction of the currents with the canyon, an offshore coastal jet passing over the canyon experienced a negative increase in relative vorticity. The flow turned anticyclonically upstream of and over the canyon, but cyclonically downstream of the canyon and offshore. Inshore, the current was flowing in the opposite direction, creating a region of shear between. Calculation of vertical transport from the horizontal velocities and density field indicated that the canyon under these flow conditions would enhance downwelling. Sediment transport within the canyon would be influenced by stratification, which can reduce vertical transport. The anticyclonic eddy over the canyon may have acted to concentrate and downwell particles. Measurements in the anticyclonic region had highest particle concentrations as well as strong downward velocity. It was not determined if particles were advected out of the canyon or sank within the canyon. The fate of different particles would depend on their sinking rate, advection by currents, upwelling or downwelling, and entrapment within eddies.

The interaction of flow with a canyon is diverse and complex, dependent on direction, stratification and wind, among other factors. The relationship between forcing and response is also complex and time-dependent. The above studies have shown that flows encountering a canyon will be deflected in some way, and experience changes in vorticity. Upwelling and downwelling occur as a result of the canyon interaction. However, it was also shown that downwelling or upwelling can induce a relaxation response of reversed flow, also associated with relaxation after a wind forcing event. Canyons transport water on and off the shelf, which is important for transport of nutrients, pollutants and sediment. Canyons could trap eddies, and in turn trap particles within the water column, which can have further impact on biota, as discussed in the next sections.

2.4.4 Microfauna and macrofauna field studies

A second mode of canyon studies relates to fauna distributions and species. The distributions of microfauna such as zooplankton and macrofauna such as fish and crustaceans, often vary in relation to the topography. Canyons can have greater diversity and population sizes than regions outside the canyon.

Vetter and Dayton (1998) studied Scripps and La Jolla Canyons, which are two shallow canyons that branch from the La Jolla Fan Valley and come close to the shore. The study examined macrofaunal communities, detritus and sediment. The canyons had different deeper communities than at comparable depth elsewhere on the slope. It was concluded the canyons, compared to outside regions, provided better food and habitat. The canyon sediment supported more biomass, although the sediment itself was not organically enriched as originally hypothesised. However, canyon communities were believed to experience more organic enrichment and physical disturbance. Detritus tended to enter from the canyon head rather than falling through the water column, which favoured colonies in the shallow parts of the canyons.

Allen et al. (2001) studied Barkley Canyon off the coast of Vancouver Island, Canada, by collecting physical and biological data. The survey was conducted during summer when upwelling conditions prevailed. CTD casts, and moored

current and temperature data indicated a cyclonic eddy within and above the canyon rims, which was apparently due to vortex stretching as water 'fell' into the canyon as it traversed it. Near the rim level the flow was upcanyon, so that it exited onto the shelf nearer shore than when it encountered the canyon. Deeper in the canyon circulation was cyclonic. The examination of zooplankton indicated that most were passively advected by the currents. Within the canyon zooplankton was advected shorewards and some were trapped within the eddy.

Sánchez-Velasco and Shirasago (1999) studied surface and subsurface distributions of neritic and oceanic taxa in relation to oceanographic processes around Palamos Canyon, in the northwest Mediterranean Sea. The oceanic group were concentrated with the slope current waters that intruded into the submarine canyon while the neritic group were concentrated on the shelf. A large cyclonic eddy offshore of the slope current may also have concentrated the taxa. The distribution of these microzooplankton was related to the bathymetry, and would consequently affect the distribution of predators.

Macquart-Moulin and Patriti (1996) examined several canyons off the French coast in the Mediterranean Sea for distribution of zooplankton. They found that species with diurnal migrations greater than the shelf depth were accumulated over the canyons. The canyons acted to trap species after travelling across the shelf on their nocturnal migration During the night, when they had migrated to the surface, they may have entered or left the area or been advected by the currents, but at night when they migrate to the deep, they became trapped within the canyon. The canyons may have contributed a funnelling effect. There would not be advection out of the canyon during the day, so high concentrations in that area would be assured.

In the above studies, submarine canyons showed a consistent trend of increasing abundance and variety of fauna within a region. This was attributed to increased productivity by supporting the lower end of the food chain, and also advection and entrapment by the canyon circulation.

2.4.5 Marine megafauna studies

D'Amico et al. (2003) reviewed the distribution of three cetacean species in the Mediterranean, specifically the Liguro Sea. The objective of this study was to relate the marine megafauna with oceanographic characteristics that could be used to predict the megafauna distribution in the future for the dual purpose of managing marine protected areas and acoustic risk mitigation i.e. protecting mammals from anthropogenic noise threats. The distributions of sperm and fin whales were correlated with doming from cyclonic circulation, which upwelled nutrient-rich water to the eutrophic level. This also correlated with high chlorophyll *a* values. Cuvier's beaked whales were sighted in subsequent years in a submarine canyon offshore of Genoa, in agreement with their preference for steep bathymetry. Thus the bathymetry and circulation patterns affected the distribution of megafauna.

Monterey Bay, with the Monterey Submarine Canyon, has been acknowledged as an area frequented by blue whales. One particular episode of upwelling accompanied by unusually high numbers of blue whales was studied by Schoenherr (1991). The study involved using acoustic techniques and net tows to estimate the populations of euphausiids in the canyon, particularly near where whales were sighted. Whale presence was counted during these cruises, and their behaviour was identified as feeding or non-feeding. The whales were seen surface feeding and sub-surface feeding. The blue whales were found near the highest concentrations of krill biomass and thick scattering layers, particularly on the southeast edge of the canyon. As the extended upwelling period ceased, the biomass decreased and the blue whales departed the area.

The Monterey Bay was further studied by Croll et al. (2000), among others, to establish the trophic links of the system. Upwelling-favourable winds induced upwelling from late February to late (boreal) summer, which was obvious through colder surface temperatures. Chlorophyll *a* values indicated increased productivity in mid-March. An early increase in backscatter from zooplankton faded but in July the backscatter increased dramatically and the blue whales arrived. In July the euphausiid population was composed largely of adults. The blue whales were found to feed on the densest patches of euphausiids between 150 m and 200 m on the canyon rim. The whales' focus on the canyon arose not because it was identifiable

by cooler water, but because associated with it were high density euphausiid swarms. Croll et al. (2000) suggested the euphausiids' choice of habitat was tied to the high productivity, the ability to migrate down 100 m in to the canyon and to remain in the sheltered areas where currents were weak, to reduce swimming effort.

Hooker, Whitehead and Gowans (1999) examined the distribution of cetaceans in the Gully, a large canyon off the coast of Nova Scotia. The region was under consideration for marine conservation due to the development of offshore petroleum activities. Of the more than ten species sighted, some showed statistically significant preferences for particular water depths, and some were most often sighted during late summer when the sea surface temperature was higher. The Gully was confirmed to have a greater abundance and diversity of cetaceans than elsewhere along the shelf. Estimation of the food requirements of bottlenose whales in the Gully (Hooker, Whitehead & Gowans 2002) indicated that a greater spatial area might need to be conserved in order to ensure sustained prey for the whales.

These studies show conclusively that canyons around the world are locations of increased and diversified populations of whales and other marine fauna. There are thus many practical, anthropic considerations that necessitate extensive study of canyons, such as for planning marine protection from expanding usage of the continental shelf for oil exploration, commercial fishing and naval activities.

2.5 ROMS and Canyon Modelling

Studies of the effect of topography on ocean circulation began some decades ago, with analytical models. As canyon topography was difficult to model, the flow across a channel was considered instead. Later models included a finite channel, i.e. a canyon, of infinite narrowness, then square canyons, rounded canyons, and finally realistic topography. The models grew in complexity, not only in the topography used but also in the complexity of describing the fluid flow. Options included variations in the boundary conditions and forcing, the stratification (varying density with depth) and inclusion of non-linear terms in the equations of motion. The development of computers allowed numerical models to be implemented more successfully, growing in complexity and realistic simulation.

ROMS (Regional Ocean Modelling System) evolved from SCRUM (*S*-Coordinate Rutgers University Model) as the next *s*-coordinate model (Haidvogel et al. 2000), although it is to be superseded by TOMS (Terrain-following Ocean Modelling System). Its features include the non-linear terrain-following *s*-coordinate system that can be configured for high resolution near the surface or bottom of the ocean, and curvilinear horizontal coordinates which means the grid can be shaped to a non-rectangle. The full UNESCO equation of state is used with potential temperature and salinity. ROMS uses an Arakawa 'C' grid with centred second-order finite-difference approximation and a staggered vertical grid. Another feature of ROMS that improved accuracy and efficiency is the use of split-explicit time-stepping. The momentum equations are progressed by direct time step while the free surface is advanced by a smaller time step.

ROMS was tested in a simulation of the North Atlantic Basin by Haidvogel et al. (2000). The results of several simulations under different conditions – model parameters, domain size and resolution – indicated that ROMS was capable of producing a realistic simulation of the North Atlantic Basin. The domain size and boundary conditions were important, as was the surface salinity boundary condition. Higher vertical resolution near the surface was also required to resolve surface forcing effects. All simulation over 10 years showed a drift in 'total' temperature and salinity within the domain.

Terrain-following σ-coordinates and the non-linear 'cousin' *s*-coordinates have one major problem: an error in calculating the current-driving forces over slopes. The error arises from the truncation error in calculating the pressure gradient over steep bathymetry. This calculation involves two large terms of similar size and opposite sign. The grid is considered consistent if one grid point is entirely below the adjacent grid points of the above layer, and vice versa. Haney (1991) documented the error that arises in this calculation. The error is reduced with increased horizontal and vertical resolution, providing the grid remains consistent. Removing a reference state (thus reducing the size of the terms) also reduces the truncation error. In practical terms there is a limit to applying these remedies, and the model is usually considered useful if the error can be considered negligible.

Allen et al. (2003) compared SCRUM, ROMS' predecessor, to laboratory simulations in order to evaluate the model for a submarine canyon. The discrepancy between the laboratory and numerical models was found to be mostly due to the truncation error in calculation of the vertical advection. This was a result of strong vertical gradients, vertical shear and sloping topography.

ROMS has been applied to a variety of situations that indicate its usefulness in the present study. The circulation off the west coast of Iberia is similar to that of Western Australia. There is a poleward boundary current with a weaker equatorward undercurrent (Peliz et al. 2002). Simple dynamics suggest the poleward surface current is generated from a cross-shore pressure gradient, and results in downward tilting of the isopycnals. The deeper isopycnals are compressed and a countercurrent (the equatorward undercurrent) forms (Peliz, Dubert & Haidvogel 2003). The Iberian poleward eastern boundary current is seasonal, occurring in winter only as in summer strong equatorward winds dissipate it and/or push it offshore. A simple model of these currents showed that it acts very like the Leeuwin Current, with upwelling wind causing modification of the current with a shelf current forming in the reverse direction, and downwelling-favourable winds enforcing and creating a secondary coastal jet (Peliz, Dubert & Haidvogel 2003). Peliz et al (2003) also simulated this system using ROMS, with realistic bathymetry that included two canyons and a promontory. The model indicated that these topographic anomalies caused the surface current to diverge and form anticyclonic eddies. The topography helped trap these anticyclonic eddies. The undercurrent, crossing a strong density gradient between the eddy and shelf, formed a cyclonic eddy, which orbited around the anticyclonic eddy. The cyclonic signature was only visible in the deeper current. Several cyclonic eddies formed by this process. Where the shelf was smooth, instabilities in the surface current created meanders, which led to the formation of cyclonic eddies and an eddy dipole. This eddy dipole was not trapped and migrated offshore. The eddy dipole mechanics encouraged this separation from the shelf.

Lujteharms, Penven and Roy (2003) applied ROMS to the Agulhas Current around South Africa, to examine shear eddies formed there. The south west of South Africa was simulated using an arc-shaped grid that conformed to the coastline, with higher

resolution near land. The simulation ran for 10 years. The boundaries were nudges toward seasonal values for the Agulhas Current. Comparison with available hydrographic data demonstrated that there were some differences between simulation and reality, but overall the model reproduced the main features sufficiently to give confidence.

2.6 Concluding Remarks

This review of literature covers diverse topics pertinent to this study of the Perth Canyon. Four topics were reviewed. The principles of oceanography formed the underlying basis for the physical oceanographic study. The currents and climate of the study region were examined, to understand what factors might be important during analysis. Other studies of submarine canyons were described, which demonstrated the behaviour of currents around canyons and the relationship between marine fauna and canyons that has been found elsewhere. This section was particularly important as it provided direction for the Perth Canyon study undertaken here, and offered comparison with other canyons. Finally the use of ROMS, which was applied in this study, was examined in other studies to demonstrate its usefulness in simulating submarine canyons.

CHAPTER 3

Analysis of Leeuwin Current Features in a Time Series of Temperature Logger Data from the Perth Canyon, 2002–2005

3.1 Summary

Temperature loggers were moored on the rim of the Perth Canyon, Western Australia, in several non-consecutive periods over 2002–2004. Seven moorings were positioned on a plateau in 500 m of water on the northern rim with another mooring at the canyon head. The different locations yielded very different data, particularly near the surface. The loggers were positioned to sample the whole water column, including the Leeuwin Current and Undercurrent. This study explored the water column's response to climatological forcing and the meandering of currents as well as canyon effects, including the occurrence of upwelling and downwelling over the rims. Perceived features ranged temporally from seasonal to less than a day. The well-mixed layer and stratification changes were apparent. Seasonal changes in temperature agreed with other Leeuwin Current studies. Changes related to Leeuwin Current's movement and water responses to wind forcing, such as the summer sea breeze and winter storms, were evident. The response to storms showed the water column mixing, restratifying, downwelling, and upwelling as the wind changed direction and strength. Changes lasting only a day were associated with sea breezes (diurnal winds), internal waves, and solitary waves. The bottom loggers indicated upwelling and downwelling events each occurred up to 20% of the time.

3.2 Introduction

Temperature remains one of the most important and useful methods to analyse the ocean. It is an important determinant of density, thus affecting geostrophic flow, and may be used as a means of identifying different water bodies (in conjunction with salinity) and water of different depths; it is also easy to measure with readily available equipment. Water temperature change at a depth has thus been used to determine the presence of upwelling and downwelling. Sea surface temperature

from satellite imagery can indicate different surface water masses and, to some degree, current direction and the presence of mesoscale eddies.

Temperature changes can also indicate various processes around submarine canyons. Bosley et al. (2004) used a series of current and temperature loggers in Astoria Canyon (USA) to find oscillations of tidal and inertial periods. The temperature range at different depths was as great as between depths, indicating a large variation in thermal structure over time. When thermal gradient estimates were used, the water at 200 m shifted vertically by 98 m over eight days.

Sobarzo, Figueroa and Djurfeldt (2001) also used temperature loggers with current meters in their submarine canyon study. The loggers, which were placed in shallow water next to the canyon, recorded surface cooling as a response to wind and a major response to a passing storm. The strong winds mixed the water to at least 40 m. Following the storm, cooling was observed at 80 m; the shallower loggers recorded cooling after this. Most temperature logger data are analysed in conjunction with other data—usually current meters moored simultaneously, meteorological data, and hydrographic cruises; however, much information can be obtained from temperature data alone.

A submarine canyon's presence could have various effects on water flow. The extreme changes in depth and direction of isobath are expected to affect currents that encounter these changes, for example altering vorticity and inducing eddies (Klinck 1996; Peliz et al. 2003). Initially, deviations in the current would occur as the current followed the isobaths. For more extreme changes, the current would break away and cross the isobaths. Eddies could become trapped in the canyon. Canyons are reputed to induce or enhance upwelling and downwelling (Klinck 1996; Sobarzo, Figueroa & Djurfeldt 2001) as a result of the vorticity changes from water curving around the canyon. The canyon's presence could also affect internal waves and increase mixing (Hickey 1995).

The Perth Canyon, as a feeding habitat for pygmy blue whales, is important in Western Australia's coastal oceanography as well as for endangered species conservation, which provided the impetus behind this study. This study employed

moored temperature loggers to investigate physical processes around the Perth Canyon. Whenever possible, the features discerned in the data are described and correlated with known forcing factors. The data provided insight into the processes affecting the ocean near the Perth Canyon and the thermal structure variability.

3.2.1 Study area

The Perth Canyon is a large, deep canyon, which meanders off the shelf of Western Australia, starting 27 km west of Rottnest Island (from the lighthouse), offshore of Perth. The canyon starts at the 200 m contour, and drops to 1000 m within 6.5 km. The canyon mouth opens out onto the abyssal plain at over 4000 m below the surface. The Perth Canyon is the only canyon in the southern part of Western Australia's west coast and, consequently, the continental shelf's most prominent feature (von der Borch 1968). The canyon bathymetry is shown in Figure 3.1a. The region is of particular interest, as during summer it is a feeding area for pygmy blue whales (*Balaenoptera musculus brevicauda*), which are an endangered species. The presence of feeding whales indicates oceanic processes associated with the canyon support a high biomass.

The major current passing over the Perth Canyon is the Leeuwin Current. Much has been written about the Leeuwin Current in recent decades (e.g. Cresswell 1996; Feng et al. 2003; Fieux, Molcard & Morrow 2005; Godfrey & Ridgway 1985; Hughes, Weaver & Godfrey 1992; Ridgway & Condie 2004; Smith et al. 1991; Thompson 1984; Thompson & Veronis 1983; Woo 2005); consequently, understanding of this poleward current along the Indian Ocean's eastern boundary has been achieved only quite recently. The Leeuwin Current is a strong, narrow current comprised of meanders and eddies, which flows inshore of the northward-flowing West Australian current. The Leeuwin Current is characterised as warm, of low salinity, and nutrient poor, which accounts for the Western Australian coast's low productivity compared with other eastern boundaries.

Underneath the Leeuwin Current is the Leeuwin Undercurrent, which is believed to be weak and northward flowing. Much less is known about this current, but reversals in current direction have been ascertained at ~300 m and below (Jones et al.

1996; Thompson 1984; Woo 2005), while the Leeuwin Current extends down to around 250 m. The Undercurrent core at 400–600 m should interact strongly with the shelf slope whereas the Leeuwin Current may be too shallow to interact with the shelf except near the shore.

The Leeuwin Current's driving force is a large meridional pressure gradient (e.g. Godfrey & Ridgway 1985; Smith et al. 1991; Thompson 1984; Woo 2005), which does not exhibit seasonal variations, but is influenced by interannual variations like El Niño-Southern Oscillation (Feng et al. 2003). Seasonal variation in the current strength is due to the wind seasonality. In winter, the Leeuwin Current is stronger and runs deeper. In summer, strong southerly winds retard the Leeuwin Current and force it offshore (Feng et al. 2003; Smith et al. 1991). These southerly winds cause a northward shelf flow—the Capes Current—to develop; cooler water upwelled near Capes Leeuwin and Naturaliste is the source of this current (Gersbach et al. 1999; Pearce & Pattiaratchi 1999). These seasonal variations and the Leeuwin Current meandering are expected to affect the temperature profile by e.g. warming, cooling, or increasing and decreasing stratification.

The wind climate of southwestern Western Australia affects the types of features that are expected to occur. The wind has a bi-seasonal nature, which is referred to here as 'summer' and 'winter' winds (corresponding to austral seasons). The summer winds persist between October and April/May; the land heating during the day and cooling during the night produces a pressure differential, which drives a sea breeze that characterises these summer winds (Pattiaratchi et al. 1997). This sea breeze was observed offshore above the canyon during recent field excursions. The wind is thus easterly (offshore) from approximately midnight to midday or early afternoon then changes to south-southwesterly (alongshore or onshore) (Pattiaratchi et al. 1997). The net wind stress, however, is from the south, as southerly winds are strongest. Winter winds are weaker and rotate through all directions with the passage of pressure systems, so that there is no persistent direction. The transition between summer and winter occurs over several weeks when the two patterns mingle.

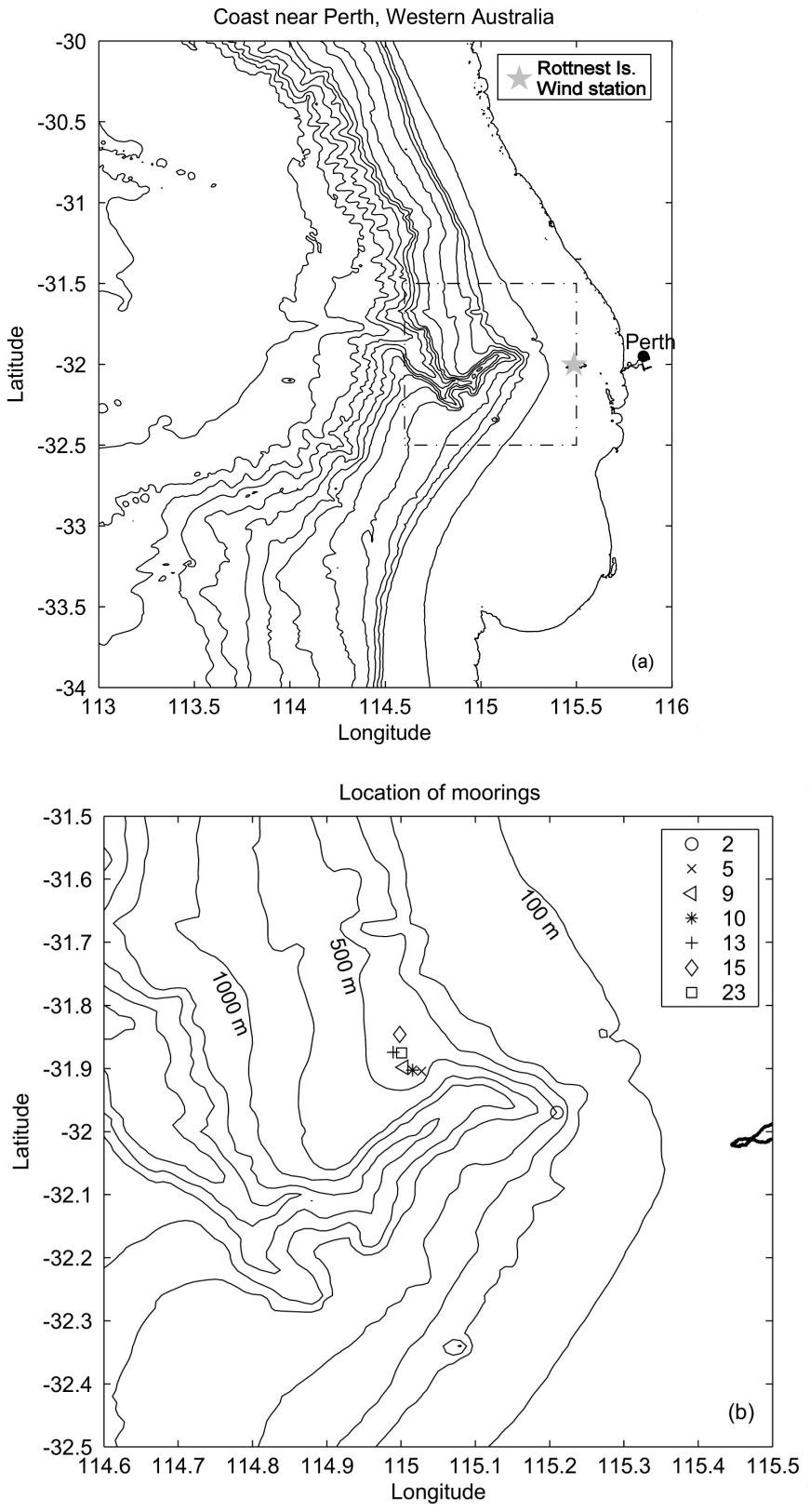

Figure 3.1. a) Location of the Perth Canyon along the WA coast. The head is near Rottnest Island, due west of Perth. Depth contours from the coast are [100, 200, 300, 500, 750, 1000, 1500, 2000, 2500, 3000, 4000] m. b) Location of the seven moorings for which data was retrieved. Six were on a 500m plateau and one (No. 2) was at the head of the canyon.

The other main wind factor is the occurrence of storms, which are mostly associated with the winter wind regime period. Strong winds, which change direction as the storm front passes through, usually characterise these events.

3.3 Data Collection

Results from seven moorings of temperature loggers from early 2002 to mid 2004 are presented. All temperature readings were obtained with Vemco Minilog TR 8-bit temperature loggers (precision of ± 0.2 °C, thermal lag time of approximately 45 s). Each instrument was programmed to sample temperature at a prescribed interval logged with its onboard clock (± 4 s day^{-1}). The loggers were attached to vertical risers set to rise from the bottom to within 50 m of the sea surface. These risers were part of moorings that were set for sea noise loggers. In total, ten moorings with temperature logger strings were deployed, of which three were lost, one provided partial data sets and six provided full data sets. The coordinates, sampling period, and sample increment for moorings used in this paper are presented in Table 1. The mooring locations are shown in Figure 3.1b.

The strong currents associated with the Leeuwin Current and gyres affected the field deployments. Field trips into the canyon between March and June 2002, for example, encountered surface currents that extended to 250 m depth (from CTD casts), with surface velocities estimated at 1–1.5 m s^{-1} (2–3 knots, based on vessel GPS drift in low wind conditions), associated with the Leeuwin Current. These strong currents were problematic for moorings—pulling surface gear down and tilting the risers. Three temperature strings were lost due to submersion, which ultimately, compressed or imploded sub-surface or surface buoys. The Perth Canyon is used heavily for naval practice and by trap and long-line fishers. Sub-surface vessel activity or fishing gear resulted in the riser of two moorings being cut; one at 200 m depth (mooring 13, see Table 1), and one at 390 m depth with subsequent loss of all midwater loggers and bottom logger failure on one mooring. What remained of these moorings was recovered by grappling.

Table 3.1. Mooring number, mooring locations (risers), using chart datum WGS874, successful sampling period, logger depths, and sampling interval for strings of temperature loggers. Time is local WST (UTC +800 h).

*For mooring 13, the riser was cut at 200 m depth on 17 August; beyond this date, only the bottom logger depth was accurately known.

#	Latitude Longitude	Start time	End time	Approx. logger depth (m)	Bottom depth (m)	Interval (mins)
2	31° 58.206' S 115° 12.601' E	17/1/2002 17:50	13/5/2002 19:20	75, 300, 370, 485	500	30
5	31° 54.262' S 115° 01.659' E	17/1/2002 14:30	21/6/2002 12:40	50, 100, 200, 300, 450	450	30
9	31° 53.879' S 115° 00.227' E	14/10/2002 09:40	20/12/2002 12:30	50, 100, 200, 300, 400, 450	450	15
10	31° 54.142' S 115° 00.932' E	18/2/2003 10:50	10/6/2003 12:00	40, 90, 190, 290, 330, 440	440	30
13	31° 52.464' S 114° 59.362' E	10/6/2003 8:40	29/9/2003 16:00 17/8/2003 15:30*	*250, 300, 350	452	20
15	31° 50.752' S 114° 59.899' E	26/2/2004 17:00	3/8/2004 12:50	186, 356, 426	426	30
23	31° 52.532' S 115° 0.039' E	30/12/2004 15:00	15/6/2005 17:30	222, 365	430	30

Risers were set up for moorings 5–23, as per Figure 3.2. Mooring 2 differed; it had a long light surface line attached to the upper buoys at 50 m depth and no ground line or sea noise logger. The long ground line (shown in Figure 3.2) was intended to allow a sea noise logger to be lowered, to isolate this logger from the riser (data not reported here); and as a target for grappling should the acoustic release have failed or if the riser was cut. This last function proved most useful. The riser was 7 mm polypropylene line, with 30–60 kg of buoyancy in the floats. Lanyards spliced into the riser on land set the vertical locations for the temperature loggers clipped on during deployment.

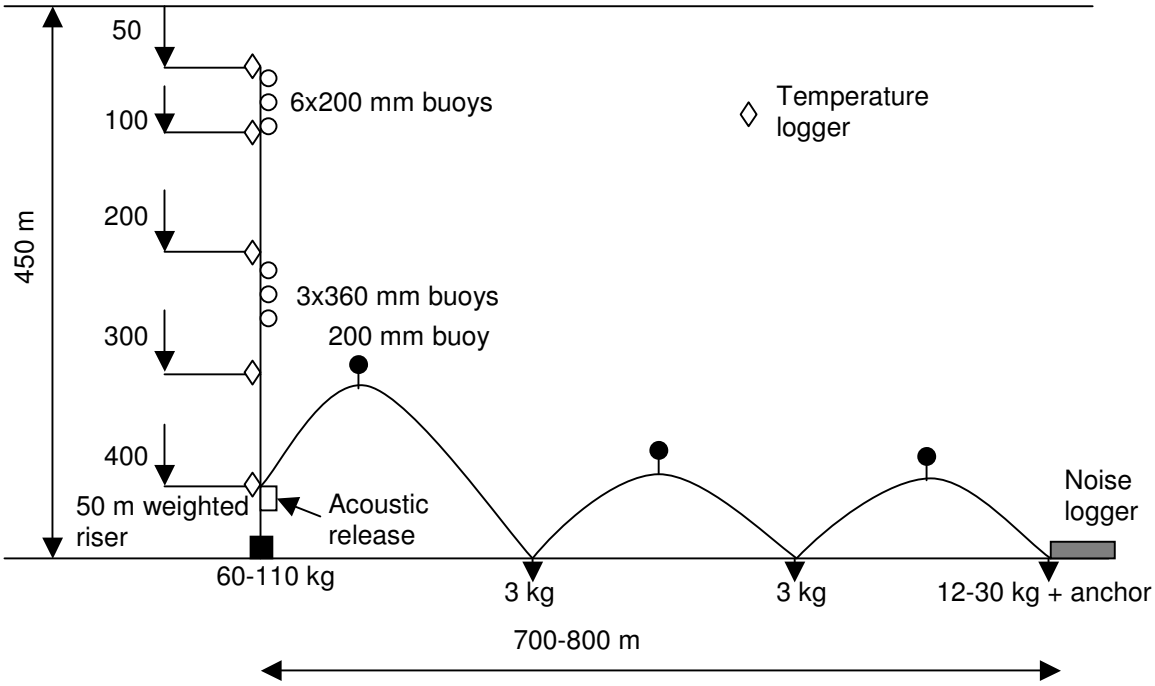

Figure 3.2: Arrangements of moorings 5–23 (not to scale, bights exaggerated).

The actual depth of loggers in the water column depended on the water depth at the riser deployment location and the riser tilt. It was difficult to control accurately the loggers' vertical depth before deployment, given the uncertainties in the charted depths around the Perth Canyon, wind and current-driven drift during deployment or the logger not initially being positioned accurately over the intended location. The probable depth error, including riser tilt, was ± 10 m, with the error in deeper loggers less than this. The true water depth of each deployment was obtained using a Simrad EQ60 sounder operating at 38 kHz. Moorings were deployed and recovered using local fishing vessels up to 20 m length.

Supplementary data used in interpretation included wind data from Rottnest Island's meteorological observing station (acquired through the Bureau of Meteorology) and sea surface temperature satellite images. The wind data were separated into north/south and east/west components with each component plotted. Winds from the south and west were positive, as vectors in a normal coordinate system. Satellite imagery (not shown) used to help identify the Leeuwin Current's location and behaviour was accessed through the Department of Land Information, and copyright

is vested in the State of Western Australia. The satellite imagery was used primarily as a qualitative indicator of the currents' and eddies' locations and their movement into and out of the Perth Canyon region. Cloudiness often inhibited satellite imaging.

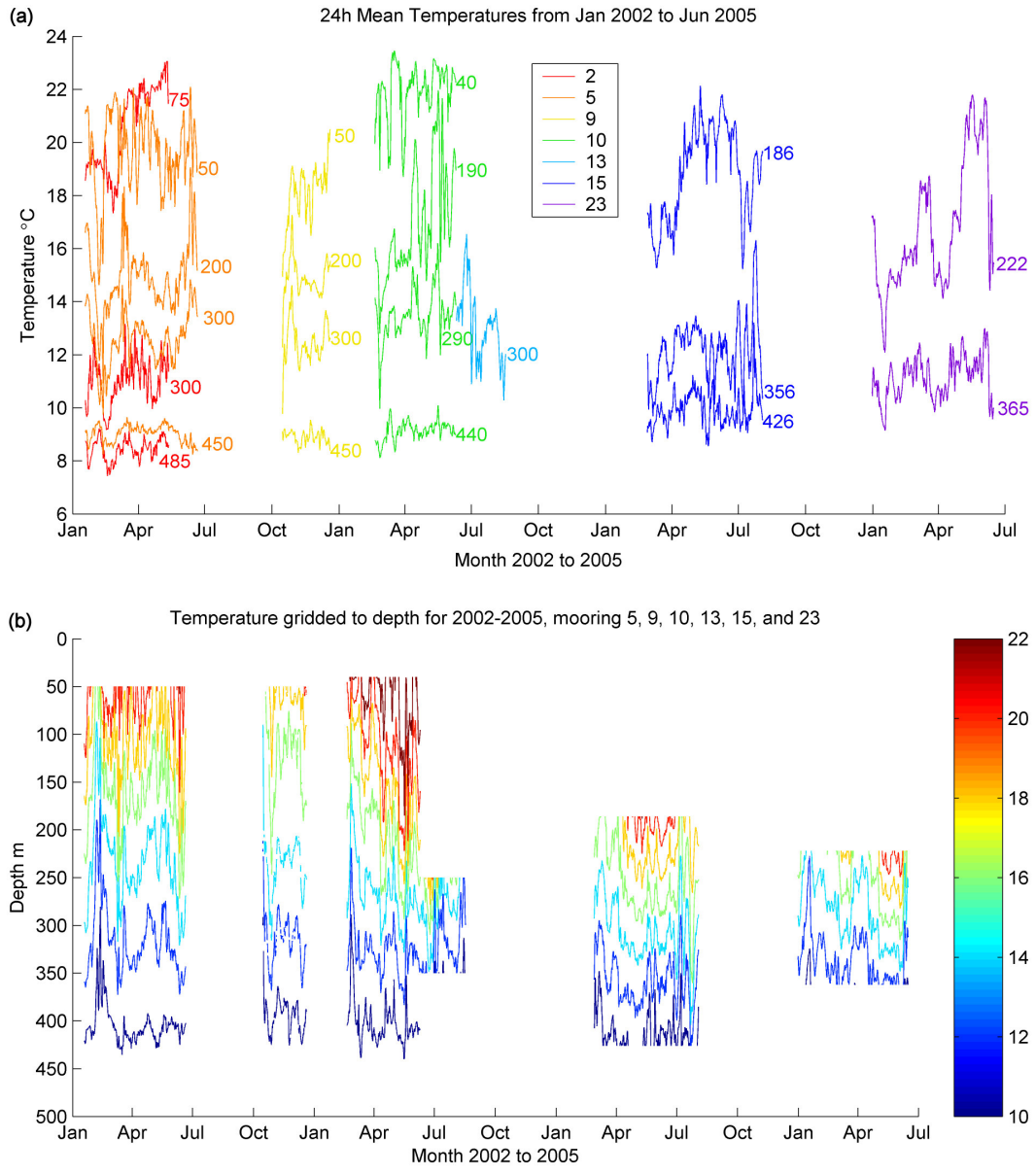

Figure 3.3. a) The complete data set at depths nearest to [50 200 300 450] m for moorings 2, 5, 9, 10, 13, 15 and 23 (which are in chronological order). Depths are labelled adjacent to the data, which have been averaged over 24 hours. b) Seasonal variations indicated by changes in temperature versus depth. All data have been averaged over 24 hours, interpolated to depth and isotherms plotted.

3.4 Results and Discussion

The temperature loggers gathered data over four years with most data collected in the first six months of each year. The abridged data are depicted in Figure 3.3a, which shows loggers at selected depth only, and the data series have been smoothed. Moorings 2 and 5 operated during the first months of 2002, indicating the effect of different locations. Mooring 2 was placed at the canyon head while the mooring 5 (and subsequent moorings) was located on a plateau on the north rim. Figure 3.3b shows the data interpolated to depth, with isotherms plotted for all moorings on the plateau. This format provides a better overview of the seasonal changes.

3.4.1 The Leeuwin Current and seasonality

The most important influence on temperature structure was the Leeuwin Current—the dominant local current at this location and depth range. The Leeuwin Current warms the surface and down to 300 m, and can be narrow and meandering. At the canyon head, the Leeuwin Current effect was quite different from at the plateau, 21 km away on the north rim. The canyon head usually experienced only the Leeuwin Current's edge (although this result is biased towards summer conditions). Temporally, the Leeuwin Current's meandering could occur over weeks and produce changes of 6 °C near the surface, as shown in Figure 3.4 (feature 1); the Leeuwin Current—or a branch of it—flowed around the canyon head (as validated by SST images) to cause the dramatic shift depicted in mooring 5 in this figure. However, the significant changes evident in Figure 3.3 at a moderate (several days to several weeks) temporal scale were also likely due to the Leeuwin Current.

Figure 3.3b shows the data also concurred with the Leeuwin Current's seasonal variation as described in the literature (e.g. Feng et al. 2003; Smith et al. 1991), i.e. stronger and deeper in winter so the temperature was warmer near the surface. Although the mid-scale variation was due to the Leeuwin Current's meandering, eddies, etc., this seasonality was a product of the wind. The start of winter, 2002, lacked the warmth evident in other years, which might have been due to El Niño conditions from early 2002 to mid 2003 weakening the Leeuwin Current.

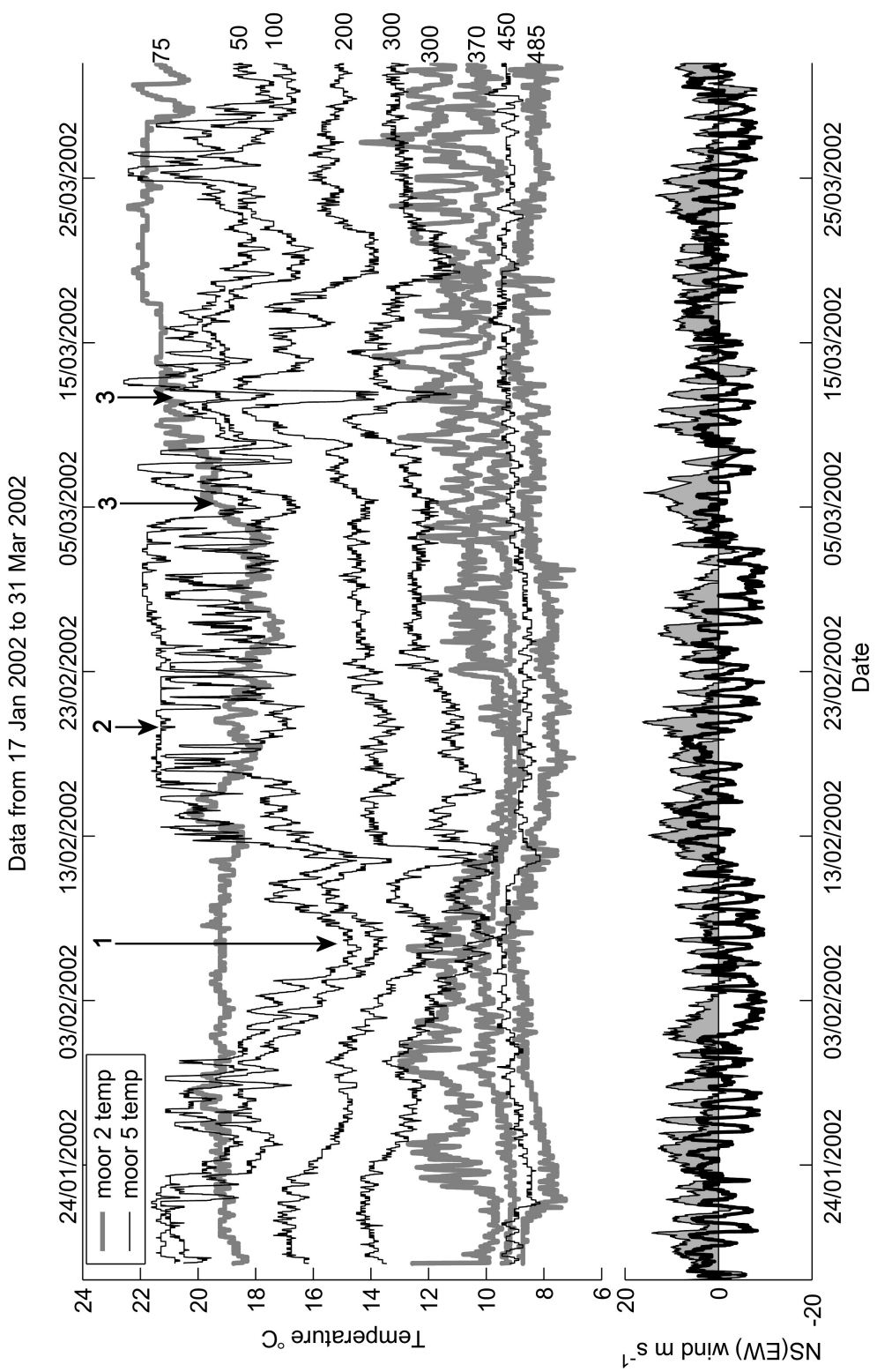

Figure 3.4. Moorings 2 and 5 from 17 January 2002 (date of deployment) to 31 March 2002 (upper axis). Wind (lower axis) is divided into N–S (shaded, southerly positive) and E–W (line, westerly positive) components. To the right of the data are numbers that indicate the approximate depth of the temperature loggers. These mooring overlap in time but are at different locations around the canyon, and show quite different signals. 1) The Leeuwin Current shifts. 2) The well-mixed layer. 3) Brief decreases in temperature.

The second wind-related seasonal variation was connected to the wind characteristics in different seasons, which manifested as different patterns of temperature change. In summer, the mixed layer was apparent as a constant temperature at the 50 m logger (Figure 3.4 feature 2), and changes in temperature were either brief (a day or less) or lasted over a week and due to the Leeuwin Current. Figure 3.4 provides an example of typical summer events. In winter, the response to the passage of weather systems manifested as variations at the surface and in the mid-water column changing in the order of days (e.g. Figure 3.6). The transition between these predominant patterns coincided with the change in the wind regime, which occurred during April–May and October–November. The pattern components are discussed below.

3.4.2 Sea breeze

The wind's influence at smaller timescales appeared throughout the data as the wind caused mixing and shifting of water. The sea breeze's effect is shown in Figures 3.4 and 3.5. The alternating sea breeze and land breeze constitute a diurnal driving force that occasionally manifested itself in the data as a periodic variation in the temperature near the surface. The sea breeze effect could extend up to 200 m, although, in some cases, it was difficult to isolate from other concurrent periodic changes (see section 3.4.4). Analysis of two incidents of wind and temperature showed there was a strong coherence with wind, but the phase varied from 0 to ± 180 degrees for the east/west or north/south component of the Rottnest Island wind data. Figure 3.5 shows an example 'out of phase' where south-westerly wind was associated with cooler temperatures and north-easterly wind was associated with warmer temperatures. The dotted vertical lines in Figure 3.5 indicate the correspondence of wind and temperature, and hence the phase relationship. This phase relationship was consistent in all clear sea breeze oscillations during November 2002.

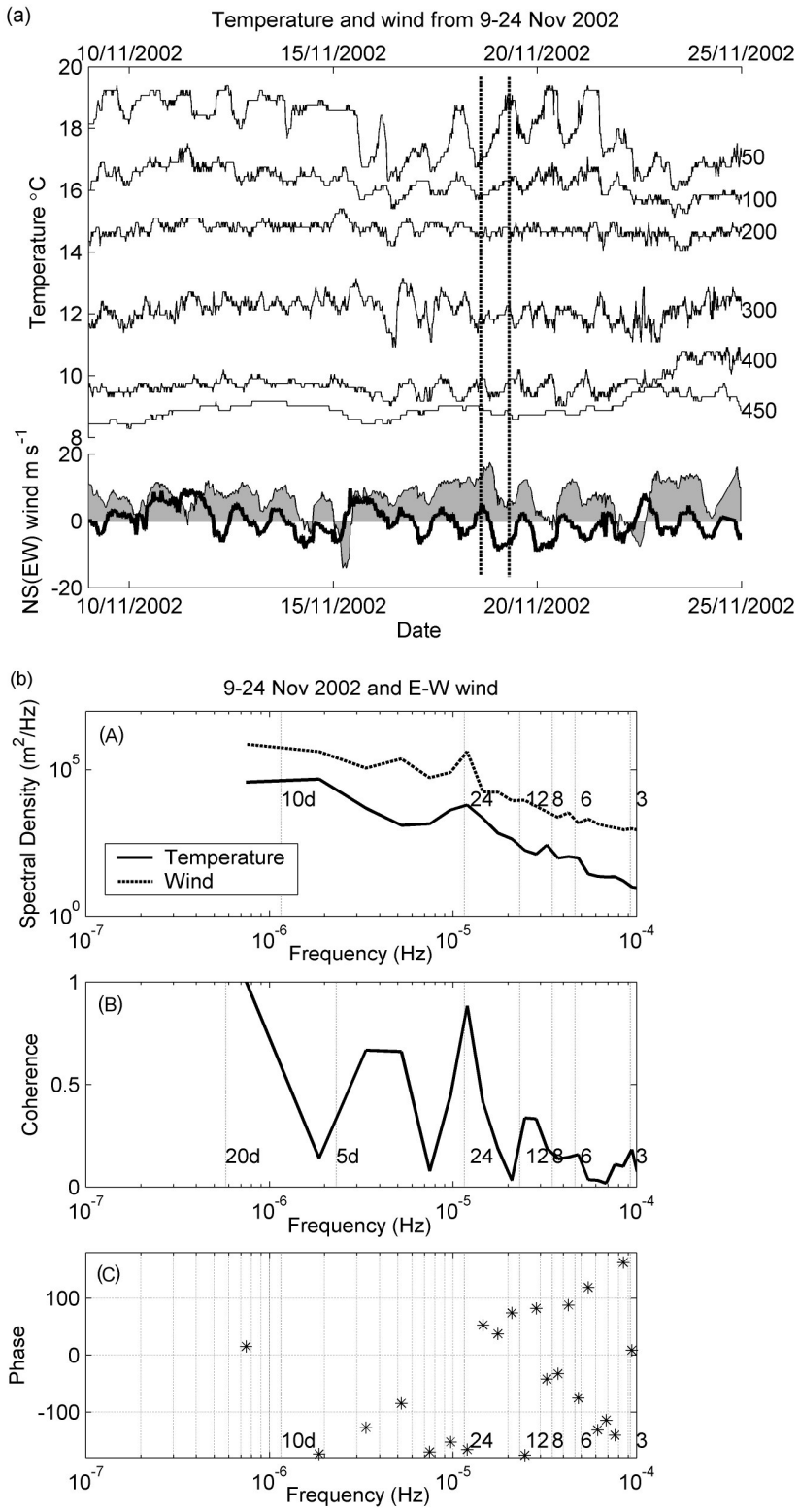

Figure 3.5. a) Upper axis: Mooring 9, 9–24 November 2002. Vertical lines indicate correspondence of wind and temperature during sea breeze and land breeze forcing. Lower axis: the N–S (shaded line) and E–W (heavy line) wind speed components. Southerly and westerly winds are positive. The temperature shows diurnal variations at the surface correlated with wind, but non-diurnal variations at 400 m. b) Spectral analysis of November 2002 50 m temperature with E-W wind component, showing strong 24 hour signal in A) spectral density, B) coherence, and C) 180° out of phase.

3.4.3 Storms

The second conspicuous wind event type was storms, which occurred several times in data collected during winter. These consisted of strong winds that cycled around anticlockwise over several days, and repeated this cycle for a series of storm fronts. Dramatic temperature changes were produced in a short period during storms. The greatest temperature change recorded during a storm was 8 °C at 250 m over three days during June/July 2003; however no loggers above this depth were recovered. An excellent example of a storm, which occurred in May 2003, is shown in Figures 3.6 (temperature data with wind broken into N-S and E-W components) and 3.7 (isotherms, wind speed and direction). Figure 3.7 indicates that during the storm, on May 19, the vertical shift of isotherms was 100 m in a day, denoting vertical displacement of water of this magnitude if no horizontal advection is assumed. This cooling was fairly simultaneous throughout the water column, as was the subsequent

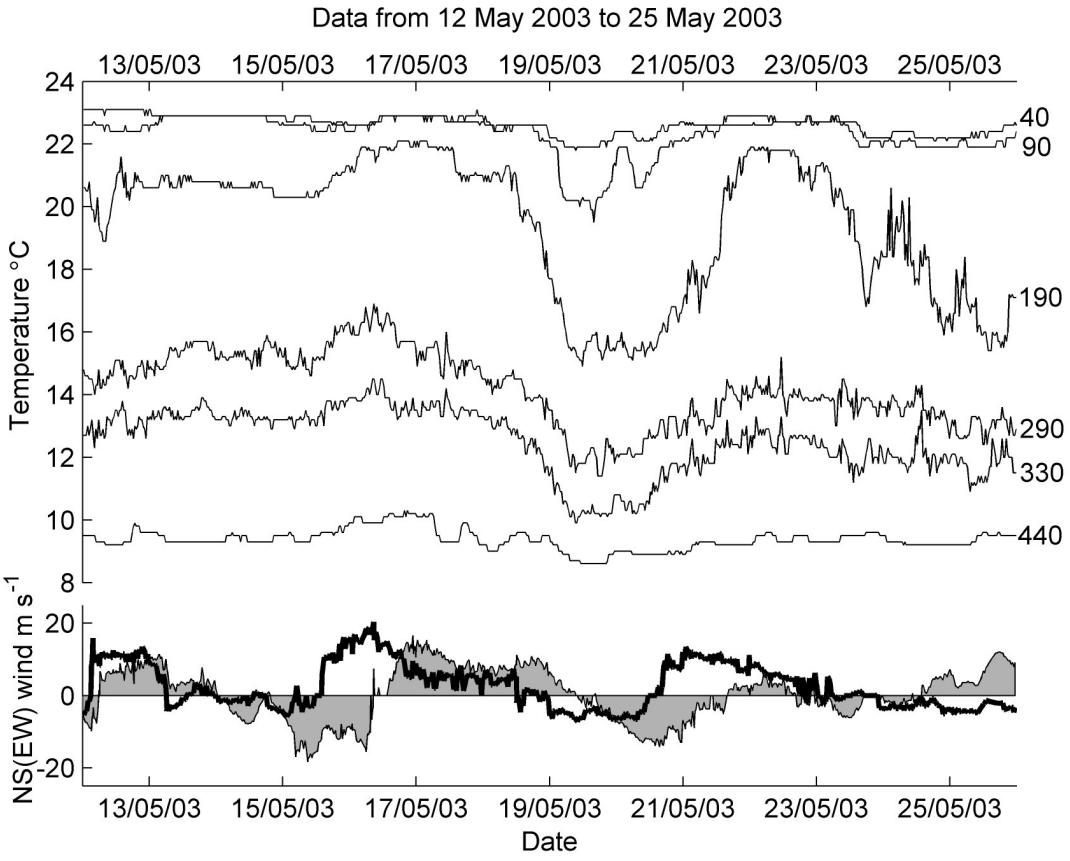

Figure 3.6. Temperature loggers for mooring 10, 12-25 May 2003, for the upper axis. The lower axis shows the North-South (shaded line) and East-West (heavy line) wind speed components. Southerly and westerly winds have positive values.

warming. At 190 m the temperature increased and decreased over a few days, as if oscillating while regaining equilibrium; a similar oscillation occurred after the June/July 2003 storm. These oscillations did not correspond directly to changes in wind stress or atmospheric pressure the way the temperature changes responded to the initial storm front.

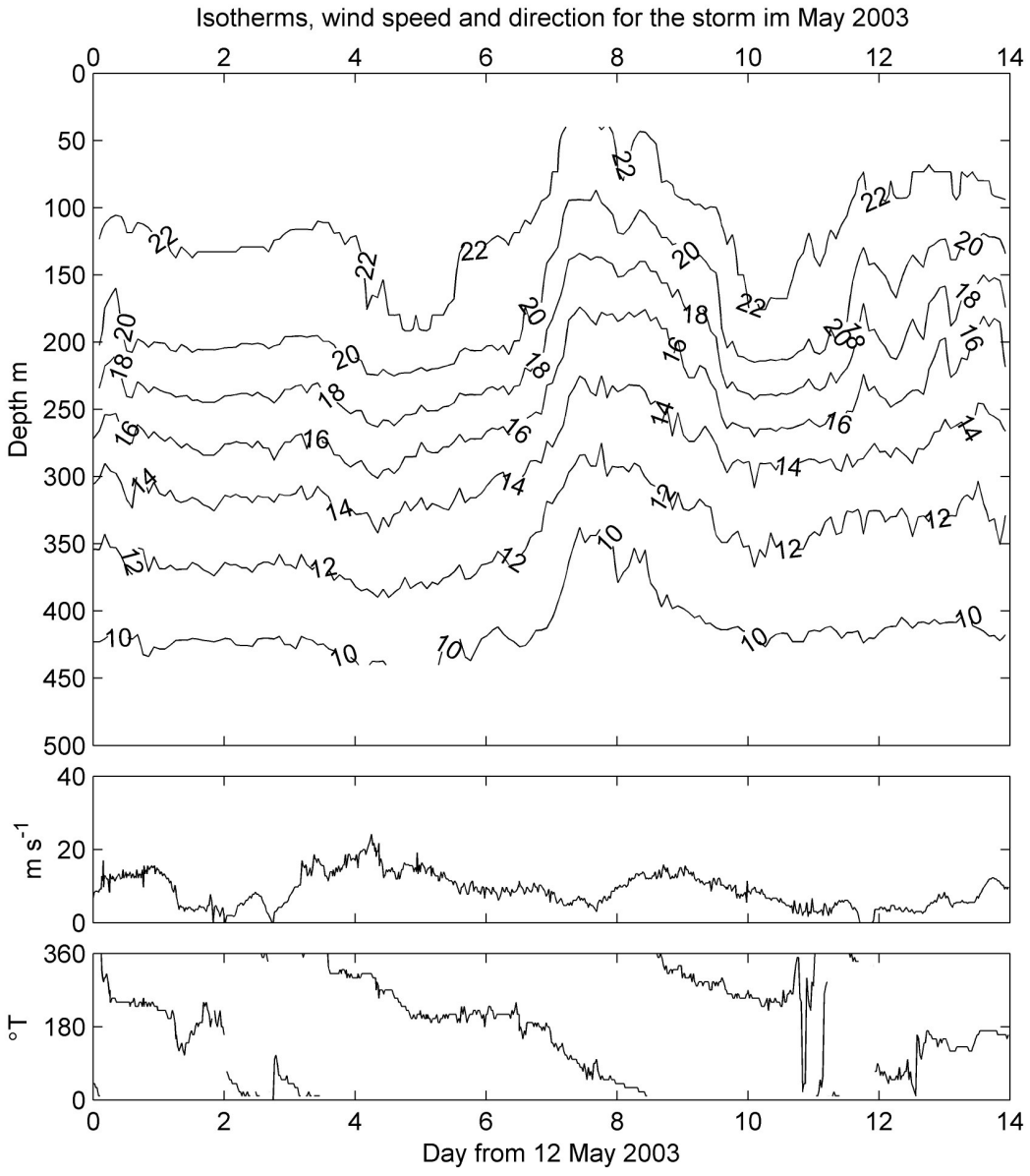

Figure 3.7. Stratification changes during the May 2003 storms, showing non-directional wind speed and wind direction on the lower axes. Temperature has been gridded to depth and 2 hour intervals and isotherms are plotted.

The effect of the wind is summarised. The strongest winds caused mixing and reduced stratification to ~200 m, which the 190 m logger registered as warming. Upwelling, cooling, and re-stratification occurred as the winds slackened. Strong vertical transport after wind relaxation has been reported in model (Ardhuin, Pinot & Tintore 1999) and field (Hickey 1997) studies. However, upwelling or downwelling could also be wind-forced, as a result of surface waters shifting laterally (Ekman transport), with a variable depth extent depending on the depth of the wind-driven layer. The strong southerly winds might be expected to induce offshore transport for much of the shelf water, which could be replaced by water upwelled from within the canyon to over the rims. The approximate relationship between wind direction and temperature was determined. The initial warming/mixing was associated with northerly–westerly winds, which turned southwest and caused cooling (upwelling, restratification). At the end of the cooling period, the wind was often weak and rotated through northeast. As the wind returned northwest to southwest and strengthened, the water warmed.

3.4.4 Other near-diurnal changes

The wind's short-term influences were primarily storms and sea breezes, but the sea breeze was not the only source of periodic changes. Periodic or pulse-like changes ranging from 0.5 to 1.1 days with a mean of 0.88 days (st. dev. = 0.15 days) were present throughout the data with a variety of origins, for example internal waves or inertial oscillations. The strongest periodicities were near one day, and these changes, particularly at the surface, were recognised as being from the sea breeze oscillation and possibly tides or solar warming, although sea breeze was the only confirmed cause. Solar warming would be very weak at 50 m, and the tidal signature at this location was very small because of its proximity to an amphidrome. Periodicities near the inertial period of 0.94 days could occur at all depths, including while a sea breeze pattern was apparent at the surface; for example, Figure 3.5a shows the 400 m oscillations had a shorter period (~0.9 days) than the 50 m oscillations.

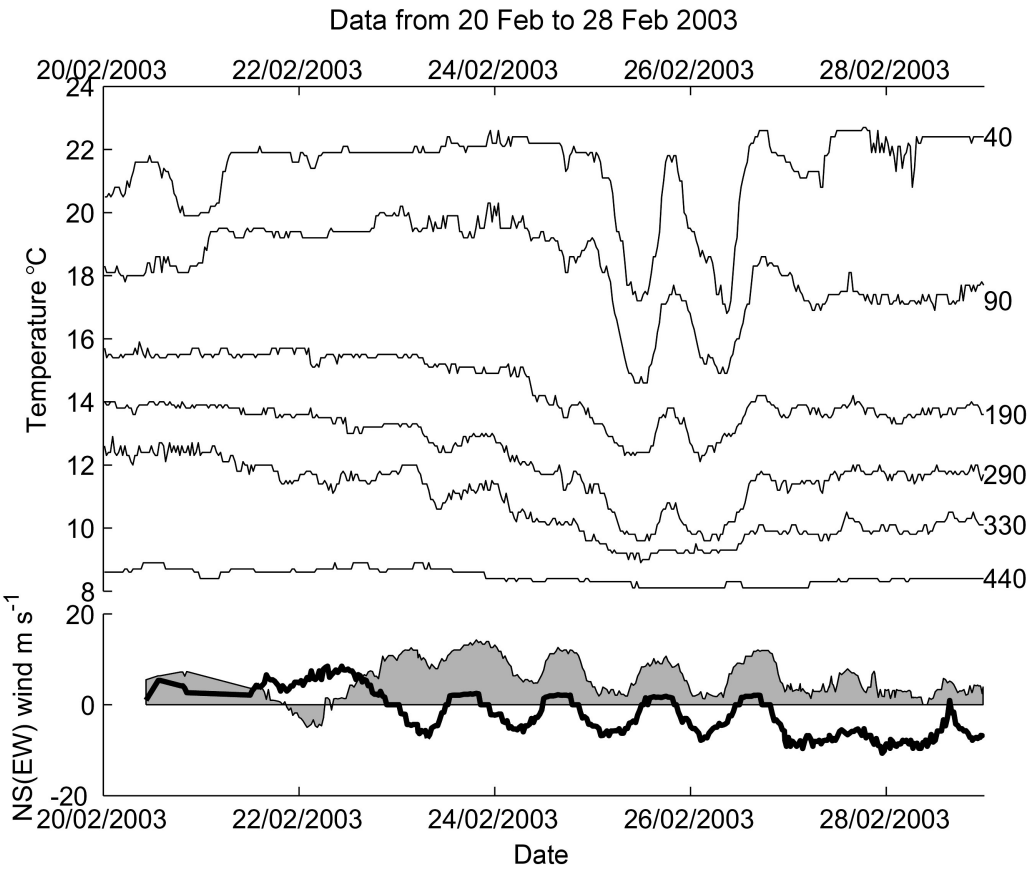

Figure 3.8. Temperature for mooring 10, 20-28 February 2003. Logger depths are indicated by numbers to the right of the data. Wind is divided into N-S (shaded, southerly positive) and E-W (line, westerly positive) components. The interesting feature is two consecutive momentary decreases in temperature which extend right through the water column.

On several occasions, the temperature dropped several degrees and rose again in one day, occurring as a single pulse. These changes could appear throughout the water column. Figure 3.4 (features 3) indicates other examples, and Figure 3.8 depicts this event occurring on two consecutive days. Of five such changes examined, the period ranged from 0.6 day to 1 day and the change was usually visible to 400 m. The isotherm showed typically ≤50 m displacement near the surface, a maximum displacement of 50 to 200 m between 100 and 200 m depth, and decreasing displacement towards the bottom logger. These changes might be attributed to a solitary wave passing through, although there is no possible corroboration with e.g. current measurements. The period is around 20 times larger than the Brunt-Väisälä period of ~0.5 hours and did not usually match the tidal period. Other internal

gravitational-gyroscopic waves (Pond & Pickard 1983) are more likely to have a period in the range seen here.

3.4.5 Upwelling

The question arose of whether water can be transported from within the canyon onto the shelf. If the canyon channels deeper water nearer to shore, it would be important as a mechanism to supply nutrients to the area. The surface current is downwelling-favourable, and although the undercurrent favours upwelling, it is weaker. However, the canyon might encourage sporadic but stronger upwelling to occur, supplying nutrients to the shelf. The temperature loggers were a poor measure of upwelling over the canyon rims because the temperature between 400 and 500 m was markedly uniform (based on CTD casts by the authors, as well as the data from the temperature loggers). A 0.3 °C change, for example, could mean an isotherm shift of over 60 m, and the temperature logger precision was only 0.2 °C. To estimate the magnitude and frequency of upwelling or downwelling occurrences at the canyon rims, the deviations greater than one standard deviation from the mean were examined for all loggers moored below 400 m.

The temperature series were long enough to provide a good seasonal average temperature. Two standard deviations equalled one third of the temperature range of the loggers moored at 440–450 m on the plateau, and approximately one quarter of the range of the logger moored at 426 m on the plateau (mooring 15) and mooring 2 at the canyon head. The latter two had a larger range probably due to location and depth. The consistency of this statistic for the three loggers moored at approximately the same depth yet different times suggested this was a reasonable way to make comparisons.

An upwelling event was defined as when the temperature was below the mean minus one standard deviation, and a downwelling event was defined as when the temperature was above the mean plus one standard deviation. In Table 3.2, the number of upwelling and downwelling days is the number of measurements defined as upwelling or downwelling times the sample period and converted to days, i.e. the total time spent beyond the threshold. The proportion of upwelling or downwelling

days are given as a percentage of the total sampling time. The number of major events indicates the number of times the 24-hour mean temperature was beyond the threshold for more than a day. These events could last over a week.

Table 3.2 shows that upwelling predominated in early 2002 (moorings 2 and 5), but in other years, incidences were approximately equal for the time sampled. In 2003 (mooring 10), the upwelling events occurred largely within the first month (February–March); otherwise, events occurred roughly every month. Moorings 2 and 5 showed concurrent incidences, indicating these two locations recorded similar features at the canyon rim.

Table 3.2. Statistical analysis of the bottom temperature loggers from moorings 2, 5, 9, 10 and 15 to estimate upwelling and downwelling occurrences.

Mooring	2	5	9	10	15
Depth m	485	450	450	440	426
Mean °C	8.43	9.02	8.88	9.11	9.9
St. Dev.	0.45	0.34	0.27	0.39	0.70
Range	3.39	2.06	1.62	2.3	5.47
2*S.D./Range	0.27	0.33	0.33	0.34	0.26
Upwelling days	18	28	13	21	23
Downwelling days	13	20	14	23	25
Period	17/1/02–13/5/02	17/1/02–21/6/02	14/10/02–20/12/02	18/2/03–10/6/03	26/2/04–3/8/04
No. days	115	155	67	112	159
% time upwelling	16	18	20	18	14
% time downwelling	12	13	21	19	15
No. major events up/down	5/6	6/4	5/4	2/4	5/6

The effects of upwelling or downwelling were complicated by the changing vertical thermal structure. The causes of upwelling or downwelling were diverse. In many cases, the change occurred throughout the water column; some such examples mentioned above were storms or internal waves. This analysis highlighted the deep water response to such changes. In other cases, the deep water change opposed the surface change. Storms produced strong downwelling and upwelling, but weaker wind events had a response similar in magnitude to the influence of circulation, i.e. the Leeuwin Current's location.

3.4.6 Spatial sensitivity

The temperature behaviour at the canyon head (mooring 2) and rim (mooring 5) could be compared for January to April 2002. At a timescale of days, the data near the surface showed very different patterns at the head and on the plateau. The plateau was far more sensitive to the Leeuwin Current moving whereas the head tended to be in the coastal margin of the Leeuwin Current at most times. (The bias toward summer measurements may have affected this result.) As remarked above, however, the bottom loggers revealed similar long-term trends in warming and cooling in both locations. A mid-depth comparison was not possible, as mooring 2 had no loggers at that depth. It was estimated, however, that the two locations might be similar up to 200 m below the surface for large-scale changes.

At a shorter time scale, the moorings were quite different. Mooring 2's shallowest logger recorded a more stable near-surface temperature (Figure 3.4), which was apparently always within the well-mixed layer at 70 m—unlike mooring 5 at 50 m. Near the bottom, mooring 2 showed much greater rapid variations, which might be associated with turbulence at the canyon head. Carter and Gregg (2002) commented that turbulent mixing could be enhanced towards the head of a canyon.

From only two concurrent moorings, it may be concluded that a distance of 21 km, or the difference from the head to the plateau, is sufficient to measure different thermal variations, particularly at the small temporal scale or near the surface. At the canyon rim depth near 500 m, changes appear which encompass this region containing both moorings.

3.5 Conclusions and Recommendations

The data collected from seven moorings deployed over four years indicated a high degree of complexity in the water temperature around the Perth Canyon. Few recorded features were repeated often; the data from each mooring appeared quite different from other moorings. Of the various features recognised as recurrent, some were attributed to the expected factors of weather or current changes. The main points of the above analysis can be summarised as:

- The influence of the mixed layer and thermocline boundary appeared in much of the data from the temperature loggers at 100 m and above. The wind strength affected the mixed layer depth. Location (of the mooring relative to water masses) also appeared important to the mixed layer depth.
- The temperature in the top 200–300 m depended on the Leeuwin Current. Periods of extensive cooling and warming occurred as the Leeuwin Current shifted location to cover the canyon, divert around it, or draw cooler water into the region. Extreme changes were rare, as the current was usually in the vicinity of the canyon. Factors other than the Leeuwin Current produced changes of the same magnitude but at different time scales.
- The greatest changes in temperature were observed when loggers were in the thermocline, where a logger could theoretically record a change of 6–8 °C in a day. (Thermocline gradients are 0.1–0.2 °C m^{-1}, vertical velocity 10^{-3}–10^{-4} m s^{-1}; so, water could rise 80 m in a day.) The greatest recorded change over 24 hours was 5 °C.
- Rapid changes in temperature, e.g. dropping ~4 °C in a day, occurred often throughout the data. In winter, such rapid changes occurred in the middle depths; in summer, they occurred near the surface. Different mechanisms appeared to be involved for each. In winter, storms were the main instigator. In summer, wind events did not appear to be the cause; internal waves were considered a likely cause, thought there was no corroborating evidence to provide proof.
- Periodic variations of about one day were probably not tidal, but might have been inertial period or sea breeze related. The correlation with sea breeze

was apparent for some surface loggers. Deeper loggers showed periodicity that was shorter than the sea breeze time scale.

- Occasional brief intrusions of cool water occurred. These could extend throughout the water column and usually lasted a day. The cause was not identified as a wind or weather event, but was suspected to be internal wave packets.
- The stablest temperature was observed by the loggers at the bottom or in the well-mixed layer. Bottom loggers showed only small, slow changes in temperature, but often conformed in these trends with the shallower loggers, sometimes several hundred metres above the bottom. These small changes might represent a large shift in the isotherms, but such a distance is difficult to estimate.
- Upwelling and downwelling at the canyon rims at ~450 m depth, i.e. where water might pass into or out of the canyon, occurred on average once a month, with 14–20% of days considered upwelling-affected and 12–21% of days considered downwelling-affected.
- Mooring location impacted significantly the variations that were observed; the plateau and the canyon head showed similar changes only near the rim.

The canyon region is vastly complex, and while the data presented here revealed much that occurs, further analysis would benefit from comparable data away from the canyon and data collected during the second half of the year (winter and spring). This would particularly aid in analysing seasonal events, such as the appearance of blue whales.

CHAPTER 4

Dynamics of the Surface and Sub-Surface Currents Off South-Western Australia: A Numerical Study

4.1 Summary

The surface and subsurface circulation off south-west Australia was simulated using the Regional Ocean Modelling System (ROMS), a primitive equation ocean model with terrain-following *s*-coordinates. The major currents in this region—the Leeuwin Current and Leeuwin Undercurrent—were reproduced by specifying only temperature and salinity distributions from climatology. The application of wind stress subsequent to the model reaching a quasi-steady state, resulted in the generation of the seasonal Capes Current, a northward flowing current on the continental shelf associated with coastal upwelling. The simulated currents compared well with the observed current patterns including the location and maximum current speeds. Shelf topography variations and bottom shear instability, which generated vorticity, influenced eddy formation. Eddies separated from the Leeuwin Current and the Leeuwin Undercurrent, migrated westward, and left the model domain through merging, dissipating or passing across an open boundary. In this simulation, the Undercurrent produced mostly cyclonic eddies due to strong negative vorticity where the current flowed against the continental slope. The Leeuwin Current produced anticyclonic warm-core eddies initiated from the formation of meanders which were strongest at the surface. The eddy field was dominated by anticyclonic eddies at the surface and cyclonic eddies at 500 m. The interaction between the Leeuwin Current and Leeuwin Undercurrent led to the formation of eddy pairs.

4.2 Introduction

The Leeuwin Current, off the coast of Western Australia, is recognised as one of the few examples of a poleward eastern boundary current which maintains its flow

throughout the year although there are seasonal and inter-annual variability. In recent years there has been several studies examining the dynamics of the Leeuwin Current and associated currents (e.g. Cresswell 1991, 1996; Feng et al. 2003; Hughes, Weaver & Godfrey 1992; Pearce 1991; Ridgway & Condie 2004; Smith et al. 1991; Woo 2005). The Leeuwin Current system consists of three major currents: the Leeuwin Current (LC), the Leeuwin Undercurrent (LU) and the shelf current systems consisting of the Capes and Ningaloo Currents. Examples of other eastern boundary poleward currents, which are all part of a surface current/undercurrent system, include the Iberian Poleward Current (Peliz et al. 2003; Peliz et al. 2002) and the California Undercurrent, also known as the Davidson Current (Barth, Pierce & Smith 2000). These poleward currents are baroclinic, but wind forcing can modify the surface currents. The interaction of these current systems with topography has been lately explored (Barth, Pierce & Smith 2000; Hughes, Ofosu & Hickey 1990; Peliz et al. 2003). However, there has been little work done on the Leeuwin Undercurrent and its interaction with the Leeuwin Current and the shelf topography.

The Leeuwin Current traverses the Western Australian coastline from the North West Cape at ~21°S, heading southwards to Cape Leeuwin then turning and following the shelf into the Great Australian Bight (see Figure 2.3). The Leeuwin Current is a narrow (~100 km), relatively shallow (<300 m) current which transports warmer water of tropical origin southwards along the shelf break. The salinity is initially lower than ambient in the north, but increases as the Leeuwin Current water ages and entrains water from the eastern Indian Ocean (Cresswell 1991; Woo 2005). The Leeuwin Current is driven by an alongshore geopotential gradient that overwhelms the (prevailing) wind stress (Godfrey & Ridgway 1985; Thompson 1984) and is in geostrophic balance. The onshore flow resulting from a meridional pressure gradient induces downwelling and the poleward geostrophic current which is located over the 200 m depth contour (Ridgway & Condie 2004).

The Leeuwin Undercurrent, which has not been studied in much detail, has been identified in field data as a sub-surface equatorward current beneath the Leeuwin

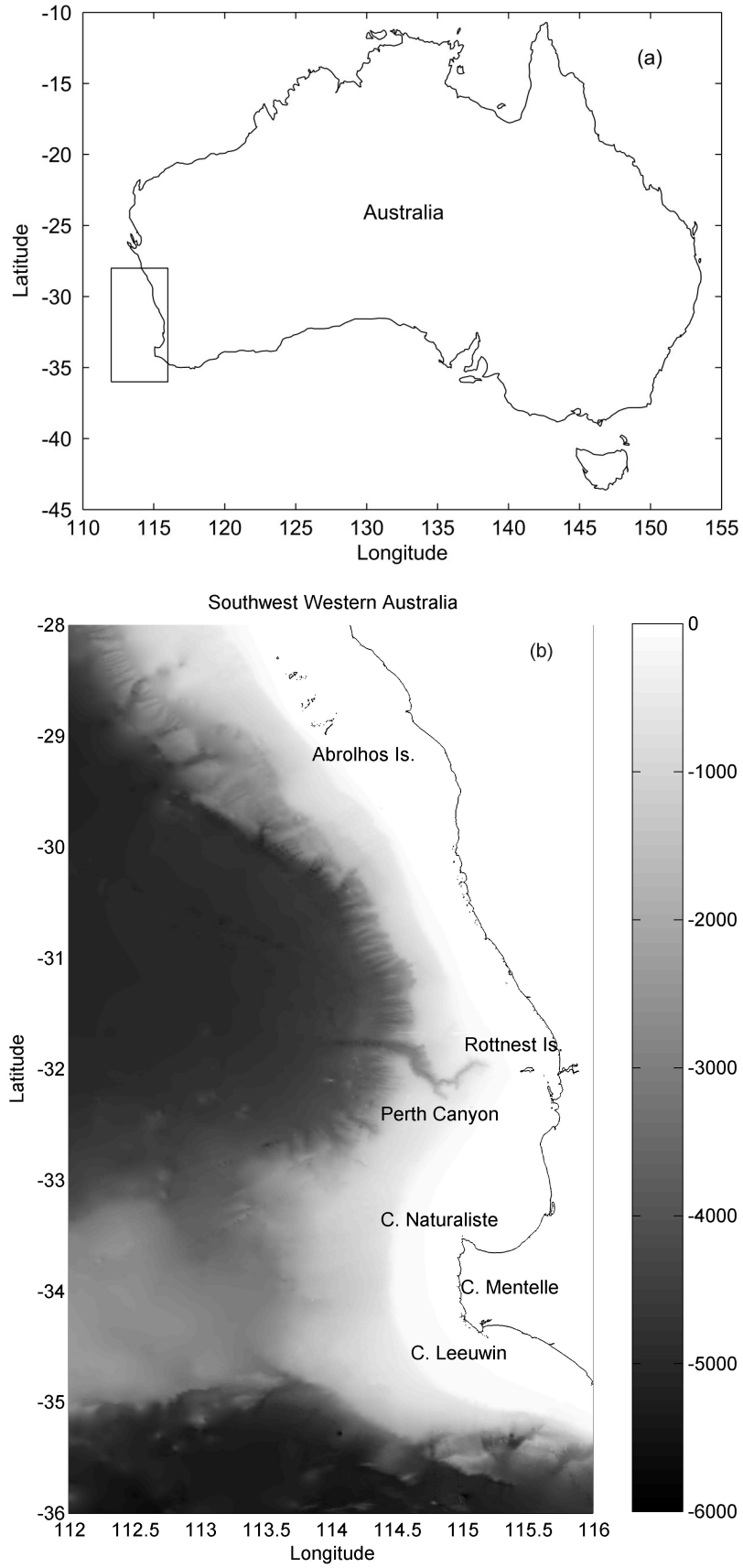

Figure 4.1. a) Australia indicating location of b) a section of Western Australia showing coastline and bathymetry including the Perth Canyon and other land features. Depth is shown in m.

Current (Thompson 1984) driven by a deeper steric height gradient (Godfrey & Ridgway 1985). The Undercurrent transports Sub-Antarctic Mode Water (SAMW), which is formed south of Australia and consists of water with a high dissolved oxygen concentration (Woo 2005).

The seasonal Capes Current, which flows equatorward on the shelf during summer, has similarly been the subject of limited study. The Capes Current is defined as a cooler water mass (due to coastal upwelling) sourced between Capes Naturaliste and Leeuwin (Figure 4.1b) or as far south as Pt. D'Entrecasteaux, that flows north along the shelf, inshore of the Leeuwin Current (Gersbach et al. 1999; Hanson, Pattiaratchi & Waite 2005; Pearce & Pattiaratchi 1999; Woo 2005). Here, the wind stress overcomes the alongshore pressure gradient resulting in the surface layers moving offshore, colder water upwelling onto the continental shelf and flowing northwards.

The wind regime along much of the WA coast is bi-modal with distinct summer and winter regimes. In summer, the predominantly southerly wind directly opposes the Leeuwin Current and drives the Capes Current. The southerly wind stress is enhanced by the daily sea breeze system which develops strong southerly winds in the afternoon (Pattiaratchi et al. 1997). This sea breeze has been observed 100 km offshore of Perth during recent field cruises. During winter the wind changes with the passage of weather systems; the direction is variable and the wind is weaker except for strong periods associated with storms.

The Perth Canyon is situated at 32°S, offshore from Perth and Rottnest Island (Figure 4.1b). The shelf depth at the head of the canyon increases rapidly from 200 m to 1000 m and the canyon floor deepens to open onto the abyssal plane at 4000 m. Around 100 km long, the canyon has a bend at its mid-point, with two short tributary canyons along the south rim. Near the head the canyon bends slightly with another gully to the north. The sides of the canyon are steep, especially near the bottom; slopes of 30-50% are common. The canyon rims are mostly below the Leeuwin Current's depth.

Eddy formation in the Leeuwin Current is particularly energetic, especially in winter when the Leeuwin Current is stronger (Fang & Morrow 2003; Feng et al. 2005).

Fang and Morrow (2003) using satellite altimeter data identified three main regions along the West Australian continental shelf where eddies are generated and one such region was situated at ~32°S which is over the Perth Canyon. The formation of multiple meanders in the Leeuwin Current interleaved by cyclonic circulation of cooler water may be followed through satellite imagery (Pearce & Griffiths 1991). Anticyclonic eddies were pinched off the main current and their formation was often accompanied by cool core eddies, to comprise an eddy pair (Pearce & Griffiths 1991).

Several model studies of the Leeuwin Current have been undertaken over the last few decades (e.g. Batteen & Rutherford 1990; Griffin, Wilkin, Chubb et al. 2001; Hughes, Weaver & Godfrey 1992; Weaver & Middleton 1989). These focus on the entire eastern boundary of the Indian Ocean and used temperature and salinity gradients and/or water inflow to produce a southward current along the eastern boundary, thus assessing the mechanisms by which the Leeuwin Current arises. For example, Hughes, Weaver and Godfrey (1992) attributed the Leeuwin Current to thermohaline forcing from the warmer east Pacific water passing through the Indonesian flow-through, rather than merely the existence of a flow-through providing an additional source of water to the Indian Ocean. Some models (e.g. Weaver & Middleton 1989) recognised a weaker undercurrent flowing northward underneath the Leeuwin Current.

The Iberian Poleward Current (IPC), which has been modelled with ROMS (Peliz, Dubert & Haidvogel 2003; Peliz et al. 2003), is particularly similar to the Leeuwin Current. The IPC is also driven northwards by an alongshore density gradient (Peliz et al. 2002). The model of the IPC produced an undercurrent at ~500 m, which interacted with the surface current and formed cyclonic and anticyclonic eddies. The Iberian Undercurrent was discontinuous and appeared to be less well-established compared with the Leeuwin Undercurrent (Peliz et al. 2003). There were several canyons and a promontory that acted as eddy formation sites on the Iberian coastline model. The WA coastline also has several sharp curves and the Perth Canyon is a particularly strong bathymetric feature that has been neglected in other models.

This paper discusses the application of ROMS to West Australia's southwest coast to investigate the surface and subsurface currents, and ultimately their interaction with the Perth Canyon. The paper is structured as follows: Section 4.3 details the model set-up, including modifications to the bathymetry from the raw bathymetry data, the initial conditions and parameters of the model, and the wind forcing adapted from real data. Evaluation of the error from using an *s*-coordinate model is also described. Section 4.4 describes the evolution of the Leeuwin Current and Undercurrent, and the Capes Current with the application of wind stress, and demonstrates that the model is a reasonable representation of reality. Section 4.5 investigates the cyclogenesis within the Leeuwin Current and Undercurrent and the role of topography. The circulation within Perth Canyon is discussed in Chapter 5.

4.3 Set-up

This study used ROMS (Regional Ocean Modelling System) version 1.0 (Haidvogel et al. 2000). ROMS uses *s*-coordinate levels, where *n* levels are spaced between the ocean surface and bottom, with adjustable vertical spacing so that, for example, resolution can be increased at the surface and/or the bottom. Thus the levels follow the terrain. This has an advantage over vertical discretisation in that slopes are not required to be approximated in a stepwise manner.

4.3.1 Bathymetry

The bathymetry was based on Australian Bathymetry and Topography Grid data at 0.01° resolution accessed from the Geoscience Australia website (Petkovic & Buchanan 2002, see acknowledgements), and interpolated to a model grid with higher resolution near the Perth Canyon. The model domain with zonal (at 32°S) and meridional grid resolution is shown in Figure 4.2. A much larger domain than the immediate area of the Perth Canyon—the ultimate focus area of study—was required for the representation of the geopotential anomaly across the domain to drive a realistic Leeuwin Current. Initial model runs revealed that the maximum current speed depended on the length of the domain. The domain was also extended offshore to allow the offshore movement of mesoscale eddies which otherwise became trapped between the Capes (i.e. Capes Naturaliste, Mentelle and Leeuwin,

see Figure 4.1b) and the boundary (see Figures 4.1 and 4.2). The domain was also lengthened to allow bathymetry modifications near the boundaries. (This is discussed in Section 4.3.4 as it related to the choice of boundary conditions in the model.) Hence, the final bathymetry covered ~8° latitude and ~5° longitude. As the boundaries were the least realistic part of the model, a domain of this size also kept boundary effects away from the canyon.

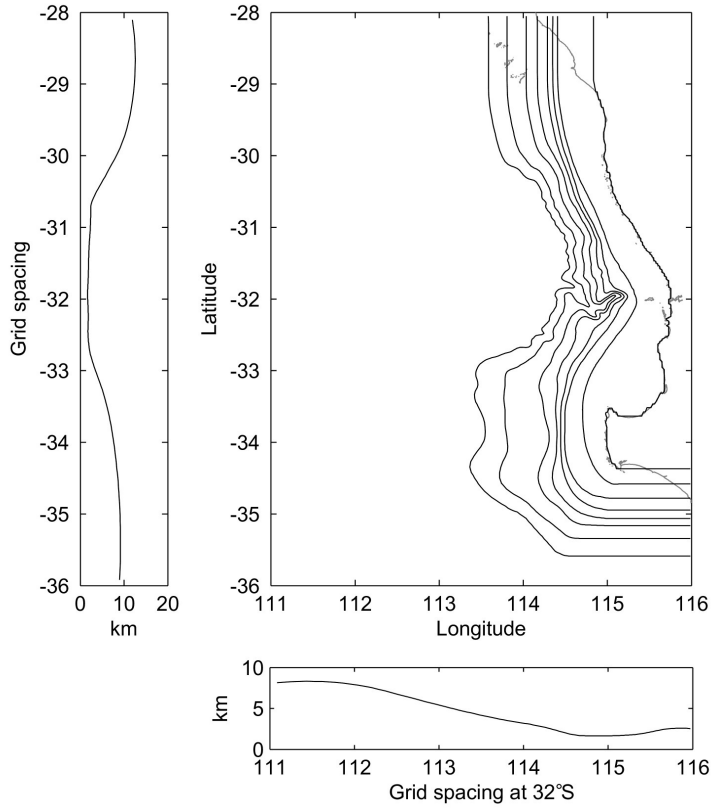

Figure 4.2. Model domain with contour lines at [100 250 500 750 1000 1500 2000] m and at the land mask boundary. The actual coastline is plotted in grey. The meridional grid spacing is indicated to the left of the domain and the latitudinal spacing at 32°S, where the canyon is bisected, is shown below the domain.

Several bathymetric parameters have been suggested to produce functional *s*-coordinate models. Robustness r was suggested as a useful parameter for model stability, where $r = \frac{\Delta h}{2h} = \frac{h_1 - h_2}{h_1 + h_2}$, h_1 and h_2 being the depth at adjacent points in the model's horizontal grid. Values of $r < 0.2$ were considered to provide robustness (Beckmann & Haidvogel 1993). The second parameter was slope steepness, where some researchers (e.g. She & Klinck 2000) have preferred limits of less than 10%.

To fit these parameters, the bathymetry was transformed, gridded, and selectively smoothed. First, the depth maximum was decreased by halving the depth below 1000 m relative to 1000 m (e.g. 2000 m became 1500 m, 3000 m became 2000 m), and the maximum depth was set to 2100 m. This accomplished three objectives; it increased vertical resolution in deep areas, reduced the slope of the very steep shelf and canyon below 1000 m, and maintained the overall shape and length of the canyon (which would not have been possible if the bathymetry was simply cut at 2100 m). These changes were not considered important as the circulation above 1000 m was of primary interest. The seamount off Cape Leeuwin (visible in Figure 4.1b) was manually removed and minimum depth was truncated to 30 m to increase vertical s-layer spacing in the shallow regions of the shelf. The resultant bathymetry was further modified as described in Section 4.3.4, to straighten and open the boundaries and facilitate the functionality of the boundary conditions.

The modified bathymetry was then adapted to the model grid, which was sparser than the raw bathymetry. The model grid spacing ranged from 12 km near the boundaries to 1.7 km at the canyon. The grid spacing is indicated in Figure 4.2. The land area was also masked, matching close to the coastline. Islands were not masked, as this caused instabilities when wind forcing was applied.

Smoothing was applied to reduce the sharpness of the truncation boundaries, and to constrain the slopes to the steepness and robustness criteria mentioned above. The smoothing regime involved weighted averaging of each point with all surrounding points, with equal weighting given to the point and the weighted average of the surrounding points. Latitudinal and longitudinal robustness parameters were calculated alternately. The smoothing was preferentially applied to those points that were outside the limit for r, and periodically applied to every point in the model domain. In this manner, the requirements of the steepness parameters were also met, with most slopes being less than 8%.

4.3.2 Initial conditions

The model was initiated with zero velocity and a flat free surface, with temperature and salinity from the World Ocean Atlas (Levitus & Boyer 1994; Levitus, Burgett &

Boyer 1994) The temperature and salinity gradients, which yield the density or geopotential pressure gradients, provided the only driving force during model initialisation. Other forcing, i.e. wind, was applied when the model had fully developed, after 150-200 days of simulation.

The salinity and temperature data were interpolated to the model grid as horizontal layers, then smoothed with the same weighted averaging scheme used for the bathymetry. The smoothed values were interpolated depthwise to the 20 *s*-coordinate levels. For the *s* levels, $\theta_s = 3$, $\theta_b = 0.1$ and $T_{cline} = 30$. The transformation between z and s coordinates is given by $z = h_s + (h - h_s)C(s)$ where

$$C(s) = (1-\theta_b)\frac{\sinh(\theta_s s)}{\sinh(\theta_s)} + \theta_b \frac{\tanh\left[\theta_s\left(s+\frac{1}{2}\right)\right] - \tanh\left(\frac{\theta_s}{2}\right)}{2\tanh\left(\frac{\theta_s}{2}\right)}$$

and $-1 \leq s \leq 0$ is the fractional depth and h_s is the depth of the s layer.

4.3.3 Model parameters

For the model, a non-linear equation of state was used. The default third order advection, Laplacian mixing scheme was used, with mixing coefficients of 10 m^2 s^{-1} for viscosity and tracer diffusion. Mixing was along geopotential surfaces. A Large-McWilliam-Doney scheme was used for vertical mixing with the coefficient for vertical mixing of tracers at 5 x 10^{-6} m^2 s^{-1} and vertical mixing of momentum at 5 x 10^{-5} m^2 s^{-1}.

4.3.4 Boundary conditions and bathymetry boundaries

Conditions for open boundary were selected to promote uninhibited inflow and outflow. Boundary values were calculated using radiation boundary conditions for the south, west and north boundaries and a 1-cell gradient boundary condition for the eastern boundary. After the model reached a quasi-steady state, the eastern boundary was switched to radiation conditions, which helped maintain stability at this boundary.

The bathymetry was also modified to improve flow at the boundaries. At the northern boundary, the shelf was straightened to run perpendicular to the boundary for one degree latitude. The south-eastern bathymetry was modified so that the shelf turned eastward below Cape Leeuwin to run perpendicular to the eastern boundary for one degree longitude. No isobaths crossed or approached the southern boundary. These modifications allowed the Leeuwin Current to flow directly in the northern open boundary and out the eastern boundary while minimising bathymetric gradients at boundaries, particularly gradients across the boundary.

4.3.5 Wind forcing

Other than the initial density gradient and boundary nudging of tracers back to original values, there was no forcing applied other than wind forcing, and there was no heat gain or loss across the air-sea interface to affect the density gradient. The wind forcing was based on wind data from the Australian Bureau of Meteorology meteorological observation station on Rottnest Island (see Figure 4.1b), collected from 2001-2002, which was assumed to be representative for the region. This assumption was moderately realistic, given Smith et al. (1991) found that wind along the Western Australian coastline was largely in phase and of similar strength. Wind vector data from images courtesy of NASA/JPL-Caltech showed little variation in wind direction across the longitudinal range of the model domain, but up to 90° difference in direction between the north and south boundaries. Often the Capes were a boundary for wind direction to change – the wind usually being more southerly to the Capes' south. The wind speed variations also coincided with direction changes.

The wind data was averaged into quarter-day intervals. The wind velocity was then converted to a wind surface stress τ by $\tau = C_D \rho_{air} u^2$, with $C_D = \left(0.63 + 0.066[\mathrm{s\,m^{-1}}] \times u\right) \times 10^{-3}$, u = wind speed, ρ_{air} = density of air (Pugh 1987). A final condition that $-0.4 < \tau < 0.4$ N m^{-2} was applied, as higher wind stress would result in model instability. Finally the wind stress was separated into vector components.

Wind was applied on day 241, when the model was considered sufficiently developed to a quasi-steady state and the subsequent 120 days of unforced run continued to produce realistic results. Two sets of wind stress data were applied to the model, starting from day 241: (1) wind stress based on wind starting from 17-Sep-2001, which was two to three weeks before the summer sea breeze winds started (referred to as 'spring'); and (2) wind stress based on wind starting from 1-Jan-2001, covering from mid-summer through autumn (referred to as 'summer'). Wind stress was applied for 140 days. After ~120 days the strong and/or persistently southerly winds generated increased mixing; this modified alongshore density gradient weakened the driving force of the Leeuwin Current. The model run then became unrealistic and was terminated.

4.3.6 Evaluation of the model error

The use of *s*-coordinate layers was considered an advantage because the steep bathymetric slopes could be more accurately represented. The drawback to terrain-following layers, however, is the additional error arising when calculating the horizontal pressure gradient. The reason for this error is that in *s*-coordinate or σ-coordinate models the horizontal layers do not follow isopycnal or geopotential surfaces, particularly over steep surfaces. The horizontal pressure gradients are calculated by correcting for the vertical hydrostatic pressure gradient along the *s*-layers, which does not contribute to driving horizontal currents (Ezer, Arango & Shchepetkin 2002; Haney 1991). A truncation error arises from this correction, due to the similar magnitude of the terms involved (Allen et al. 2003; Haney 1991). This source of error within the model leads directly to anomalous pressure gradients driving the currents. Steeper slopes enhance the error with very steep slopes resulting in model instability. Increasing the resolution reduces this problem (Ezer, Arango & Shchepetkin 2002; Haney 1991) but is not always a feasible solution. An alternative is to adjust the bathymetry so that the slopes are less steep – a tactic that was adopted in this study.

Following Beckmann and Haidvogel (1993), the model was run with no forcing, i.e. no temperature or salinity gradients at initialisation, to assess the model error. The currents that formed without explicit forcing were erroneous. For initial conditions,

temperature and salinity values representing the mean depth profile for the model domain were applied to every grid point, so that theoretically there were no horizontal gradients.

The model error rapidly built over the 20 day run, with the currents near their maximum speed after approximately 10 days. The maximum speed exceeded 0.2 m s^{-1} after 20 days. At the surface, currents followed the shelf break north and south toward the canyon, then diverted offshore at the midpoint of the domain, to produce a weak countercurrent. The strongest currents were between 100 m and 400 m depth, where the shelf was very steep and the pycnocline strong. At this depth, the southerly current flowed along the shelf north of the canyon and formed an anticyclonic eddy on the north rim of the canyon (Figure 4.3). Weak eddies also formed off Capes Naturaliste and Leeuwin. Below 500 m, strong currents—at most 0.05 m s^{-1}—also developed over regions of steep slope.

The vertical velocities in the error run were small (in the order of 10^{-5}) except near steep slopes. The error near the steep bathymetry reached 1 x 10^{-3} for single cells and 10^{-4} for adjacent cells. The location of the high vertical velocities changed during the run, although particular locations showed some bias for positive or negative *w* within the canyon.

The features visible in the error run, i.e. the strong current north of the canyon and the anticyclonic eddy that formed within the canyon, emerged at the start of the real model run, so were suspected to be erroneous. A series of three anticyclonic eddies developed in the canyon and migrated offshore. After 100 days, however, the southward shelf-slope current leading into the canyon was no longer apparent and after 150 days a northward Undercurrent developed. It was therefore assumed that despite the erroneous currents' non-negligible strength, the circulation forced by the density gradients overrode these currents as the model spun up and reached quasi-equilibrium. Therefore, the error due to the pressure gradient calculation was not considered prohibitive to using this model.

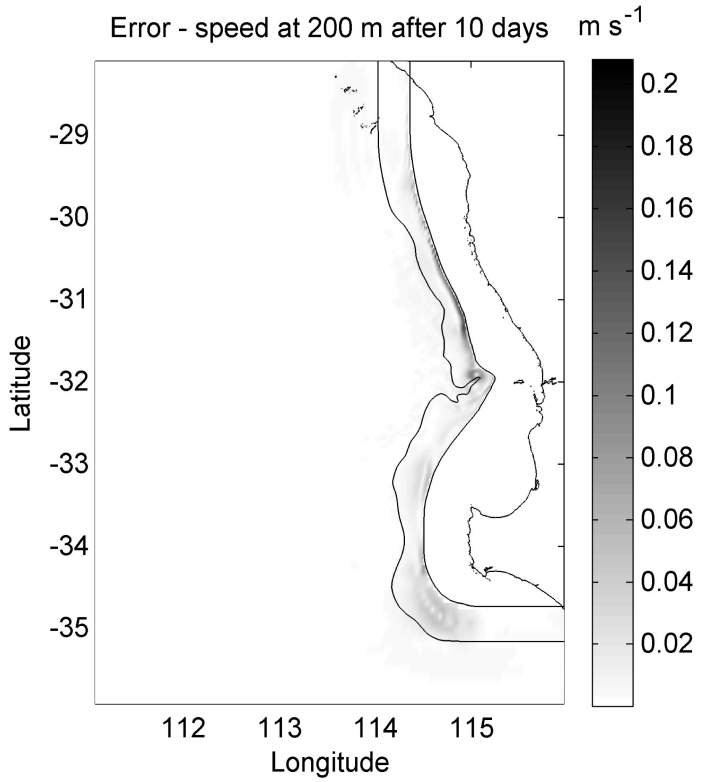

Figure 4.3. The speed of the erroneous currents formed after 10 days in the model error evaluation run. The error is concentrated over the steep shelf slopes and a small eddy has formed within the canyon. Bathymetry contours shown at 200 and 1000 m.

4.4 Model Results

In this section the major features of the simulation—the currents and eddy field—are described and verified against a variety of data. Appendix A (CD-ROM) contains Quicktime movies of the output from the three model runs.

4.4.1 Model development and the Leeuwin Current

The model initialisation run started with density gradient forcing only (i.e. no wind forcing) and was run for 360 days. The model displayed a southward surface current that flowed along the shelf break, representing the Leeuwin Current (Figure 4.4a). After 30 days, meanders appeared and eddies formed over the canyon and along the southern shelf. The meanders enlarged and a series of anticyclonic eddies formed over the canyon, migrated southwest, and merged to form a mesoscale eddy west of the Capes. Meanders in the current south of the Capes also formed an eddy, which migrated west.

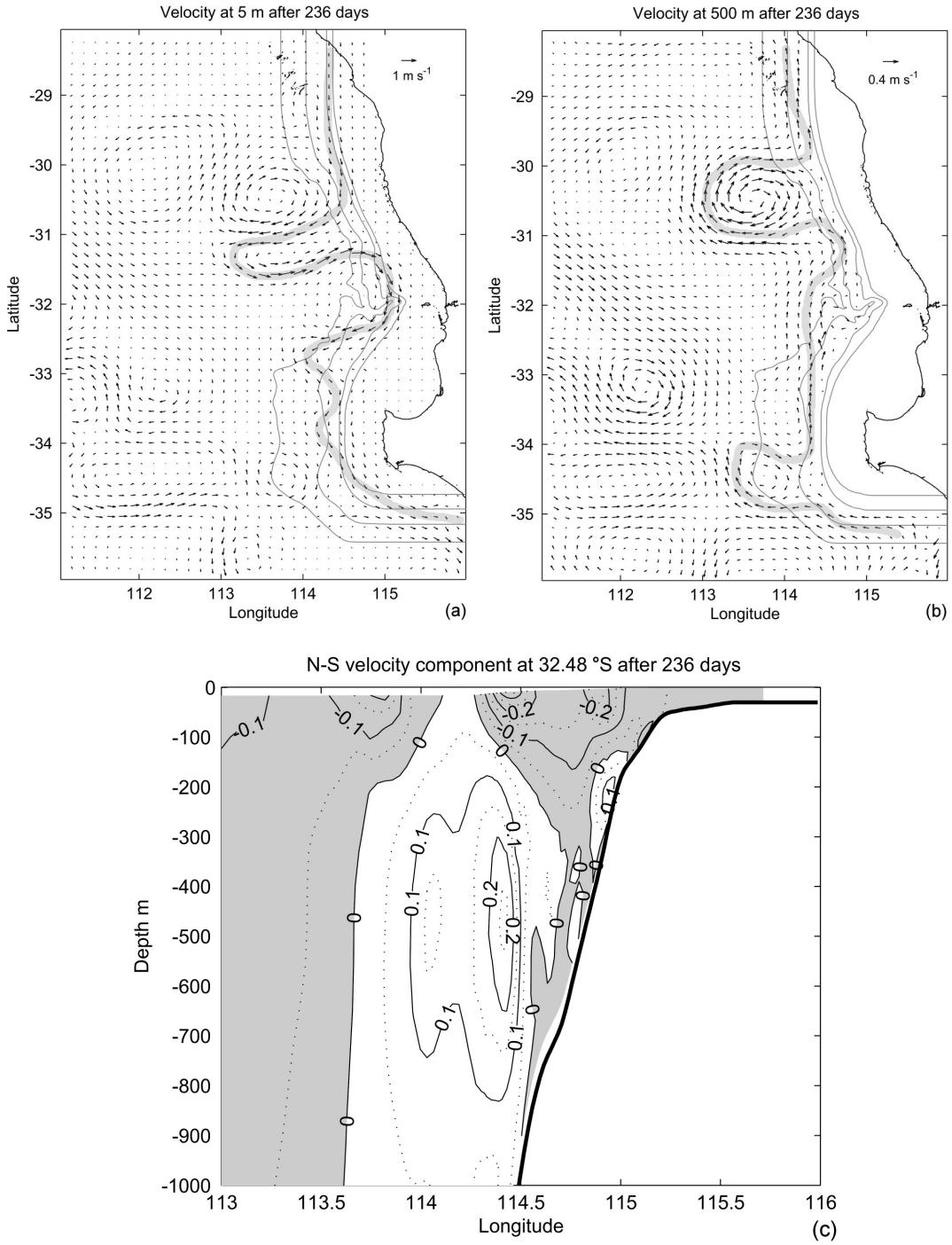

Figure 4.4. a) The velocity field of the initialisation run at the surface (5 m) after 236 days. The grey line, drawn by eye, indicates the main flow path of the Leeuwin Current. b) The velocity field of the initialisation run at the depth of the Undercurrent (500 m) after 236 days. The grey line, drawn by eye, indicates the main flow path of the Undercurrent. c) A cross section of the initialisation run along 32.48°S showing the north-south velocity component with depth. The negative velocity (e.g. the southward LC) is shaded. Labelled solid contours mark 0.1 m s^{-1} intervals and dotted contours mark the intervening 0.05 m s^{-1} values.

The simulated Leeuwin Current, like the actual current, was sourced from the northern shelf and offshore, with a stream coming from the northeast of the domain to reach the shelf north of the canyon. Between 100 and 200 days, the current reached quasi-equilibrium, where as many eddies were migrating offshore and exiting the domain, as were forming. Generally the current was <1 m s^{-1} for the southward flow and within the eddies. Localised transient high-speed currents occurred as brief jets of water during the model run. After 300 days currents speeds up to 1.6 m s^{-1} were achieved, and the maximum current speed ceased to increase.

The predicted Leeuwin Current speeds were comparable to the measured Leeuwin Current. During recent field excursions, surface currents of up to 1–1.5 m s^{-1} were estimated from vessel drift in calm seas (Section 3.3.2). A field cruise (Chapter 6) found a strong structure of eddies and meanders along the shelf slope and maximum currents of 0.8 m s^{-1}. These speeds compare exactly with the simulation. The eddy structure likewise is reproduced; this is discussed in Section 4.4.3. Current literature suggested the Leeuwin Current extends down to at most 250 m around 32°S (Feng et al. 2003). The simulated surface currents, i.e. those with maximum velocity at or near the surface, rapidly diminished in speed by 200 m depth (Figure 4.4c). The model thus reproduced realistic Leeuwin current speeds and depth extent.

4.4.2 The Leeuwin Undercurrent

At 300 m and below, the Leeuwin Undercurrent was visible as a northerly flow that remained adjacent to the continental slope. After development, it flowed disjointedly northward forming cyclonic eddies, which detached and migrated offshore. Figure 4.4b indicates the path of the bulk of water in the Undercurrent. The Undercurrent's speed at its core depth of 400–600 m (Figure 4.4c) was around 0.3 m s^{-1} and reached a maximum of 0.5 m s^{-1}. Smith et al. (1991) noted an equatorward current below the Leeuwin Current with a maximum speed at 450 m and Thompson (1984) measured a northward subsurface current speed of up to 0.4 m s^{-1} at 300 m. Woo et al. (2005) recorded the presence and distribution of the water mass marked by an oxygen maximum at 400–510 m along the WA coast (21–35°S), which is the domain of the Undercurrent. Field ADCP and Lowered ADCP data confirmed that there often existed a subsurface velocity maximum at 400-600 m in a direction contrary to

shallower flow, and a region of shear, or zero velocity, which occurred at 250–350 m or just beneath the Leeuwin Current (Section 6.5.3). The Leeuwin Undercurrent, similar to the Leeuwin Current, is driven by an alongshore geopotential gradient (Smith et al. 1991; Thompson 1984; Woo 2005); this is reflected in the model forcing which only specified the temperature and salinity distribution within the model domain which in turn generated a realistic Leeuwin Undercurrent.

4.4.3 The eddy field

After the model reached quasi-equilibrium, the Leeuwin Current was comprised of many eddies and meanders. Periodically eddies or eddy pairs detached from the Leeuwin Current and migrated offshore. Initially, at the surface, anticyclonic eddies generated through Leeuwin Current meanders dominated. The Undercurrent tended to generate cyclonic eddies, which detached from the slope and migrated offshore. These eddies were strongest or well formed at the core depth of the Undercurrent (400-600 m). Subsequently, these cyclonic eddies manifested near the surface, often in cyclonic-anticyclonic pairs. Historical field data collected had insufficient spatial coverage to indicate if subsurface eddies were of a predominantly different direction to surface eddies, or rather if eddies were confined to either the surface or the Undercurrent, particularly during formation. However, a recent examination of an eddy pair generated within the Leeuwin Current indicated a very different vertical structure for each type (Feng et al. submitted). Specifically, the anticyclonic eddy had a maximum velocity at the surface that was diminished at 250 m, while the cyclonic eddy's velocity remained near constant to 250 m. The thermal structure of the cyclonic eddy was characterised by strong upwelling below 300 m while the anticyclonic eddy was characterised by a bowl shape at the surface. These results strongly resemble the eddies simulated in this study.

Anticyclonic eddy formation regions included the shelf curvature south of the Abrolhos Islands, Perth Canyon or just to the north, the shelf off Cape Naturaliste and the shelf southwest of Cape Leeuwin (Figure 4.1b). The Undercurrent generated cyclonic eddies primarily at the same locations as the Leeuwin Current. However, the Undercurrent encountered the shelf features at these locations from the opposite

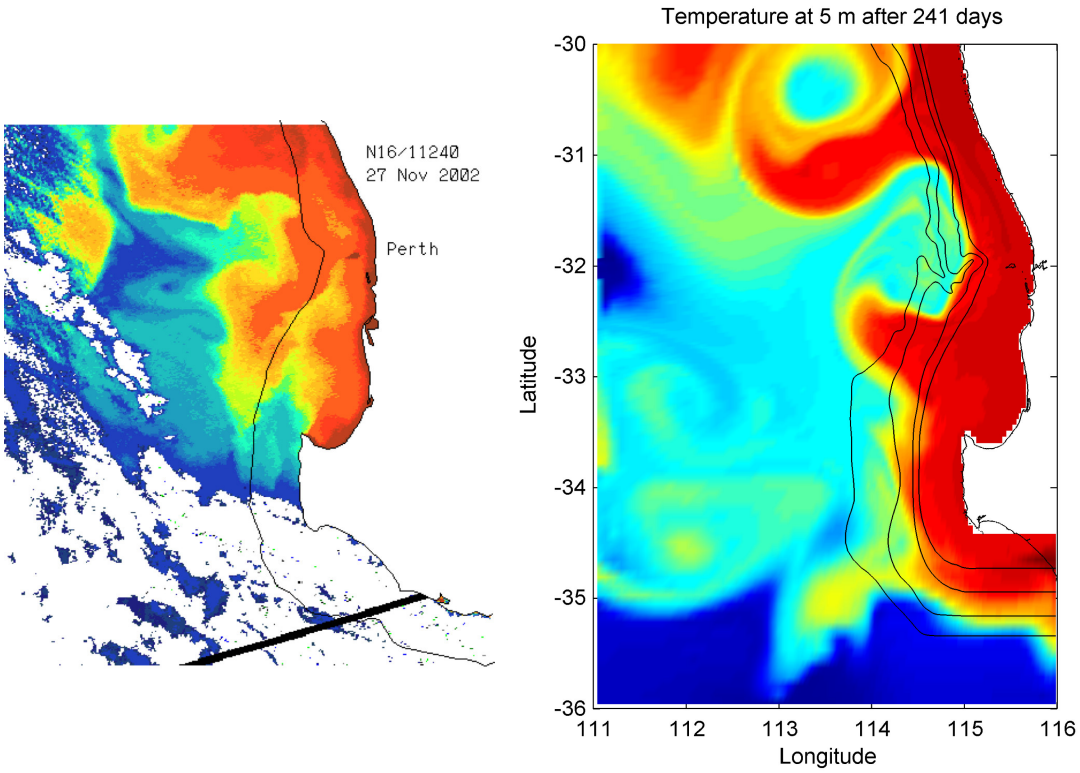

Figure 4.5. a) NOAA satellite images of the Leeuwin Current in November 2002. The warmest water (shown in red/orange) represents the Leeuwin Current, while the coolest water is in blue; white patchy areas are clouds. The thin black line marks the approximate edge of the continental shelf. Image by Alan Pearce, courtesy of WASTAC. b) A model image from day 241 of the initialisation run, showing an eddy offshoot north of the canyon, the Leeuwin Current close to shore over the canyon allowing cooler water over the canyon, and another eddy offshoot to the south of the canyon.

direction, so the eddy formed at a different location (e.g. the north side instead of the south side of a topographic feature). The northernmost and southernmost locations where eddies formed may yield erroneous eddy formation rates because the shelf was modified at these points. The northernmost was least realistic as isobaths turned northwards rather than following a diverging northwest path.

Figures 4.5 and 4.6 show examples of the flow and eddies formed in the Leeuwin Current from the no-wind simulation and satellite SST images. These were selected to show that similar broad-scale features, such as eddy location, were reproduced within the model. Figure 4.5 shows the Leeuwin Current close to the shelf, with an eddy pair separating from the Current near 31°S, cool water drawn in over the canyon and another anticyclonic eddy forming at the Cape Naturaliste shelf south of

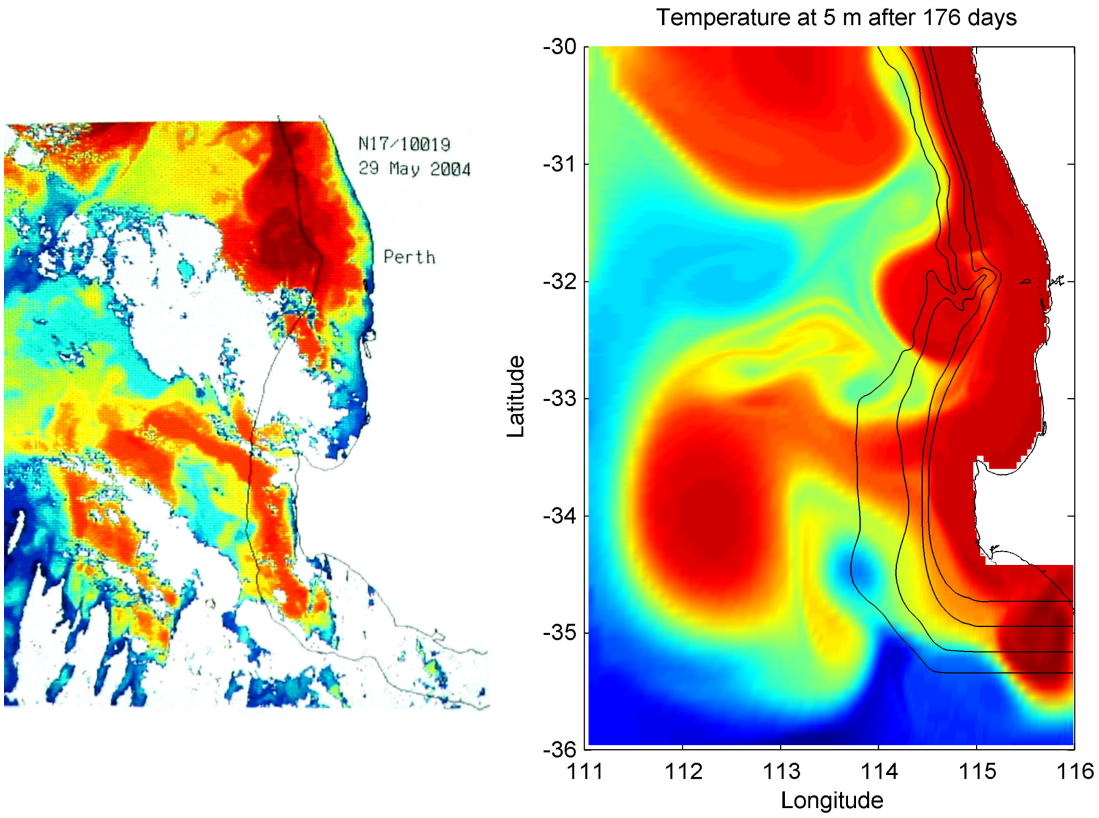

Figure 4.6. a) NOAA satellite images of the Leeuwin Current in May 2004. The warmest water (red) represents the Leeuwin Current, the coolest water is blue; white patchy areas are clouds. The thin black line marks the approximate edge of the continental shelf. Image by Alan Pearce, courtesy of WASTAC. b) A model image from day 176 of the initialisation run showing an anticyclonic warm-core eddy over the canyon, an eddy detaching from the Leeuwin Current from near Cape Naturaliste, and cooler water being drawn up into the Leeuwin Current north of the canyon.

the canyon. Figure 4.6 shows the Leeuwin Current again flowing along the shelf break. In this scenario, cool water was being drawn between the current and a warm-core eddy above 31°S (at the northern boundary of both images), an anticycloniceddy was situated over the canyon, and another anticyclonic eddy had separated from the current near Cape Naturaliste but whose connection had not completely severed.

Neglecting very weak eddies (<0.2 m s^{-1} boundary velocity at all depths) and very small eddies (<0.25° diameter), at any one time, between 5 and 10 eddies were present in the model domain (an area of ocean approximately 4° longitude by 8° latitude). The typical number of eddies was 7 or 8. Eddy residence time within the model domain varied from weeks to months. On average, eddies exited the domain at a rate of once per 2-3 weeks and eddies merged every ~25 days. The frequency of

eddy formation on the shelf was 3-4 weeks, with formation more often near or in the Perth Canyon. Eddies also formed through eddy splitting, but very rarely. Other eddy 'losses' were due to eddies dissipating. These statistics were evaluated by comparison with altimetry data for the modelled region. Eddy formation rates were estimated at one eddy per 2.5–4 weeks on average; the rate varied inter-annually and was higher during winter than summer (Griffin, Wilkin, Pearce et al. 2001). The number of simulated eddies within the domain at any time was similar to the number in the altimetry data, and the rate of eddy formation was also similar, indicating the model's accuracy.

4.4.4 Wind forcing: the Capes Current and seasonal responses

The wind forcing was included in the model to examine the interaction between the currents driven by an alongshore potential gradient and the opposing wind stress. The upwelling-favourable southerly winds that predominate during summer were the main focus for two reasons: (1) the Capes Current results from these seasonal winds (Gersbach et al. 1999; Pearce & Pattiaratchi 1999) and (2) upwelling induced by these winds could impact on productivity (Hanson, Pattiaratchi & Waite 2005). In the model, cooler water appeared on the shelf between the Capes after the start of the sea breeze pattern, four weeks after the spring wind forcing was initiated (i.e. the middle of October). Data from the Rottnest Island 50 m Coastal Station indicated cooling by October 6, 2001, around the start of the sea breeze pattern. This preceded the model's cooling response by ~10 days, which seems a reasonable agreement for this simulation with the limited wind stress magnitude. The cooler water appeared along the whole length of the coast, but was most pronounced at the Capes (Figure 4.7). This suggested that cooler water was upwelled along the whole coast in response to Ekman transport offshore driven by the southerly winds. Water advected northwards produced additional cooling of shelf waters.

For the simulation starting with summer winds, the Capes Current formed immediately. It began to disappear, with the Leeuwin Current moving onshore, during April when the southerly winds weakened and the sea breeze was absent. The two simulations thus replicate the entire Capes Current season, with realistic responses to the seasonal changes in the wind stress.

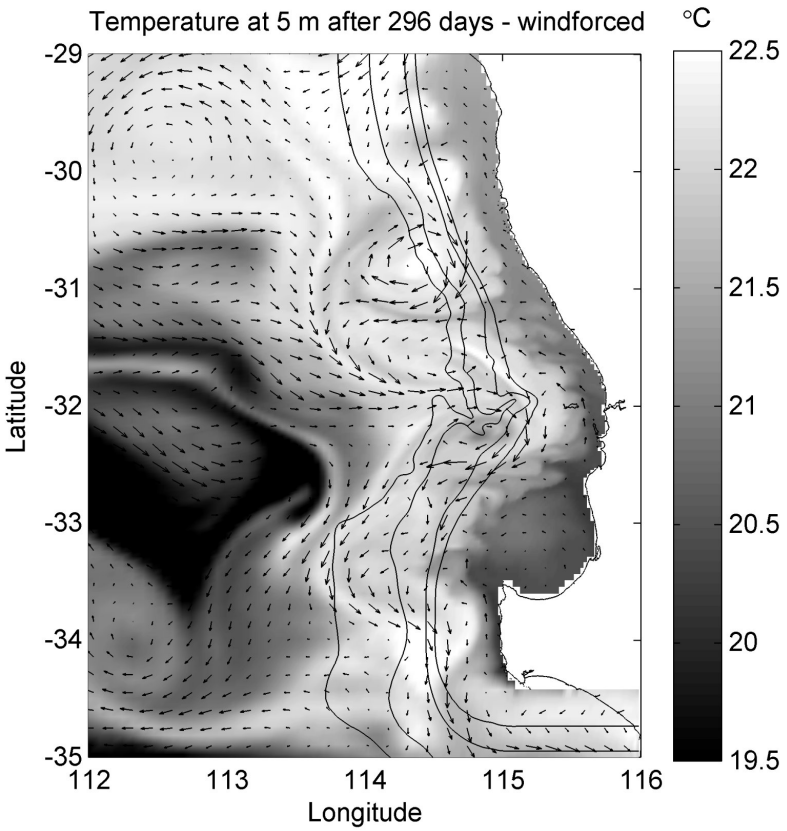

Figure 4.7. The temperature at 5 m of day 296 of the model run after 55 days of wind forcing starting from January, showing the Leeuwin Current flowing down the slope with several eddies along the slope. The Capes Current is visible as cooler water on the shelf. Velocity field indicated with arrows, maximum speed 0.75 m s^{-1}.

Figure 4.8a provides an example of a cross-section of model results at Cape Mentelle (Figure 4.1b) from early February, which shows upsloping isotherms indicating upwelling, the northward velocity of the Capes Current on the shelf and the southward Leeuwin Current further offshore. The upwelled water originated from a depth of 50-150 m and is thus sourced from the lower layers of the Leeuwin Current and thus is still low in nutrients (see also Hanson, Pattiaratchi & Waite 2005). Figure 4.8b shows a field transect off Cape Mentelle obtained from RV *Southern Surveyor* during October–November 2003. The pattern of isotherms is very similar but the temperature is several degrees warmer due to the absence of surface heat fluxes in the model. The simulated Leeuwin Current maintains its 22 °C temperature along the entire shelf, which is reduced only by mixing. With the absence of heat loss in this simulation, upwelling was the only possible mechanism that could produce surface cooling.

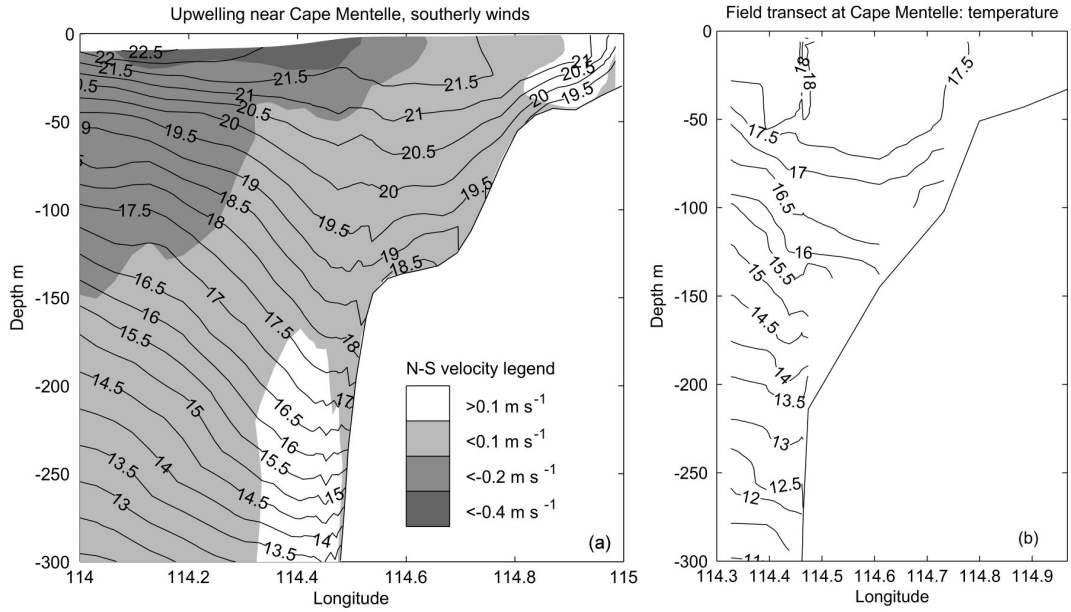

Figure 4.8. a) Typical temperature-depth profile of a wind-forced run showing upwelling at the Capes: Cape Mentelle, between Capes Naturaliste and Leeuwin. The land boundary is at 115°E, the boundary of the graph. The north-south velocity is shaded—the white indicates the Capes Current and Undercurrent, the dark grey the Leeuwin Current. b) Field transect at Cape Mentelle from November 2003.

The Capes Current velocity responded rapidly to changes in wind strength, so speeds of 0.5–1 m s^{-1} were produced as an immediate response to strong southerly wind forcing, but mean speeds were ~0.2 m s^{-1}. This agreed well with data from the field cruise, which indicated northward flow from south of Cape Leeuwin all the way up the shelf, with speeds near 0.2 m s^{-1} and constrained to inside the ~150 m contour along most of the shelf. The simulated Capes Current exhibited a similar constraint to the bathymetry. The Capes Current simulated here conforms to descriptions in the literature (Gersbach et al. 1999; Pearce & Pattiaratchi 1999) of a current that is narrow and confined to the shelf, and is wind-driven by short upwelling periods.

Billows, which are a feature commonly visible on SST images, appeared in the region of shear between the Leeuwin and Capes Currents (Figure 4.7). However, the simulated coastal water differed from that in the SST images due to the absence of radiative heating or cooling, which renders the shoreline water warmer in summer and cooler in winter. Compare the model image in Figure 4.7 with the satellite images in Figure 4.5 (November) and Figure 4.6 (May), which show warm and cool

shores respectively. The simulated Capes Current appears similar to the satellite images but for these differences.

4.5 Eddies and Eddy Formation

Eddies formed in the model could be categorized into two types, which were distinct in formation, location and direction but often occurred in conjunction: (1) formed in the Leeuwin Current as a warm-core anticyclonic eddy with a maximum velocity at the surface, which decreased rapidly with depth; and (2) formed in the Undercurrent, had a maximum velocity and coherent structure at 400–600 m but became weaker towards the surface, and was almost always cold-core cyclonic. Anticyclonic eddies did not appear to form in the Undercurrent except in two instances: within the Perth Canyon where the complex topography resulted in eddies of both directions, and at the south-eastern boundary of the domain, which was ignored as a boundary effect. Consequently, at the surface, anticyclonic eddies associated with the Leeuwin Current dominated the eddy field, but as the depth increased, these became indistinct and cyclonic eddies associated with the Undercurrent dominated. This transition is shown in Figure 4.9. This correlation of eddy type with depth appears to arise from the model's finite domain and the mechanisms that associate with the specific currents involved, as discussed below.

Surface eddy formation was linked to the formation and development of meanders in the Leeuwin Current. Meanders developed where shear from the Leeuwin Current's base against the slope (near the shelf break at 100 m for example) created positive (anticyclonic) vorticity. The flow then separated from the shelf and meandered anticyclonically. Initially the current rejoined the slope, but the anticyclonic meander grew, formed a closed eddy that separated from the current and migrated offshore. This process strongly replicated that described by Pearce and Griffiths (1991) although the formation of meanders was attributed to instability in the alongshore jet and topography interaction was not mentioned. In these simulations, the shallow Leeuwin Current and the smoothed bathymetry did not encourage the eddy generation (except over the canyon at 200 m) that might occur over real bathymetry. However, the locations of shelf edge curvature appeared to influence the location of eddy formation and development. This may have been due to the

interaction of the Undercurrent with both the bathymetry and the Leeuwin Current rather than direct interaction of the Leeuwin Current and bathymetry.

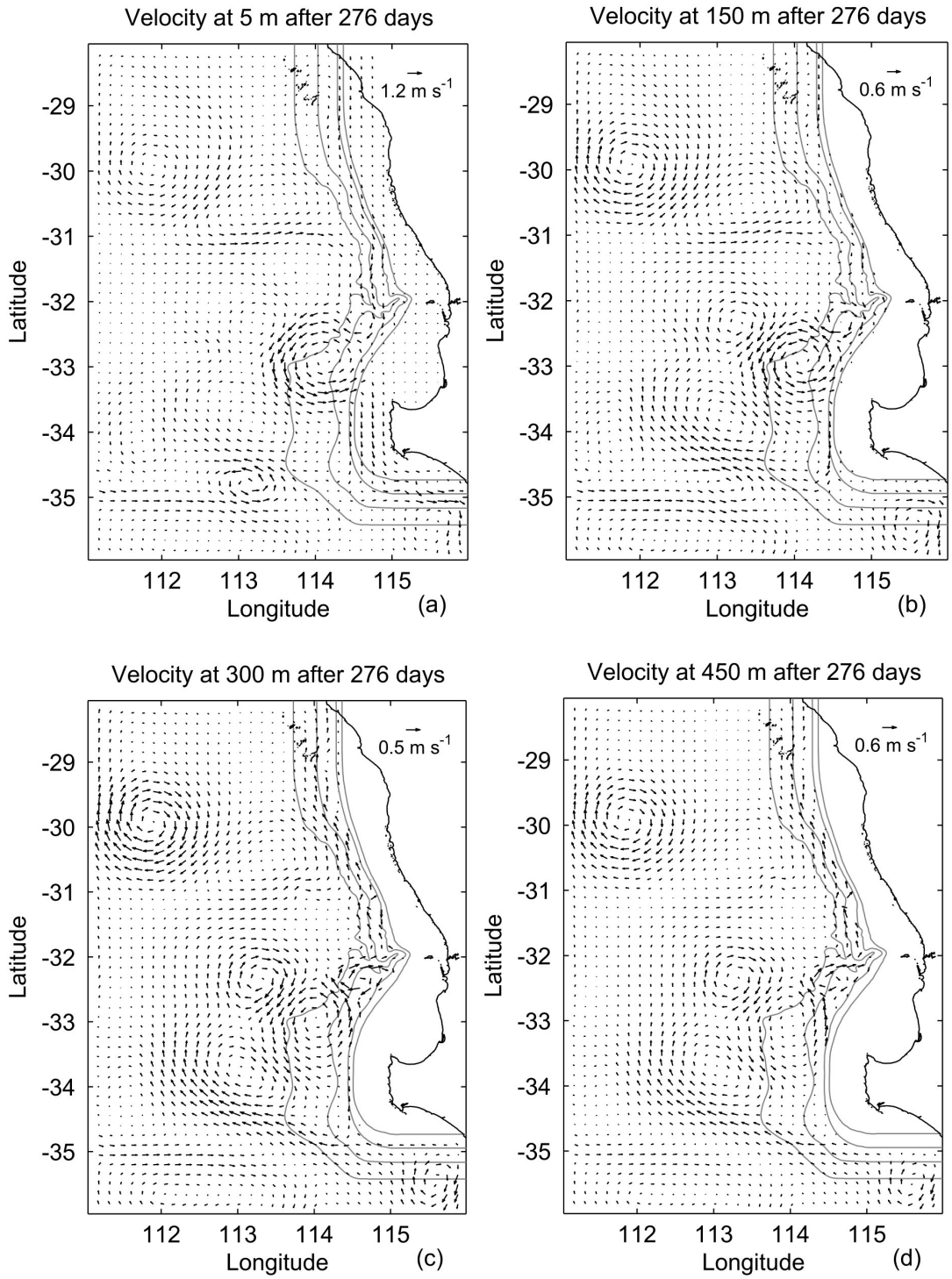

Figure 4.9. Changes in the current with depth. The anticyclonic eddies dominate near the surface, and the cyclonic eddies dominate in the Undercurrent. The labelled arrow indicates the approximate maximum velocity. a) at 5 m. b) at 150 m. c) at 300 m. d) at 450 m.

The Undercurrent also formed shear instabilities between the current and the shelf slope, generating cyclonic vorticity. As the flow detached from the slope, the depth increase enhanced the negative vorticity, encouraging the eddy formation. The shelf break bathymetry supported this mechanism because where the shelf turned sharply onshore, the current was unable to follow the isobaths and detached, moving to deeper water to form cyclonic eddies (see Figure 4.10a). Thus, the bathymetry determined the location of eddy formation within the Undercurrent, unlike the Leeuwin Current, because the slope at 500 m had sharper corners than at 100 m. The canyon was a special case because its extended bathymetric curves allowed several eddies of different directions to form within it, constrained by the canyon walls.

The formation of eddy pairs with the cyclonic eddy core in the Undercurrent and the anticyclonic eddy forming in the Leeuwin Current indicated the interaction between the two currents. The synchronicity of formation of eddies to create eddy pairs can be interpreted as reducing shear friction within the water column. The eddies at depth and at the surface tended to form or position themselves such that, as much as possible, the flow collimated itself over the entire water column and/or the surface and depth flow were perpendicular to cross paths. Only where the surface and subsurface currents flowed straight along the shelf did they flow in opposite directions.

A description of typical eddy pair formation is shown schematically in Figure 4.10b and may be described as follows: Initially a meander forms in the Leeuwin Current, which develops, into an anticyclonic eddy (marked A in Figure 4.10b). The dashed line shows the bound of warm Leeuwin Current water. Grey dashed arrows in Figure 4.10b represent a cyclonic eddy B (located to the north of A), forming in the Leeuwin Undercurrent at the same time as the anticyclonic eddy A starts to form at the surface. Eddy B can appear at the surface after eddy A has developed, often entraining a branch of warm water to flow around B, enclosing cooler oceanic water (solid grey arrow). As A detaches from the main flow, cooler water drawn north along the shoreward rim of A can form a new cyclonic eddy C. Eddy C can become part of the same process if another anticyclonic eddy forms to the south, or can pair up with A also. Eddies A and B are not necessarily the same diameter, but the smaller eddy orbits around the larger eddy in an eddy pair.

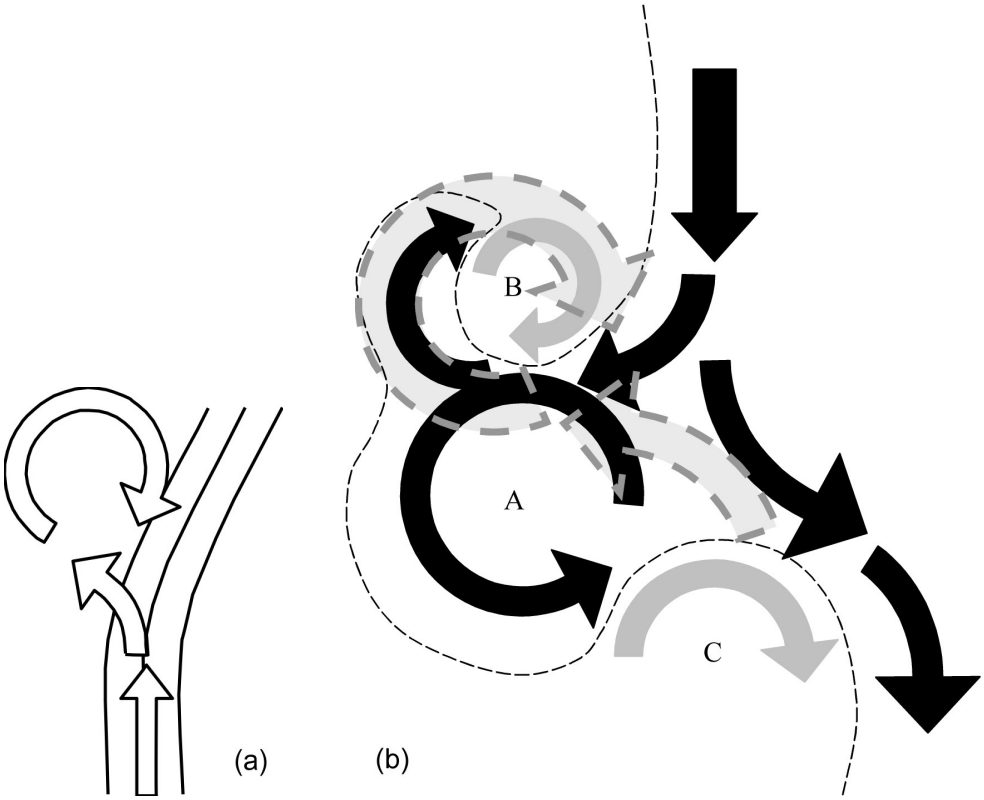

Figure 4.10. a) Schematic of generation of cyclonic eddies associated with bathymetric curves. b) Formation of eddy pairs in the Leeuwin Current and Undercurrent. The black arrows are the Leeuwin Current and the thin dashed line represents the warm water boundary. The solid grey arrows are cooler offshore water and the grey dashed arrows are the Undercurrent. A=Leeuwin Current anticyclonic eddy. B=Undercurrent cyclonic eddy paired with surface eddy. C=New eddy forming from ocean water drawn between the Leeuwin Current and anticyclonic eddy.

In the case of the canyon, eddies tended to form in several places, and the eddy pair mechanism described above was not essential. The Perth Canyon's size and complexity meant that multiple eddies could form within it. The Leeuwin Current only interacted with the canyon at ~200 m, where the flow would separate from the isobath and form an anticyclonic eddy trapped within the tip of the canyon. This only occurred if the Leeuwin Current flowed southward following the 200 m isobath when it encountered the canyon. When the Undercurrent encountered the canyon it could break away from the shelf at ~500 m and form a cyclonic eddy over the southern rim. A cyclonic eddy could also form along the canyon axis to the east (i.e. upcanyon) of where the Undercurrent crossed the canyon axis. The eddy location and size depended on where the Undercurrent crossed the canyon. This eddy formation only occurred below the rim of the canyon, i.e. where it was partly

enclosed. Hughes, Osofu and Hickey (1990) depicted this eddy formation as an undercurrent interaction with a canyon, i.e. a current that is below the rim of a canyon. She and Klinck (2000) found a similar feature of eddy formation with a canyon, which was attributed to momentum advection causing separation of the upstream flow, and stretching vorticity inside the canyon. Pressure gradient errors are likely to be most problematic within the canyon. The Perth Canyon's complex circulation pattern is further discussed in Chapter 5.

4.5.1 Comparison with a model of the Iberian Poleward Current

The Iberian Poleward Current system is similar to the Leeuwin Current System; consequently, its recent modelling is worth discussing in comparison. The driving forces for the two current systems are similar. The Iberian Poleward Current experiences seasonality because, unlike the Leeuwin Current, the wind can override the alongshore density gradients, inducing upwelling currents. This system has been modelled using ROMS also (Peliz, Dubert & Haidvogel 2003; Peliz et al. 2003).

A weak equatorward undercurrent accompanied the Iberian Poleward (surface) Current. There were two canyons and a promontory with which the currents interacted to generate eddies. Near these bathymetric features, anticyclonic eddies formed as surface current meanders induced the undercurrent to separate from the shelf and turn back around anticyclonically. The bathymetry trapped the anticyclonic eddies and several smaller cyclonic eddies formed and circulated around the anticyclonic eddy as satellites, before eddies detached from the shelf (Peliz et al. 2003). Initially, the cyclonic eddy signal did not reach the surface although the anticyclonic eddy appeared throughout the water column. If the shelf bathymetry did not trap the anticyclonic eddy, an eddy dipole formed and migrated offshore. This formation of eddies is greatly resembled by that shown in the current study; points of similarity were the interaction between the surface current and undercurrent producing coupled eddies, the interaction with bathymetry, and the predominance of anticyclonic eddies at the surface and cyclonic eddies at depth. The primary difference was that in the present study the cyclonic eddies appeared first within the undercurrent while the anticyclonic eddies did not extend so strongly through the water column.

4.6 Concluding Remarks

The numerical model ROMS was used successfully to simulate the surface and sub-surface current systems along the south-west coast of Australia including the Perth Canyon. The model, forced using only temperature and salinity derived from climatology, simulated a Leeuwin Current and Leeuwin Undercurrent which reproduced the location and magnitudes of the currents observed from field measurements and satellite imagery. The model also accurately predicted the locations of eddy formation, and the timescales of the eddy field (formation and migration rates) compared favourably with observations. Wind forcing modified the surface current system with the Leeuwin Current migrating offshore and generating a northward flowing Capes Current on the shelf. The wind stress also resulted in coastal upwelling.

Eddy formation was related to the interaction between the Leeuwin Current and Undercurrent. Eddies in the Leeuwin Current and Undercurrent were frequently coupled, with the formation of anticyclonic eddies in the Leeuwin Current complementing the formation of cyclonic eddies in the Undercurrent to create eddy pairs. Although the eddy field at the surface and at depth was related, anticyclonic eddies dominated the surface flow and cyclonic eddies dominated at 500 m. Eddies were formed near the shelf break and then migrated offshore over several weeks or months. Flow along the shelf break caused shear to generate vorticity, and bathymetric contours affected the location of eddy formation by inducing flow separation and vorticity stretching.

CHAPTER 5

Numerical Simulation of Circulation in the Perth Submarine Canyon to Determine the Influence of Current Interactions on Marine Microfauna and Megafauna

5.1 Summary

Western Australia's current system was simulated with ROMS to examine the Perth Canyon's circulation, where, despite the region's oligotrophy, the Perth Canyon annually attracts feeding blue whales. Two currents entered the canyon's vicinity; the Leeuwin Current interacted weakly with the canyon, whereas the deeper Leeuwin Undercurrent interacted strongly with the canyon, resulting in eddies forming within the canyon. There was no steady state; the flow field changed continually with few repeated characteristics. Recurrent eddies, however, produced regions where upwelling or downwelling predominated during the model runs. Deep upwelling was stronger within the canyon than elsewhere on the shelf, but near-surface vertical transport was strong everywhere when wind forcing was applied. Upwelling alone appeared to be insufficient to transport nutrients to the euphotic zone, because the canyon rims are deep. Increased upwelling combined with entrapment within eddies, and strong upwelling-favourable winds that could assist mixing, might be sufficient to account for the relatively high productivity attributed to the canyon. The Leeuwin Current is otherwise a strong barrier to upwelling of nutrients.

5.2 Introduction

Submarine canyons have been the subject of many oceanographic studies for their effect on local circulation and, not unrelated, importance in marine habitats. Canyons have frequently been associated with feeding marine megafauna, appearing in systems where enhanced upwelling boosts productivity. An excellent example is Monterey Canyon, where intense upwelling periods and subsequent euphausiid abundance increase attracted many blue whales (Croll et al. 2000; Schoenherr 1991).

Studies analysing the circulation in submarine canyons using field and modelling approaches are increasing in number. Numerical modelling has advantages over field studies, through easier data generation, and analytical models, which are unwieldy because of the non-linearity required to model the system effectively. Canyon modelling principles were established using an idealised slice into a shelf (e.g. Allen 1996; Haidvogel & Beckmann 1995; Hughes, Ofosu & Hickey 1990; Klinck 1988; Klinck 1996; Pedlosky 1974; Verron, Renouard & Boyer 1995).

It has been well established in model and field studies that the direction of an alongshore current determines whether upwelling or downwelling is favoured. The current direction determines whether water is transported onshore or offshore, resulting in downwelling or upwelling. As wind direction may dictate currents, strong winds in favourable conditions can increase cross-shelf exchange (Klinck 1996; Skliris, Hecq & Djenidi 2002).

The presence of a canyon alters the cross-shore pressure gradient to enhance the cross-shelf transport and therefore upwelling or downwelling (e.g. Allen 1996; Boyer, Zhang & Pérenne 2000; Granata et al. 1999; Klinck 1996; She & Klinck 2000; Skliris, Hecq & Djenidi 2002; Sobarzo, Figueroa & Djurfeldt 2001; Song & Chao 2004). When a current encounters a curve in the bathymetry it will initially try to follow the curvature. For example, the currents will try to flow around the canyon head, following the bathymetry, increasing in speed as the current squeezes between the coast and canyon. On encountering narrow canyons, however, the shelf curves too sharply, and the flow will cross isobaths, which can result in column stretching and vorticity changes. In some cases, a closed eddy forms within the canyon.

She and Klinck (2000) used ROMS (see Section 5.3.2) to examine an idealised canyon, resembling Astoria Canyon off the western coast of North America, under constant upwelling-favourable and downwelling-favourable winds. Under upwelling-favourable winds, the alongshore flow showed little effect near the surface, which was beyond the canyon bathymetry's influence. A cyclonic eddy formed within the canyon rims at 150 m, near the head and towards the upstream rim, with onshore flow farther down the canyon axis. At 300 m, the flow followed

the isobaths, with strong onshore flow on the upstream slope and weaker offshore flow on the downstream slope. Under downwelling winds, the situation was largely reversed, but the vertical transport was reduced.

Stratification affects the bathymetry's vertical extent of influence. Stronger stratification limits influence, so flow above the canyon may be beyond its influence (Klinck 1996; She & Klinck 2000; Skliris, Hecq & Djenidi 2002). With weak stratification, the bathymetry exerts an influence over a greater depth (She & Klinck 2000; Skliris, Hecq & Djenidi 2002); thus, in strong stratification cases, the enhancement of cross-shelf exchange by canyons is limited.

Few studies, however, have included downwelling-favourable systems (Klinck 1996; Skliris, Hecq & Djenidi 2002), undercurrent interactions with canyons (Hughes, Ofosu & Hickey 1990), or canyons with realistic or non-idealised bathymetry (e.g. Ardhuin, Pinot & Tintore 1999; Skliris, Hecq & Djenidi 2002; Skliris, Lacroix & Djenidi 2004). This study attempted all the above with a case study of the Perth Canyon, which is a whale feeding hot spot. A strong downwelling-favourable poleward surface current (the Leeuwin Current) and a weak undercurrent in the reverse direction (the Leeuwin Undercurrent) dominated this region.

From 2000 to 2004, the Perth Canyon was the subject of collaborative research (the WAXA Blue Whale Project), funded through Australian Defence, to study pygmy blue whales sighted along the WA coast, particularly near the Perth Canyon in summer. An associated goal was to study the whales' habitat—the Perth Canyon—to understand its suitability to whale feeding. Observation during the WAXA Blue Whale Project revealed that whales frequent the canyon to feed on krill (*Euphausia recurva*). The ultimate purpose of this canyon modelling study was to determine why the canyon had an abundance of the whales' prey. Possible mechanisms included prey aggregation, and food provisions for the prey, culminating in large swarms forming. This information could eventually be used to predict when and where krill concentrations would be highest; thus, the whales' appearance might be anticipated.

The primary aim of simulating the Perth Canyon's circulation was to better understand how the ocean interacts with the canyon, particularly under the local wind and current conditions. Topics in this paper include formation of eddies in the canyon and the occurrence and location of vertical motion. Analysis was extended to the forcing conditions associated with these fluid movements, such as weather. The Perth Canyon was expected to significantly affect the local currents, beyond the effect of the continental shelf's curvature.

In this chapter, Section 5.3 describes the modelled area's physical setting, including the currents and wind, and briefly reports the model set-up. Section 5.4 discusses circulation in the canyon, including the occurrence of upwelling and downwelling. Section 5.5 discusses the model results' implications for productivity and aggregation of krill swarms.

5.3 Methods

5.3.1 Study area

The Perth Submarine Canyon starts at the 200 m contour, 48 km west of Perth, Western Australia, and is approximately 100 km long. Near the head, it is approximately 10 km wide and rapidly reaches depths greater than 1000 m. At the shelf slope, it is 3 km deep and cuts to 4 km deep in the abyssal plain. Note that the canyon 'head' refers to the canyon's shoreward section (~10-15 km), and the 'tip' refers to the head's shoremost point. The canyon has bends at 10 km and 50 km from the tip and small branches south at 40 km and 50 km (Figure 5.1). The bend at 50 km is referred to as the 'dogleg'. The Perth Canyon could be summed up as long, steep-sided, narrow, and deep, and it substantially intrudes into the continental shelf.

Two permanent currents flow in the Perth Canyon's vicinity. The Leeuwin Current, at the surface, flows south (poleward) along the shelf break and is up to 300 m deep at 32°S. The Leeuwin Current reaches speeds over 1 m s^{-1}, although the average speed is approximately 0.4 m s^{-1} (Feng et al. 2003; Smith et al. 1991). The Leeuwin Undercurrent flows brokenly equatorward up the continental slope with a maximum velocity at 450–550 m and speeds of 0.1–0.4 m s^{-1} (Thompson 1984, Chapter 6).

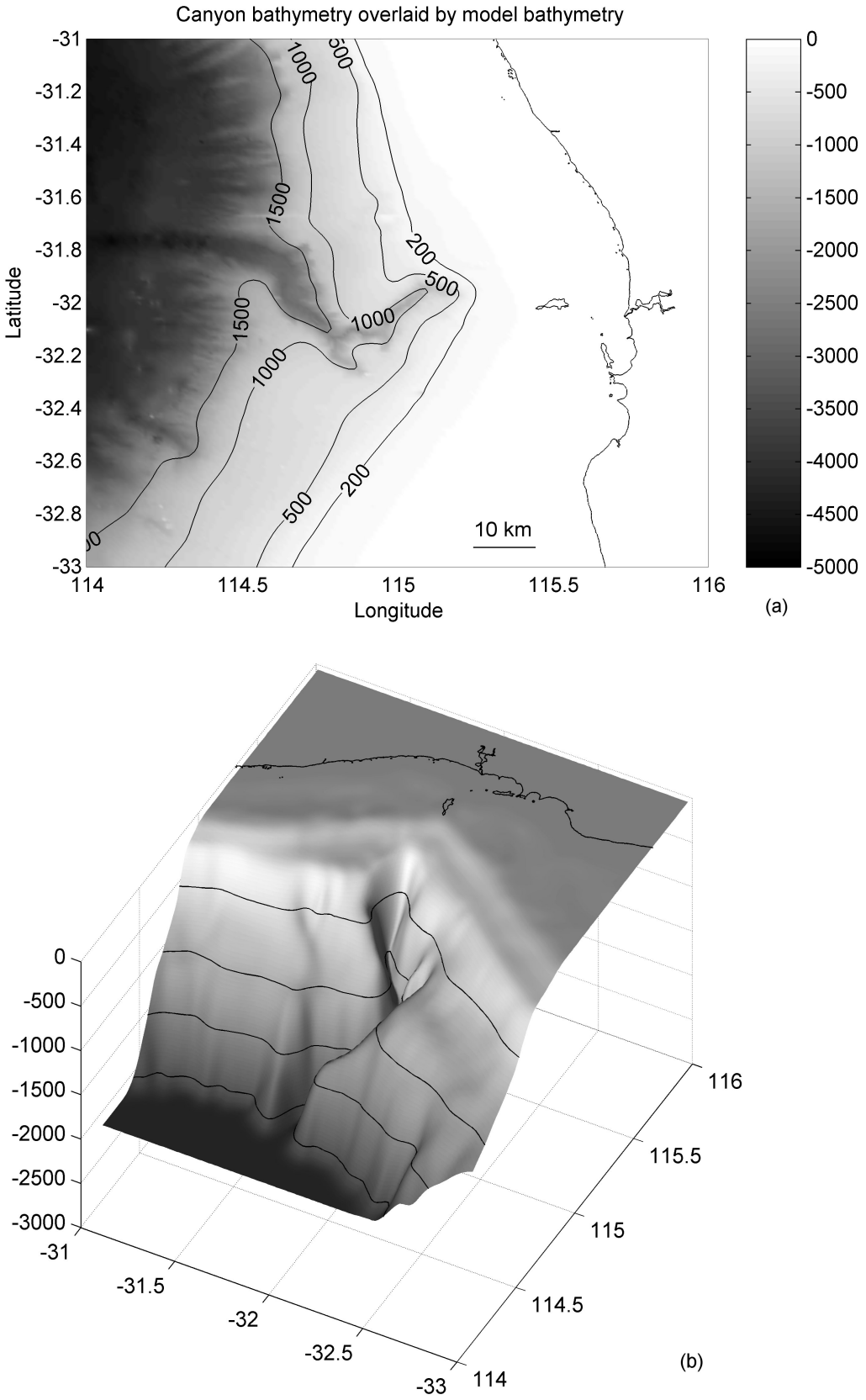

Figure 5.1. a) Canyon bathymetry (shaded—refer to colour bar for depth) overlaid with model bathymetry (contour). The real and model bathymetry depths are equivalent above 1000 m; however, the model bathymetry has been smoothed. An approximate scale at 32°S is shown. b) Three-dimensional figure of canyon.

The wind regime at 32°S consists of strong southerly winds during summer (October–April), which are modulated by a sea breeze pattern. In winter, the wind is weaker and the direction variable, as weather systems pass. Strong winds associated with storm fronts usually occur during winter (April–October). The transition between summer and winter winds usually occurs within a month or two as one pattern begins to interrupt the other. The southerly summer winds oppose the Leeuwin Current, causing it to weaken and shallow (Feng et al. 2003). These winds also create the Capes Current—a northward-flowing current restricted to the shelf and sourced by shallow upwelling (Gersbach et al. 1999; Pearce & Pattiaratchi 1999).

5.3.2 The model set-up: ROMS

ROMS (Regional Ocean Modelling System) was developed by teams at Rutgers and UCLA (Haidvogel et al. 2000). The model was chosen because it uses the terrain-following *s*-coordinate system for vertical coordinates (Haidvogel, Wilkin & Young 1991), which transforms the *z*-coordinate to layers that conform to the bathymetry. This reduces the bathymetry approximation that would occur with a stepwise vertical grid.

The major drawback of a terrain-following coordinate system is the error associated with calculating the horizontal pressure gradient, which requires correcting for the hydrostatic pressure term. The error is primarily due to truncation when subtracting two large values of similar size. This error generates spurious currents, which may be a significant problem, depending on the application. In Chapter 4 it was established for this model that although spurious currents and eddies appeared, particularly around the canyon, the 'real' density-forced currents swamped these currents after the model had developed fully. The model required about 160 days to develop, i.e. reach quasi-equilibrium.

Chapter 4 described the model set-up in detail. Briefly, the model domain ranged from 111 to 116°E and 28 to 36°S. The canyon was located centrally near the eastern land boundary (at 32°S and 115°E). Shelf topography was straightened

above 30°S and below 34°S to be perpendicular to the north and east boundaries, respectively. Horizontal resolution varied from ~10 km near the north, south and west boundaries, to ~2 km near the canyon. The depth below 1000 m was halved relative to 1000 m, which reduced steepness and depth without losing the canyon's shape below 1000 m. The topography was then cut below 2100 m and above 30 m. All islands were ignored, as they caused instability when wind stress was applied. The topography was smoothed to fit robustness $r < 0.2$ (Beckmann & Haidvogel 1993; Haidvogel et al. 2000) and slope steepness less than 10% (following e.g. She & Klinck 2000). The model used 20 *s*-coordinate layers with $\theta_s = 3$, $\theta_b = 0.1$ and $T_{cline} = 30$, so that the vertical resolution was higher near the surface.

Initial model forcing included temperature and salinity gradients adapted from the World Ocean Atlas 1994 (Levitus & Boyer 1994; Levitus, Burgett & Boyer 1994). Wind forcing was applied to the developed model after 240 days, using quarter day forcing of real wind from Rottnest Island 2001 to 2002 (see Figure 5.1a). The three model runs included the initialisation run, with no wind forcing, and two wind-forced runs. The first wind-forced run used wind from summer 2001, and the second used wind from spring 2001. The three runs were referred to as 'no-wind' or 'initialisation', 'summer', and 'spring', and Quicktime movies of the runs are included in Appendix A (CD-ROM). The model output was collected every five days, although a test run at one-day resolution was conducted for comparison. The results presented below, unless stated otherwise, refer to these three runs, with a duration of 200 days for the no-wind and 100 days each for the wind-forced all at five-day resolution. The wind-forced runs were terminated after 100 days of wind forcing degraded the density gradient driving the Leeuwin Current.

Ground-truthing and model verification (Chapter 4) indicated the model successfully reproduced the Leeuwin Current, the Undercurrent, and the Capes Current when summer wind forcing was applied. The Capes Current, however, did not interact directly with the canyon. The model was found to be realistic in the location and magnitude of the currents formed. Cyclonic eddies forming in the Undercurrent and anticyclonic eddies forming in the Leeuwin Current constituted an interesting bias.

5.4 Results

5.4.1 Circulation

Before discussing the circulation in the canyon, the major currents in the model will be described. The Leeuwin Current was composed of jets, meanders, and eddies; its usual speed was ~0.6 m s^{-1}, and its maximum speed was ~1 m s^{-1}. It flowed southward along the shelf break, near the 200 m isobath, and over the Perth Canyon, extending to an approximate depth of 200 m. The Leeuwin Undercurrent flowed northward against the shelf slope at 400–600 m and frequently formed eddies where the shelf curved. The Undercurrent's usual speed was <0.3 m s^{-1} with a maximum of 0.5 m s^{-1} and across the canyon, it had a mean of ~0.1 m s^{-1}. The Capes Current was associated with water upwelled from approximately 100 m and was constrained inside the ~150 m isobath, so it did not pass over the canyon. Its velocity depended on the wind and could reach 0.3 m s^{-1}. A three-dimensional section of the model is shown in Figure 5.2. The southernmost extent is a slice through the canyon, just south of Rottnest Island. The Leeuwin Current was observed as a meander in the surface water; the Undercurrent was more diffuse, with a deeper maximum velocity. On the shelf, the wind forcing turned the flow northward.

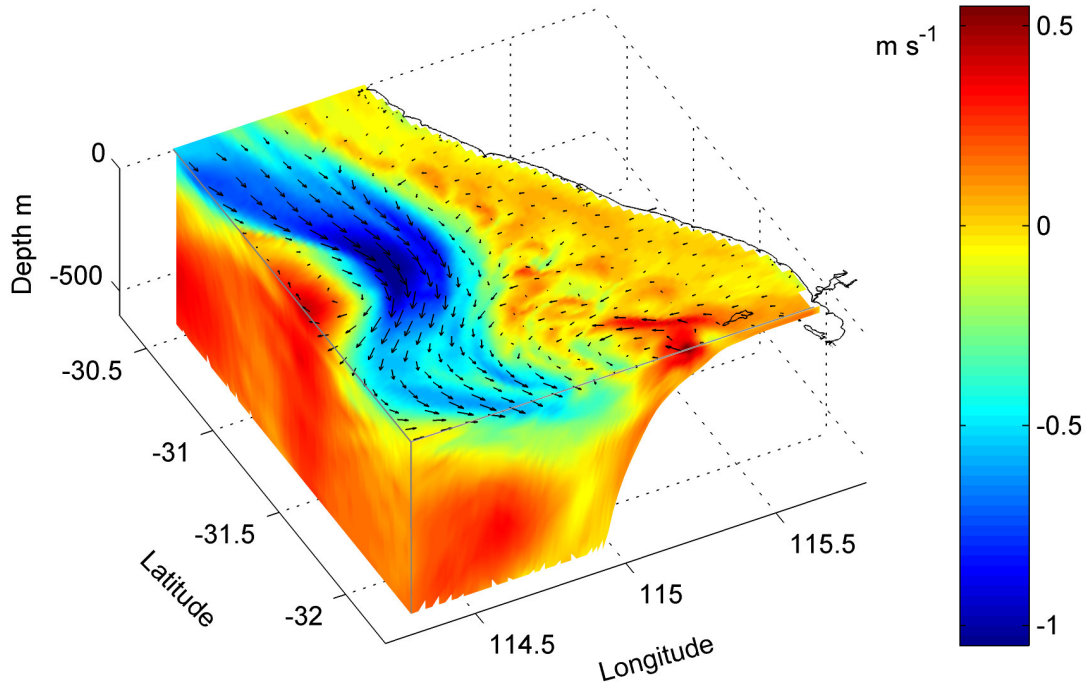

Figure 5.2. The southward (blue) Leeuwin Current and northward (red) Undercurrent in a three-dimensional section from the spring run. Maximum depth is 750 m.

5.4.1.1 Circulation in the canyon

The circulation in the canyon changed continually during the model runs (see Appendix A: canyon movies). No steady state or typical flow pattern was present in the circulation and flow features persisted for days to weeks. Consequently it was difficult to generalise the flow in the canyon. However, it was possible to define six patterns or 'cases' (described in Appendix B) that could approximately describe the flow at any time. Discriminating features included the location of eddies and meanders in the Leeuwin Current and Undercurrent and the thermal structure at several depths. The presence of shelf cooling associated with the Capes Current was insignificant, as it rarely or never impacted on canyon circulation. The consistent features that permitted such a classification suggested the currents were influenced by the bathymetry.

Some ambiguity arose where the circulation was between two patterns or patterns shared some of the same features. Approximately 100 days was required for all patterns to manifest, which was in the order of a season. The patterns occurred in no specific order, and the pattern frequency distribution varied between runs. This result signified that the canyon circulation was highly variable and changed rapidly. The effect of any particular pattern remained a finite period of days to weeks.

In the following discussion, the circulation associated with the canyon is described in general terms and some specific examples are given. The surface circulation is described first.

5.4.1.2 The surface and the Leeuwin Current

The strong stratification above 400 m and the Leeuwin Current and Undercurrent's distinctness limited the depth extent of the canyon's influence above its rim. The above-rim flow appeared to interact with the canyon only within 200 m of the rim, so the canyon's influence extended to the surface at the canyon tip, but deepened rapidly with the shelf slope. This indicated that except at the canyon tip, the Leeuwin Current was not influenced by the canyon. However, the shelf curvature at approximately 150–250 m depth blends with the canyon tip. This curvature at the

canyon head encouraged cyclonic circulation around the canyon, but when the Leeuwin Current separated from the shelf, it helped form anticyclonic eddies.

Circulation examples are provided in Figures 5.3, 5.4, and 5.5. The figures indicate the surface flow (5.3a, 5.4a, and 5.5a) had little relation to the bathymetry, but the shelf constrained the flow at 200 m (5.3b, 5.4b, and 5.5b). In Figure 5.3 the Leeuwin Current is forming a closed anticyclonic eddy, indicated by the pool of warm water to the canyon's north, and as this eddy separates, cooler water was being drawn in behind it. (This is a case 5, with the variation of cool water drawn in behind the anticyclonic eddy.) In Figure 5.4, the Leeuwin Current crosses over the canyon head, almost following the shelf's curve (This is a case 1 with the anticyclonic eddy south of the canyon and the Leeuwin Current meandering onshore). In Figure 5.5 (wind-forced output corresponding to Figure 5.2) the Leeuwin Current's core meanders across the middle of the canyon, bounded by cooler oceanic water offshore and cooler Capes Current water onshore. At 200 m, warmer water pushes down against the shelf at the canyon head despite surface cooling from the wind. (Figure 5.5 is a case 6 with wind forcing.)

5.4.1.3 The Undercurrent and eddy formation

The Undercurrent interacted strongly with the canyon to form eddies, which could be centred over the axis or the rims. The eddies changed as the Undercurrent shifted, so within five–ten days they could disappear or grow and migrate offshore. The examples in Figures 5.3–5.5 (panels c and d) show some of the variety.

In Figure 5.3's example, the Undercurrent followed the bathymetry as it approached the canyon, but broke away and crossed the canyon where the 500 m isobath deviated around the canyon head. The Undercurrent continued in an anticyclonic circulation, which was centred just south of the canyon mouth, and also formed a cyclonic eddy north of the region shown. Part of the jet that crossed the canyon broke away and formed a cyclonic eddy at the canyon head. This upwelled cool water into the head, whereas the anticyclonic eddy caused a warm pool of water to dominate the rest of the canyon.

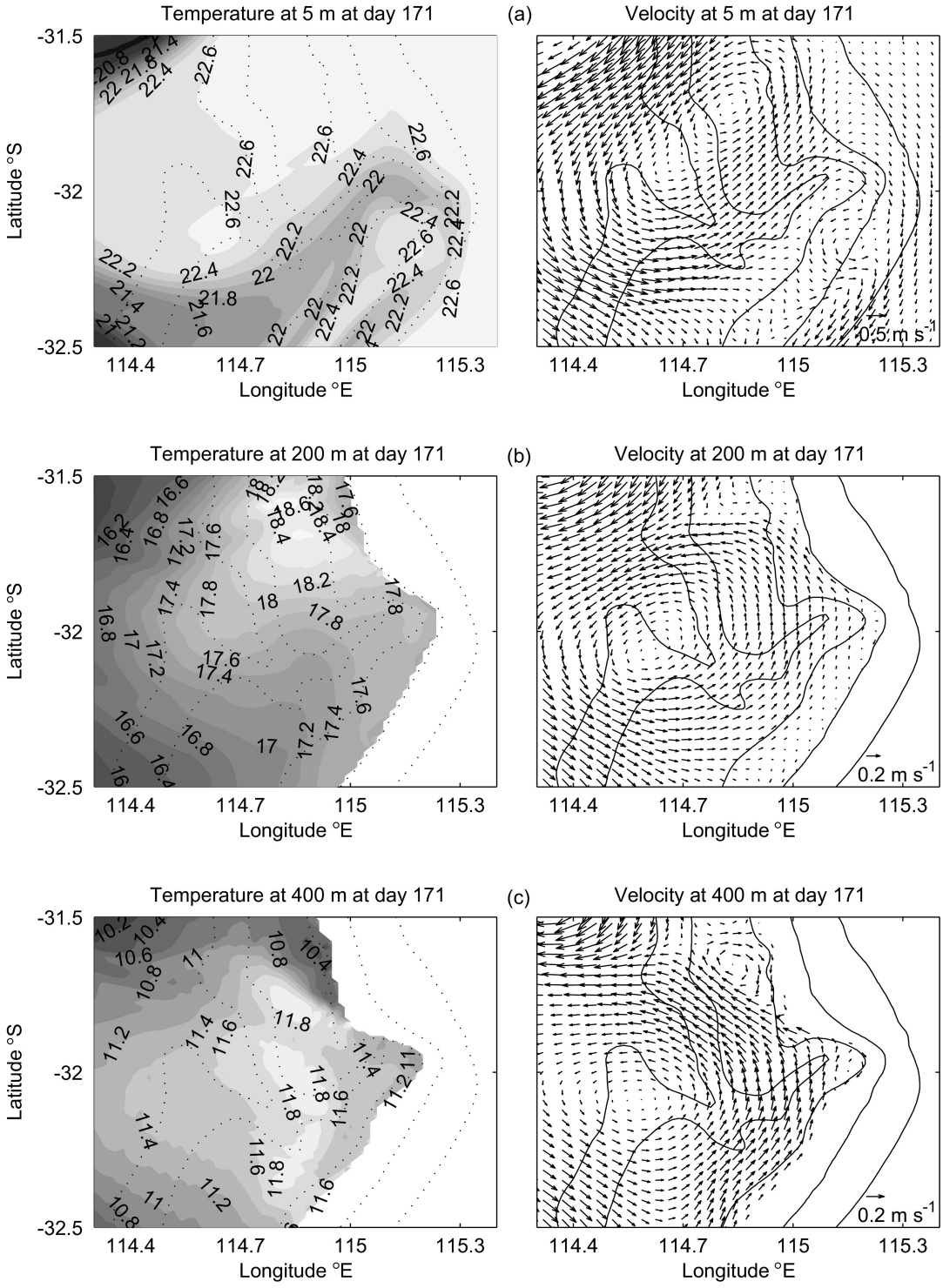

Figure 5.3. Continues next page.

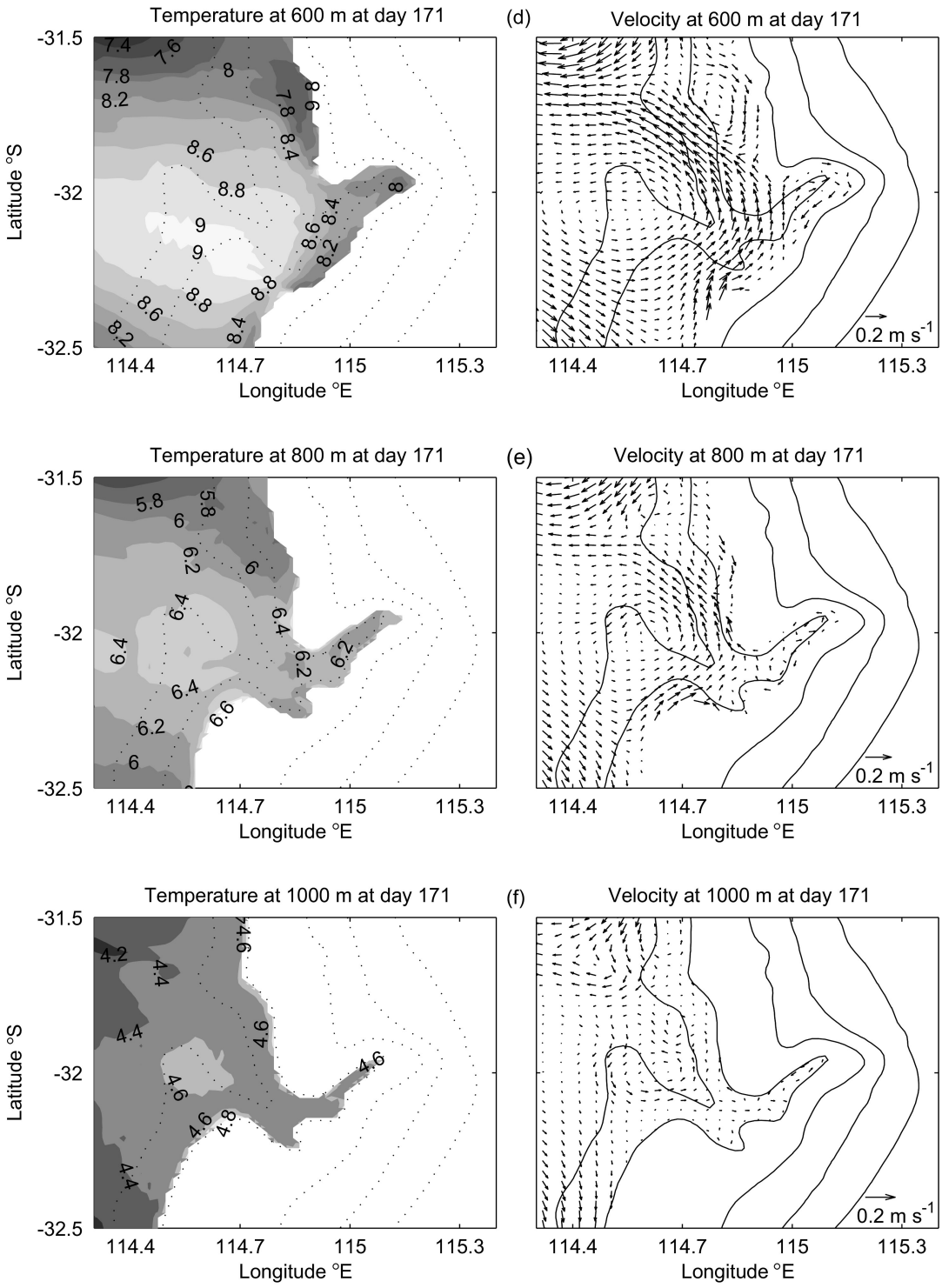

Figure 5.3. Day 171 of the no-wind run showing temperature (left pane) and velocity vectors (right pane). a) 5 m. b) 200 m. c) 400 m. d) 600 m. e) 800 m. f) 1000 m. Bathymetry contours at [100, 200, 500, 1000, 1500] m.

The example in Figure 5.4 shows the Undercurrent away from the shelf and crossing the canyon mouth. As the model output indicated an anticyclonic eddy to the south (Figure 5.4a), it could be assumed that, before entering the depicted region (west side

of Figure 5.4c), the Undercurrent flowed against the slope until it was drawn offshore to follow the anticyclonic eddy's northern side. As the Undercurrent entered, it then curved cyclonically as it continued past the canyon mouth.

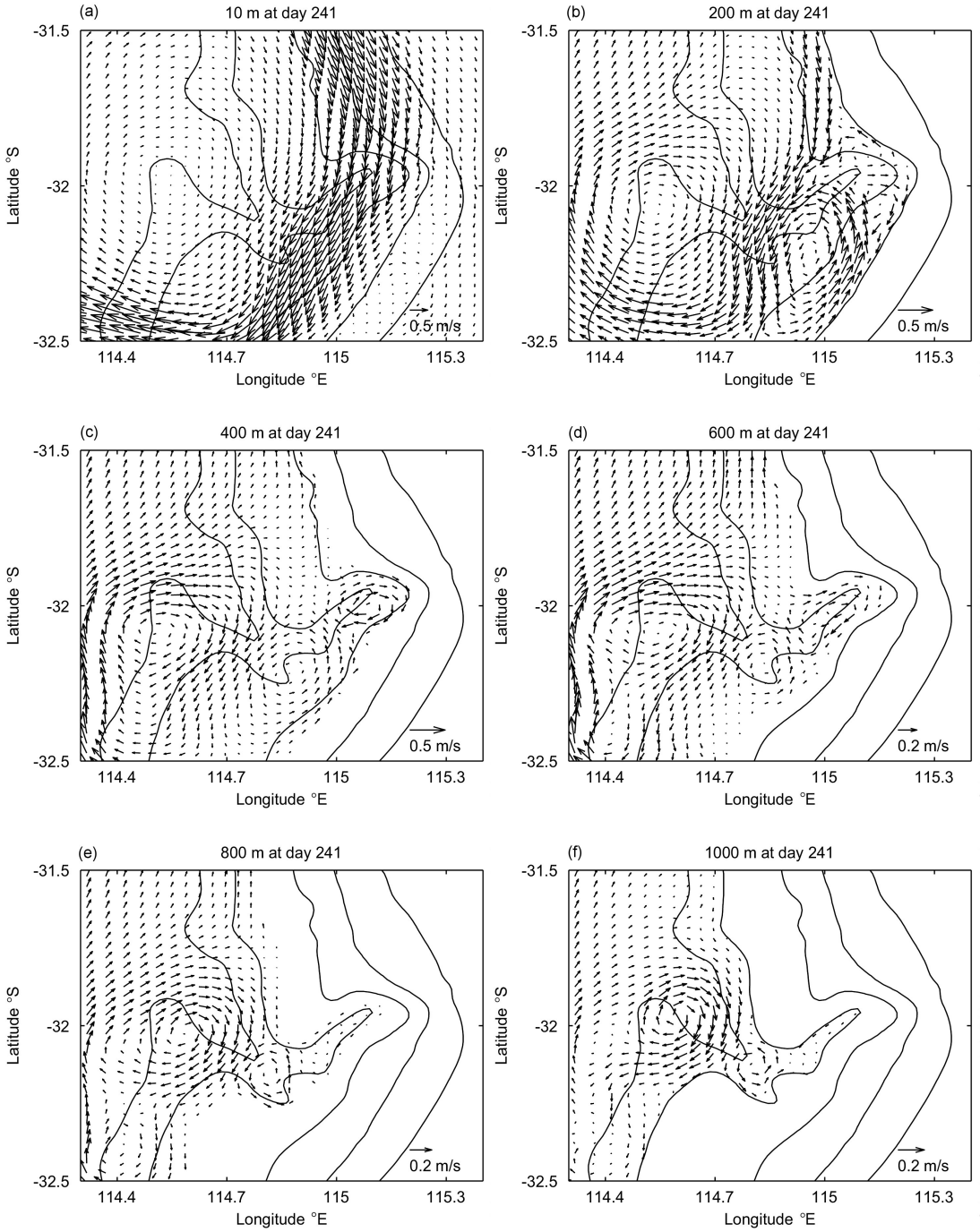

Figure 5.4. Day 241 of the no-wind run showing velocity at different depths. a) 5 m. b) 200 m. c) 400 m. d) 600 m. e) 800 m. f) 1000 m. The Leeuwin Current is inshore over canyon, and forms an anticyclonic eddy to the south of the canyon. Bathymetry contours at [100, 200, 500, 1000, 1500] m.

Elsewhere on the continental slope this situation might be a simple eddy pair, but because the Undercurrent crossed the canyon far offshore, a series of eddies formed within the canyon. The large cyclonic eddy over the mouth was part of the eddy pair. The southward-flowing part of this eddy generated an anticyclonic eddy near the dogleg, which became more centred over the axis at greater depth. This anticyclonic eddy in turn generated a cyclonic eddy in the head, which was over the south rim at 200 m, but centred over the axis at 600 m. At 1000 m, the circulation was elongated within the canyon head (not visible in Figure 5.4 at this resolution).

In a typical eddy pair, the cyclonic eddy is north of the anticyclonic eddy at formation, while a second cyclonic eddy can form from cool water drawn to the anticyclonic eddy's south (Figure 4.10b). Part of an eddy pair during development is shown in Figures 5.3 and 5.4. One of the eddies was over the canyon while the other was outside the depicted area and the canyon's influence. Figure 5.3 shows the anticyclonic eddy over the canyon, but moving offshore to allow a new cyclonic eddy to form over the canyon. Figure 5.4 shows the cyclonic eddy over the canyon and the anticyclonic eddy to the canyon's south. The eddy pair formation process could thus occur with either eddy over the canyon, indicating the canyon contributed to eddy pair formation, but the process was not consistent.

An example from a wind-forced run, in which the Leeuwin Current and Undercurrent were across the canyon, is shown in Figure 5.5. An anticyclonic circulation, which joined the Undercurrent north of the canyon, was present at the head. A tiny cyclonic eddy was at the canyon tip at 400 m. At 800–1000 m, a cyclonic eddy was apparent over the canyon mouth. No strong eddies that were formed from the Undercurrent were in the canyon. The Leeuwin Current and Undercurrent meandered such that they crossed perpendicular to each other, which reduced shear. The thermal structure indicated surface downwelling and deeper upwelling towards the head, with the interface at approximately 400 m. This pattern resembled recent field transects in the Perth Canyon (Chapter 6).

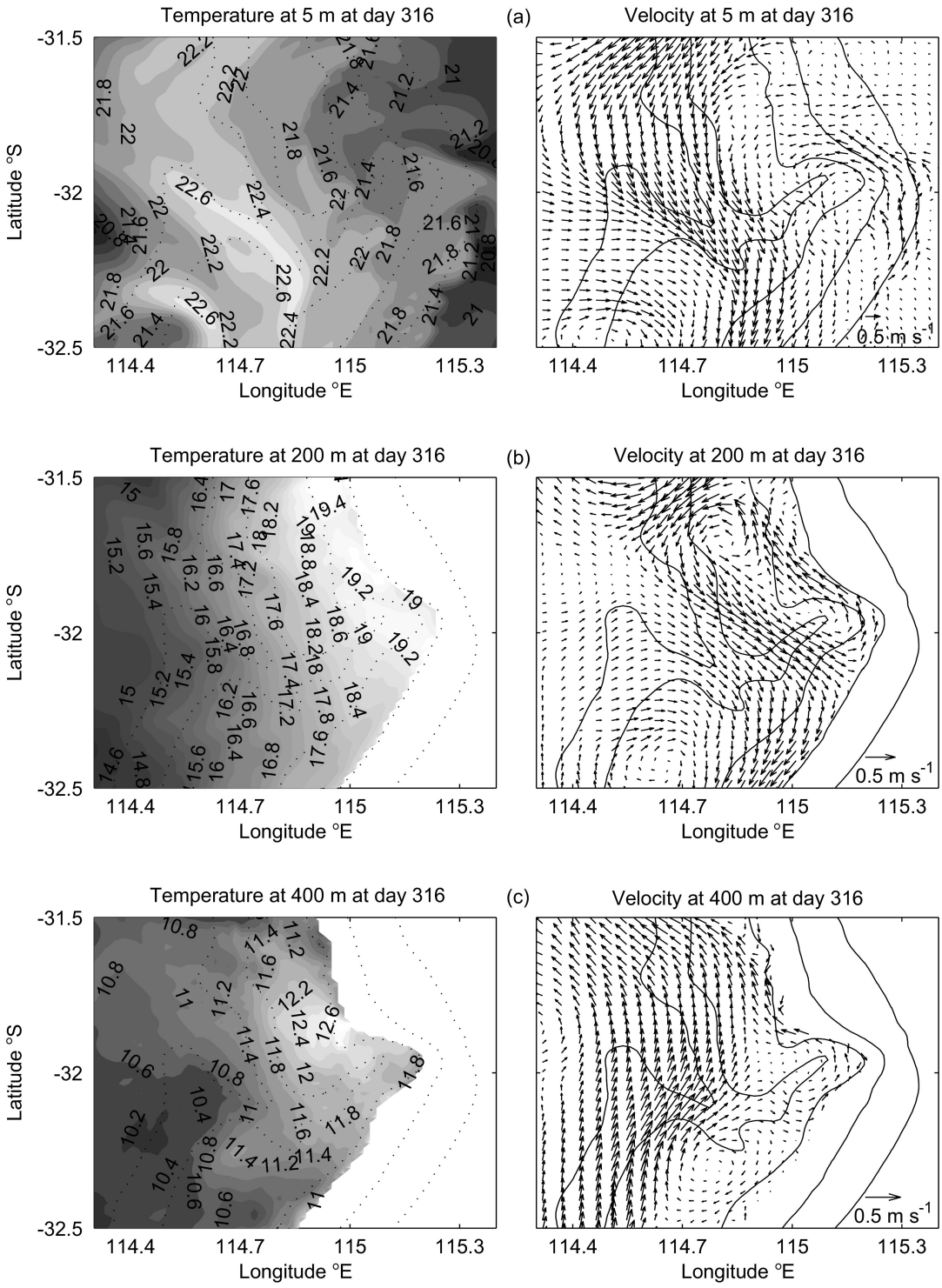

Figure 5.5. Continues next page.

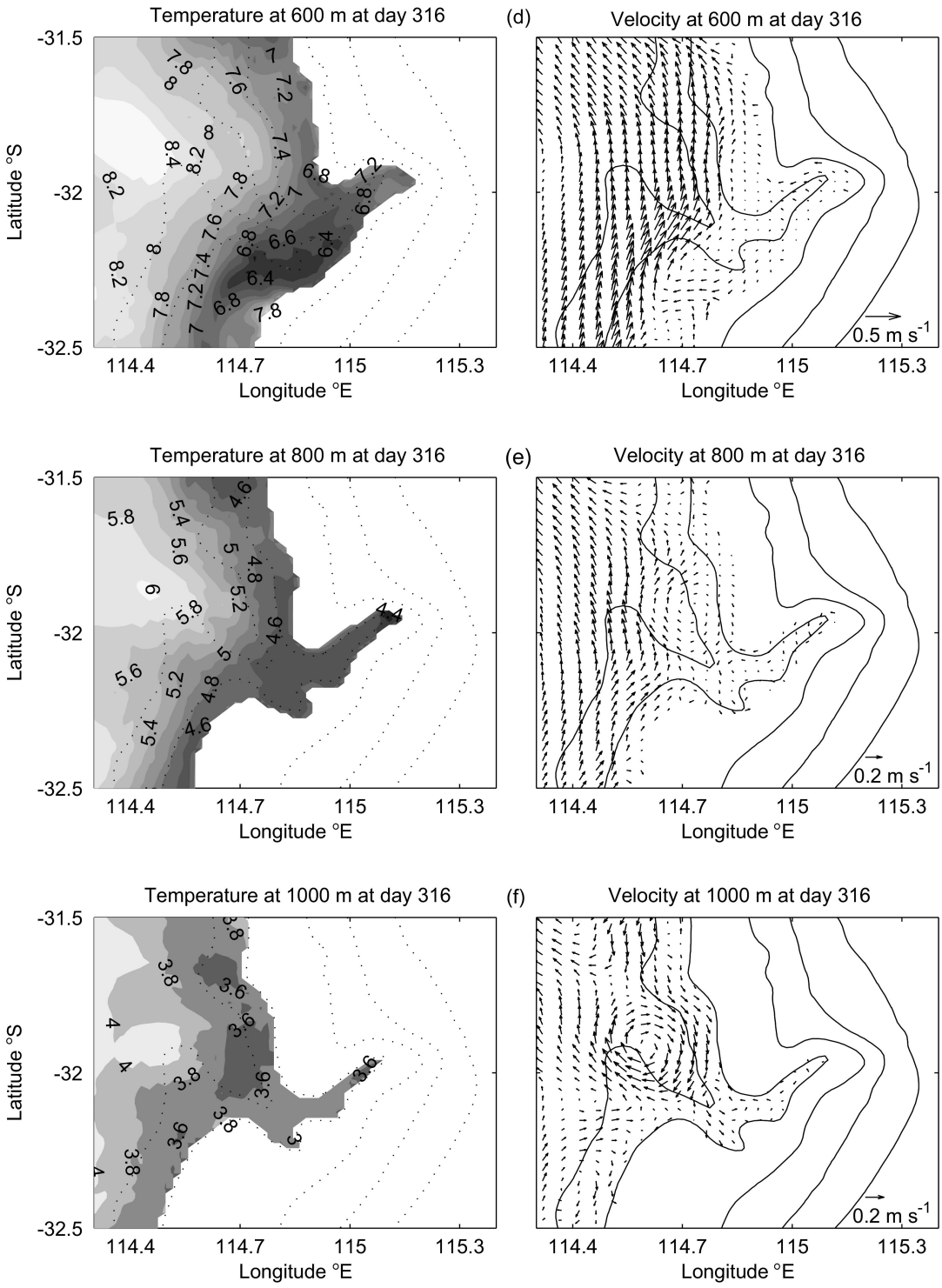

Figure 5.5. Day 316 of the spring wind-forced run showing temperature (left pane) and velocity vectors (right pane). a) 5 m. b) 200 m. c) 400 m. d) 600 m. e) 800 m. f) 1000 m. Bathymetry contours at [100, 200, 500, 1000, 1500] m.

5.4.1.4 General summary of circulation

The canyon circulation was variable, but internally consistent, as the above examples showed. The Undercurrent interacted most strongly with the canyon. Within the canyon, eddies formed continually, bounded by the flow across the canyon and its rims. Small eddies forming in the canyon head would disappear, grow and migrate, or morph into one eddy of a pair. Any Undercurrent flow northward across the canyon would induce a cyclonic eddy upcanyon (i.e. closer to the head), and a flow crossing southward would induce an anticyclonic eddy upcanyon. These 'eddy-generating flows' could be part of another eddy.

A chain of fairly circular eddies of alternating direction aligned along the axis could form because the canyon's length was several times its width. At 1000 m, however, the canyon between the dogleg and the head was too narrow, and the flow became an elongated eddy along the canyon axis. An estimated Rossby internal radius of deformation at several depths showed that at 1000 m depth the Rossby radius became the same as the width (~12 km), whereas above this, e.g. in the Undercurrent, the canyon was wider than the Rossby radius. This could account for the change in eddy shape.

The deeper circulation was congruent with the surface circulation by minimising shear and juxtaposing eddies of opposite directions. Despite this, a confident extrapolation of deep circulation from surface flow did not seem possible because the canyon introduced a greater complexity to the circulation. Furthermore, wind forcing decreased the relationship between surface flow and flow at depth. The eddy field at depth remained coherent, but wind-driven surface flow obscured surface features. The Undercurrent's path and location of eddies might be identified from field or remote sensing measurements if the surface features are identified clearly; if the bathymetry were considered, smaller features could also be estimated. Extrapolating from field data, however, would be a difficult undertaking unless the data were high resolution. As discussed in Section 5.5, the small-scale circulation might be important to the canyon region.

5.4.2 Upwelling and downwelling

Vertical transport is usually measured by proxy, using a tracer, such as temperature, to indicate the displacement of water. Temperature is commonly used because it decreases monotonically with depth (ignoring fine structure) and is easy to measure in the field. Detection of vertical displacement with temperature requires a comparison: either spatial, temporal, or with a mean state. However, a numerical model facilitates use of the vertical velocity, w, which is calculated from the horizontal velocity components u and v. Upwelling, thus, is indicated by positive w values.

Based on the literature (e.g. Klinck 1996), it was expected the Leeuwin Current would produce downwelling, whereas the Undercurrent would produce upwelling. The model agreed with the literature and the author's recently collected field data (next chapter) that the Leeuwin Current pushed isotherms down against the shelf and the Undercurrent pushed isotherms up against the shelf. This occurred in the canyon and elsewhere on the shelf. Horizontal isotherms indicated a boundary occurred at ~400 m. Isotherm depression or doming in the warm-core anticyclonic or cold-core cyclonic eddies indicated eddy-generated upwelling and downwelling. Beyond these, the canyon produced effects on a small scale, which could influence vertical motion. Furthermore, within the canyon, vertical advection, rather than horizontal advection, caused greater temperature changes.

The characteristic flow described in Section 5.4.1 is now examined using temperature to identify its effect on upwelling. The Leeuwin Current over the canyon pushed warm water down into the canyon (e.g. Figures 5.3 and 5.5). If a mesoscale anticyclonic eddy formed over the canyon, the isotherms were depressed near the canyon mouth (e.g. Figure 5.3c–f), as the circulation extended through the water column. In this case, with the Leeuwin Current offshore and the Undercurrent across the middle of the canyon, upwelling due to a cyclonic eddy forming in the canyon head caused cooling. Cool water upwelled on the north rim, where the cyclonic eddy and Undercurrent flows diverged (visible in Figure 5.3c). As the eddy grew, the upwelled water was transported around the eddy to produce a cold spot on the eddy's south side (Figure 5.6). Hence the location of highest vertical velocity

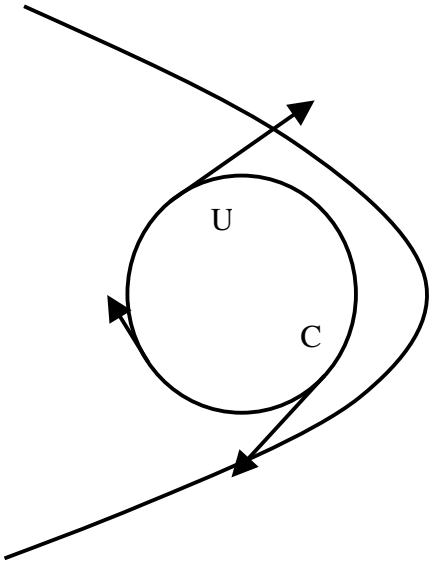

Figure 5.6. Schematic of an eddy in the canyon head. U—upwelling, C—cool water. Similar to the eddy in the head in Figure 5.3c,d. The isobath could represent the 500 m isobath.

does not correspond to the coldest temperature, due to horizontal transport. This cyclonic eddy was present for approximately 50% of the simulation. In contrast, where the Leeuwin Current meandered around the canyon head nearer to shore (e.g. Figure 5.4a), the cyclonic eddy drew cooler water from offshore over the canyon almost to the head, possibly allowing upwelling in the canyon (except at the tip).

To determine if the canyon induced more upwelling than otherwise occurred along the shelf, the vertical flux was examined throughout the domain. The vertical velocity at 100 m, 200 m, and 500 m was collated from the three model runs (spanning 200 days for the no-wind run and 100 days each for the wind-forced model runs), with data every five days. Output at higher temporal resolution showed more detail, but the five-day output was found adequate to represent the trends in vertical flow w for the no-wind run (Figure 5.7). Several parameters were calculated. The mean vertical velocity was calculated to determine if there were certain areas of predominant upwelling or downwelling. The total absolute velocity indicated locations that had the most vertical transport in either direction. The standard deviation indicated the range and variation in different areas. As the sample number was small, a normal distribution was assumed, and several histograms of w suggested

this is a reasonable assumption. A Student's t-test indicated that the areas with mean $|w| > 1.5 \times 10^{-4}$ m s^{-1} in Figure 5.7a were significantly different (P=0.9) from a mean of zero.

5.4.2.1 Upwelling in the no-wind run

For the no-wind model run, the regions of highest vertical flow were near the shelf, particularly within the canyon. The vertical flow within the canyon was stronger, by an order of magnitude, at 500 m than at 200 m or 100 m; at 200 m the flow did not interact greatly with the canyon. In contrast, away from the canyon, the vertical transport near the shelf was similar in magnitude at 200 m and 500 m, but higher at 100 m. Along the shelf edge, the regions of highest vertical flow were those associated with eddy formation.

Within the canyon, there were several distinct areas where the flow was predominantly either upwelling or downwelling at 500 m (Figure 5.7a). At the head, the flow was upwelling at the north rim and downwelling at the south rim, which concurred with Figure 5.6 for a recurrent cyclonic eddy. At the dogleg, the flow was downwelling on the north rim, and the south rim showed downwelling on the spur's south side and upwelling on the south side of the two gullies bracketing the spur.

Examination of the standard deviation of *w,* the vertical velocity, for the canyon region (Figure 5.7b) indicated some of the changeability or persistence of upwelling or downwelling. It revealed if the net velocity over time was due to large incidences, up or down, or small incidences primarily in one direction. The canyon head had a standard deviation similar in size to the mean velocity, and the dogleg had a larger standard deviation than the mean. Examination of the data from nine locations in the upwelling or downwelling regions visible in Figure 5.7a confirmed this. The canyon head locations were either predominantly upwelling or downwelling, with few incidences in the other direction. At the dogleg, the flow was stronger and more variable, often varying between upwelling and downwelling, and a few large events biased the mean. The results from four locations (two upwelling and two downwelling, two at the canyon head and two at the dogleg, but on opposite rims) are shown in Figure 5.8; the locations are marked in Figure 5.7a.

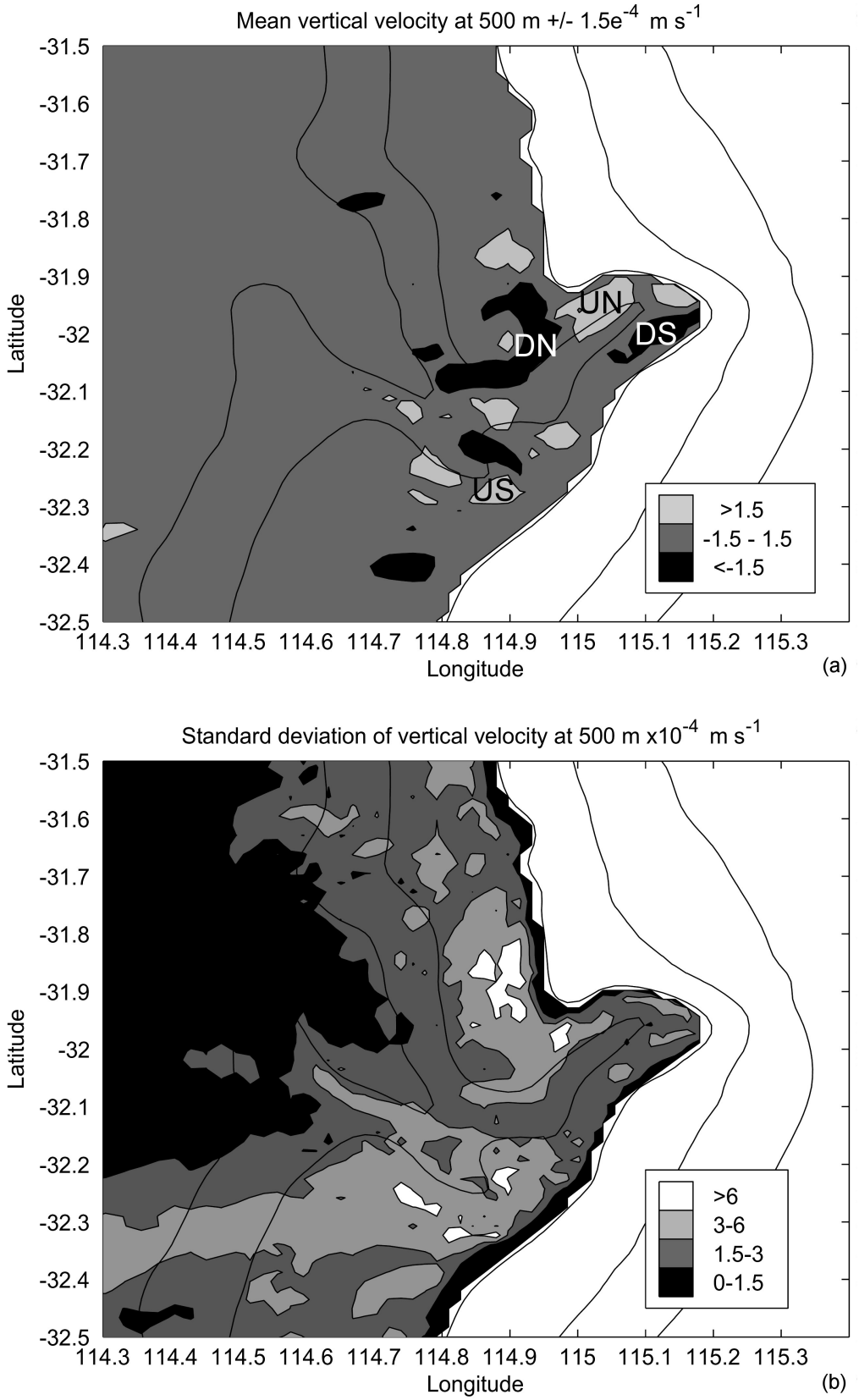

Figure 5.7. a) Regions of mean vertical velocity for the no-wind model run, days 161–361. Black indicates mean velocity <-1.5 x 10^{-4} m s^{-1}, i.e. downwelling; light grey indicates mean velocity >1.5 x 10^{-4} m s^{-1}, i.e. upwelling. U—up, D—down, N—north, S—south. b) Standard deviation of mean vertical velocity (m s^{-1}).

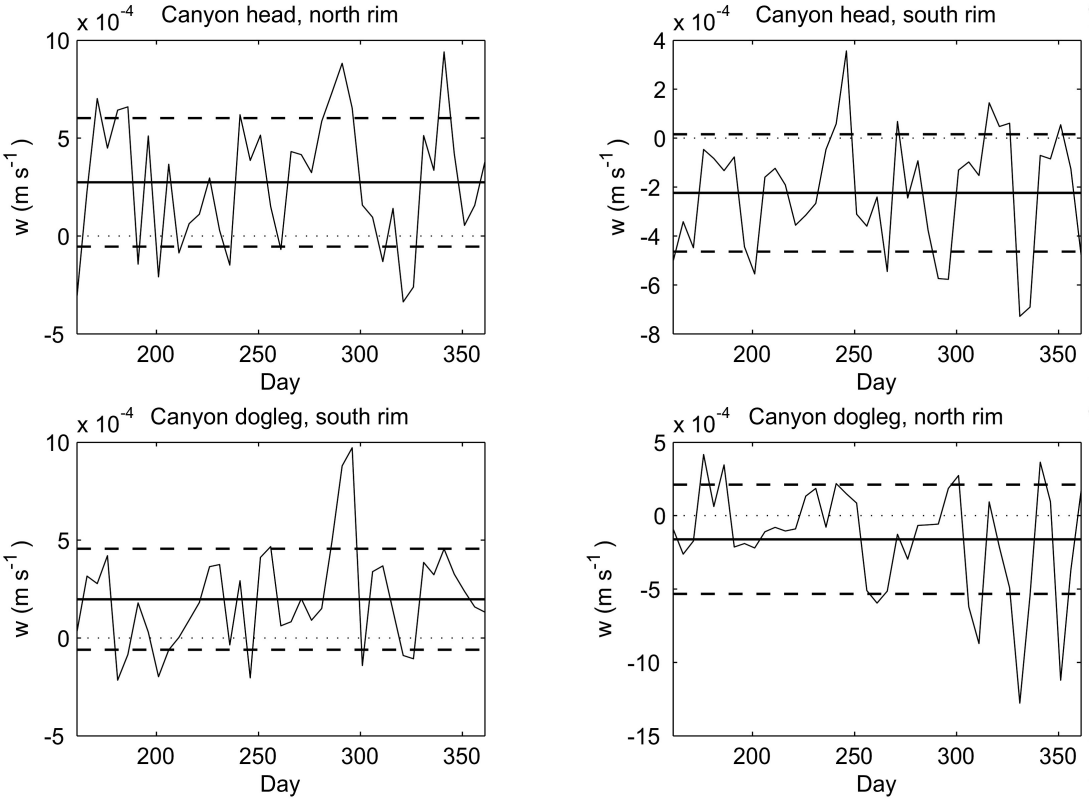

Figure 5.8. Vertical velocity at selected locations in the canyon head at 500 m. Locations are indicated in Figure 5.7a.

Integration over the canyon head region (114.61–115.20°E, 31.81–32.31°S) assessed if there was net flow into or out of the canyon at the head for the model run, hence if water was being circulated onto the shelf. The integrated mean at 500 m was predominantly upwelling over time, and the standard deviation was similar in magnitude to the mean.

Two substantive downwelling events (196–201 and 311 days) and three strong upwelling events (176, 276, and 296 days) occurred. The canyon circulation at these times did not show identical features, but it could be generalised that a cyclonic eddy centred over the south rim would produce a net upwelling. An anticyclonic or cyclonic eddy centred on the north rim could produce net downwelling. This is because the eddy asymmetry affected the size of the region (i.e. the size of the eddy's side) in which upwelling or downwelling occurred. This was similar to Ardhuin et al.'s (1999) results modelling a Mediterranean canyon, where they found upwelling was produced when eddy flow predominantly impinged on one rim. Allen (1996)

also noted that non-linearity shifted the pattern downstream (compared with a linear model) causing asymmetry in the circulation, which greatly increased upcanyon flow because the onshore stream was located over the canyon.

5.4.2.2 Upwelling in the wind-forced runs

With wind forcing, the vertical flow increased by a factor of two to four, and was enhanced over a much larger area (Figures 5.9a and 5.9b—summer run). The canyon was not a focal point, even at 500 m, which was well below the wind's direct influence. The coarse (five-day) temporal resolution was insufficient to represent *w* over time, which could change direction every day or two. The spatial pattern of mean vertical flow, however, was similar for one-day and five-day outputs (compared for 60 days), suggesting the five-day mean was reasonably accurate.

The spring (not shown) and summer runs showed different patterns, but there were similarities at the canyon head. The wind-forced runs' mean *w* patterns also resembled the no-wind run's pattern within the canyon, although the magnitude was different. This showed that the circulation patterns evolving in the canyon recurred, with or without wind, over a hundred days. These runs may be too short, however, to provide a good mean flow result, suggesting a season is a short time in which to determine a mean. As discussed in Section 5.4.1.1, 100 days were required to manifest six flow cases, which supports this.

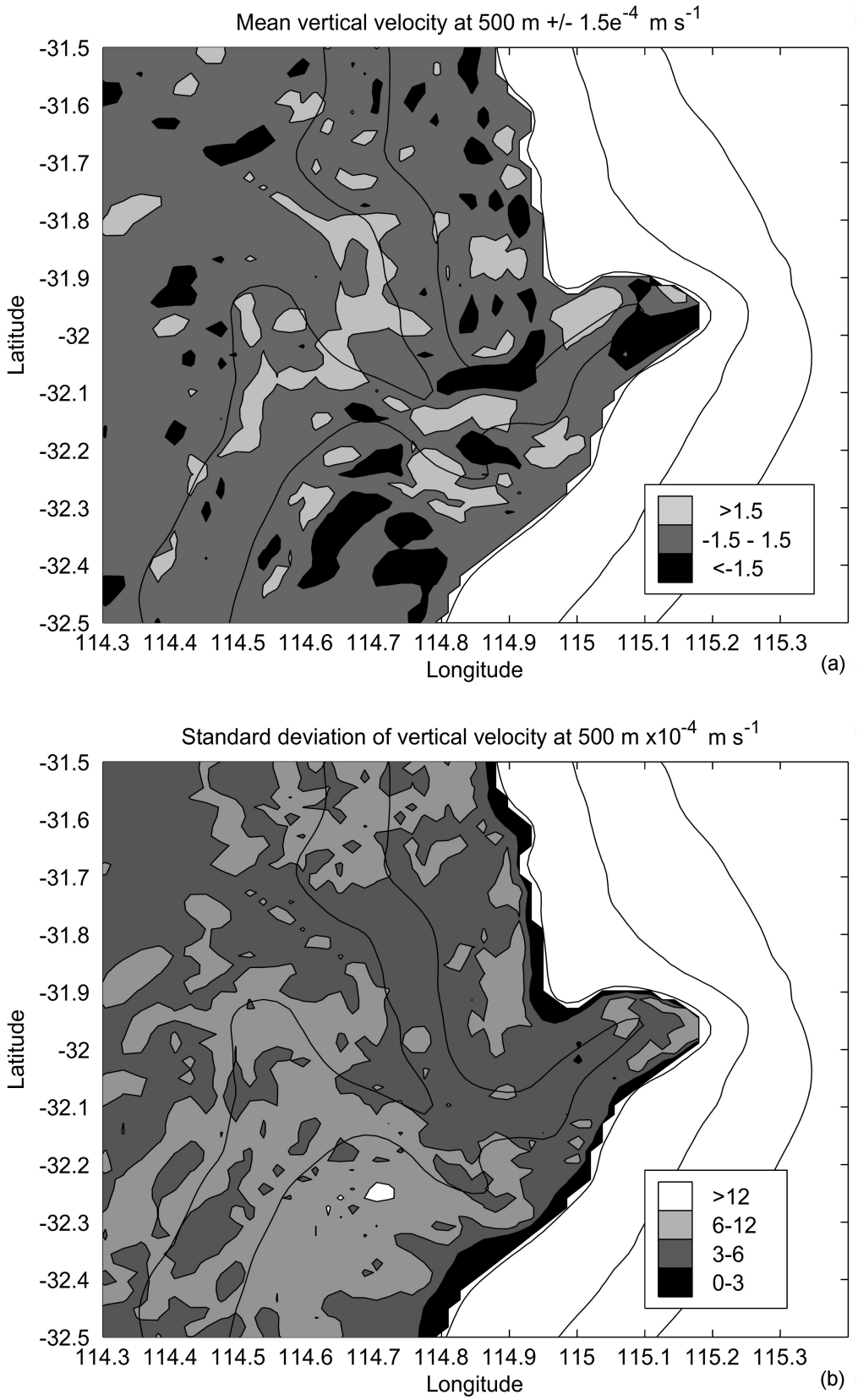

Figure 5.9. a) Vertical velocity for the summer wind-forced model (wind starting January 1, over 100 days). b) Standard deviation for the same run. Note the different scale compared with Figure 5.7b.

5.2.3.3 Comparison with temperature time- series.

The vertical velocities were calculated from the temperature time series presented in Chapter 3 by interpolating the depth of isotherms from the temperature loggers. These were compared with the vertical velocities from the numerical model, as shown in Table 4.1. The model output was an instantaneous calculation at 5 day intervals, while the field data's velocity was calculated from the change in the linearly interpolated isotherm depths over 15 to 30 minute intervals. Horizontal advection was assumed to be zero.

Table 4.1. Mean and maximum velocities (m s^{-1}) for the windforced and non-windforced model runs, and calculated from temperature logger data. *Field data given over entire water column i.e. ranging 50–450 m. Lowest velocities were recorded at the top or the bottom of this depth range.

	No wind run	Wind runs	Field data*
200 m mean	$\pm 3 \times 10^{-4}$	$\pm 5 \times 10^{-4}$	$\pm(1.5–2) \times 10^{-3}$
200 m max.	$-6–12 \times 10^{-4}$	$\pm 2 \times 10^{-3}$	$\pm(5–10) \times 10^{-3}$
500 m mean	$\pm 4 \times 10^{-4}$	$\pm 4 \times 10^{-4}$	–*
500 m max.	$\pm 2.5 \times 10^{-3}$	$-2.5–4.5 \times 10^{-3}$	–*

The velocities from the field data are at least two to three times larger than those from the numerical model. Apart from the difference between how the vertical velocity was derived, the explanation for this discrepancy is probably that the model does not reproduce the vertical velocity precisely.

Comparing the net distance isotherms travel over 5 day intervals for the model and field temperature data on the plateau, both evince changes of the same range, which was less than 150 m. This agreement over a coarse scale is as good as might be expected from the model's limiting spatial and temporal scales.

5.4.2.4 Summary of upwelling

The circulation frequently included the Undercurrent across the middle of the canyon and cyclonic circulation over the dogleg or against the rims, which produced upwelling to at most 200 m. The cyclonic eddy within the canyon head, which

occurred when the Undercurrent crossed the canyon over the dogleg, was similarly frequent. The Leeuwin Current, however, maintained downwelling along its path, and usually diverted around these upwelling regions.

It was apparent the canyon's presence modified the flow by encouraging eddies to form, which impacted on the degree of upwelling that occurred, particularly below the canyon rims. The Undercurrent favoured upwelling through favouring the formation of cyclonic eddies. It was also evident the Leeuwin Current's location controlled the upwelling within the top few hundred metres. The Leeuwin Current's meanders drew in water from offshore, which decreased stratification and mixed with the Leeuwin Current, to influence where upwelling might be increased. Incidentally, eddies are often indicated in sea colour images as having increased chlorophyll where the water masses mix.

5.5 Discussion

This study posed the question: how does the Perth Canyon affect biological productivity? From anecdotal evidence, i.e. the presence of feeding whales, the Perth Canyon has episodes of high productivity that can produce sustainable quantities and dense swarms of krill. This modelling study was used to examine the ocean's physical interaction with the canyon and infer how this would affect productivity in the region.

The hypotheses regarding increasing productivity and prey density are well established and can be found in many canyon studies. It is perhaps not surprising that the Perth Canyon, along the whole WA coast, is a region of relatively high productivity on an oligotrophic coastline. The two mechanisms considered the 'usual suspects' for promoting dense krill swarms are upwelling and entrapment. This study aimed to determine which mechanisms played a role—and to what degree—within the Perth Canyon and if episodic events or seasonal changes were important. Canyons have been cited as both causing and enhancing upwelling, which can bring deep, nutrient-rich water towards the surface and the productive euphotic zone. Canyons also enhance downwelling, and the current direction determines the vertical transport. The other mechanism, entrapment, refers to the

ability of eddies or canyons to 'trap' material within them, increasing residence time and encouraging aggregation, which could also boost productivity.

Upwelling was evaluated using temperature and vertical velocity. The vertical temperature structure along the shelf indicated that between the Leeuwin Current and Undercurrent was a barrier to upwelling and downwelling at 300–400 m. The circulation within the canyon, however, also contributed to upwelling and downwelling, and was able to produce upwelling to above 300 m, particularly at the head and around the canyon rims. The vertical velocity indicated that recurrent patterns within the canyon were associated with regions prone to upwelling or downwelling. The canyon rims are well below the euphotic zone, so even water upwelled onto the shelf would not be upwelled to the euphotic zone. Mixing, which may be provided by the wind, would then become important. The summer winds caused shallow upwelling from a depth of 100 m, onto the shelf, to produce the Capes Current, which was too shallow to originate from below the oligotrophic Leeuwin Current or within the canyon.

An abundance of eddies were formed and trapped within the canyon. It was not verified if these eddies could trap material, although the literature supported this hypothesis (Allen et al. 2001; Bosley et al. 2004; Sánchez-Velasco & Shirasago 1999; Vetter & Dayton 1998). Previous studies indicated closed eddies formed in narrow canyons where the canyon was narrower than the Rossby radius (Ardhuin, Pinot & Tintore 1999; Hughes, Ofosu & Hickey 1990; She & Klinck 2000). Ardhuin et al. (1999) simulated a secondary circulation within a canyon, similar to the multiple eddies that occurred in this study. Rossby radius estimates for the Perth Canyon were a similar order of magnitude to the canyon width at the head and deep in the canyon. Below 1000 m, the circulation became elongated where the canyon was very narrow.

Eddies forming within the canyon were initially confined and had to grow to escape the canyon, unlike eddies forming against the open shelf. Furthermore, at least one eddy was within the canyon at all times, even if it was very weak. The canyon circulation also appeared to produce flow that impinged against the rims, which could cause entrapment (Allen et al. 2001). Specifically, the Undercurrent crossed

the canyon, encountered the wall, and diverged, with a part forming a closed upwelling eddy in the head, similar to that observed in She and Klinck (2000, e.g. figure 6b) or Ardhuin et al. (1999).

In summary, the canyon did not generate upwelling of water straight to the euphotic zone, but it did encourage upwelling to below the Leeuwin Current. Other mechanisms must be invoked to bring the nutrients into the euphotic zone. The persistent southerly winds might assist by increasing the mixed layer depth and encouraging shallow upwelling on the shelf. The occurrence of eddies within the canyon should also encourage aggregation and prolong the residence of nutrients and biota as well as contribute to the vertical transport. These factors contribute to the likelihood of the canyon being a high productivity area, although alone they would be ineffectual. The Leeuwin Current always acted as a barrier to upwelling, which, theoretically, the southerly winds might reduce. This was not replicated in the model, however, possibly owing to the short period modelled compared with the timescale of Leeuwin Current meanders. Other mechanisms, such as internal waves, that could contribute to upwelling and mixing were unable to be modelled and must be evaluated using other means.

5.6 Conclusions and Recommendations

The Perth Submarine Canyon's circulation was analysed using ROMS to simulate a large section of the southwest Western Australian coastline. The model generated a realistic Leeuwin Current and Undercurrent from density gradients, and produced a Capes Current with wind forcing. The Undercurrent interacted strongly with the canyon, whereas the Leeuwin Current interacted with only the canyon head at around 200 m depth; however, the Undercurrent and Leeuwin Current interacted with each other.

The circulation in the canyon had no steady state, but changed continually on a timescale of days to weeks. Eddies sometimes recurred within the canyon, indicating the canyon regulated the circulation. A season was found to be too short to typify the flow or its variability. The formation of eddies within the canyon conformed to other studies where closed eddies formed (Ardhuin, Pinot & Tintore 1999; Hughes, Ofosu

& Hickey 1990; She & Klinck 2000). The Perth Canyon, which is crooked and longer than many other studied canyons, formed several eddies along its length, which were circular but became elongated at 1000 m and below, where the canyon was narrower.

The Perth Canyon tended to have strong vertical transport, particularly associated with the Undercurrent. The results showed that eddies forming within the canyon usually produced infrequent strong events or weaker, but recurring, events that generated localised vertical transport. The addition of wind increased the vertical transport everywhere. The Leeuwin Current formed a barrier, which limited upwelling, so it may be assumed upwelling of nutrients to the euphotic zone would depend on the Leeuwin Current's location and thickness. Upwelling within the canyon tip was favoured when the Leeuwin Current shifted offshore. The wind could assist with upwelling and mixing, and the formation of eddies within the canyon could increase residence time in the canyon for nutrients and biota.

Applying heat exchange (insolation, exchange to atmosphere), which might allow a wind-forced model to run for longer without degrading the density gradients, could improve these results. This would then allow a statistical evaluation and a better assessment of seasonal changes.

CHAPTER 6

Physical Properties and Processes in the Perth Canyon, and Their Links to Productivity and Blue Whales

6.1 Summary

The oceanography of the Perth Canyon was examined through two field excursions combined with previous results from field analysis and numerical simulations. Water properties were assessed to identify water masses and vertical movement. The distribution of chlorophyll in the surface layers indicated high spatial variability, with a deep chlorophyll maximum at ~80 m. The input of nutrients to the euphotic zone occurred sporadically as the Leeuwin Current generally suppressed upwelling, although the Perth Canyon increased nutrient concentrations within its rims. The circulation measured during the field cruises showed many of the same features, such as eddies, that appeared in the simulation of circulation. Aggregations of krill and other acoustic backscatter targets were concentrated near the head of the canyon at a range of depths, which may have been promoted by the circulation. Overall, it appeared that many factors might contribute favourably to the appearance of feeding blue whales at the Perth Canyon during summer, but none would be sufficient alone. The canyon could promote both upwelling and aggregation to boost productivity and attract the whales while the seasonal changes in the wind and light cause seasonal productivity variations.

6.2 Introduction

The Perth Canyon is a significant feature of the south-western continental shelf of Western Australia (WA) (Figure 6.1). It is a large, deep canyon and hundreds of kilometres from any other canyon of comparable parameters. The Perth Canyon region recently came under intense study because it is a feeding area for pygmy blue whales (*Baelenoptera musculus brevicauda*) during summer. Little was known about the whales, including their population size, feeding habits, and where they

reside during other parts of the year. Also unknown – and the focus of this study – was how the canyon region attracts whales. The primary hypothesis was that processes associated with the canyon create conditions that promote the dense krill swarms that have since been observed and sampled (R. McCauley, unpublished data) and on which the whales feed.

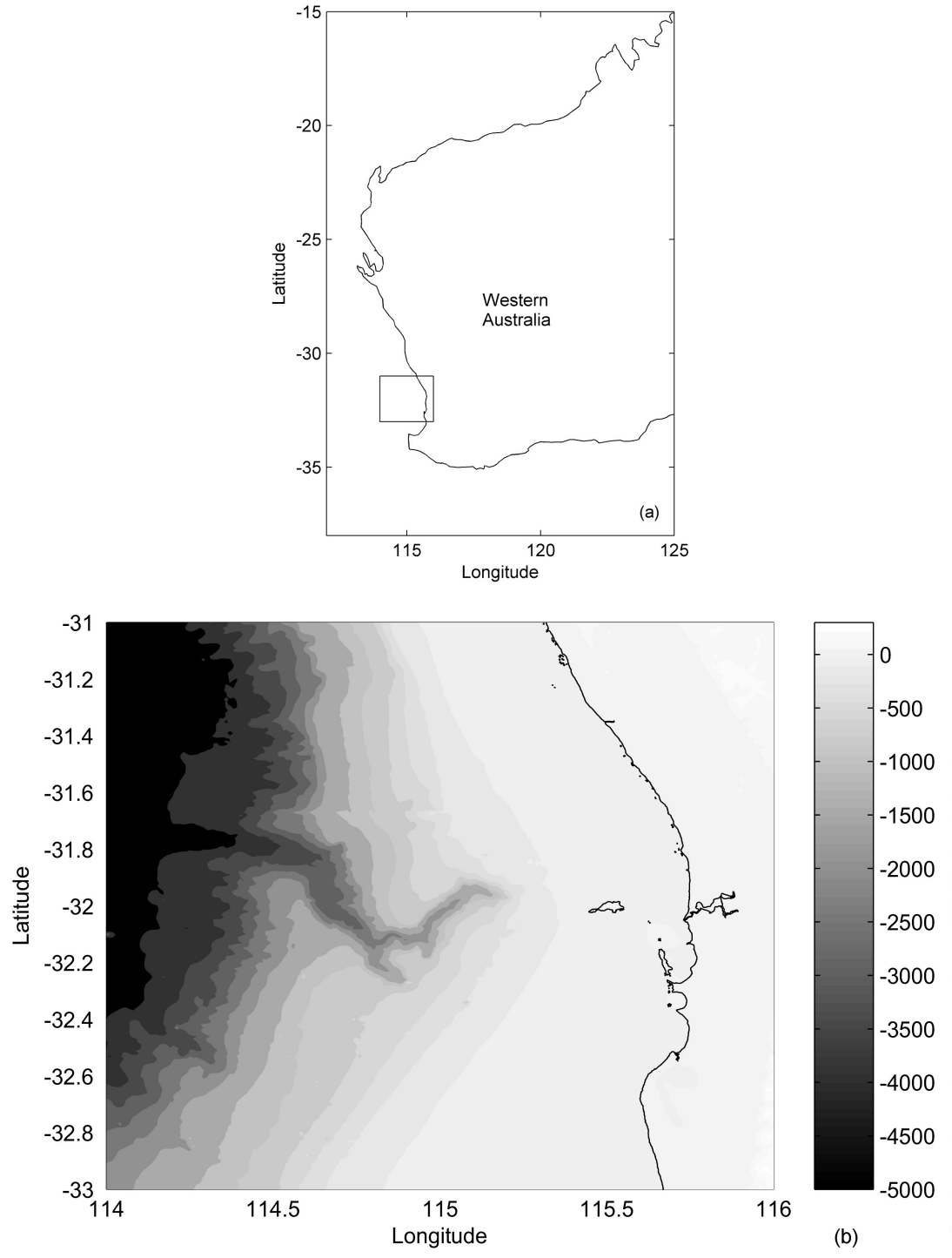

Figure 6.1. a) Australia showing inset of b) Perth Canyon bathymetry with depth in m.

A number of studies associated feeding marine megafauna with topographic features like canyons (Croll et al. 2000; D'Amico et al. 2003; Hooker, Whitehead & Gowans 2002; Schoenherr 1991). One of the more intensely studied cases is Monterey Canyon in Monterey Bay, California, USA. The canyon itself has been the subject of much oceanographic study (Carter & Gregg 2002; Croll et al. 2000; Landry & Hickey 1989; Petruncio, Paduan & Rosenfeld 2002), including as a centre of upwelling. Upwelling in Monterey Bay occurs from late winter through to late summer (boreal seasons). Primary production increases in mid-March, and the period of maximum zooplankton abundance occurs a few months later in summer. This coincides with the highest abundance of blue whales (Croll et al. 2000). The whales target very dense patches of prey, which in Monterey Bay occur at the surface and subsurface at around 150 m. The prey prefer the steep topography of the canyon rims (Schoenherr 1991), where they can remain in highly productive upwelling areas throughout their diurnal migrations (Croll et al. 2000). Blue whale sightings in Monterey Bay were concentrated along the rims of the canyon, similar to sightings at the Perth Canyon.

The studies of other canyons provided some suggestions for investigating the physical processes that may ultimately be linked to the presence of whales in the Perth Canyon. Upwelling would be an important mechanism for biological productivity and has often been associated with canyons. However, the surface current over the Perth Canyon is the poleward-flowing Leeuwin Current, which is oligotrophic and suppresses upwelling (Pearce 1991). Previous chapters searched for evidence of upwelling or downwelling in the Perth Canyon, to characterise its occurrence. The offshelf or onshelf transport of organic detritus can be funnelled through a canyon (Allen et al. 2001; Granata et al. 1999; Macquart-Moulin & Patriti 1996). The canyon circulation can include strong eddies which can trap material within them. Vorticity stretching and geostrophic balance within the canyon can also lead to advection of e.g. microzooplankton against the slope. Such aggregation within canyons boosts density and residence time. These processes found in other canyons form the basis for the analysis of a broad collation of data.

The aim of this study was to elucidate the physical oceanographic processes that occur in relation to the Perth Canyon. A derivative from this was to understand the

relationship to the biological oceanographic aspects, and thence to apply this to the appearance of the blue whales. The data dealt with in this paper were primarily from two cruises. However, the analysis combined these data with other data, including from temperature loggers and whale sightings collected over several years, and numerical simulation results.

6.3 Study Area

The Perth Canyon is a relict of the Swan River drainage system, cutting into the shelf west of Perth and Rottnest Island. At the canyon head the depth plunges from 200 m to 1000 m. The canyon mouth opens onto the Abyssal plain at 4000 m. In between, the canyon curves sinuously over 100 km, with a sharp bend halfway referred to as 'the dogleg', as shown in Figure 6.1b. Two small branches are present on the south rim near the dogleg. Features to note on the north rim are a plateau delineated by the 500 m contour, and a small gully on the eastern side of this plateau. These can be more clearly seen in Figure 6.2b.

The Leeuwin Current, a poleward eastern boundary current, flows along the shelf break and hence over the canyon (Figure 2.3). This is a strongly downwelling-favourable current, so the upwelling that is found on other eastern ocean boundaries does not occur on the Western Australian coastline. There are many studies regarding the Leeuwin Current and its dynamics (e.g. Cresswell 1996; Fang & Morrow 2003; Feng et al. 2003; Godfrey & Ridgway 1985; Pearce & Griffiths 1991; Smith et al. 1991; Thompson 1984; Weaver & Middleton 1989). The Leeuwin Current flows year round, but weakens in response to strong southerly winds in summer. It consists of meanders, jets and eddies, with the main flow over 100 km wide at 32°S. The southward flow there extends to around 300 m depth, but may extend 100 m deeper when running strongly, or 100 m shallower when weakened by winds (Smith et al. 1991).

Inshore of the Leeuwin Current is a seasonal, northward-flowing current called the Capes Current (Figure 2.4). The Capes Current is sourced by cool upwelled water from the bottom of the Leeuwin Current between the Capes Naturaliste and Leeuwin

at around 34°S, in response to the strong and persistently southerly winds during summer (Gersbach et al. 1999; Pearce & Pattiaratchi 1999).

Underneath the surface flow, the Leeuwin Undercurrent (Figure 2.3) has a net velocity northward with measured speeds of 0.1–0.4 m s^{-1}, (Smith et al. 1991; Thompson 1984). The Undercurrent stays close to the shelf and has a maximum velocity at around 500 m. The Undercurrent is driven by an equatorward pressure gradient, which is thought to be linked to the presence of the Leeuwin Current above it (Thompson 1984; Woo 2005).

6.4 Assimilated Data

The work described in this chapter combines data from field cruises with other data and results from previous studies of the Perth Canyon, including from the previous chapters. Summaries of the results from previous analyses are included in this section.

6.4.1 Field trips

Two oceanographic cruises collected data from the Perth Canyon. Cruise 1 (ID SS09/2003) took place in late spring 2003 (24 October–9 November) and cruise 2 (ID SS02/2004) in mid summer 2004 (29 January–4 February). Both cruises were on the National Facility—Ocean Research Vessel Southern Surveyor, owned and operated by Australia's CSIRO (Commonwealth Science and Industrial Research Organisation).

Cruise 1 covered the southwestern coast of WA (Figure 6.2a) from just north of the Abrolhos Islands (27.5°S) to Point D'Entrecasteaux (35°S) and included transects both along-axis (31/10/2003) and across-axis (7/11/2003) of the Perth Canyon (Figure 2b). CTD casts for the along-axis transect were made at 3000 m, 2500 m, then spaced along the axis to 1000 m, then up the canyon head towards Rottnest Island at 750 m, 530 m, 370 m, 290 m, 180 m, 130 m, 100 m, and 50 m. CTD casts on the across-axis transect were made along the 115.02°E line at depths of approximately 300 m, 500 m, 600 m and 1000 m (south rim), and 1000 m, 500 m,

400 m and 300 m (north rim), which were approximately equally spaced. This transect crossed the plateau delineated by the 500 m isobath on the northern rim of the canyon (visible in Figure 6.2b), which is referred to subsequently as 'the plateau'.

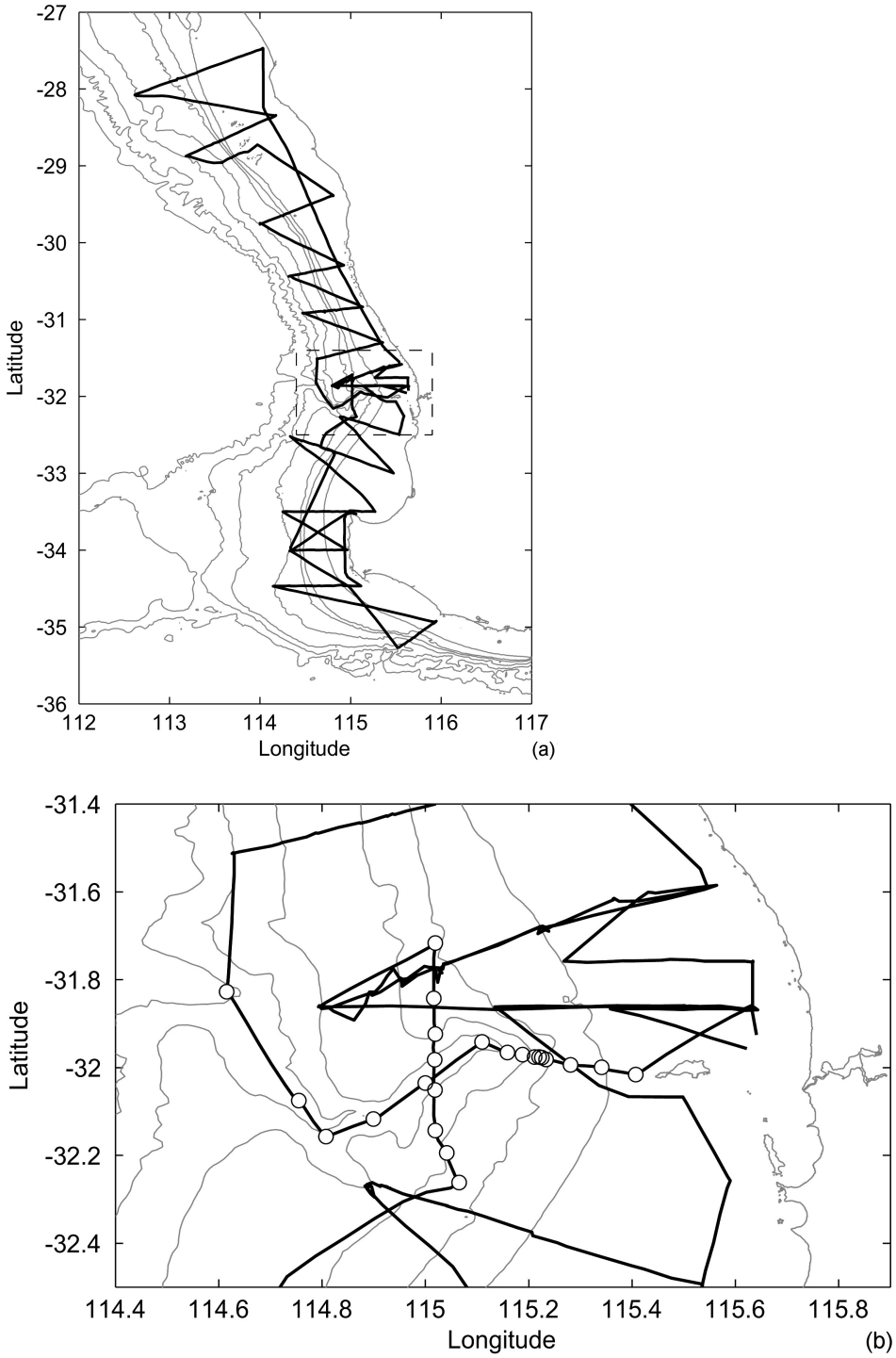

Figure 6.2. a) Cruise 1 track. b) Cruise track and CTD station locations for Rottnest transects along axis and across canyon axis for cruise 1 (SS09/2003). Bathymetry contours at 100, 200, 500, 1000, 2000 and 3000 m. The along-axis transect started at the 3000 m contour and finished at 50 m. The across-axis transect went approximately between the 300 m contours at 115.02°E.

The second cruise (29/1/2004-3/2/2004) focused only on the canyon (Figure 6.3). This cruise took place at the start of the peak time for blue whale sightings, which is February-March. Several blue whales were sighted during the cruise. The hours between 2 am and 2 pm were devoted to CTD stations, and between 2 pm and 2 am to trawling (Engel pelagic fish trawl or EZ plankton net) for fish, krill or significant acoustic scatter targets that appeared on the vessel's echo sounder. Details of this biological study are dealt with elsewhere (McCauley et al. in prep.) although the echo sounder data was utilised in the analysis here (see Section 6.5.5). CTD casts were made in an approximate grid designed to include several latitudinal and longitudinal transects and also provide reasonable spatial coverage. The transects included one at 115.02°E to repeat cruise 1's measurements, and additional casts to form an along-axis transect to 2500 m and to increase sampling around the head. Some consideration in the analysis was made for temporal variations as most transects were not measured in one day. For example, the along-axis transect was a combination of casts from days 1, 2 and 6.

Each cruise gathered data from a CTD (for temperature, salinity and pressure) mounted on a rosette that carried additional instruments to measure fluorescence,

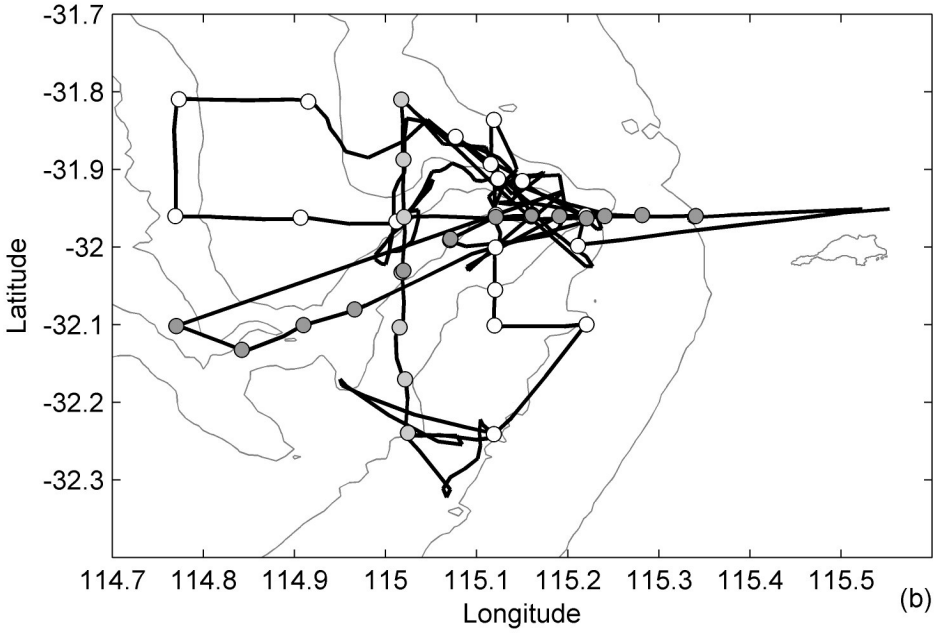

Figure 6.3. CTD station locations and cruise track for cruise 2 (SS02/2004). Bathymetry contours at 100, 200, 500, 1000, 2000 and 3000 m. Along-axis stations in darker grey, across-axis stations in lighter grey.

dissolved oxygen, and light (PAR) readings, with the remaining spaces on the rosette were occupied by Niskin bottles to sample for nutrients (silicate, nitrate and phosphate) and calibration. Cruise 1 had in addition a transmissometer for light transmission in the water. Cruise 2 used a Lowered Acoustic Doppler Current Profiler (LADCP) for stations where the depth was greater than the ship's ADCP could register (~300 m). Both cruises used the ship ADCP continuously. The biological productivity for cruise 1 is presented in Twomey et al. (submitted); C. Hanson undertook biological measurements during cruise 2.

6.4.2 Numerical model

The circulation of the southwest of Western Australia and the Perth canyon was simulated with ROMS (Regional Ocean Modelling System, Haidvogel et al. 2000). The application of ROMS to the region was described in Chapter 4 and the analysis of circulation in the canyon in Chapter 5. The simulations indicated that upwelling generally occurred at the depth of the Undercurrent, but the Leeuwin Current acted as a barrier against upwelling to the surface. Upwelling in the canyon penetrated closer to the surface when the Leeuwin Current diverted inshore or offshore. The Perth Canyon generated many eddies in the Undercurrent, which strongly affected the vertical transport, particularly through the formation of cyclonic eddies within the canyon or along its rims. Furthermore, these eddies would theoretically increase residence time within the canyon for passive tracers and also encourage aggregation of biota.

6.4.3 Temperature loggers

Strings of temperature loggers were moored on the Perth Canyon rim discontinuously over four years (Chapter 3). One mooring was located at the head of the canyon and seven others were located on the plateau delineated by the 500 m isobath on the northern rim of the canyon (Figure 3.1). The temperature changes revealed the processes that affect the water in the canyon's vicinity, which included weather and climate, meanders of the Leeuwin Current, and internal waves. The canyon may have had increased mixing near the head. The canyon head and plateau showed different features, which reflected a spatial scale (~20 km) relevant to the movement of water. The loggers also indicated that upwelling and downwelling at

the level of the canyon rim (500 m in this case) happened sporadically; 14–20% of the time was upwelling-affected and a similar period was downwelling-affected.

6.4.4 Whales

Population surveys of pygmy blue whales were undertaken between 1999 and 2004 by the Centre for Whale Research (boat), Western Australian Museum and Western Whale Research (aircraft), and Curtin University of Technology (passive acoustics). The manifold purposes were to estimate the population size and trend of the whales, to form a database of identified individuals, tag individuals with satellite GPS trackers, obtain samples for DNA analysis, and research the behavioural patterns of the whales. The blue whales were noted to be migratory feeders, with a migration and feeding pattern dictated by the sequence of productive areas peaking in prey abundance. Typically, blue whales feed on a large mass of very dense prey, then move on. A similar pattern was expected in the Perth Canyon, where sightings could number above 30 whales on one day, though it is unlikely that such numbers would be sustained for an extended period in an area not renowned for high productivity. Annual mean whale call rates determined from passive acoustics over 2000-2005 indicated annual variability suggestive of an oscillatory seasonal visitation pattern, although correlation with variables such as the Southern Oscillation Index (to denote El Niño periods) has not been established (R. McCauley, pers. comm.).

Figure 6.4a shows the aerial survey flight paths and Figure 6.4b the aerial blue whale sightings (data from WAM). This combines three survey regions: conducted from the canyon south to Geographe Bay (Figure 2.1); conducted over the canyon exclusively; and conducted from the canyon north to 31°S. The surveys all included the canyon, but despite this bias it became clear that there were many more whales in the canyon than away from it. Hence the surveys were focused on the canyon to conserve effort. The aerial surveys gave the best spatial coverage for whale distributions. The boat surveys (data from CWR, Figure 6.4c), in contrast, targeted the whales, so effort was concentrated on where the whales were most consistently found. This was the northern rim on the plateau and a tributary branch (the 'gully') on the eastern side of the plateau. Most whale sightings occurred in a water depth range of 300-600 m.

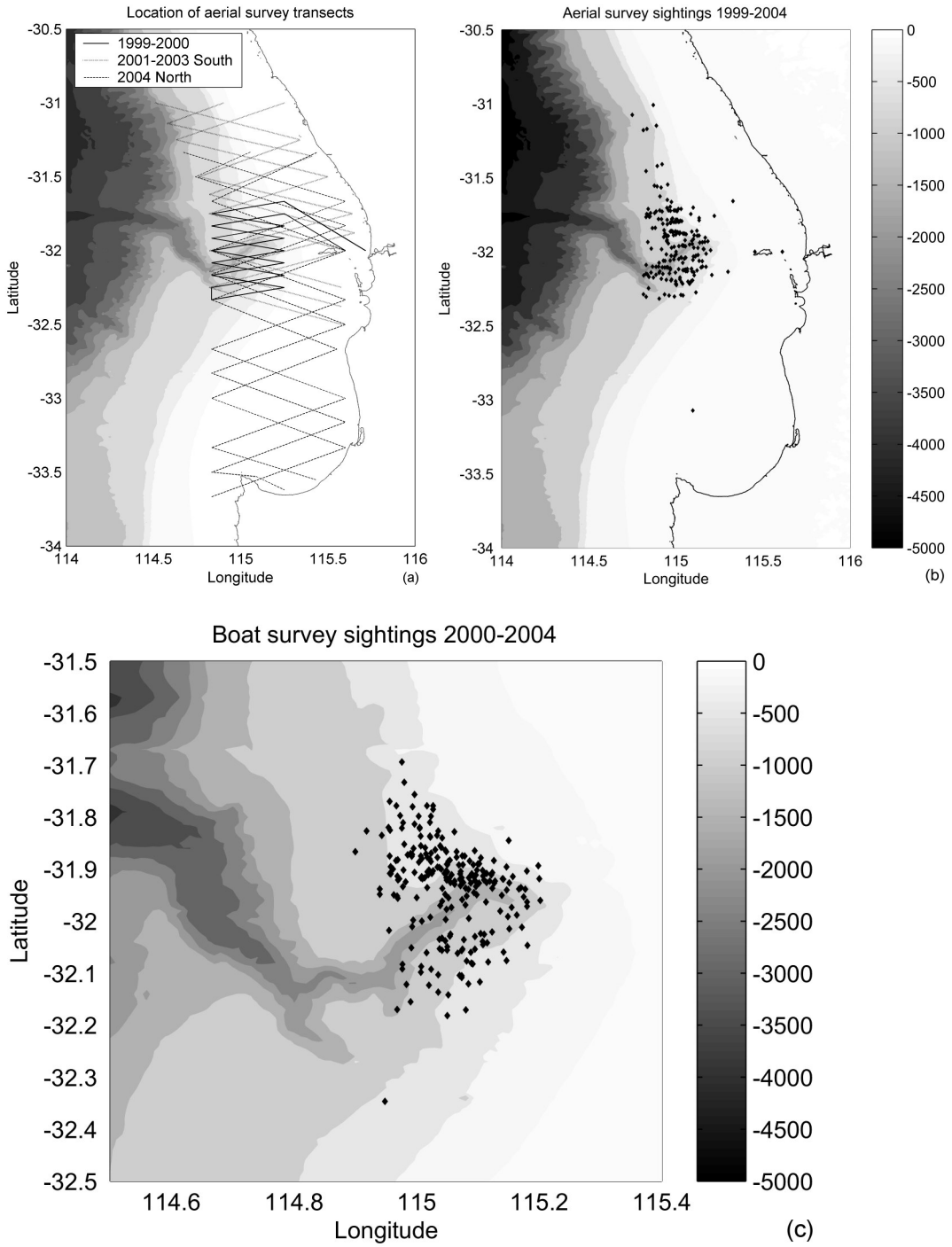

Figure 6.4. a) Location of the three aerial survey paths. b) Location of aerial sightings of pygmy blue whales. c) Boat survey sightings of pygmy blue whales. For boat surveys: total whales = 425, total survey miles = 11 423, total survey hours = 1 366.

The mean whale resighting period (from boat surveys) was 21.3 ± 8.3 days (± 95% C.I.) which suggested whales stayed within or near the canyon for two to four weeks. Satellite tags provided additional information on several whales' movement (Jenner and Gales, unpublished data). Of four whales that were tagged, one was found to

stay in the canyon for 8 days during March 2002, foraging around the rims and the head of the canyon. A whale tagged in December 2002 in Geographe Bay around 1.5° south of the canyon was located 43 days later in the subtropical convergence zone at 122°E. The third tagged whale in late March 2004 spent the subsequent 16 days traversing a region between the canyon (32°S) and the shelf break at 31°S. The fourth tagged whale from late March 2004 traversed the shelf up north to the Abrolhos but further offshore, having travelled perhaps 425 km in 7 days.

6.4.5 Echo sounding data

During cruise 2 the RV Southern Surveyor operated Simrad EA500 (12 kHz) and EK500 (38kHz) single beam sonars. The acoustic backscatter, combined with targeted EZ net tows, showed that krill (*Euphausia recurva* predominantly) occurred in a deep scattering layer at 300–500 m during the day (R. McCauley, pers. comm.). At night, this layer rose up to the chlorophyll maximum at ~80 m, presumably to feed. Other aggregations occurred just below the Leeuwin Current, at the boundary between water layers. Also during the day, krill formed small dense clusters near the rims of the canyon at 200–300 m, which dispersed at night to form new patches. The echo sounder records indicated the greatest biomass was over the canyon rims, near the head. An echo sounder was also used during other field trips to deploy and retrieve moored equipment. On one trip a whale was detected diving directly down towards the deep scattering layer at ~420 m, while during another trip the echo sounder showed a whale making diving lunges through the deep scatter layer at almost 500 m (R. McCauley, pers. comm.), which is believed to be typical feeding behaviour.

6.5 Analysis

The field cruise data were analysed to produce a description of the physical characteristics and the hydrology of the canyon during the two cruises. The data were then combined with other data described in Section 6.4 to further illuminate processes within the canyon.

6.5.1 Temperature, salinity and oxygen: Water masses

The temperature, salinity and oxygen values elucidated the major water masses present, as shown in the T-S-O diagram in Figure 6.5. The surface water was Leeuwin Current water as the cruises did not go offshore far enough to reach oceanic water; the Capes Current water was sourced from the Leeuwin Current's base (Gersbach et al. 1999; Pearce & Pattiaratchi 1999). In cruise 1, near the surface, the top ~150 m showed variation in salinity and temperature which conformed to a typical Leeuwin Current signature of 35.7–35.8 psu and 16-19 °C for this latitude and season (Feng et al. 2003). During the second cruise the range of T-S values was much greater. This was due to the surface temperature being ~3 °C warmer for cruise 2 and the stratification having an irregular, step-like structure nearer the canyon head, which caused greater variation away from the mean stratification. The stratification during cruise 2 was stronger, as the temperature at 450 m (the base of the thermocline) coincided for both cruises. Below the well-mixed layer (WML), which had a depth of up to 80 m, the thermocline extended to over 400 m. The LC and thermocline are in the range of the (South) Indian Central Water (ICW) at 32°S, marked by the salinity maximum.

The Sub-Antarctic Mode Water (SAMW) at 350–550 m, marked by an oxygen maximum (Figures 6.5 and 6.6) (Woo 2005), is the domain of the Leeuwin Undercurrent. A second thermocline between 550 and 750 m marked the transition to the salinity minimum of the Antarctic Intermediate Water (AAIW) (Wong 2005; Woo 2005). An oxygen minimum at ~1300 m marked the intrusion of another water mass, believed to be an intrusion of North-West Indian Intermediate Water (NWIIW) (Rochford 1961; Woo 2005), or possibly Upper Circumpolar Deep Water mixed with higher salinity water from the northern Indian Ocean (Fieux, Molcard & Morrow 2005). Examination of historical data (not shown) along the WA coastline, revealed that the signal of this water mass changed from the north by becoming cooler, less saline and more oxygenated near the Perth Canyon. Further south the signal disappeared further, becoming more oxygenated and blending signatures with adjacent water masses, until it disappeared south of Australia in the Great Australian Bight. Below 2000 m was the Indian Deep Water (IDW) marked by a salinity maximum (Tomczak & Godfrey 1994). No water masses deeper than the IDW were sampled, as the maximum depth measured was 3000 m.

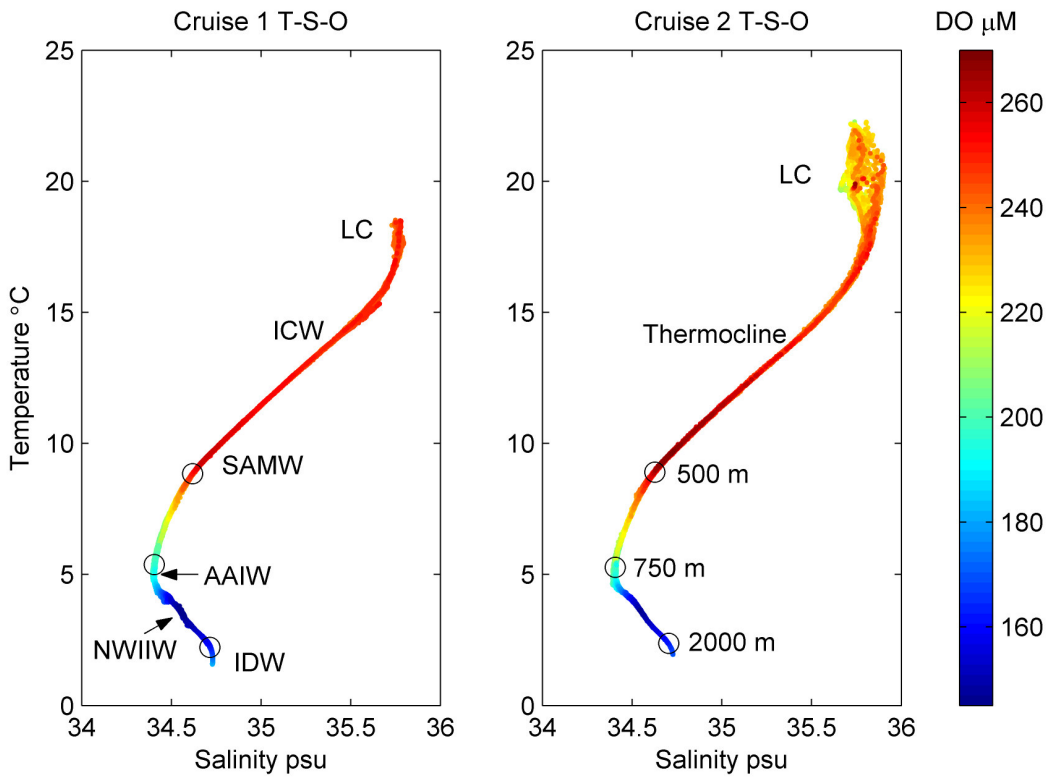

Figure 6.5. Temperature-salinity-oxygen plot for both cruises. Dissolved Oxygen (DO) in µM indicated by colour. Depths marked by circles, 500 m, 750 m and 2000 m, are labelled for cruise 2 only and are accurate to within 50-80 m. Above ~400 m the depth is poorly estimated by T-S values. Water bodies, labelled for cruise 1 only, are indicated as Indian Deep Water (IDW), Sub-Antarctic Mode Water (SAMW), Antarctic Intermediate Water (AAIW), North-West Indian Intermediate Water (NWIIW), and Indian Central Water (ICW). The Leeuwin Current (LC) and the thermocline, which starts at 50-80 m, are also labelled for cruise 2.

Figures 6.6 and 6.7 show all data collected from the CTD in cruise 1, with the ADCP data. Figures 6.8 and 6.9 show the CTD data, LADCP and ADCP data from cruise 2. Along-axis, i.e. cross-shelf, transects from both cruises revealed similar patterns for the isotherms and isohalines (Figures 6.6 and 6.8). The isotherms from the surface to 400 m indicated the Leeuwin Current caused downwelling against the shelf. On the shelf, the isotherms above 200 m lifted towards the surface, denoting upwelling to the Capes Current. This was more marked in cruise 1 when the Leeuwin Current was further offshore and the Capes Current was wider. There was a salinity maximum below the WML which was 50 m deep offshore and reaching near 200 m depth at the shelf, following the 18–20 °C isotherms. This feature was more defined in cruise 2 (visible in Figures 6.8 and 6.9), and accounted for much of the spread in the T-S diagram (Figure 6.5) near the surface. The isotherm depths for both cruises

became horizontal below the thermocline at 450 m, within the Undercurrent, and below this depth the isotherms indicated upwelling against the shelf/head of the canyon. The upwelling and downwelling against the shelf conformed to the expectations of equatorward and poleward currents respectively at an eastern boundary.

6.5.2 Chlorophyll, oxygen and transmission: Shallow–midwater variation

Fluorescence, transmission and oxygen were measured during CTD casts. Fluorescence was used as a proxy for chlorophyll *a*, although for cruise 2 fluorescence was converted to chlorophyll *a* using the empirical relationship established through chlorophyll *a* extractions. The fluorescence, oxygen and transmission for along-axis and across-axis transects are shown in Figures 6.6 and 6.7 respectively for cruise 1, and Figures 6.8 and 6.9 respectively for cruise 2.

Chlorophyll was elevated within the Leeuwin Current above the ~13 °C isotherm. Both cruises showed depression of isotherms and fluorescence to below ~200 m in the canyon head (along-axis transects). Over the canyon axis the deep chlorophyll maximum (DCM) was at ~90 m in both cruises, but was pushed up onto the shelf at the head, to around 50 m where the water depth was less than 200 m. The maximum fluorescence occurred at different locations in each cruise. In cruise 1 the fluorescence maximum offshore was high and thin, while over the canyon head the fluorescence maximum was weaker and broader. In cruise 2 the fluorescence maximum along the axis was nearer the head. There was a second, weaker fluorescence maximum at the 16–17 °C isotherms, at 150 m deepening to 250 m near the head, which seemed to be associated with a sharp thermocline near the base of the Leeuwin Current and a secondary oxygen minimum. In the cross-axis transects, chlorophyll *a* was concentrated over the rims in each cruise.

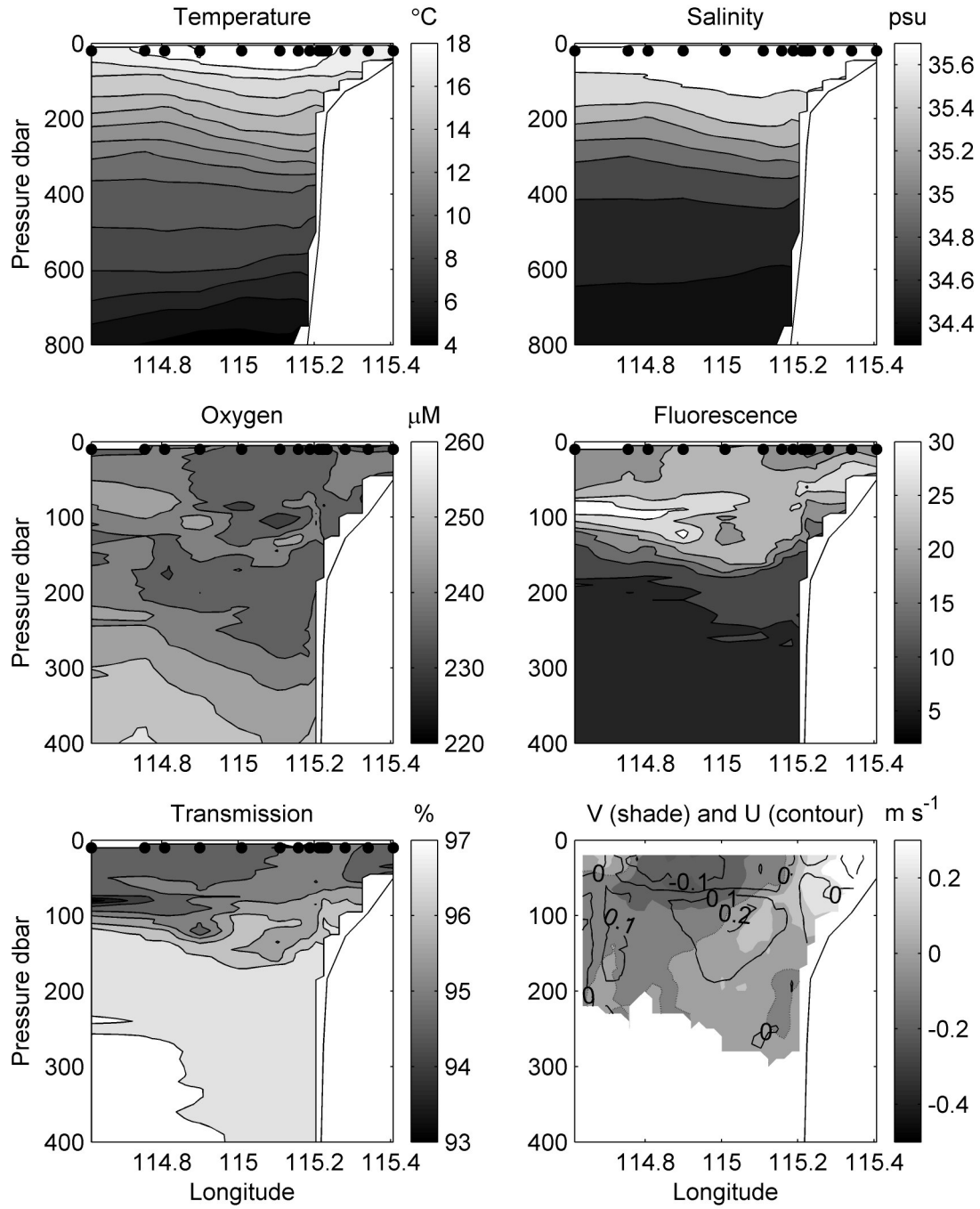

Figure 6.6. CTD and ADCP data for cruise 1 along the canyon axis. Note fluorescence has arbitrary units. CTD station locations are marked with (●). ADCP shows north-south velocity V shaded and east-west velocity U in contour; northward and eastward are positive.

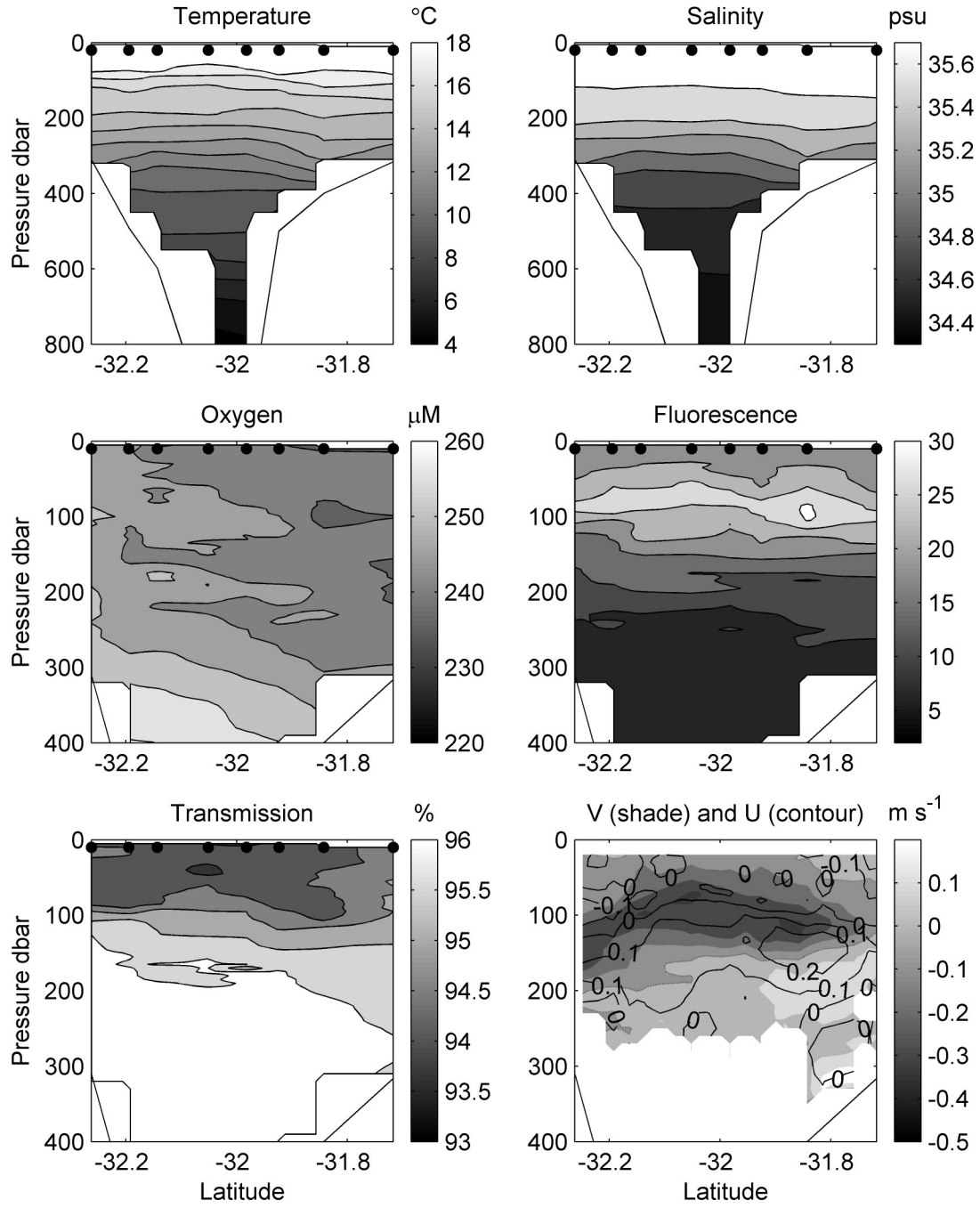

Figure 6.7. CTD and ADCP data for cruise 1 across the canyon axis. Note fluorescence has arbitrary units. CTD station locations are marked with (●). ADCP shows north-south velocity V shaded and east-west velocity U in contour; northward and eastward are positive.

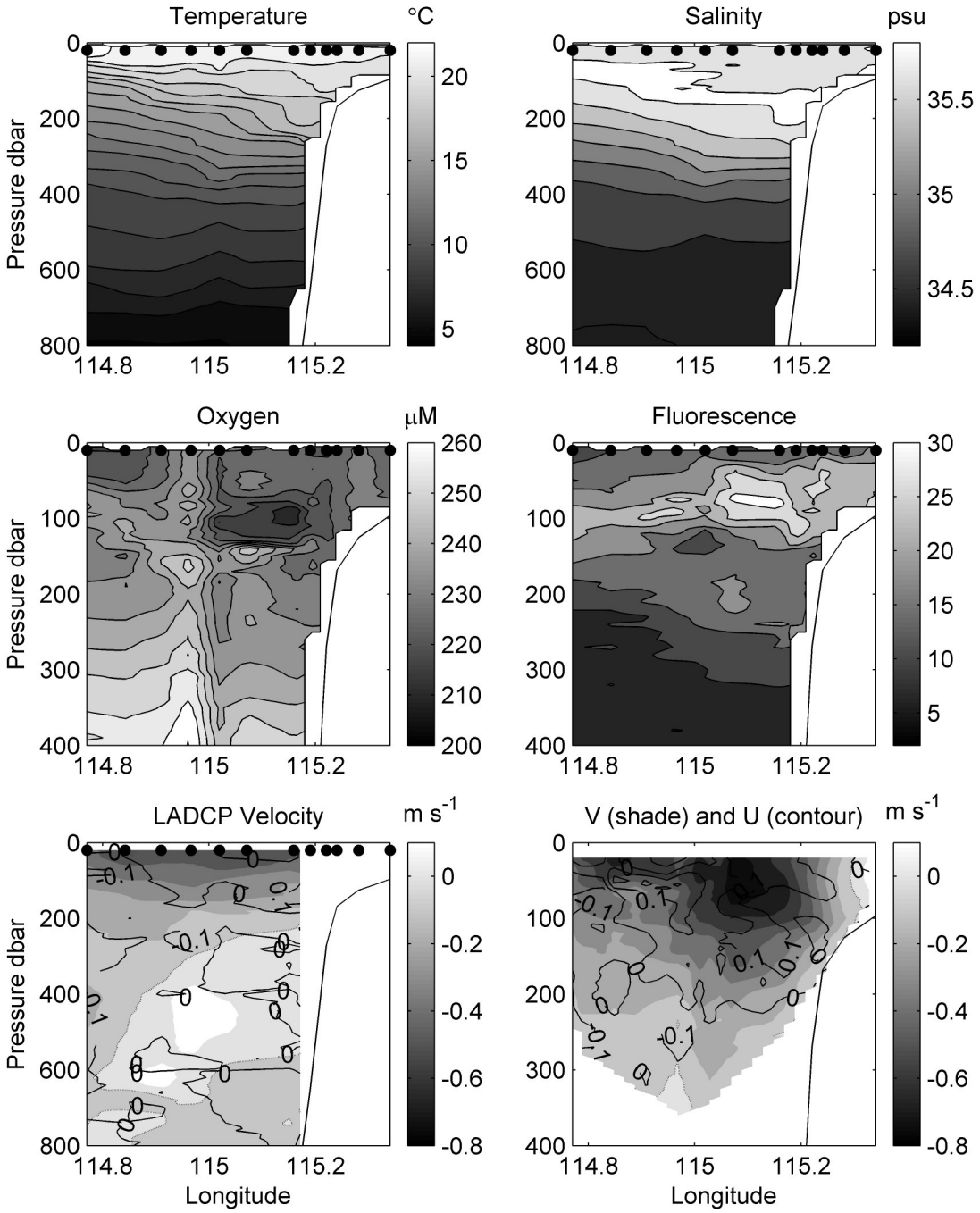

Figure 6.8. CTD and ADCP data for cruise 2 along axis transect (darker grey stations in Figure 6.3). Fluorescence has arbitrary units. CTD station locations are marked with (●). Note that the ADCP transect is along the 32°S line rather than following the axis, for better continuity. This transect was completed on consecutive days, unlike the along-axis transect. LADCP and ADCP show north-south velocity V shaded and east-west velocity U in contour; northward and eastward are positive.

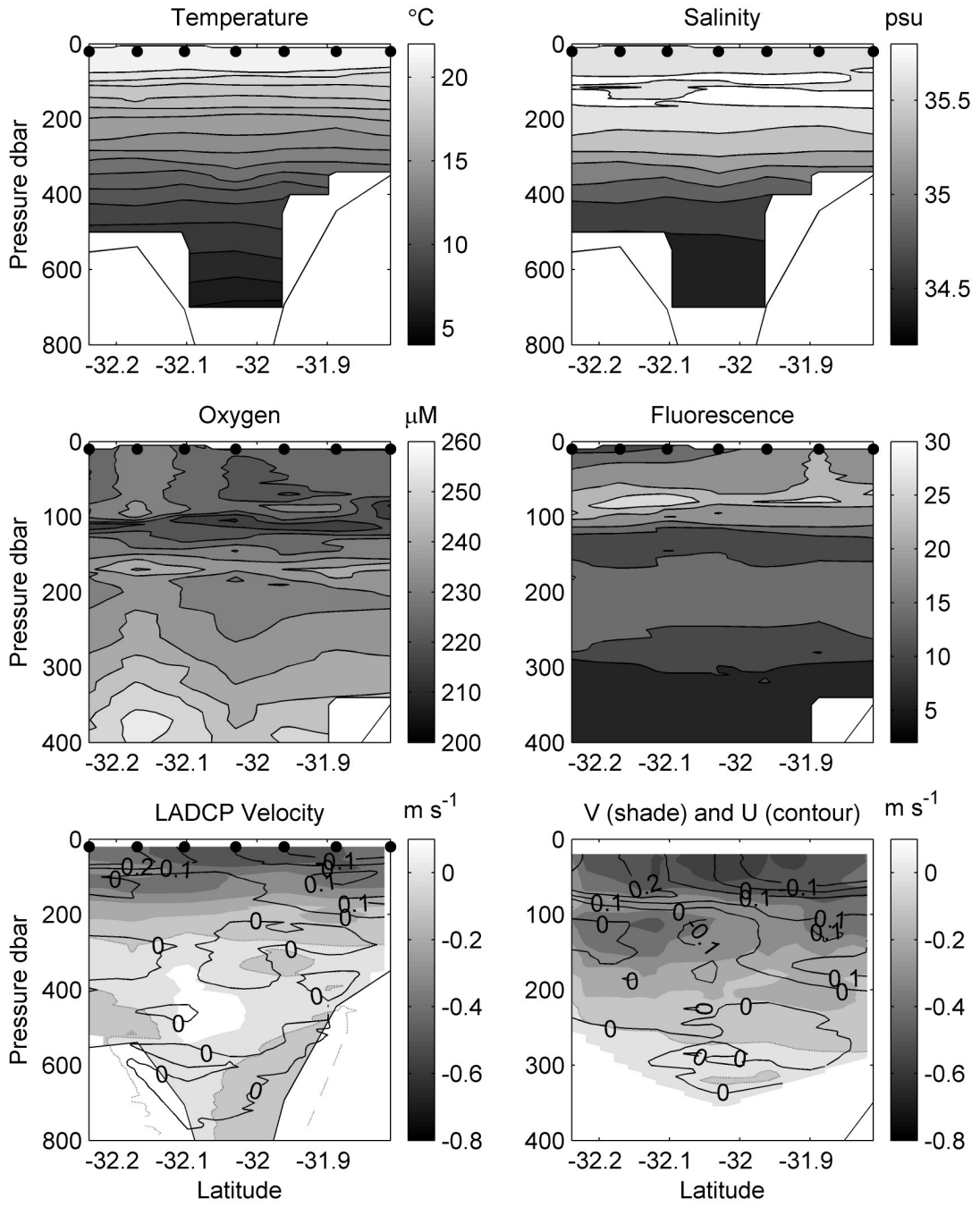

Figure 6.9. CTD and ADCP data for cruise 2 across axis transect (lighter grey stations in Figure 6.3). Fluorescence has arbitrary units. CTD station locations are marked with (●). LADCP and ADCP show north-south velocity V shaded and east-west velocity U in contour; northward and eastward are positive.

Cruise 2 also permitted a spatial and temporal examination. Figure 6.10a indicates the mean chlorophyll *a* between 50 and 100 m, Figure 6.10b the maximum chlorophyll *a* value at each location, Figure 6.10c the depth of the chlorophyll *a* maximum, and Figure 6.10d the temperature at 50 m. The chlorophyll *a* showed

patchiness over the canyon on a scale of at least several nautical miles. High depth-integrated concentration patches occurred near the head though the highest values were elsewhere on the rims, but the depth of the maximum value was variable. The temperature shows similar distribution to the chlorophyll maximum and its depth. From Figure 6.10 it was inferred that the most productive regions were near the canyon head. It was also found that within a day the DCM at one location could vary in depth or magnitude, which was feasibly due to advection. Surface chlorophyll was not a good indicator of deep chlorophyll as often the highest fluorescence in the DCM was matched by a low surface measurement.

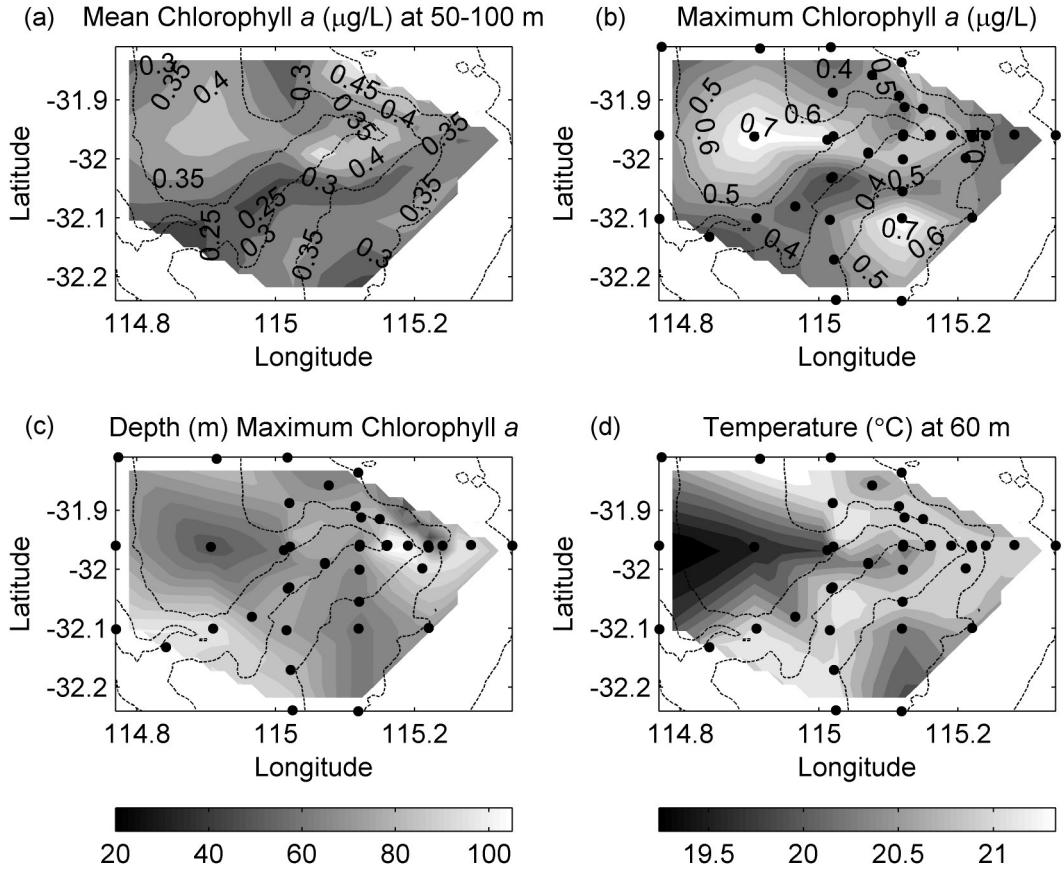

Figure 6.10. a) Mean chlorophyll *a* concentration between 50 and 100 m for cruise 2. b) Maximum measured chlorophyll *a* concentration for cruise 2. c) Depth of chlorophyll *a* maximum in m. d) Temperature at 60 m, the approximate mean depth of the chlorophyll *a* maximum. Station locations marked as (●).

Transmission reflected the fluorescence, loosely correlating low transmission with high fluorescence. Transmission also decreased with depth but was uniform below 100-200 m as the fluorescence stabilised. Oxygen was related to fluorescence, with a

local maximum and/or minimum around the DCM, associated with respiration. Consequently the spatial variation of oxygen correlated with the fluorescence as well as the depth variation. An oxygen minimum occurred just below the DCM as demonstrated by Woo et al. (2005), associated with sinking and decaying detritus.

6.5.3 Circulation: ADCP, LADCP and model

The ADCP and LADCP (cruise 2 only) data clearly denoted the Leeuwin Current, Capes Current and reversal of flow with depth ascribed to the Leeuwin Undercurrent (Figures 6.6–6.9, 6.11). The Capes Current was bounded by the ~300 m isobath over the canyon contour in cruise 1 (though away from the canyon it was bounded by the 150 m contour) and in cruise 2 was apparently closer to shore though measurements at the onshore Leeuwin Current boundary were few. Sea surface temperature (SST) satellite images confirmed the Leeuwin Current was over the canyon in both cruises. During cruise 1 there were several warm-core eddies with diameter 30–60 km, shifting in and out of the canyon region, while during cruise 2 the core of warmest water seemed to be offshore of the survey zone. The maximum surface current speed for cruise 1 was 0.2–0.4 m s^{-1} and in cruise 2 was up to 0.8 m s^{-1} though this varied during the five days of the cruise. These tallied well with literature values and indicated that the velocity was variable.

For cruise 1, during the along-axis transect (Figure 6.6), the surface flow was southwestward over the canyon, turning northwestward west of the dogleg. At ~80 m the flow over the canyon was southwestward and below ~150 m the flow was eastward (onshore). The surface flow turned northward over the head and against the slope at 115.2°E, delineating the shelf current boundary. At the time of the across-axis transect, the surface flow was weak and south-southwestward over the canyon, but westwards at the north end of the transect and eastwards at the south end. The Leeuwin Current was strongest between ~50 m and ~150 m. With increasing depth the flow turned more eastward then northeastward. The deeper currents tended to be opposite in direction to the surface currents, indicating that 1) surface flow did not indicate flow below e.g. 100 m and 2) between the surface and 150 m there was current shear. The data suggested cyclonic circulation centred west of the dogleg and anticyclonic circulation over the canyon head during cruise one.

For cruise 2 (Figure 6.11), the Leeuwin Current was strongest at 115-115.1°E, between the head and dogleg. Satellite SST images indicated that southerly flow coincided with the warm Leeuwin Current. At the onshore boundary of the Leeuwin Current the flow was changeable, as the boundary of southerly flow extended to the

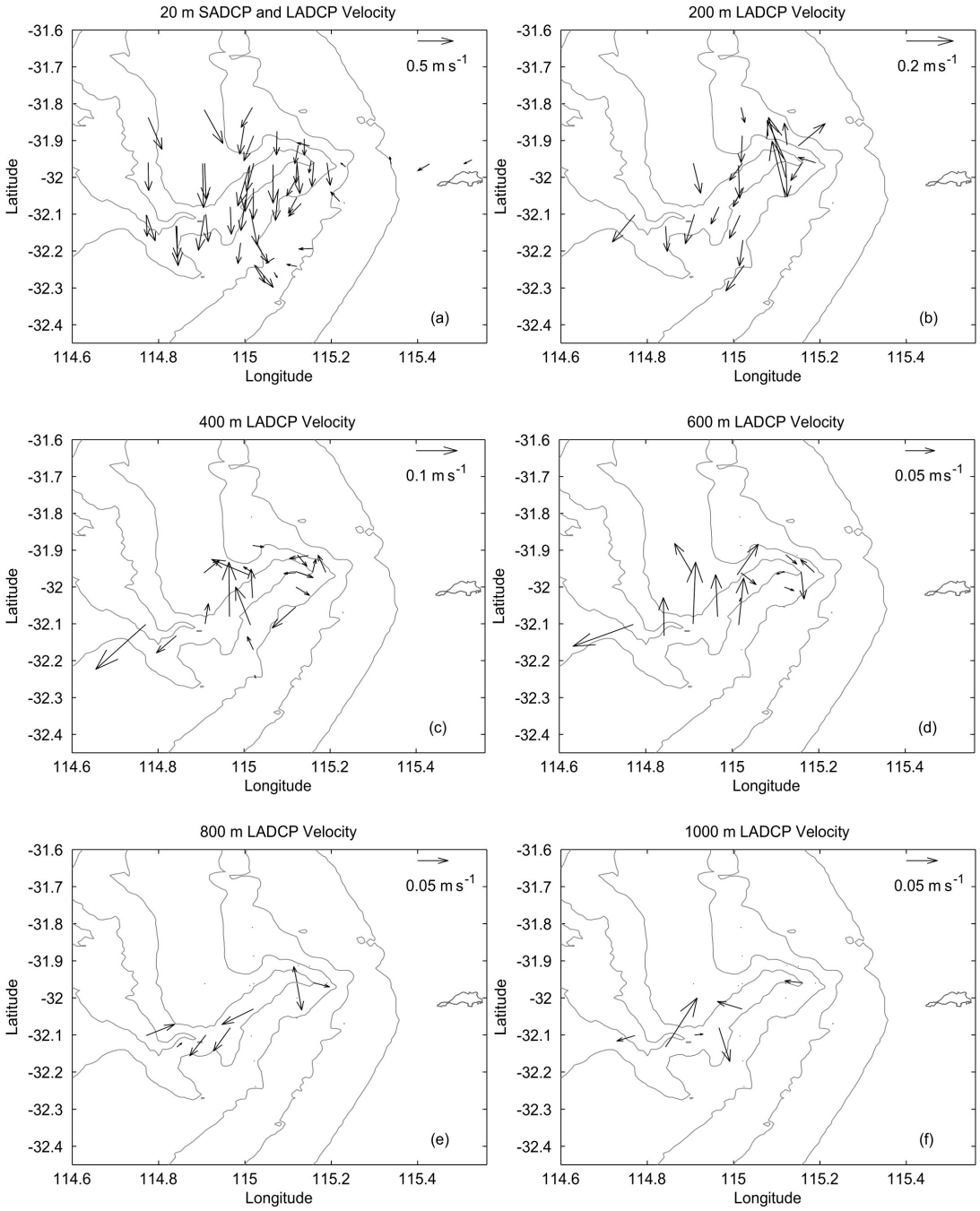

Figure 6.11. a) Cruise 2 LADCP and gridded SADCP velocity measurements at 20 m. b) LADCP velocity at 200 m. The same at c) 400 m. d) 600 m. e) 800 m. f) 1000 m. Canyon bathymetry contours are at 100 m, 200 m, 500 m, 1000 m, 2000 m, and 3000 m.

head of the canyon at the start of the cruise but then shifted offshore. This may have been due to a strong wind event early in the cruise. Note in one location at the head (in Figure 6.11) there are two vectors in different directions, which represent different times. Within the head of the canyon there was a northward jet at 180-280 m at 115.12°E (Figure 6.11b), between a cyclonic eddy over the tip and an anticyclonic eddy connected to the southward Leeuwin Current flow. This eddy formation was assisted by the canyon bathymetry starting to interact with the current at this depth, as occurred in the numerical simulation, although a strong wind event during cruise 2 might have prompted this pattern to develop. The Undercurrent was evident at 400-600 m as a reversal of the Leeuwin Current, flowing up to 0.15 m s^{-1} northwards over the canyon dogleg at 114.95°E (Figures 6.11c, 6.11d). The flow further down the axis suggested anticyclonic circulation. There was also a cyclonic eddy trapped by the Undercurrent in the head of the canyon. Deeper measurements of the circulation (Figures 6.11e, 6.11f) indicated a high degree of spatial and temporal variability, with no circulation features resolved by the sampling resolution.

The field-measured circulation within the canyon was similar to that simulated with ROMS (see Chapter 4). The model indicated that the canyon's influence began at around 100 m above the rim—the canyon starts at 200 m depth—and that an anticyclonic eddy would form between the Leeuwin Current and the canyon rims at around 200 m. The simulations evinced a tendency for eddies to form and fill the canyon at all depths, which these field data supported with variable flow directions throughout the canyon. The model results also concurred with the cross sections along the canyon axis, where the Undercurrent pushed isotherms up against the head, the Leeuwin Current depressed the isotherms towards the head, and there was shallow upwelling onto the shelf where the Capes Current was present.

According to the whale observation data, the most important region is the tip of the canyon including the plateau and adjacent gully. Figure 6.12 shows the typical circulation at 500 m in the canyon head, based on the model output. Typical in this case means the flow resembled this around half the time; for the remaining time the circulation in the tip was variable, with multiple weak eddies or occasionally an anticyclonic eddy. The black arrows indicate the Undercurrent crossing the canyon

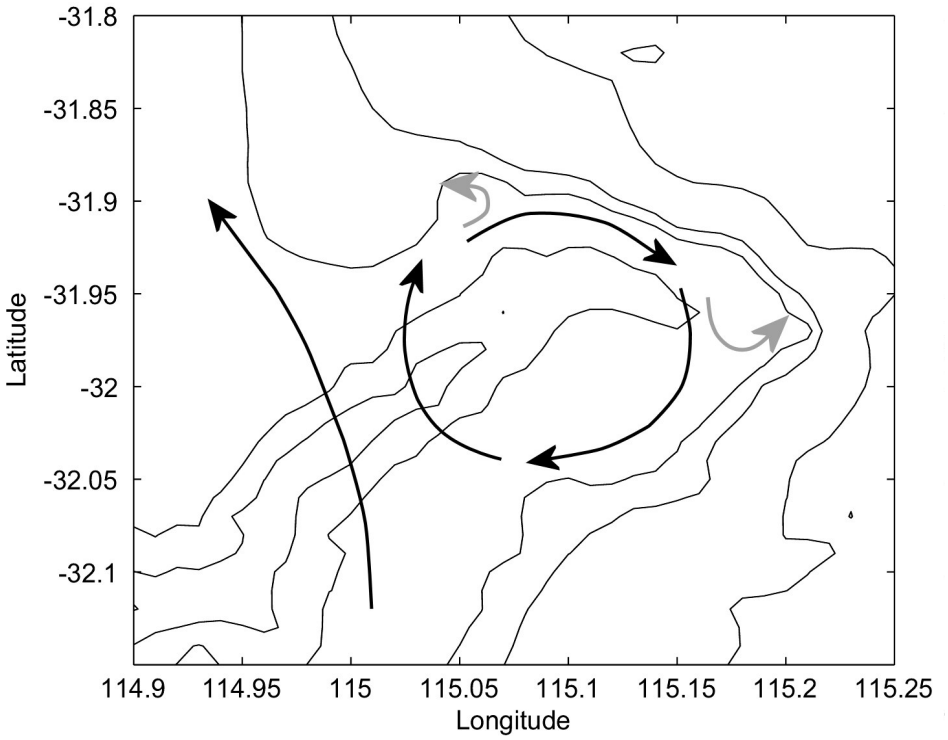

Figure 6.12. Circulation in the tip of the canyon at 500 m, based on model output overlayed on real bathymetry. Black arrows indicate typical model features. Grey arrows indicate features not confidently modelled due to resolution and smoothing of the bathymetry, but inferred based on typical response to bathymetric curves and LADCP velocities. Isobaths shown are 100 m, 200 m, 500 m, 1000 m and 2000 m.

and inducing the cyclonic eddy in the head of the canyon. Grey arrows indicate smaller circulations that were inferred from the model but were not well reproduced due to the bathymetry smoothness and resolution limitations of the model. The important features to note include: 1) the divergence of flow that impinges on the plateau, 2) the upwelling cyclonic eddy, 3) the small trapped eddies in the tip and gully. The field data shows a northward arrow in the tip (at 400-600 m) that may be due to a small anticyclonic circulation. The gully was not measured by ADCP.

6.5.4 Nutrients

6.5.4.1 Spatial distribution on shelf

The nutrient data from cruise 1 were compared near and away from the canyon to assess whether or not the canyon's presence affected the nutrient concentration. Figure 6.13 shows nitrate values at four depths (750 m, 500 m, 300 m and 200 m). At 1000 m (not shown) there was no bias towards the canyon although the region

from 30.5°S to 32.5°S was enhanced. At 750 m colder water and increased nutrients against the slope denoted upwelling due probably to the northward undercurrent. The canyon indicated upwelling throughout and increased nutrients over a wider area of shelf slope. At 500 m a similar pattern appeared, though upwelling was confined to the 500 m isobath and within the canyon head. At 300 and 200 m there were high concentrations over the dogleg and offshore part of the canyon associated with

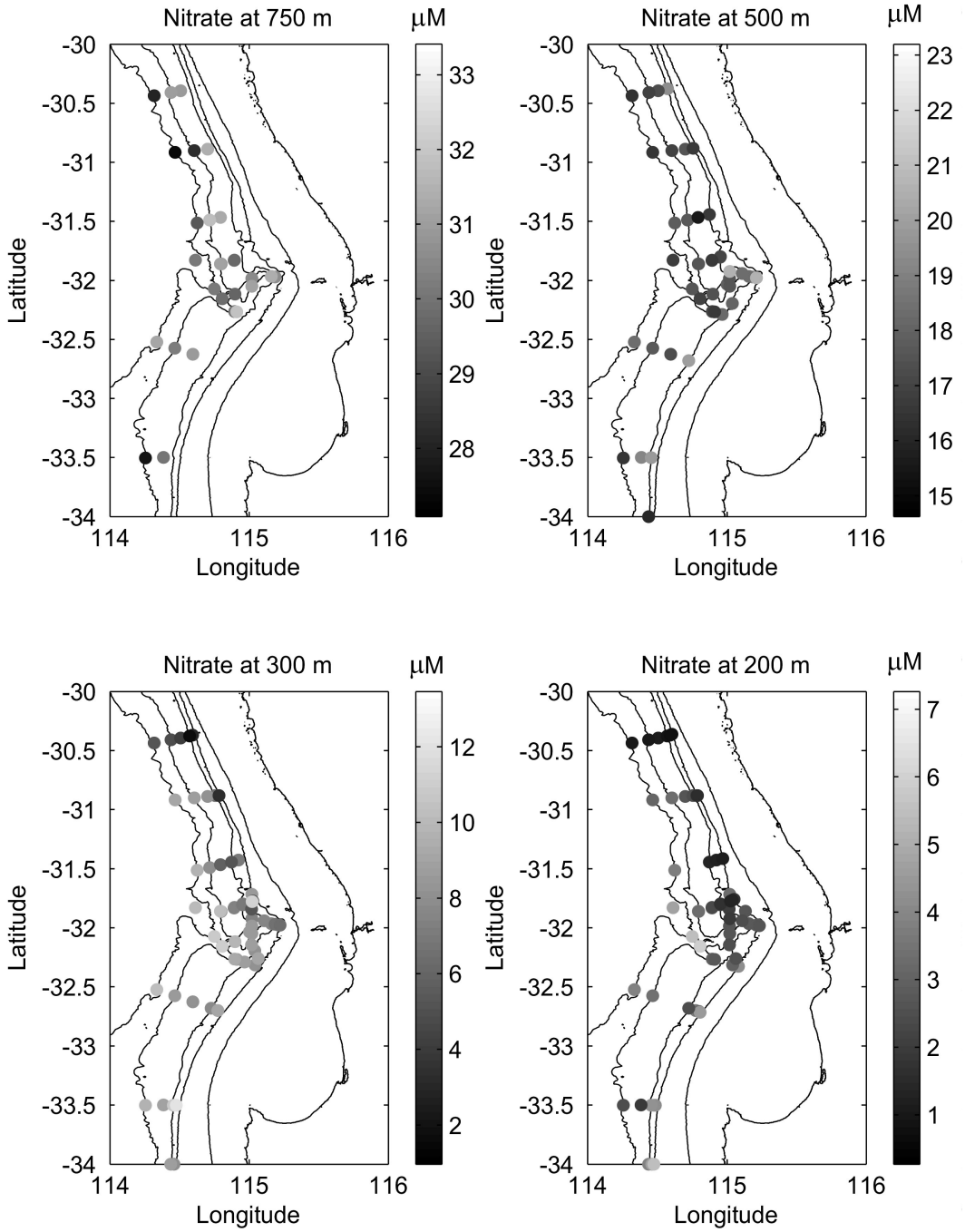

Figure 6.13. Nitrate values from cruise 1 along shelf at four different depths. Nitrate concentrations are in µM. Contours are at [200, 500, 1000, 1500, 2000] m.

doming in a cyclonic eddy, and low concentrations suggesting downwelling against the shelf due to the Leeuwin Current. Above 200 m the nitrate values were affected by uptake by biota, which rendered futile a spatial comparison. The nutricline began just below the DCM and above this, nutrient concentrations were very low (near detection limit). In conclusion, below ~400 m the canyon permits a greater volume of upwelled water, which produces nutrient enhancement, but above this depth the surface circulation directs upwelling. Nutrients near the surface are rapidly utilised.

6.5.4.2 Nitrate input from temperature time series

The field data were used to construct a curve associating nutrients with temperature for this region. Nitrate was chosen as the most important nutrient to consider. A piecewise curve was fitted to relate nitrate from cruise 2 to temperature. The data from cruise 2 were chosen to better represent the bulk of the temperature logger data, because of the similar time of year.

It was found that between 5 °C and 17 °C the square root of nitrate concentration was linearly proportional to temperature. The relationship above 17 °C was weak as the nitrate values were highly variable, but it was approximated with a third order polynomial to allow for a local nitrate maximum around 18 °C which occurred often in the data. Above 20 °C the nitrate concentration was low and constant. The data above 20 °C were therefore neglected. To connect the linear relationship with the cubic, the nitrate concentration (μM) values were calculated for each equation, then data between 16 and 17 °C were combined using a weighted average to allow smooth transition between the two.

$$nitrate(\mu M) = \begin{cases} (-0.4369 * t + 8.0438)^2 & t < 17°C \\ -0.2047t^3 + 11.1823t^2 - 203.144t + 1227.98 & 16 < t < 20°C \end{cases}$$

The temperature t is in °C. The above relationship was applied to the temperature data collected from the moored temperature loggers. To exemplify the nutrient variation, the temperature at 150 m was calculated by linear interpolation for all possible moorings. This depth was chosen as sufficiently shallow that the nutrients were likely to be mixed into the euphotic zone and utilised. Figure 6.14 indicates the nitrate values corresponding to the temperature at 150 m.

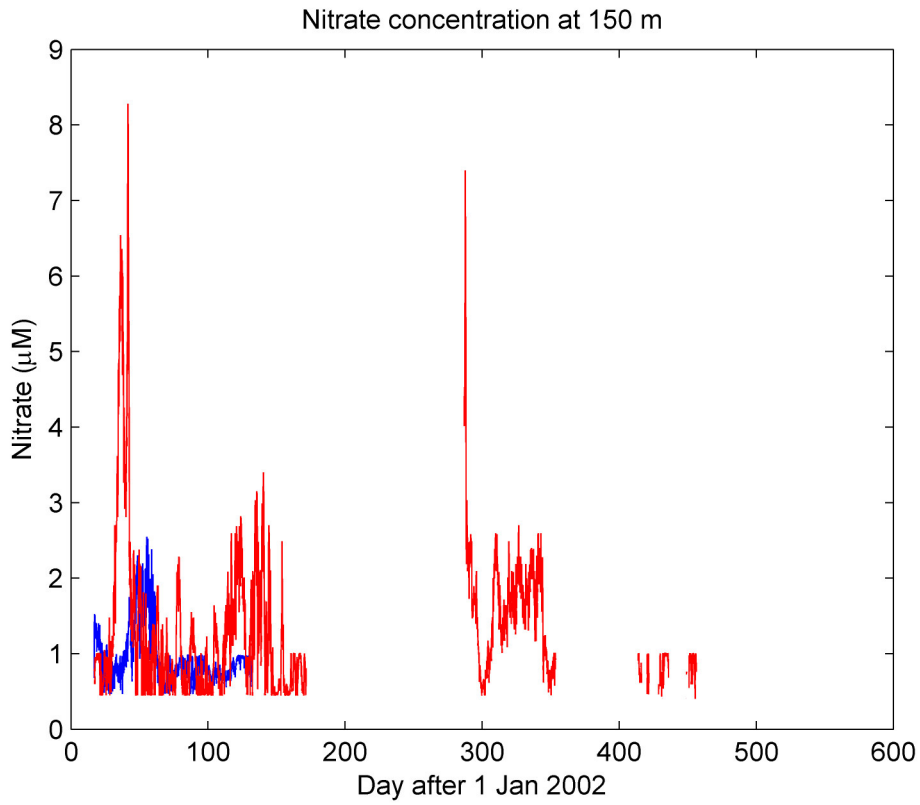

Figure 6.14. Nitrate values at 150 m for four moorings. Blue is a mooring on the canyon head, red are three moorings on the north rim of the canyon.

Over the period for which data were collected, there were occasional (1 per 6 months) increases over 4 µM, which lasted for a short period, sometimes for only a day or two that was attributed to wave pulses (Chapter 3). There were longer periods where the range reached 2-3 µM, at no particular time of year. However, often there were months in which the concentration was around 1 µM, which was around the baseline concentration for water at 150 m. In summary, nitrate (and by association, all nutrients) inputs of high concentration were rare and usually brief. Inputs of moderate concentration could last longer and occur more frequently, but there were times when months passed without change from 'usual' water values. However, data from the temperature loggers moored in different locations at the same time showed disparate results, indicating that upwelling may occur in localised areas of the canyon. Non-synchronous upwelling events in distinct locations may be possible, which would allow a higher frequency of upwelling. Once brought onto the shelf, the upwelled water may disperse around the canyon and into the euphotic zone. Furthermore, internal waves breaking at the canyon head could increase vertical

mixing (Hickey 1997), with one mooring indicating strong mixing near the head. Drifting strings of temperature loggers operating at high temporal resolution also recorded internal waves with periods of 3 hours to 24 hours around the canyon head.

6.5.5 Acoustic backscatter layers

The echo sounder backscatter data revealed aggregations at a range of depths. The scatter layers and clusters, when sampled with nets, consisted of krill and other zooplankton, and myctophid fish (R. McCauley, pers. comm.). Figure 6.15 indicates the locations of short transects across the rim during the day and night. Two blue whales were observed feeding near the transects' locations during the cruise. Figure 6.16 shows the daytime acoustic backscatter data from the EA500 (12 kHz) and the EK500 (38 kHz), adjacent to data from a CTD cast taken during that transect and corresponding ADCP and LADCP velocities. The vertical lines in the backscatter

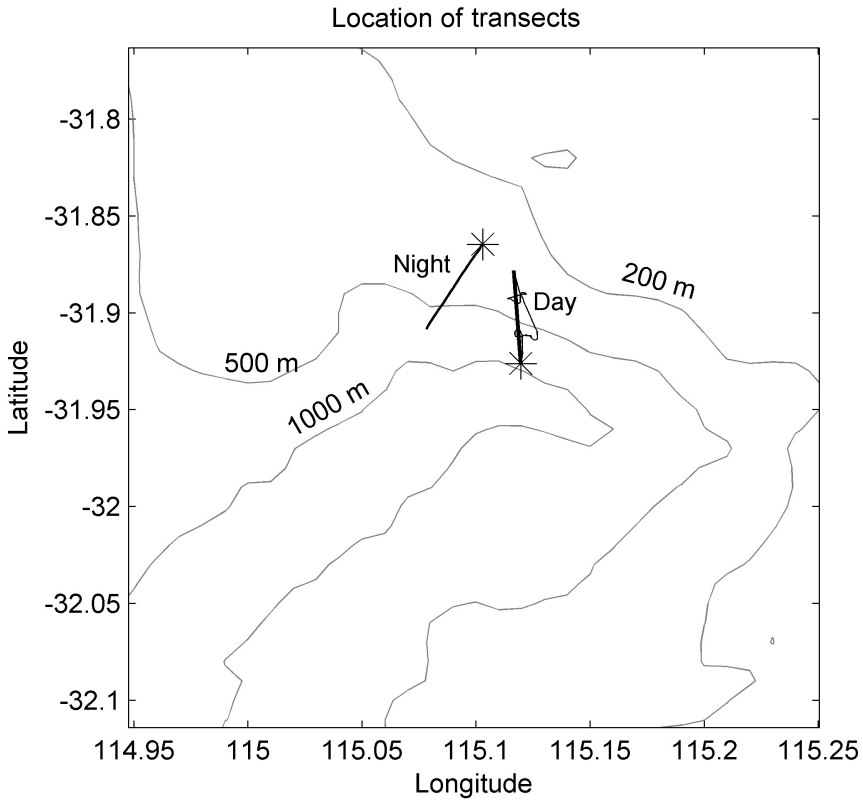

Figure 6.15. Location of transect for Figure 6.16 (Day) and Figure 6.17 (Night). The thin line denotes actual vessel path and the heavy line to which the backscatter was mapped. The asterisk denotes the start of the transect.

were due to noise. The backscatter showed a deep scatter layer below 400 m, composed of the krill that the blue whales feed on. This recurrent deep scatter layer coincided in depth with the bottom of the thermocline, and also with the oxygen maximum, though this did not cause the sharp layer boundary. The deep scatter layer was present in all parts of the canyon, though there was patchiness. Estimates of biomass by mean backscatter between 400 and 500 m indicated higher concentrations were found near the head. Near the rims, usually between 200 m and 350 m, were small swarms or schools, visible with the EA500. Several of these were sampled by EZ net and found to contain krill (R. McCauley, pers. comm.). In the upper 200 m were several thin layers visible with the EK500 that corresponded to fine structure in the water column, visible in temperature, oxygen, fluorescence maximum and velocity. The layer near 200 m corresponded to the bottom of the Leeuwin Current and the start of the pycnocline (visible best with salinity).

Figure 6.17 shows backscatter data collected at 38 kHz during the night and includes ADCP data and CTD data from a station close in time and location to the transect. During the night, the deep scatter layer, which was at ~400 m during the day, migrated to near the surface and remained in the region of the fluorescence (i.e. chlorophyll) maximum. The oxygen content was higher at this time and would be consumed by the krill during the night, then replenished during the day by phytoplankton. The scatter layer at 200 m again corresponded to the bottom of the Leeuwin Current, marked clearly in the salinity, oxygen and velocity.

Spatial analysis of backscatter was difficult because the scatter layer depths were variable (e.g. the fluorescence maximum was not at a consistent depth but could range 50-100 m which was enough to bias results). The data also contained a lot of noise, due to strong winds and use of the vessel's dynamic positioning system, which had to be excluded. However, the backscatter signal was consistently stronger against the rims near the head for data from the day or the night for 50-100 m, and 400-500 m during daytime.

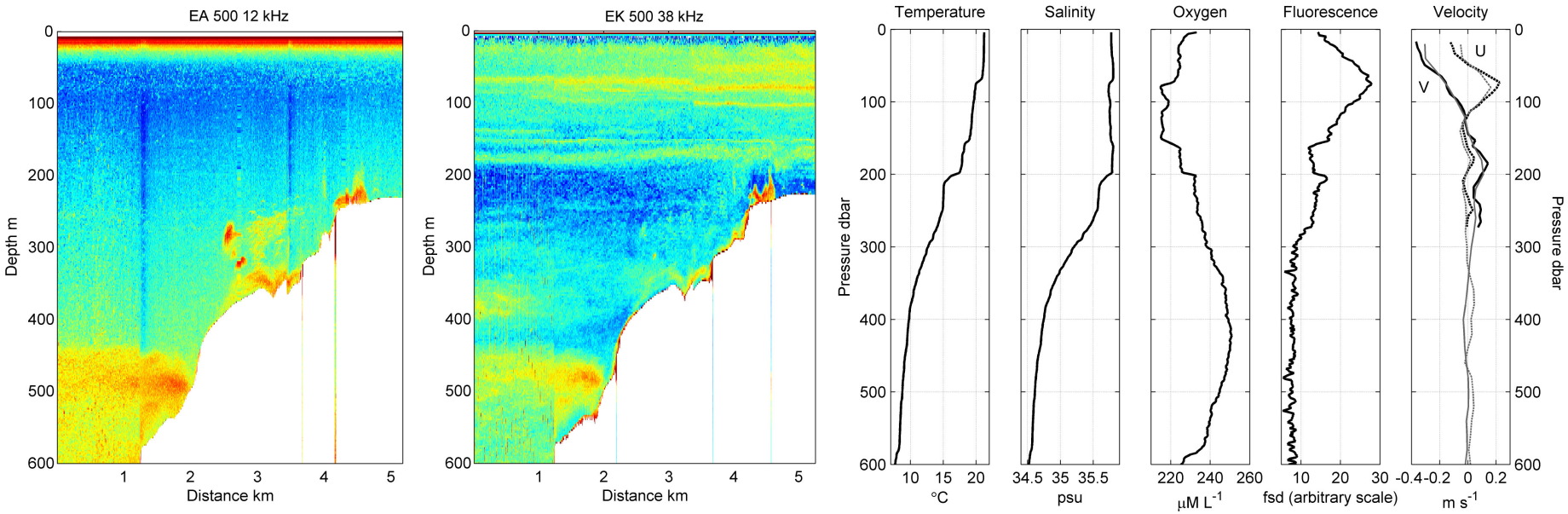

Figure 6.16. Acoustic backscatter during the day, taken from cruise 2, EA500 (left) and EK500 (right), on the 2 February, 9:45-12:45 WST (local time). The data have been mapped to a straight line from start to end of transect. The two different frequencies reveal different features. Data from a CTD cast taken during transect, including temperature, salinity, oxygen, fluorescence, ship ADCP and lowered ADCP.

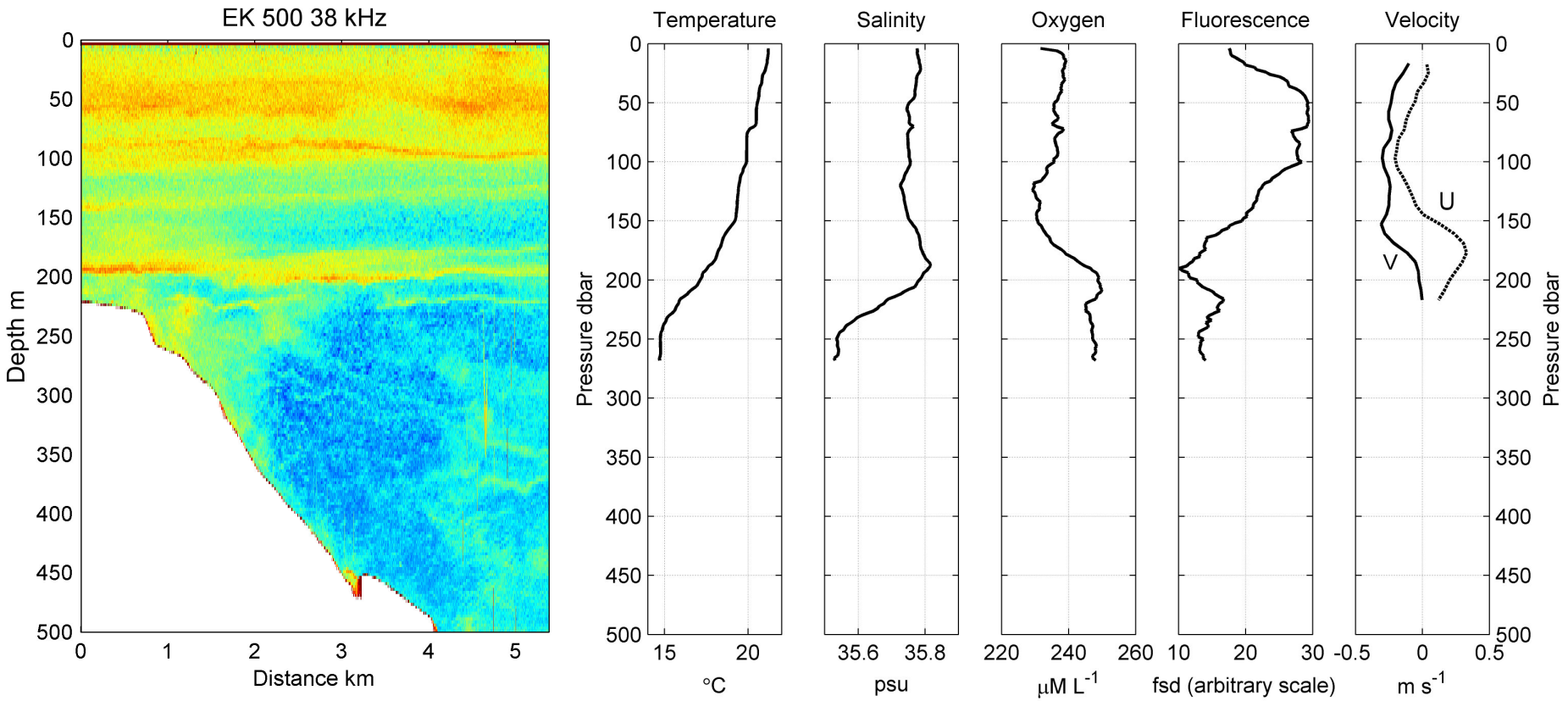

Figure 6.17. EK500 Acoustic backscatter during the night, taken from cruise 2, 3 February, 20:25-21:30 WST (local time). Data from a CTD cast taken during transect, including temperature, salinity, oxygen, fluorescence and ship ADCP.

6.6 Discussion

6.6.1 Physical oceanography of the Perth Canyon

The physical oceanographic characteristics of the Perth Canyon can be now summarised. The Perth Canyon is primarily the domain of the Sub-Antarctic Mode Water (the Leeuwin Undercurrent), and the deep circulation of the Antarctic Intermediate Water and Indian Deep Water. The Indian Central Water occupies the shallow rims and adjacent shelf. The bottom boundary of the Leeuwin Current at around 200 m depth is influenced by the canyon. Despite this, the Leeuwin Current provides an effective boundary against upwelling all along the shelf, usually to around 400 m depth, as indicated by both model and field data. Eddies form within the canyon, below the rims, with direction dependent upon the adjacent across-axis flow, e.g. the Undercurrent usually causes cyclonic eddies to form within the canyon head. The Undercurrent favours upwelling to around 400 m. For water to upwell above 400 m requires an additional factor, e.g. storms, internal waves or pulses, or the Leeuwin Current meandering off the canyon (inshore or offshore). The temperature logger data indicated upwelling at the depth of the Leeuwin Current on the plateau occurs significantly every six months, and that the timing differs at different locations around the canyon (see Sections 3.4.5, 3.4.6 and 6.5.4.2). Canyon processes operate on scales of kilometres, as indicated by the fluorescence patchiness and temporal variability, so that fine-scale localised processes may be important to the canyon region.

The Perth Canyon is patently different to many other canyons studied on the west coast of North America (e.g. Barkley, Astoria, La Jolla, Scripps, and Juan de Fuca canyons) or Mediterranean canyons (Blanes, Palamos, and Calvi canyons), among others. Reasons include the unusual current system that exists on WA's coast, and the surface current having little interaction with the canyon. The Perth Canyon is deep and long, relatively far from the surface and the shore, and highly isolated from any other similar major shelf feature. However, like canyons in other studies, it has importance for the oceanographic processes of the region and consequently as a habitat for a range of marine fauna. Compared to the adjacent, straight shelf, it has

enhanced cross-shelf exchange and greater eddy activity, and allows a larger area of upwelling.

6.6.2 Whales in the Perth Canyon

There are several reasons why the pygmy blue whales seasonally migrate along the WA coast and aggregate in the Perth Canyon. The migration pattern of blue whales is seasonal, as there are 'greener pastures' and breeding/calving areas elsewhere that the whales inhabit at other times; the WA coast is a thoroughfare with the Perth Canyon a way station. The whales' prey depend ultimately on light and nutrients to supply the bottom of the food chain: the phytoplankton. Insolation is at a maximum during summer, when cloudiness is a minimum and the solar angle of incidence is greatest. Light was observed to penetrate to 100 m during summer. Nutrient input is controlled by the Leeuwin Current, which exhibits seasonal variation. Large phytoplankton able to migrate down to the nutricline to gather nutrients reduce the requirement for upwelling to the photic zone; deeper nutrient increases will support these plankton (Rivkin et al. 1984; Villareal & Lipschultz 1995). Such phytoplankton have been found in WA waters (Waite et al. submitted). These arguments are not dependent on the presence of a canyon.

There were two opposing arguments for when productivity would be boosted, for summer and winter conditions. During summer, the Leeuwin Current weakens and allows upwelling when the winds are strong and southerly. The shallow upwelling that occurs during summer at the Capes (Hanson, Pattiaratchi & Waite 2005) brings nutrients to the euphotic zone to boost productivity. Similar upwelling was evinced by isotherm deflection at the canyon, bringing water from 50 m to the surface over the canyon. During winter a chlorophyll bloom occurs along the coast, visible with SeaWIFS ocean colour. At this time the Leeuwin Current is stronger, the mixed layer deepens and stratification reduces which could decrease upwelling resistance. Additionally, storms assist with shallow mixing and resuspension, which boost coastal nutrients, while the Leeuwin Current entrains nutrients and matter from the coast. Storms recorded with the temperature loggers indicated deeper upwelling and mixing occurred. Hanson et al. (2005) have demonstrated that these summer and

winter seasonal mechanisms increased nutrient levels, but light limited productivity during winter.

How might this be resolved with the presence of whales during summer, which must be supported by a strong krill population? The data presented here are insufficient to resolve the seasonality problem, particularly without accounting for other factors in the annual migration of the blue whales. An analogue to the study presented by Croll (2000), regarding Monterey Bay, is hypothesised. In Monterey Bay there are two krill blooms, one at the end of winter and one in summer. The second bloom coincides with an adult krill population and the arrival of whales. We suggest that the productivity increase of winter may boost the krill population, and the productivity increase in summer further supports the generation of the krill population. So several months after the 'summer' weather begins, sufficient numbers of adult krill exist for the whales to feed upon, and they arrive en masse. This is speculation based on the physical evidence and would require an assessment of the krill population in the canyon region during the year to properly form the connections or 'trophic links' (Croll et al. 2000) between the various factors.

These seasonal arguments can apply to the entire shelf, and indeed whales have been sighted feeding e.g. along the steep shelf break north of the canyon (Figure 6.4b). However, the canyon is the focus of whale feeding and this study has demonstrated several reasons why this may occur. The Perth Canyon is a centre of greater upwelling than the adjacent shelf, as indicated by the numerical simulations, the nutrients, and the consideration that the canyon could bring deeper water on to the inner shelf because it bisects the shelf so dramatically. There was evidence of localised upwelling at different depths due to circulation features, which produced higher nutrient values. This conformed to observations (Twomey et al. submitted) of the depth-integrated chlorophyll *a* along the coastline being higher near the Perth Canyon, and an increased presence of diatoms, which indicated freshly upwelled nutrients. Apart from upwelling, the eddies induced within the canyon could increase the residence time of nutrients and encourage aggregation of biota, as has been found in other canyons (e.g. Allen et al. 2001). The dense sightings of whales feeding near the head and within the gully may be accounted for by small-scale circulation aggregating krill. The acoustic backscatter also indicated the head

contained a greater biomass (which has been observed in other canyons along the Australian shelf (R. Kloser, CSIRO, pers. comm.)).

A further mechanism to increase krill swarm density was proposed by Macquart-Moulin and Patriti (1996). Migratory euphausiids can be advected to and from the area during the night when they rise to near the surface. During the day they migrate down into the canyon, which can act as a trap or channel. Thus even if the whales consume the krill during the day, at night more will be advected to the region and descend again into the canyon. It is also possible that any krill near the canyon at the surface, will funnel down into the canyon, thus increasing the concentration at the head.

6.7 Concluding Remarks

This field study was combined with a variety of data and results from previous analyses to examine the physical process of the Perth Canyon and their association with biological processes. The Perth Canyon is a highly complex and dynamic system in a complex marine environment. The canyon topography influenced the circulation, which affected eddy formation and vertical transport. The processes associated with the canyon indicated a number of ways in which the krill density in the canyon might be enhanced, and so account for the appearance of the blue whales. It seemed probable that many factors play a contributing role, as no one factor, such as upwelling, seemed able to produce the seasonal fluctuations in productivity on its own.

CHAPTER 7

Conclusion

The physical processes within the Perth Submarine Canyon have been examined using a variety of methods, to greatly increase the understanding of this topographic feature and its impact on the marine environment. The objective of this study was to examine the physical oceanographic characteristics of the Perth Canyon, which could be applied to increase understanding of the appearance of pygmy blue whales (*Balaenoptera musculus brevicauda*) during their annual migration. This study utilised a numerical model, ROMS (Regional Ocean Modelling System) to the circulation of the WA coast and the Perth Canyon, and also analysed field data, specifically from moored temperature loggers, two field cruises on the RV *Southern Surveyor* and other subsidiary sources (e.g. satellite images, weather stations). The results from these methods were integrated to produce a complete overview of the canyon's physical processes.

Although the primary focus was the physical oceanography, attention was given to the physical–biological relationship, i.e. to examine effects on productivity that could attract the whales. It was found that productivity factors included regional and canyon-specific factors, which could all contribute to productivity in the Perth Canyon. The effect of factors that are independent of the canyon are summarised first, as they have primary control over productivity in the region. The factors that relate to or depend on the canyon are summarised second, showing how the canyon perturbs the system to affect circulation and productivity. All these factors are important to consider for the visitation of the blue whales, particularly as they are interrelated.

7.1 Canyon-Independent Factors

The physical factors that impact on productivity within the studied region, independent of the canyon, that have been determined in this study and from existing literature, are described below.

Leeuwin Current

The Leeuwin Current (LC) flows poleward along the shelf-break and suppresses upwelling along much of the WA coastline. The LC water is oligotrophic and its clarity also allows deep penetration of light. It flows year-round with continuous forcing from the geopotential gradient. The LC was clearly identified during field trips as a southward flow outside the 200 m contour over the canyon, extending to 200 m depth or more. It was measured at >1 m s^{-1} on some occasions. Numerical simulations indicated variable circulation due to meanders and eddy formation.

Coupling of the Leeuwin Current and Undercurrent

The Leeuwin Undercurrent flows equatorward against the shelf slope, following the ~500 m isobath, and is weaker than the Leeuwin Current. The Undercurrent causes isotherms to upwell against the shelf slope. The model indicated that the LC and Leeuwin Undercurrent were interrelated, so that eddies formed often as an eddy pair, with an anticyclonic eddy from the Leeuwin Current and a cyclonic eddy from the Undercurrent. These currents oriented themselves to minimise shear between them. The interrelation between these currents meant that an outside factor (e.g. topography) that generated meanders or eddies in one current would result in a corresponding change in the other current.

El Niño

The El Niño-Southern Oscillation variation across the Pacific Ocean influences Indonesian flow-through and thus the forcing of the Leeuwin Current. In El Niño years the Leeuwin Current is weaker (Feng et al. 2003) because the geopotential gradient decreases. The temperature time series from the moored loggers may have detected some effect from El Niño (Section 3.4.1) but there was insufficient time frame of data to examine what influence this might have on the canyon circulation and its impact on whale sightings.

Wind

The wind in the Perth Canyon region was seasonally varying. It was predominantly upwelling-favourable (southerly) in summer, and during winter a regime of variable winds and storms functioned. The change of wind pattern occurred in September–October and April–May in most years. The temperature loggers clearly recorded the seasonal differences due to wind. The summer wind created the Capes Current with shallow upwelling, which was demonstrated with the numerical model to coincide with the onset of southerly, sea breeze winds (Section 4.4.4). The sea breeze only affected shallow surface layers in the temperature logger data (Section 3.4.2). Storms, in contrast, affected the water column to 500 m, causing mixing, upwelling and downwelling. Upwelling also occurred as relaxation after such a strong wind event (Section 3.4.3). Both the upwelling and the mixing could affect productivity through increasing nutrient concentrations near the surface.

Light

Light is seasonally varying, with more direct, i.e. stronger and more penetrating, light during summer when the sun is closer to zenith. Also, cloudiness occurs predominantly in winter. Light is required by phytoplankton for photosynthesis, so productivity is usually a balance between light, which decreases with depth, and nutrients, which increase with depth. Light was included in discussions on productivity due to its importance (Section 6.6), although it was not studied quantitatively here.

Nutrients

Nutrients are important for productivity, and as this coast is generally nutrient limiting, all mechanisms by which nutrients could be injected into the system were important. Nutrients could be supplied by upwelling from deeper in the ocean, or brought from the shelf through resuspension (by wind) and/or entrainment by the Leeuwin Current. The nitricline along the shelf occurs at ~100 m, just below the deep chlorophyll maximum, so water lifted from below 100 m to above 100 m would be beneficial. Nutrients from below the Leeuwin Current would need assistance through wind-induced shallow upwelling or mixing to bring the nutrients into the euphotic zone. Alternatively, nutrients upwelled to below the photic zone may be

accessed by vertically migrating phytoplankton, which have been found in WA waters (Waite et al. submitted).

7.2 Effect of the Perth Canyon

Following the aims of the study presented in Chapter 1, the effect of the canyon, discovered during this study, is summarised below. This includes: the interaction of the two major currents with the canyon; the effect of wind forcing; the circulation within the canyon and the occurrence of upwelling; and the distribution of biota.

Leeuwin Current

The canyon did not strongly influence the Leeuwin Current because the current is shallow and the canyon rims are deep. The numerical model indicated that near the surface the Leeuwin Current flowed over the canyon without deviation, and only deeper, around the base of the Leeuwin, was there marked interaction with the canyon head. There was some evidence from SST and ocean colour images that eddies tended to form or reside over the canyon region, though this may be produced by the curvature of the shelf and coastline, or interaction with the Leeuwin Undercurrent.

Leeuwin Undercurrent

The Leeuwin Undercurrent interacted strongly with the Perth Canyon. The Undercurrent, as depicted in the model, flowed into the canyon following the shelf at 500 m then broke away from the shelf to cross the canyon, often near the dogleg. This encouraged eddies to form within the canyon, which could grow and migrate offshore. These eddies could induce a circulation response in the Leeuwin Current.

Eddies and circulation

Eddy formation within the canyon occurred continuously in the numerical simulations. The circulation was variable, not steady-state, though there were recurring patterns over a season or longer. The eddies were bounded by the canyon rims. The shallowest eddies, discovered in both model and field data, occurred at 150–200 m depth at the head of the canyon and were formed from southward flow in the Leeuwin Current's base. Below the canyon rims multiple eddies could form,

aligned down the axis and constrained by the rims. The model indicated that eddies at the level of the Undercurrent formed, evolved and migrated out of the canyon over a period of days to weeks. One field cruise found at least two eddies at the depth of the Undercurrent, and deeper down inconsistent flow direction indicated multiple eddies. The system favoured adjacent eddies to be of opposite directions. Eddies also formed regions of convergence and divergence against the rims. One common pattern was when the Undercurrent crossed the canyon and diverged on encountering the north rim, forming a cyclonic eddy within the head of the canyon.

Upwelling

Upwelling within the canyon was constrained underneath the Leeuwin Current. The LC's presence directly over the canyon caused downwelling as deep as 400 m, while the Undercurrent induced upwelling to the limit the LC imposed. The upper limit of upwelling was nearer the surface when the Leeuwin Current was thinner or not directly over the canyon.

The documented effect of canyons on vertical exchange was reproduced here, but through the interaction of the undercurrent and not the surface current. The model indicated that within the canyon, upwelling and downwelling were enhanced at e.g. 500 m compared to elsewhere on the shelf, or to above the canyon rims. The model indicated regions of transport predominantly either up or down that occurred in response to the circulation within the canyon. The cyclonic eddies and areas of divergence created localised upwelling. The canyon also brought deeper water closer to shore, which if upwelled could flood onto the shelf surrounding the canyon. The nutrient field data indicted a large area of nutrient enhancement below ~400 m, particularly in the canyon head.

Cooling registered by the bottom loggers could indicate the presence of water raised from below the canyon rims. The temperature loggers also indicated the presence of internal waves, which may increase mixing by breaking on the canyon rims.

Entrapment

Entrapment of material within the canyon may occur, although there was no direct evidence found in this study. Previous studies have suggested that eddies tend to trap

material or advect it against canyon rims, which can cause aggregation and increase residence time of tracers or passive advectors. The canyon's circulation described here would support the occurrence of entrapment. The echo sounder used during field cruises indicated some patchiness over the canyon axis and against the rims, with greater biomass near the canyon head. These contained high-density aggregations of krill that whales feed upon. The canyon may also act as a preferred habitat for the krill, being deep but near the coast.

In conclusion, the canyon is a region of enhanced productivity because it is more dynamically active, it provides a pathway for nutrients to reach the shelf, and acts as a focal point for the krill that gather within it. Unlike other recognized canyon upwelling systems, it is not a region of prolonged upwelling but exhibits sporadic and localised upwelling to supply nutrients, which usually do not reach the eutrophic level unless other mechanisms take effect. The reasons why summer is more favourable for blue whales are the seasonality of light and upwelling-favourable winds, which boost productivity all along the shelf. There were no reasons discovered here to indicate that the canyon would cause seasonal productivity; rather it would be a productivity-enhanced area at all times of year.

Regarding the potential for predicting the arrival of blue whales, a means to predict the krill population growth would be a useful proxy. However, the instigation of high productivity occurs below the surface so is difficult to monitor. Use of wind measurements, or sea surface temperature to monitor the Leeuwin Current, may be useful although cause and effect involving productivity over the short and long term needs to be established.

7.3 Future Work

This study of the Perth Canyon has considerable scope for extension. The first area that would benefit from improvement is the numerical modelling. The model results here were limited by the brief time in which the simulation could be run before it became unrealistic when wind forcing was applied. The reason for this was the degradation of the geopotential gradient forcing. Including features such as insolation and ocean-atmosphere heat exchange could help retain the density gradient

so that the currents continue to flow despite wind-forced mixing. Long runs could allow for a statistical analysis of the circulation, and a further examination of the seasonal differences.

The second area that could benefit is a study of the zooplankton within the canyon over time and space which would enable further links between the physical analysis of this study and the visitation of the blue whales. To predict the appearance of the whales, knowledge of their prey is vital. It may be easier to relate the changes in the krill population and distribution throughout the year to the seasonal changes described above, and possibly to make krill population predictions on a timescale shorter than a season. The Strategic Research Fund for the Marine Environment (SRFME) Biophysical Oceanographic Project is studying the links between the ocean, phytoplankton, zooplankton and fish, offshore of Perth, and may soon achieve this.

A final possible area of study is to relate the whale sighting numbers to the physical characteristics. However, this is the least feasible because it would require many years of whale survey data to produce any significant correlation with e.g. SOI, SST or an upwelling index, and all other factors relating to the migration patterns and population size must also be considered. Some effort has already been made to compare whale call numbers to the SOI (R. McCauley, pers. comm.).

This study has produced a comprehensive examination of the physical processes that occur in the Perth Canyon, and considered how these processes can affect the biological oceanography of the region, using a variety of data sources and methods. The outcomes of this research may be utilised in further studies of the Perth Canyon and in the development of policies to protect the pygmy blue whales.

References

Allen, SE 1996, 'Topographically generated, subinertial flows within a finite length canyon', *Journal of Physical Oceanography,* vol. 26, pp. 1608-1632.

Allen, SE, Dinniman, MS, Klinck, JM, Gorby, DD, Hewett, AJ & Hickey, BM 2003, 'On vertical advection truncation errors in terrain-following numerical models: Comparison to a laboratory model for upwelling over submarine canyons', *Journal of Geophysical Research,* vol. 108(C1), no. 3003, pp. 1-16.

Allen, SE, Vindeirinho, C, Thomson, RE, Foreman, MGG & Mackas, DL 2001, 'Physical and biological processes over a submarine canyon during an upwelling event', *Canadian Journal of Fisheries and Aquatic Sciences,* vol. 58, pp. 671-684.

Ardhuin, F, Pinot, JM & Tintore, J 1999, 'Numerical study of the circulation in a steep canyon off the Catalan coast (western Mediterranean)', *Journal of Geophysical Research,* vol. 104, no. C5, pp. 11115-11135.

Barth, JA, Pierce, SD & Smith, RL 2000, 'A separating coastal upwelling jet at Cape Blanco, Oregon and its connection to the California Current System', *Deep-Sea Research II,* vol. 47, pp. 783-810.

Batteen, ML & Rutherford, MJ 1990, 'Modeling studies of eddies in the Leeuwin Current: the role of thermal forcing', *Journal of Physical Oceanography,* vol. 20, pp. 1484-1520.

Beckmann, A & Haidvogel, DB 1993, 'Numerical simulation of flow around a tall isolated seamount. Part I: Problem formulation and model accuracy', *Journal of Physical Oceanography,* vol. 23, pp. 1736-1753.

Bosley, KL, Lavelle, JW, Brodeur, RD, Wakefield, WW, Emmett, RL, Baker, ET & Rehmke, KM 2004, 'Biological and physical processes in and around Astoria submarine Canyon, Oregon, USA', *Journal of Marine Systems,* vol. 50, pp. 21-37.

Boyer, DL, Zhang, X & Pérenne, N 2000, 'Laboratory observations of rotating, stratified flow in the vicinity of a submarine canyon', *Dynamics of Atmospheres and Oceans,* vol. 31, pp. 47-72.

Carter, GS & Gregg, MC 2002, 'Intense, variable mixing near the head of Monterey Submarine Canyon', *Journal of Physical Oceanography,* vol. 32, no. 11, pp. 3145-3165.

Cherubin, L, Carton, X, Paillet, J, Morel, Y & Serpette, A 2000, 'Instability of the Mediterranean Water undercurrents southwest of Portugal: effects of baroclinicity and of topography', *Oceanologia Acta,* vol. 23, no. 5, pp. 551-573.

Cresswell, GR 1991, 'The Leeuwin Current - observations and recent models', in *The Leeuwin Current: an influence on the coastal climate and marine life of Western Australia*, eds. AF Pearce & DI Walker, Perth, pp. 1-14.

Cresswell, GR 1996, 'The Leeuwin Current near Rottnest Island, Western Australia', *Marine and Freshwater Research,* vol. 47, pp. 483-487.

Croll, DA, Marinovic, B, Benson, S, Chavez, FP, Black, N, Ternullo, R & Tershy, BR 2000, *From wind to whales: Trophic links in a coastal upwelling system*,,, Final Report to the Monterey Bay National Marine Sanctuary, Contract No. 50ABNF500153.

D'Amico, A, Bergamasco, A, Zanasca, P, Carniel, S, Nacini, E, Portunato, N, Teloni, V, Mori, C & Barbanti, R 2003, 'Qualitative correlation of marine mammals with physical and biological parameters in the Ligurian Sea', *IEEE Journal of Oceanic Engineering,* vol. 28, no. 1, pp. 29-43.

Ezer, T, Arango, H & Shchepetkin, AF 2002, 'Developments in terrain-following ocean models: intercomparisons of numerical aspects', *Ocean Modelling,* vol. 4, pp. 249-267.

Fang, F & Morrow, R 2003, 'Evolution, movement and decay of warm-core Leeuwin Current eddies', *Deep Sea Research II,* vol. 50, pp. 2245-2261.

Feng, M, Fandry, CB, Majewski, L & Waite, A submitted, 'Characteristics of two counter-rotating eddies in the Leeuwin Current system off the Western Australian coast', *Deep-Sea Research II*.

Feng, M, Meyers, G, Pearce, AF & Wijffels, S 2003, 'Annual and interannual variations of the Leeuwin Current at 32ºS', *Journal of Geophysical Research,* vol. 108, no. C11, p. 3355.

Feng, M, Wijffels, S, Godfrey, JS & Meyers, G 2005, 'Do Eddies Play a Role in the Momentum Balance of the Leeuwin Current?', *Journal of Physical Oceanography,* vol. 35, pp. 964-975.

Fieux, M, Molcard, R & Morrow, R 2005, 'Water properties and transport of the Leeuwin Current and Eddies off Western Australia', *Deep-Sea Research I,* vol. 52, pp. 1617-1635.

Gentilli, J 1991, 'Homologous peri-oceanic west coast climates in the southern hemisphere', in *The Leeuwin Current: an influence on the coastal climate and marine life of Western Australia*, eds. AF Pearce & DI Walker, Perth, pp. 15-34.

Gersbach, GH, Pattiaratchi, CB, Ivey, GN & Cresswell, GR 1999, 'Upwelling on the south-west coast of Australia--source of the Capes Current?', *Continental Shelf Research,* vol. 19, pp. 363-400.

Godfrey, JS & Ridgway, KR 1985, 'The large-scale environment of the poleward-flowing Leeuwin Current, Western Australia: Longshore steric height gradients, wind stresses and geostrophic flow', *Journal of Physical Oceanography,* vol. 15, pp. 481-494.

Granata, TC, Vidondo, B, Duarte, CM, Satta, MP & Garcia, M 1999, 'Hydrodynamics and particle transport associated with a submarine canyon off Blanes (Spain), NW Mediterranean Sea', *Continental Shelf Research,* vol. 19, pp. 1249-1263.

Griffin, DA, Wilkin, JL, Chubb, CF, Pearce, AF & Caputi, N 2001, 'Ocean currents and the larval phase of Australian western rock lobster, *Panulirus cygnus*', *Marine and Freshwater Research,* vol. 52, pp. 1187-1199.

Griffin, DA, Wilkin, JL, Pearce, AF & Chubb, CF 2001, *Sea surface temperatures and currents off Western Australia, 1993-2000* CSIRO Marine Research, [CD-ROM] Version 2.0, 19 January 2001

Haidvogel, DB, Arango, H, Hedstrom, K, Beckmann, A, Paola, M-R & Shchepetkin, AF 2000, 'Model evaluation experiments in the North Atlantic Basin: simulations in non-linear terrain following coordinates', *Dynamics of Atmospheres and Oceans,* vol. 32, pp. 239-281.

Haidvogel, DB & Beckmann, A 1995, 'Wind-driven residual currents over a coastal canyon', in *Aha Huliko'a Proceedings: Flow-Topography Interactions*, Hawaii, pp. 219-224.

Haidvogel, DB, Wilkin, JL & Young, R 1991, 'A semi-spectral primitive equation ocean circulation model using vertical sigma and orthogonal curvilinear horizontal coordinates', *Journal of Computational Physics,* vol. 94, pp. 151-185.

Hamilton, LJ 1986, 'Statistical feature of the oceanographic area of south-western Australia, obtained by bathythermograph data', *Australian Journal of Marine and Freshwater Research,* vol. 37, pp. 421-436.

Haney, RL 1991, 'On the pressure gradient forces over steep topography in sigma coordinate ocean models', *Journal of Physical Oceanography,* vol. 21, pp. 610-619.

Hanson, CE, Pattiaratchi, CB & Waite, AM 2005, 'Seasonal production regimes off south-western Australia: influence of the Capes and Leeuwin Currents on phytoplankton dynamics', *Marine and Freshwater Research,* vol. 56, pp. 1011-1026.

Heezen, BC 1956, 'The origin of submarine canyons', *Scientific American,* vol. 195, no. 2, pp. 36-41.

Hickey, BM 1995, 'Coastal submarine canyons', in *Aha Huliko'a Proceedings: Flow-Topography Interactions*, Hawaii, pp. 95-110.

Hickey, BM 1997, 'The response of a steep-sided, narrow canyon to time-variable wind forcing', *Journal of Physical Oceanography,* vol. 27, pp. 697-726.

Hooker, SK, Whitehead, H & Gowans, S 1999, 'Marine protected area design and the spatial and temporal distribution of cetaceans in a submarine canyon', *Conservation Biology,* vol. 13, no. 3, pp. 592-602.

Hooker, SK, Whitehead, H & Gowans, S 2002, 'Ecosystem consideration in conservation planning: energy demand of foraging bottlenose whales (*Hyperoodon ampullatus*) in a marine protected area', *Biological Conservation,* vol. 104, pp. 51-58.

Hughes, RL, Ofosu, KN & Hickey, BM 1990, 'On the behaviour of boundary undercurrents near canyons', *Journal of Geophysical Research,* vol. 95, no. C11, pp. 20259-20266.

Hughes, TMC, Weaver, AJ & Godfrey, JS 1992, 'Thermohaline forcing of the Indian Ocean by the Pacific Ocean', *Deep Sea Research Part A. Oceanographic Research Papers,* vol. 39, no. 6, pp. 965-995.

Johnson, D 1967, *The origin of submarine canyons*, Hafner Publishing Company, Inc., New York.

Joint Panel on Oceanographic Tables and Standards 1991, *Processing of oceanographic station data*, UNESCO, Paris.

Jones, ISF, Cato, DH, Hamilton, LJ & Scott, BD 1996, *Site survey for an ocean engineering project west of Perth for July to September 1992*, DSTO Aeronautical and Marine Research Laboratory, Melbourne, DSTO-TR-0459.

Klinck, JM 1988, 'The influence of a narrow transverse canyon on initially geostrophic flow', *Journal of Geophysical Research,* vol. 93, no. C1, pp. 509-515.

Klinck, JM 1989, 'Geostrophic adjustment over submarine canyons', *Journal of Geophysical Research,* vol. 94, no. C5, pp. 6133-6144.

Klinck, JM 1996, 'Circulation near submarine canyons: A modelling study', *Journal of Geophysical Research,* vol. 101, no. C1, pp. 1211-1233.

Landry, MR & Hickey, BM (eds.) 1989, *Coastal oceanography of Washington and Oregon*, Elsevier, Amsterdam.

Levitus, S & Boyer, TP 1994, 'World Ocean Atlas 1994', in *NOAA Atlas NESDIS 4*, vol. 4: Temperature. US Department of Commerce, Washington, D.C., p. 117,

Levitus, S, Burgett, R & Boyer, TP 1994, 'World Ocean Atlas 1994', in *NOAA Atlas NESDIS 3*, vol. 3: Salinity. US Department of Commerce, Washington, D.C., p. 99,

Lutjeharms, JRE, Penven, P & Roy, C 2003, 'Modelling the shear edge eddies of the southern Agulhas Current', *Continental Shelf Research,* vol. 23, pp. 1099-1115.

Macquart-Moulin, C & Patriti, G 1996, 'Accumulation of migratory micronekton crustaceans over the upper slope and submarine canyons of the northwestern Mediterranean', *Deep-Sea Research I,* vol. 43, no. 5, pp. 579-601.

McCauley, RD, Bannister, JL, Burton, CK, Jenner, C, Jenner, M-N, Rennie, SJ, Salgado Kent, C & Pattiaratchi, CB In prep, 'Pygmy blue whales in the Perth Canyon, Western Australia'.

Morrow, R, Fang, F, Fieux, M & Molcard, R 2003, 'Anatomy of three warm-core Leeuwin Current eddies', *Deep Sea Research II,* vol. 50, pp. 2229-2243.

Pattiaratchi, CB, Hegge, B, Gould, J & Eliot, I 1997, 'Impact of sea-breeze activity on nearshore and foreshore processes in southwestern Australia', *Continental Shelf Research,* vol. 17, no. 13, pp. 1539-1560.

Pearce, AF 1991, 'Eastern boundary currents of the southern hemisphere', in *The Leeuwin Current: an influence on the coastal climate and marine life of Western Australia*, eds. AF Pearce & DI Walker, Perth, pp. 35-46.

Pearce, AF & Griffiths, RW 1991, 'The mesoscale structure of the Leeuwin Current: A comparison of laboratory models and satellite imagery', *Journal of Geophysical Research,* vol. 96, no. C9, pp. 16739-16757.

Pearce, AF & Pattiaratchi, CB 1999, 'The Capes Current: a summer countercurrent flowing past Cape Leeuwin and Cape Naturaliste, Western Australia', *Continental Shelf Research,* vol. 19, pp. 401-420.

Pedlosky 1974, 'Longshore currents, upwelling and bottom topography.', *Journal of Physical Oceanography,* vol. 4, pp. 214-226.

Peliz, Á, Dubert, J & Haidvogel, DB 2003, 'Subinertial response of a density-driven Eastern Boundary Poleward Current to wind forcing', *Journal of Physical Oceanography,* vol. 33, pp. 1633-1650.

Peliz, Á, Dubert, J, Haidvogel, DB & Le Cann, B 2003, 'Generation and unstable evolution of a density-driven Eastern Poleward Current: The Iberian Poleward Current', *Journal of Geophysical Research,* vol. 108, no. C8, p. 3268.

Peliz, Á, Rosa, TL, Santos, MP & Pissarra, JL 2002, 'Fronts, jets, and counter-flows in the Western Iberian upwelling system', *Journal of Marine Systems,* vol. 35, pp. 61-77.

Petkovic, P & Buchanan, C 2002, *Australian bathymetry and topography grid*, Canberra: Geoscience Australia. Retrieved: 22 February 2002, from http://www.ga.gov.au/general/technotes/20011023_32.jsp.

Petruncio, ET, Paduan, JD & Rosenfeld, LK 2002, 'Numerical simulations of the internal tide in a submarine canyon', *Ocean Modelling,* vol. 4, pp. 221-248.

Pond, S & Pickard, GL 1983, *Introductory dynamical oceanography,* 2nd edn, Butterworth-Heinemann, Oxford.

Pugh, DT 1987, *Tides, surges and mean sea-level*, J Wiley, Chichester.

Ridgway, KR & Condie, SA 2004, 'The 5500-km-long boundary flow off western and southern Australia', *Journal of Geophysical Research C: Oceans,* vol. 109, no. 4, p. C04017.

Rivkin, RB, Swift, E, Biggley, WH & Voytek, MA 1984, 'Growth and carbon uptake by natural populations of oceanic dinoflagellates *Pyrocystis noctiluca* and *Pyrocystis fusiformis*', *Deep Sea Research Part A. Oceanographic Research Papers,* vol. 31, no. 4, pp. 353-367.

Rochford, DJ 1961, 'Hydrology of the Indian Ocean I. The water masses in intermediate depths of the south-east Indian Ocean', *Australian Journal of Marine and Freshwater Research,* vol. 12, pp. 129-149.

Sánchez-Velasco, L & Shirasago, B 1999, 'Spatial distribution of some groups of microzooplankton in relation to oceanographic processes in the vicinity of a submarine canyon in the north-western Mediterranean Sea', *ICES Journal of Marine Science,* vol. 56, pp. 1-14.

Schoenherr, JR 1991, 'Blue whales feeding on high concentration of euphausiids around Monterey Submarine Canyon', *Canadian Journal of Zoology,* vol. 69, pp. 583-594.

She, J & Klinck, JM 2000, 'Flow near submarine canyons driven by constant winds', *Journal of Geophysical Research,* vol. 105, no. C12, pp. 28671-28694.

Skliris, N, Goffart, A, Hecq, JH & Djenidi, S 2001, 'Shelf-slope exchanges associated with a steep submarine canyon off Calvi (Corsica, NW Mediterranean Sea): A modeling approach', *Journal of Geophysical Research,* vol. 106, no. C9, pp. 19883-19901.

Skliris, N, Hecq, JH & Djenidi, S 2002, 'Water fluxes at an ocean margin in the presence of a submarine canyon', *Journal of Marine Systems,* vol. 32, no. 1-3, pp. 239-251.

Skliris, N, Lacroix, G & Djenidi, S 2004, 'Effects of extreme meteorological conditions on coastal dynamics near a submarine canyon', *Continental Shelf Research,* vol. 24, pp. 1033-1045.

Smith, RL, Huyer, A, Godfrey, JS & Church, JA 1991, 'The Leeuwin Current off Western Australia, 1986-1987', *Journal of Physical Oceanography,* vol. 21, no. 2, pp. 323-345.

Sobarzo, M, Figueroa, M & Djurfeldt, L 2001, 'Upwelling of subsurface water into the rim of the Biobío submarine canyon as a response to surface winds', *Continental Shelf Research,* vol. 21, pp. 279-299.

Song, YT & Chao, Y 2004, 'A theoretical study of topographic effects on coastal upwelling and cross-shore exchange', *Ocean Modelling,* vol. 6, pp. 151-176.

Thompson, RORY 1984, 'Observations of the Leeuwin Current off Western Australia', *Journal of Physical Oceanography,* vol. 14, pp. 623-628.

Thompson, RORY & Veronis, G 1983, 'Poleward boundary current of Western Australia', *Australian Journal of Marine and Freshwater Research,* vol. 34, pp. 173-185.

Tomczak, M & Godfrey, JS 1994, *Regional oceanography: An introduction*, Pergamon, London.

Twomey, LJ, Waite, A, Pez, V & Pattiaratchi, CB submitted, 'Variability in nitrogen uptake and fixation in the oligotrophic waters off the south west coast of Australia', *Deep-Sea Research II.*

Verron, J, Renouard, D & Boyer, DL 1995, 'Rectified flows over a finite length shelf break: a bank and a canyon case', in *Aha Huliko'a Proceedings: Flow-Topography Interactions*, Hawaii, pp. 207-218.

Vetter, EW & Dayton, PK 1998, 'Macrofaunal communities within and adjacent to a detritus-rich submarine canyon system', *Deep-Sea Research II,* vol. 45, pp. 25-54.

Villareal, TA & Lipschultz, F 1995, 'Internal nitrate concentrations in single cells of large phytoplankton from the Sargasso Sea', *Journal of Phycology,* vol. 31, pp. 689-696.

von der Borch, CC 1968, 'Southern Australian submarine canyons: their distribution and ages', *Marine Geology,* vol. 6, no. 2, pp. 269-279.

Waite, A, Muhling, B, Holl, C, Beckley, L, Montoya, J, Strezelecki, J, Thompson, P & Pesant, S submitted, 'Food web structure in two counter-rotating eddies based on $\delta^{15}N$ and $\delta^{13}C$ isotopic analyses', *Deep-Sea Research II.*

Weaver, AJ & Middleton, JH 1989, 'On the dynamics of the Leeuwin Current', *Journal of Physical Oceanography,* vol. 19, pp. 626-648.

Wong, APS 2005, 'Subantarctic Mode Water and Antarctic Intermediate Water in the South Indian Ocean based on profiling float data 2000-2004', *Journal of Marine Research,* vol. 63, pp. 789-812.

Woo, M 2005, *Summer Circulation and Water Masses along the West Australian Coast*, Doctor of Philosophy, University of Western Australia.

Appendix A. Index of CD-ROM

Whole Domain Runs

No wind initialiation run. Temperature and velocity vectors.

N0_wind_surface.qt

No_wind_500m.qt

Summer wind run. Temperature and velocity vectors.

Summer_wind_surface.qt

Summer_wind_500m.qt

Spring wind run. Temperature and velocity vectors.

Spring_wind_surface.qt

Spring_wind_500m.qt

Canyon Runs

No wind initialisation run: canyon. Temperature and velocity vectors, and isotherms in canyon cross sections.

No_wind_canyon.qt

Summer initialisation run: canyon. Temperature and velocity vectors, and isotherms in canyon cross sections.

Summer_wind_canyon.qt

Spring initialisation run: canyon. Temperature and velocity vectors, and isotherms in canyon cross sections.

Spring_wind_canyon.qt

The velocity vector scale is not consistent between movie frames.

Movies can be viewed with a Quick Time player which can be downloaded free from http://www.apple.com/quicktime/win.html.

Appendix B. Flow Cases – Summary

Case 1	The Leeuwin Current flows around the Perth Canyon over the head; ocean water has been drawn over the Perth Canyon. Below 200 m, a cyclonic eddy is over the canyon mouth, an anticyclonic eddy is near the dogleg, and a cyclonic eddy is at the canyon tip. Downwelling occurs on the shelf, but upwelling occurs in the tip at 200 m and below. An anticyclonic eddy south of the Perth Canyon might form an eddy pair.
Case 2	The Leeuwin Current is across the Perth Canyon mouth. A cyclonic eddy is on the south rim, inshore of the Leeuwin Current. The cyclonic eddy causes strong upwelling at 500 m. Cyclonic circulation occurs in the tip. An anticyclonic eddy is south of the Perth Canyon, forming an eddy pair.
Case 3	The Leeuwin Current is over the Perth Canyon's head, causing downwelling. Cool water has been drawn around the north side of a cyclonic eddy situated south of the Perth Canyon. The Undercurrent is across canyon with a cyclonic eddy in the head at 500 m; upwelling occurs on the shelf, but is constrained by the Leeuwin Current.
Case 4	An anticyclonic eddy is northwest of the Perth Canyon. Cool oceanic water has been drawn in over the Perth Canyon, forming a cyclonic eddy over the dogleg at all depths. Downwelling occurs against the shelf, and upwelling occurs in the cyclonic eddy. The Undercurrent is across the canyon mouth.
Case 5	An eddy pair is present, with the anticyclonic eddy over the Perth Canyon and a cyclonic eddy against the shelf to the south. The Undercurrent circles anticyclonically around the canyon and forms cyclonic upwelling eddies to the north and south of the canyon. Upwelling occurs deep in the canyon head due to a cyclonic eddy.
Case 6	Similar to Case 5 at surface, but Case 3 at depth. The wind forcing causes some differences because the Leeuwin Current is offshore instead of onshore, and billows form on the onshore boundary of the Leeuwin Current. The northward shelf water helped to close the

	anticyclonic circulation over the canyon. The Undercurrent meanders over the Perth Canyon rather than forming a closed circulation. Cyclonic circulation occurs against the shelf north of the canyon and in the tip, causing upwelling.

Pictorial Description of Flow Cases

Case 1

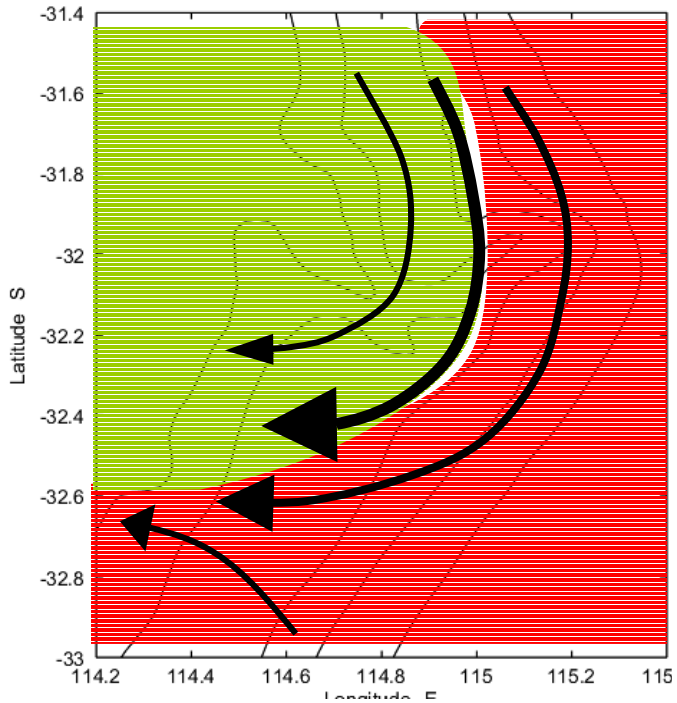

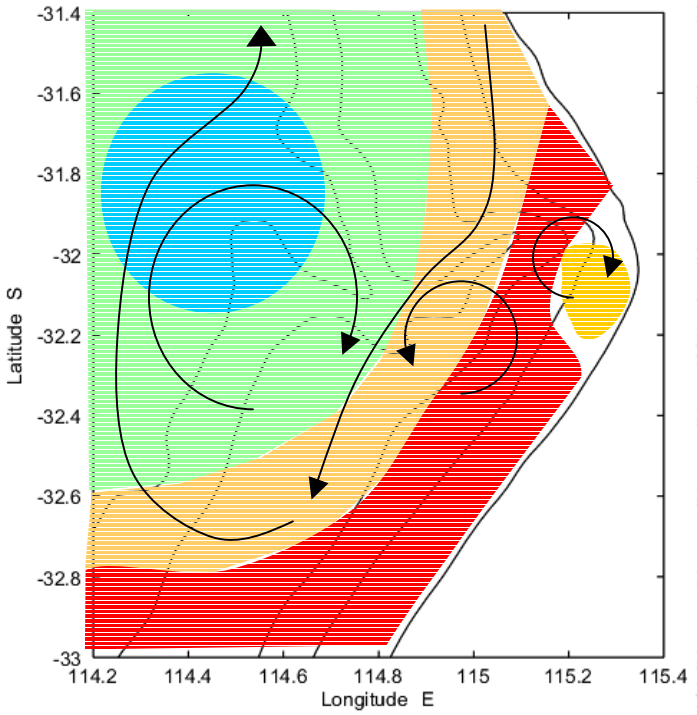

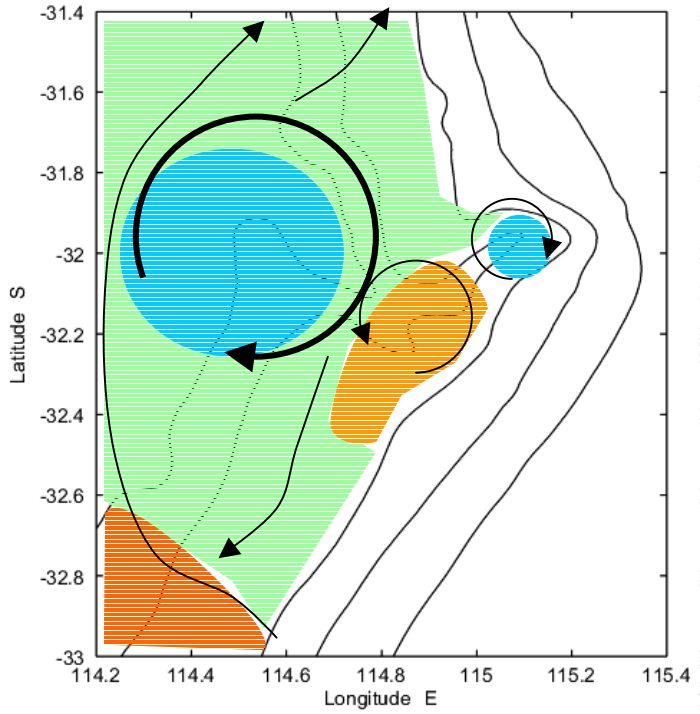

The Leeuwin Current flows around the Perth Canyon over the head; ocean water has been drawn over the Perth Canyon. Below 200 m, a cyclonic eddy is over the canyon mouth, an anticyclonic eddy is near the dogleg, and a cyclonic eddy is at the canyon tip. Downwelling occurs on the shelf, but upwelling occurs in the tip at 200 m and below. An anticyclonic eddy south of the Perth Canyon might form an eddy

Case 2

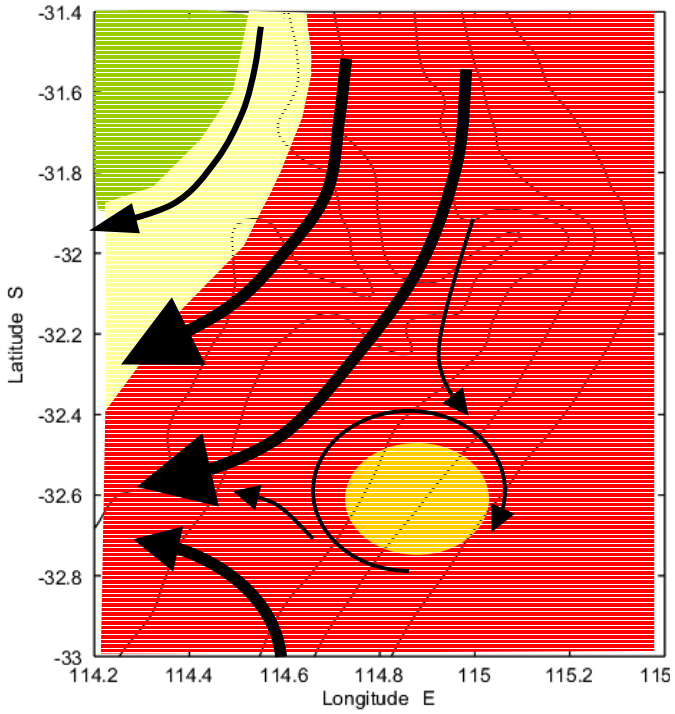

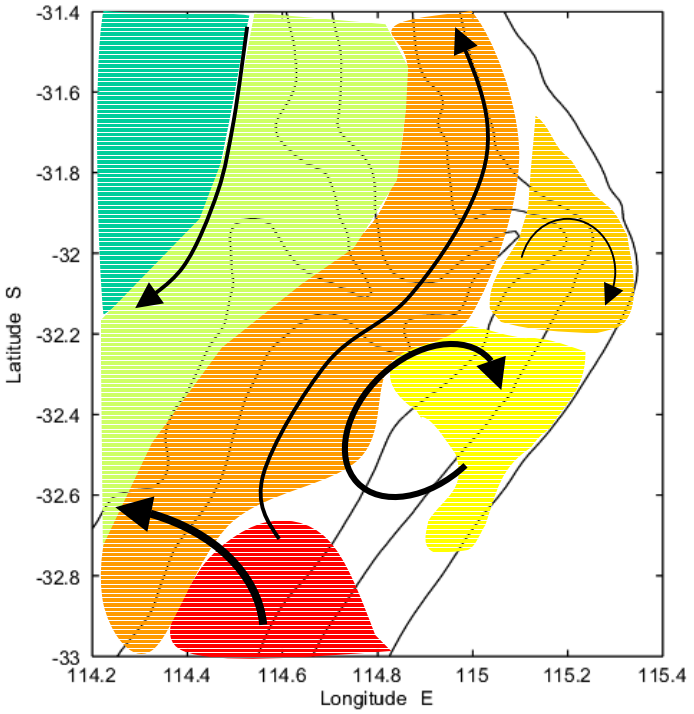

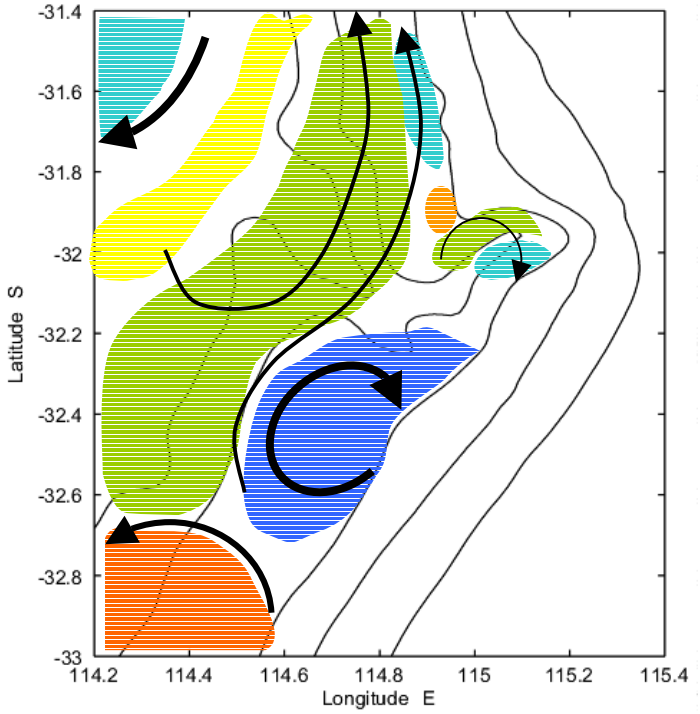

The Leeuwin Current is across the Perth Canyon mouth. A cyclonic eddy is on the south rim, inshore of the Leeuwin Current. The cyclonic eddy causes strong upwelling at 500 m. Cyclonic circulation occurs in the tip. An anticyclonic eddy is south of the Perth Canyon, forming an eddy pair.

Case 3

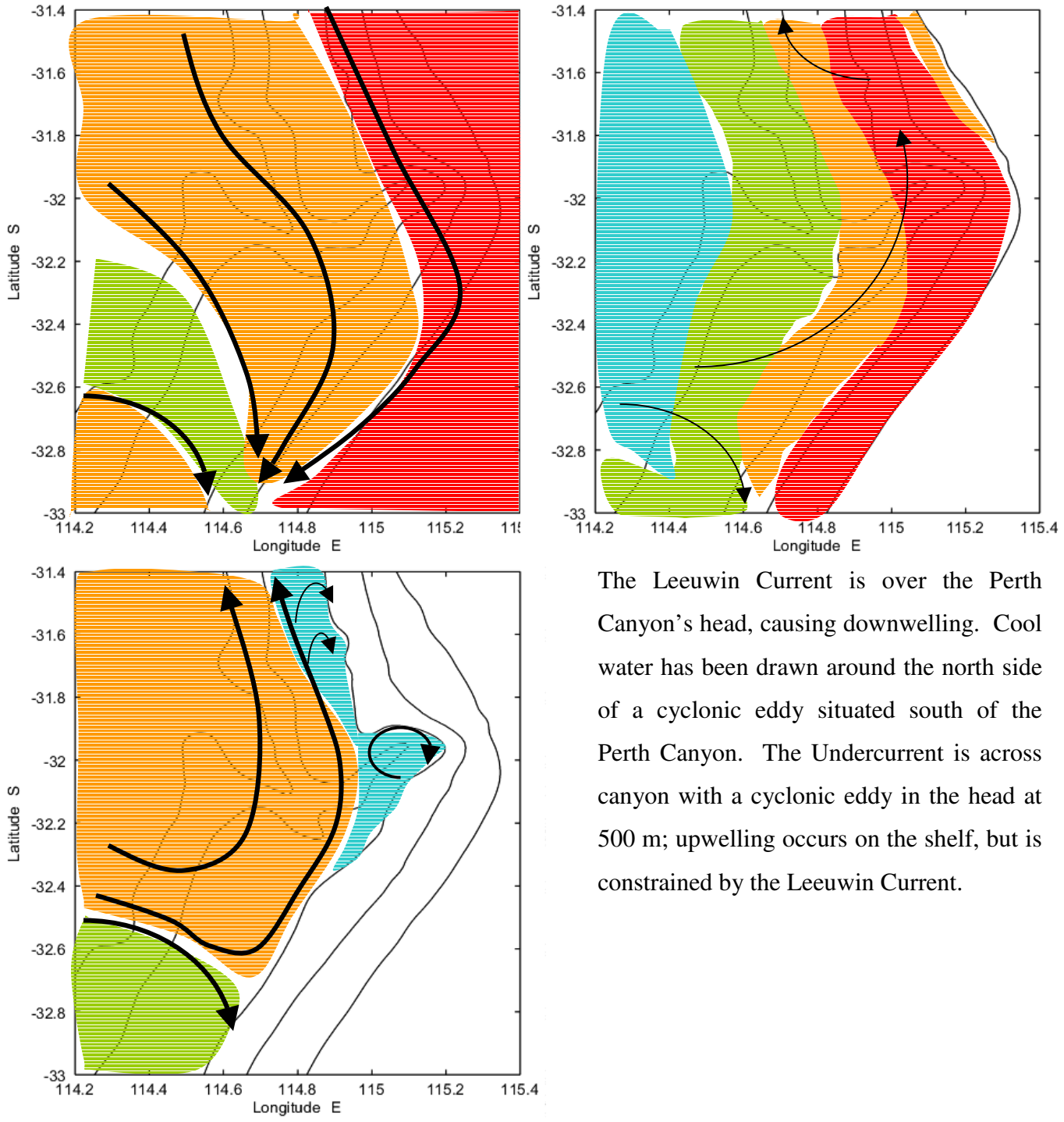

The Leeuwin Current is over the Perth Canyon's head, causing downwelling. Cool water has been drawn around the north side of a cyclonic eddy situated south of the Perth Canyon. The Undercurrent is across canyon with a cyclonic eddy in the head at 500 m; upwelling occurs on the shelf, but is constrained by the Leeuwin Current.

Case 4

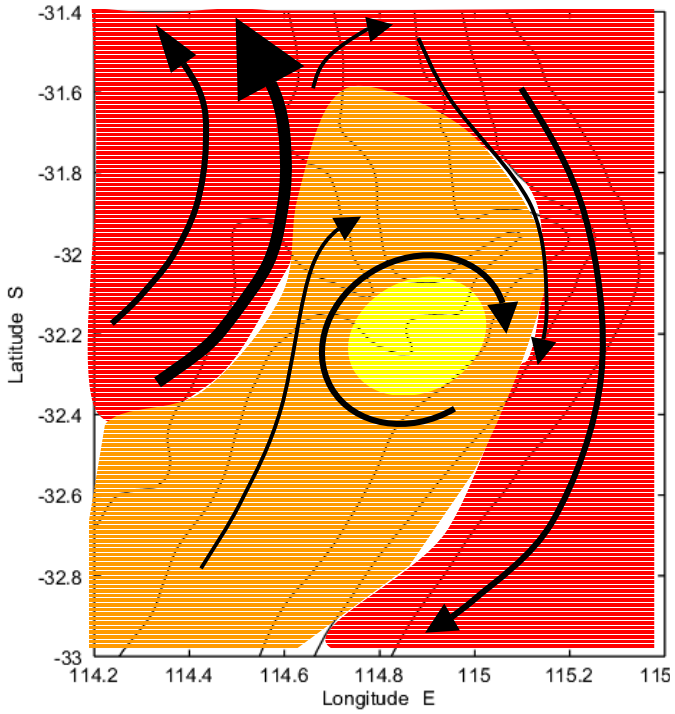

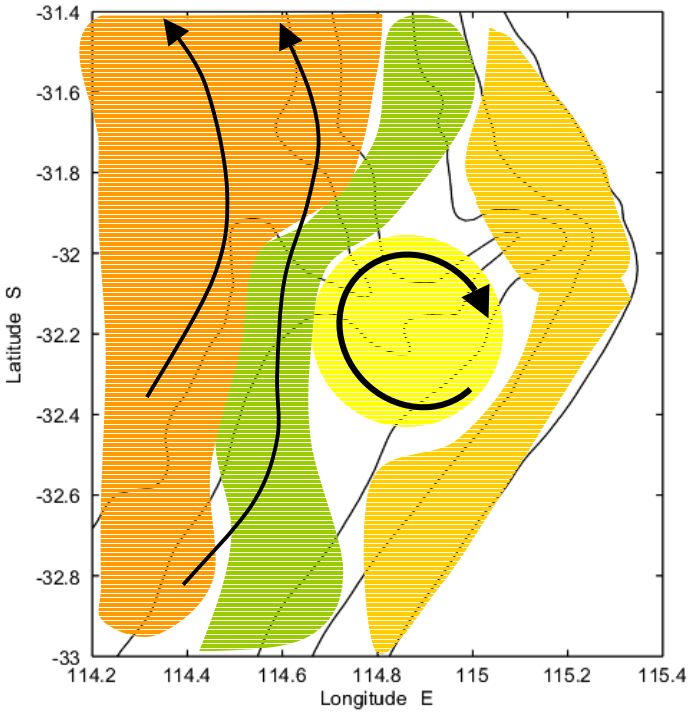

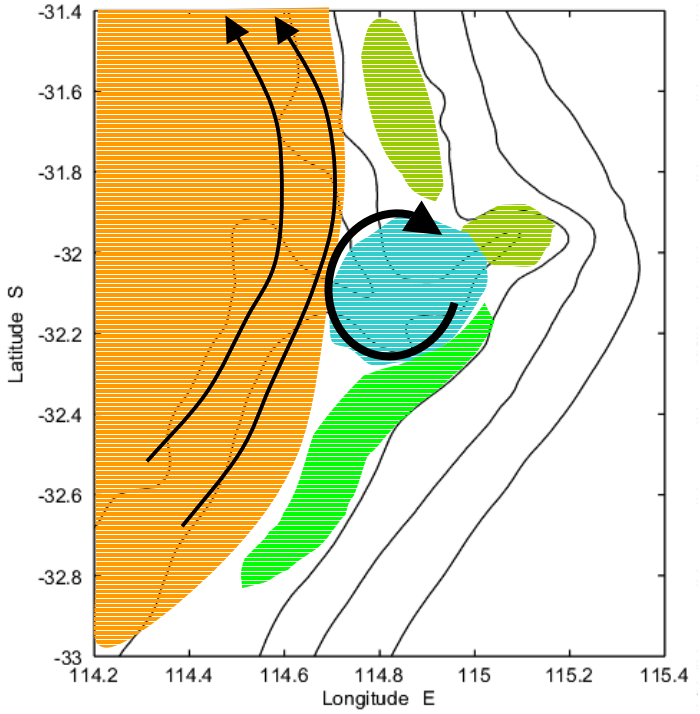

An anticyclonic eddy is northwest of the Perth Canyon. Cool oceanic water has been drawn in over the Perth Canyon, forming a cyclonic eddy over the dogleg at all depths. Downwelling occurs against the shelf, and upwelling occurs in the cyclonic eddy. The Undercurrent is across the canyon mouth.

Case 5

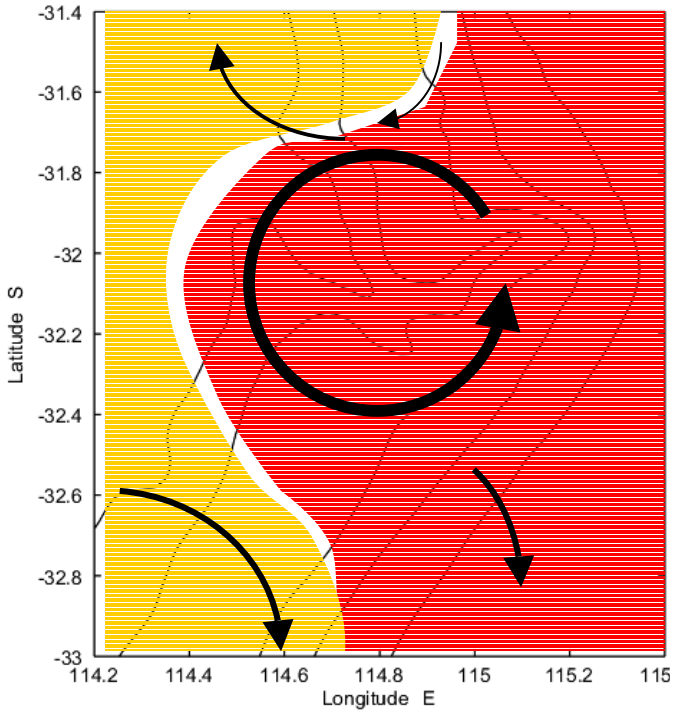

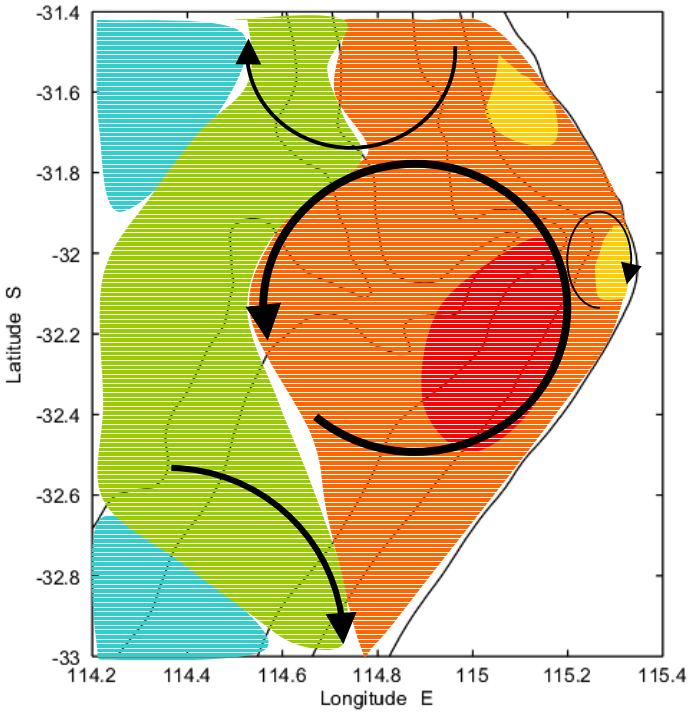

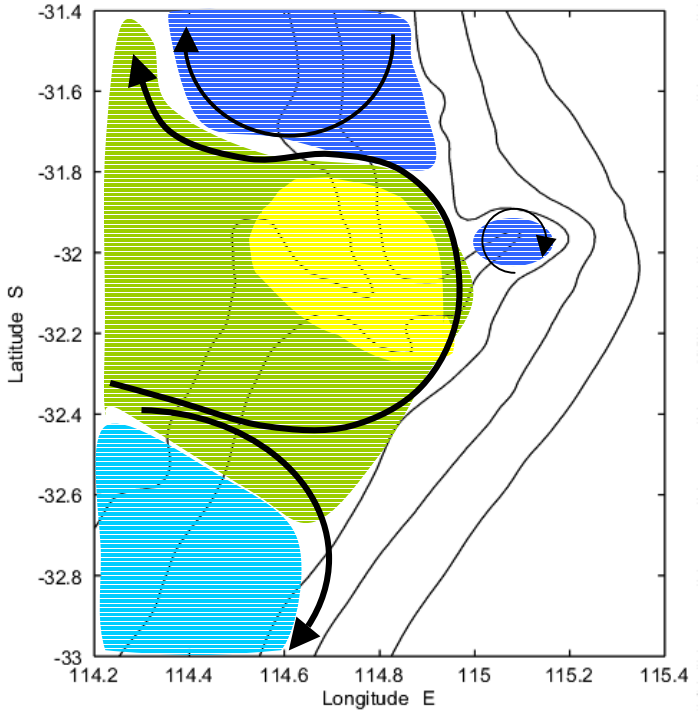

An eddy pair is present, with the anticyclonic eddy over the Perth Canyon and a cyclonic eddy against the shelf to the south. The Undercurrent circles anticyclonically around the canyon and forms cyclonic upwelling eddies to the north and south of the canyon. Upwelling occurs deep in the canyon head due to a cyclonic eddy.

Case 6 – variation 1

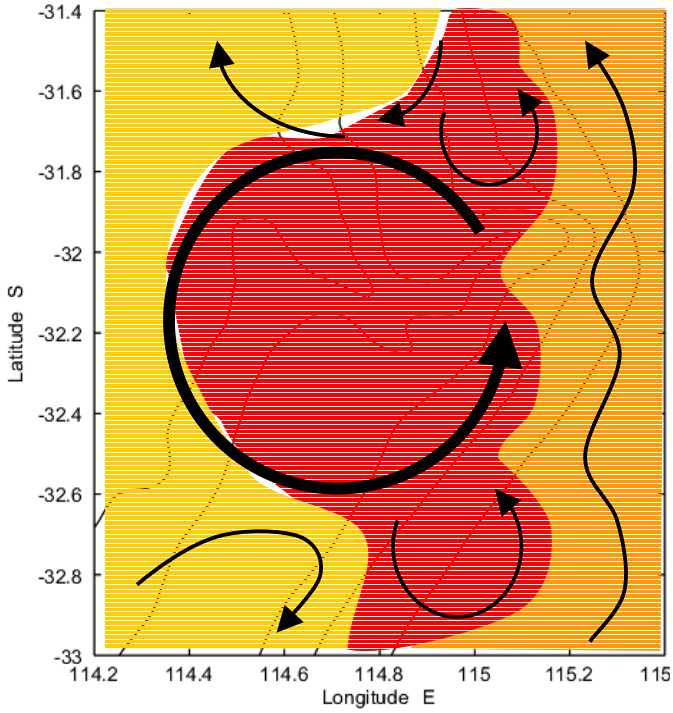

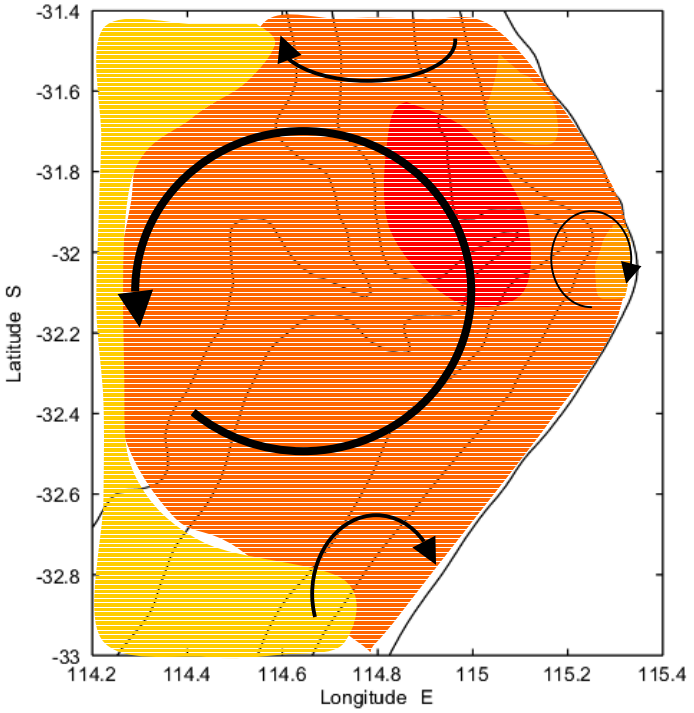

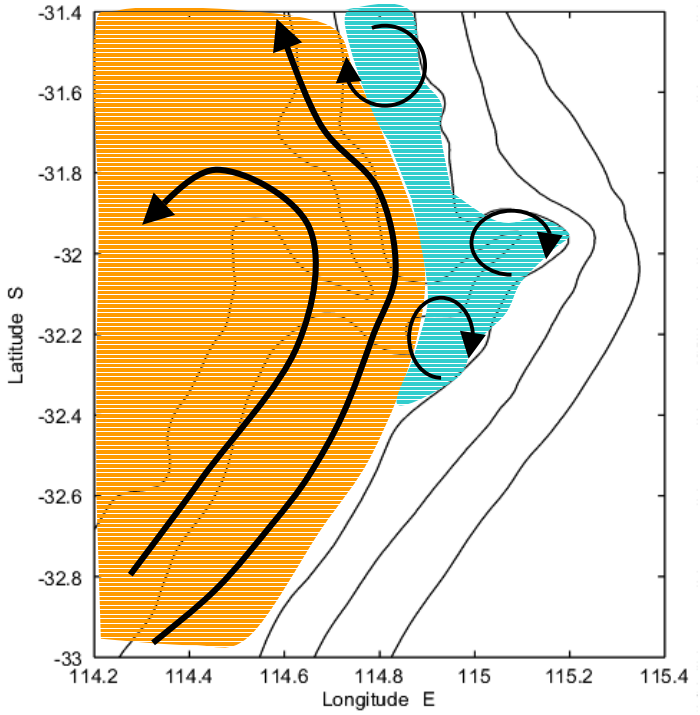

Similar to Case 5 at surface, but Case 3 at depth. The wind forcing causes some differences because the Leeuwin Current is offshore instead of onshore, and billows form on the onshore boundary of the Leeuwin Current. The northward shelf water helped to close the anticyclonic circulation over the canyon. The Undercurrent meanders over the Perth Canyon rather than forming a closed circulation. Cyclonic circulation occurs against the shelf north of the canyon and in the tip, causing upwelling.

Case 6 – variation 2

Variation 2 shows the slight differences in flow pattern that Case 6 accommodates.

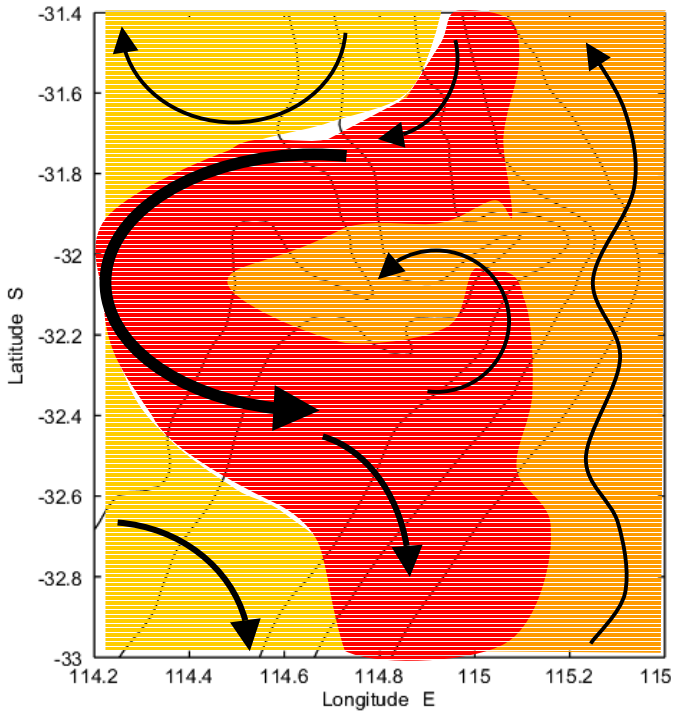

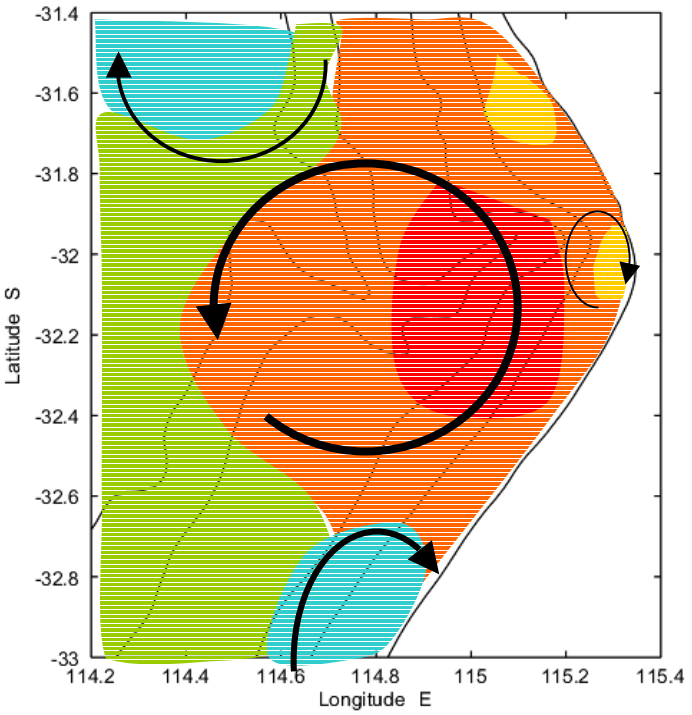

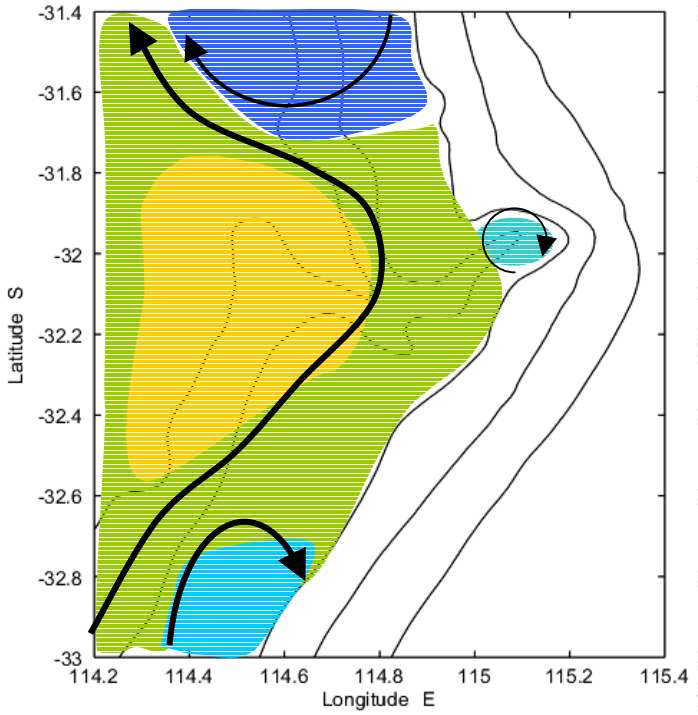

Similar to Case 5 at surface, but Case 3 at depth. The wind forcing causes some differences because the Leeuwin Current is offshore instead of onshore, and billows form on the onshore boundary of the Leeuwin Current. The northward shelf water helped to close the anticyclonic circulation over the canyon. The Undercurrent meanders over the Perth Canyon rather than forming a closed circulation. Cyclonic circulation occurs against the shelf north of the canyon and in the tip, causing upwelling.

Occurrence of Flow Cases in the Three Runs

Day	No wind	Summer	Spring
161	2		
166	2		
171	5		
176	5		
181	5		
186	2		
191	2		
196	3		
201	3		
206	6		
211	6		
216	6		
221	3		
226	3		
231	4		
236	4		
241	1	1	1
246	1	1	1
251	1	2	2
256	2	5	2
261	2	5	2,4
266	2	6	5
271	2	6	6
276	2	6	4
281	3	4	4
286	3	4	4
291	3	4	4
296	4	4	4
301	4	3	4
306	4	3	4

Day	No wind	Summer	Spring
311	4	3	2
316	2	3	6
321	2	3	6
326	3	5	6
331	5	5	6
336	5	6	1
341	1	6	2
346	2	-*	-
351	3	-	-
356	2	-	-

* - indicates the surface current became too unstable due to mixing.